Spring 5-31-2000

An integrated membrane-based chromatographic process for biomolecule isolation and purification

Xiaoping Dai
New Jersey Institute of Technology

ABSTRACT

AN INTEGRATED MEMBRANE-BASED CHROMATOGRAPHIC PROCESS FOR BIOMOLECULE ISOLATION AND PURIFICATION

by
Xiaoping Dai

Biomolecules obtained from fermentation and cell-culture processes are present in low concentrations in a complex medium/broth. For intracellular products, cells are first harvested. Subsequently, cell lysis and homogenization are undertaken to produce a homogenate. The biomolecules are next separated from the cell debris by lysate clarification. For extracellular products, the biomolecules are separated from the whole cells by clarification. The overall yield is reduced with each additional step. As the cost of bioseparation process accounts for 50-80% of the final product cost, innovations in and improvement of bio-downstream processing are greatly needed.

In this research, a cyclic process integrating a commercially available hollow fiber ultrafiltration (UF) cartridge and chromatographic resin beads was developed to reduce the number of devices and steps in bioseparation. This device consisted of ion exchange beads carefully packed on the shell side of a hollow fiber UF module. Loading of proteins on the beads on the shell side was carried out for a period of 10 - 30 minutes from the UF permeate on the shell side produced from a tube-side feed containing protein mixtures in buffer or in a cellular suspension. The eluent was next introduced either from the shell-side inlet or tube-side inlet. The chromatographic fractions were collected from the shell-side outlet. Continuous cyclic processes were also studied by repeatedly loading, washing and eluting protein(s) without applying cleaning agents to the membrane cartridge at the beginning of each cycle except the first one. A yeast-based cellular suspension containing

a binary protein mixture was also applied to this device. The target proteins were recovered and purified successfully by the continuous cyclic process.

A general mathematical model has been developed to predict pressure, flow rate and flux profiles in a bead-filled UF/MF hollow-fiber membrane module. The model was studied for a variety of operational modes in such modules, e.g., UF/MF, permeate flow control, Starling flow, elution, backflushing, etc. By using this model, preliminary mathematical descriptions for protein loading and elution behaviors in the bead-filled device have also been developed.

AN INTEGRATED MEMBRANE-BASED CHROMATOGRAPHIC PROCESS FOR BIOMOLECULE ISOLATION AND PURIFICATION

by
Xiaoping Dai

A Dissertation
Submitted to the Faculty of
New Jersey Institute of Technology
In Partial Fulfillment of the Requirements for the Degree of
Doctor of Philosophy in Chemical Engineering

Department of Chemical Engineering,
Chemistry and Environmental Science

May 2000

APPROVAL PAGE

AN INTEGRATED MEMBRANE-BASED CHROMATOGRAPHIC PROCESS FOR BIOMOLECULE ISOLATION AND PURIFICATION

Xiaoping Dai

Dr. Kamalesh K. Sirkar, Advisor   Date
Distinguished Professor of Chemical Engineering,
Sponsored Chair, Membrane Separations and Biotechnology, NJIT

Dr. Robert G. Luo, Co-Advisor   Date
Assistant Professor of Chemical Engineering, NJIT

Dr. Barbara Kebbekus, Committee Member   Date
Professor of Chemistry, NJIT

Dr. Gordon A. Lewandowski, Committee Member   Date
Chairperson and Distinguished Professor of Chemical Engineering, NJIT

Dr. Chao Zhu, Committee Member   Date
Assistant Professor of Mechanical Engineering, NJIT

BIOGRAPHICAL SKETCH

Author: Xiaoping Dai

Degree: Doctor of Philosophy in Chemical Engineering

Date: May 2000

Undergraduate and Graduate Education:

- Doctor of Philosophy in Chemical Engineering,
  New Jersey Institute of Technology, Newark, NJ, 2000

- Master of Science in Chemical Engineering,
  Chinese Academy of Sciences, Beijing, P. R. China, 1993

- Bachelor of Science in Biochemical Engineering,
  East China University of Science and Technology, Shanghai, P. R. China, 1990

Major: Chemical Engineering

Presentations and Publications:

Xiao-Ping Dai, Zhi-Fa Yang, Robert G. Luo and Kamalesh K. Sirkar,
"Lipase-Facilitated Separation of Organic Acids in a Hollow Fiber Contained Liquid Membrane Module,"
Journal of Membrane Science, 171(2), 183 – 196, 2000.

Xiao-Ping Dai, Robert G. Luo and Kamalesh K. Sirkar,
"An Integrated Process for Biomolecule Isolation and Purification,"
Biotechnology Progress, 15(6), 1095-1105, 1999.

Xiao-Ping Dai, Robert G. Luo and Kamalesh K. Sirkar.
"Pressure and Flux Profiles in Bead-Filled Ultrafiltration/Microfiltration Hollow Fiber Membrane Module,"
Submitted to Biotechnology Progress, 2000.

Xiao-Ping Dai, A. Kovvali, Kamalesh K. Sirkar,
"Pore Flow Through Reactor,"
Manuscript in preparation, 2000.

Xiao-Ping Dai, Robert G. Luo and Kamalesh K. Sirkar,
"Cyclic Operation of a Membrane-Based Chromatographic Process for
Biomolecule Separation and Purification,"
Presented at the AIChE Annual Meeting, Dallas, November 1999.

Xiao-Ping Dai, Robert G. Luo and Kamalesh K. Sirkar,
"A Membrane-Based Chromatographic Process for Biomolecule Purification,"
Presented at the 1999 International Congress on Membranes and Membrane
Process, Toronto, Canada, June 1999.

Xiao-Ping Dai, Robert G. Luo and Kamalesh K. Sirkar,
"An Integrated Process for Biomolecule Isolation and Purification,"
Presented at the AIChE Annual Meeting, Miami Beach, November 1998.

Xiao-Ping Dai, Robert G. Luo and Kamalesh K. Sirkar,
"An Integrated Process for Biomolecule Isolation and Purification,"
Presented at the 10th Annual Meeting of North American Membrane Society in
Cleveland, Ohio, May 1998.

Xiao-Ping Dai, Robert G. Luo and Kamalesh K. Sirkar,
"An Integrated Process for Biomolecule Isolation and Purification,"
Presented at the AIChE Annual Meetings, Los Angeles, November 1997.

Xiaoping Dai, Yihua Qi and Fan Ouyang,
"Vero Cell Culture on Microcarriers in a Designed Air-Lift Bioreactor,"
Chinese Journal of Biotechnology, 11(4), 399, 1995. (Chinese)

Xiaoping Dai, Yihua Qi and Fan Ouyang,
"Preliminary Investigation on Anchorage-Dependent Cell Culture by Air-Lift
Suspending Microcarriers,"
Proceedings of the 3rd Asia-Pacific Biochemical Engineering Conference,
Singapore, pp 408, June 1994. (Oral Presentation)

Xiaoping Dai, Yihua Qi and Fan Ouyang,
"Contact-Inhibited Growth Model for Anchorage-Dependent Cells,"
Proceedings of the 2nd National Symposium for Young Chinese Chemical
Engineers, Guangzhou, P. R. China, pp 485, December 1993. (Chinese)

To my husband, Gui-Hua; my grandma; my parents, Mr. and Mrs. Dai; my brother, Zheng-Kun; my sister-in-law, MeiChih and my nephew, Claudia.

ACKNOWLEDGMENT

I would like to express my sincere gratitude to my supervisors, Professor Kamalesh K. Sirkar and Professor Robert G. Luo, for their guidance, support and friendship throughout this research.

Special thanks to Professors Gordon A. Lewandowski, Barbara Kebbekus and Chao Zhu for serving as members on my committee and giving me valuable suggestions.

I appreciate the support, help and suggestions from Membrane Separations and Biotechnology Group throughout these years, including: Dr. Sudipto Majumdar, who helped me greatly in the numerical simulation part of this research; Dr. Zhi-Fa Yang, who helped me to start on the right foot when I first joined this group; Arminta Skipper and Judy Kapp, who helped me to take care of logistics; Dr. Uttam Shanhbang, Jignesh Sheth, A. Sarma Kovvali, Gordana Obuskovic, Dr. Yingjie Qin, Dr. Hua Chen, Meredith Mason, Jose Whu, Wendy Reid and Dr. Bhaumik.

And finally, I want to thank my husband, Gui-Hua Qian, who constantly supported me over all these years.

TABLE OF CONTENTS

TABLE OF CONTENTS
(Continued)

TABLE OF CONTENTS
(Continued)

Chapter   **Page**

LIST OF TABLES

LIST OF FIGURES

Figure   **Page**

Figure   **Page**

LIST OF FIGURES
(Continued)

NOMENCLATURE

A	Water permeation parameter (m/Pa.s), eq 5.1
A_1	Integration constant in eq 5.18a and eq 5.58a
A_2	Integration constant in eq 5.18a and eq 5.58a
ABS	Optical absorbance of protein
B	Parameter defined by eq 5.14
B^c	Certain value of B at which the TMP uniformity index α is same for a module with or without an ES when other parameters are same
$B^{\#}$	Certain value of B at which the TMP uniformity indicated by α reaches the highest level as a function of B when other parameters are same
B^*	Parameter defined by eq 5.32c
B^{**}	Parameter defined by eq 5.32c
$B^{/}$	Parameter defined by eq 5.34a
C_0	Initial protein concentration of liquid phase (mg/ml)
C^*	Equilibrium concentration of protein in the liquid phase (mg/ml)
C_{if}	Tube-side concentration in feed (mg/ml)
C_{if0}	Feed concentration (mg/ml)
C_{ip}	Protein concentration in liquid phase on the shell-side bed (mg/ml)
C_{is}	Lumped protein concentration in solid phase on the shell-side bed (mg/ml)
D_i	Housing internal diameter of the module (m)
D_{ieff}	Effective axial dispersion coefficient for species i (m^2/s)
d_i	I.D. of a single fiber (m)
d_o	O.D. of a single fiber (m)

d_p Diameter of beads packed on shell side (m)

E Parameter defined by eq 5.53

ES Extended section

F_1 Function defined by eq 6.30b

F_2 Function defined by eq 6.30c

J_{vz} Volume flux through the membrane at axial location z ($m^3/m^2.s$)

K Linear equilibrium constant

K_d Dissociation constant (mg/ml)

L Module length (m)

L_E Length of the extended section (m)

M Parameter defined by eq 5.13.

N Parameter defined by eq 5.13.

N_0 Number of fibers inside the module

P_{atm} Atmospheric pressure

P_E Pressure in the extended section (psig or Pa)

P_F Tube-side pressure for the situation where feed is introduced from the fiber bore (psig or Pa)

P_P Permeate side pressure for the situation where feed is introduced from the fiber bore (psig or Pa)

P_S Shell-side pressure for the situation where feed is introduced from the shell-side inlet (psig or Pa)

P_T Tube-side pressure for the situation where feed is introduced from the shell-side inlet (psig or Pa)

$Q_{F0}{}^c$ Certain value of Q_{F0} at which the TMP uniformity index indicated by α is the same as a function of Q_{F0} for a module with or without an ES when other parameters are same

$Q_{F0}{}^{\#}$ Certain value of Q_{F0} at which the TMP uniformity indicated by α reaches the highest level as a function of Q_{F0} when other parameters are same

Q_F Feed volumetric flow rate for the situation where feed is introduced from the fiber bore (m^3/s)

Q_P Permeate volumetric flow rate for the situation where feed is introduced from the fiber bore (m^3/s)

Q_S Shell-side volumetric flow rate for the situation where feed is introduced from the shell-side inlet (m^3/s)

Q_T Tube-side volumetric flow rate for the situation where feed is introduced from the shell-side inlet (m^3/s)

Q_{si} Volumetric flow rate in a single fiber (m^3/s)

q^* Equilibrium concentration of protein in the solid phase (mg/ml)

q_m Maximum protein adsorption capacity (mg/ml)

R_i Housing internal radius of the module (m)

$R_i{}'$ Solute rejection by the membrane, defined by eq.6.3

r_f Radius of free surface (m), eq 6.2

NOMENCLATURE
(Continued)

r_i	Internal radius of a single fiber (m)
r_o	External radius of a single fiber (m)
S	Constant defined by eq 6.30a
S_E	Cross-sectional area of extended section (m^2)
S_F	Cross-sectional area outside a hollow fiber in one unit cell by applying the "free surface model"
S_s	Cross-sectional area of shell side (m^2)
T	Parameter defined by eq 5.36.
TMP	Transmembrane pressure, $P_F - P_P$ or $P_S - P_T$
u_E	Superficial velocity in the extended section (m/s)
u_P	Superficial velocity in the shell-side bed (m/s)
V	Parameter defined by eq 5.54
W	Parameter defined by eq 5.54

Greek Symbols

α	Uniformity factor of TMP, defined by eq 5.42
β	Parameter defined by eq 5.17
ε	Void fraction of the bed
ϕ	Ratio of the cross-sectional areas of the shell-side bed over the ES bed
μ	Viscosity of fluid (kg/m.s)

NOMENCLATURE
(Continued)

Subscripts

E	Extended section
F	Feed side (tube side, for the situation where feed is introduced from the tube-side inlet)
L	End of the module length
P	Permeate side (shell side, for the situation where feed is introduced from the tube-side inlet)
S	Shell side (for the situation where feed is introduced from the shell-side inlet)
T	Tube side (for the situation where feed is introduced from the shell-side inlet)
z	Any length from the beginning of the module length
0	Beginning of the module length

CHAPTER 1

BACKGROUND

1.1 Introduction

Biomolecules (e.g., interferons, hormones, immunoglobulins, growth factors, DNAs) obtained from fermentation and cell-culture processes are present in low concentrations in a complex medium/broth containing various combinations of cells, cell fragments, lysed cells, colloidal materials, etc. For intracellular products, cells are first harvested. Subsequently, cell lysis and homogenization are undertaken to produce a homogenate. The biomolecules are next separated from the cell debris by lysate clarification. For extracellular products, the biomolecules are separated from the whole cells by clarification. Therefore biomolecule recovery from a fermentation broth is complicated by the large number of dissolved substances and suspended particles present in the broth.

Most bioseparation processes involve the following steps: removal of insolubles by either filtration or centrifugation, isolation of products using either adsorption or solvent extraction, purification (via chromatography and precipitation) and polishing via crystallization, or spray drying and lyophilization (Belter, Cussler and Hu 1988). The number of sequential operations needed for the purification contributes significantly to the overall costs of the downstream process. The overall yield is reduced with each additional step (van Reis, Leonard, Hsu and Builder 1991). The devices involved in these processes are complex as well. As the performance of the bioseparation is responsible for 50-80% of the final product cost, innovations in and improvement of bio-downstream processing that reduce the overall number of steps, increase yield and productivity along

1

with a reduction in the complexity of the downstream processing flowsheets are greatly needed (Sofer and Hagel 1997a; Harrison 1994).

1.2 Previous Technologies for Process Integration

A number of strategies have been suggested previously for downstream process integration. In one strategy, specialized adsorbent beads/particles or membranes are employed. Nigam, et al. (1988) have suggested using specially prepared adsorbents consisting of small, porous adsorbent particles such as chromatography beads entrapped within a reversible hydrogel matrix (e.g. agarose, diameter of the beads is 1.2-1.4 mm, adsorbent content is 35%), or adsorbent particles encapsulated within a thin (50-100 μm) hydrogel membrane (e.g. calcium alginate, size of spherical capsule is 1.3 mm, adsorbent content is 60-65%). The pore size of the hydrogel can be tailored such that the desired product in the crude extract can readily diffuse through the hydrogel matrix or membrane to the adsorbent. Colloidal contaminants are completely excluded from contacting the adsorbent particles (Figure 1.1). The authors recovered recombinant β-lactamase from unclarified broths and homogenates using these immobilized adsorbents.

Expanded bed adsorption (EBA) is a recently developed new unit operation that recovers proteins from crude feed-stock in a single pass operation without prior clarification (McCormick 1993; Thömmes, Halfar, Lenz and Kula 1994; Chang and Chase 1996; Diehl 1998; Finette, Baharin, Mao and Hearn 1998). In this technology, a suitable stationary phase is fluidized in a mobile phase with the liquid feed stream directed upwards. Elution can be carried out either in the upward direction or downward direction (Figure 1.2). The EBA is a tool in the initial phase of downstream processing.

STREAMLINE^R adsorbent is a matrix developed by Amersham Pharmacia Biotech (Uppsala, Sweden and Piscataway, NJ) for expanded bed adsorption. The beads consist of a porous 6% or 4% highly cross-linked agarose as the basic structure. Most beads have a particle size range 100-300 µm with a mean particle size of 200 µm. To provide fluidization characteristics suitable for using the matrix to capture protein from the whole fermentation broth, inert crystalline quartz particles are incorporated into the basic bead structure. This ensures a rapid separation of the matrix from the surrounding liquid phase. Ion exchange or affinity ligands are covalently attached to the base matrix (Amersham Pharmacia Biotech 1999a; Thömmes 1999). The adsorbents exhibit a Gaussian like distribution of particle size and particle density which allow the beads to find their suitable position in the column to reduce the axial dispersion in the expanded bed (Figure 1.2) (Amersham Pharmacia Biotech 1999b).

However, the expanded bed design does not allow for complete removal of viable cells for some applications; the eluate was found to have viable cells to the extent of 0.01% of that of the applied feedstock (Chang and Chase 1996). Dilution or nuclease pretreatment of the feedstocks are needed before application to the bed for high biomass containing feedstocks (Chang and Chase 1996; Shiloach and Kaufman 1999). Further, successful operation of the expanded bed depends on achieving a stable bed where the mixing in the column is very limited. Achieving a stable bed was found to be difficult when dealing with intracellular products (Johansson, Jagerstern and Shiloach 1996).
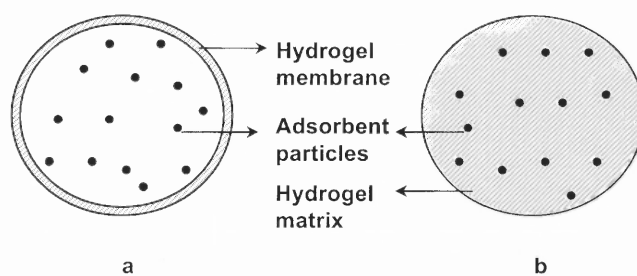
Figure 1.1 Small, porous adsorbent particles encapsulated within a thin hydrogel membrane (a) or the adsorbent particles entrapped within a reversible hydrogel matrix (b) (Nigam, Sakoda and Wang 1988).

a
Adsorption

b
Upward
elution

c
Downward
elution
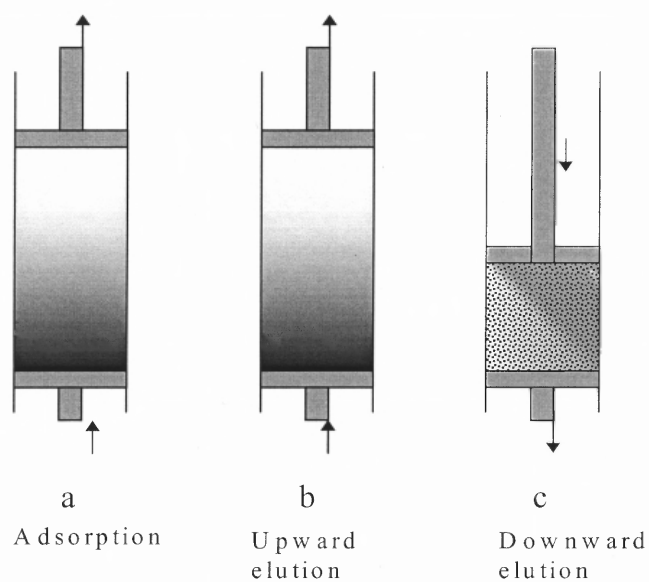
Figure 1.2 Expanded bed adsorption and elution. (a) Adsorption. (b) Upward elution. (c) Downward elution

In membrane adsorption processes (Figure 1.3), ligands are grafted on the surfaces of pores in microporous or macroporous membranes; biomolecule adsorption is achieved by convecting the filtered broth through the pores (Thömmes and Kula 1995; Zeng and Ruckenstein 1999). This idea was introduced as a technology especially suited

for large-scale processes. It can be operated either in dead-end mode or in crossflow mode. This process has the integrative aspects of capture and purification steps with the possibility of processing large amounts of product in a comparatively short time. Membrane-based adsorption can be generally distinguished from particle-based adsorption by the fact that the interaction between a solute (protein) and a matrix (immobilized ligand) does not take place in the dead-ended pores of a particle, but mainly in the through-pores of a membrane. Binding capacity is reached by using membranes of sufficient internal surface area, yielding configurations of very large diameter to height ratios (d/h). Reduced pressure drop in membrane adsorption process allows increased flow rates and productivity. Without pore diffusion as the limiting step in packed bed adsorption, membrane adsorption separates molecules on the basis of different binding kinetics, and not just sorption equilibrium isotherms of the species.
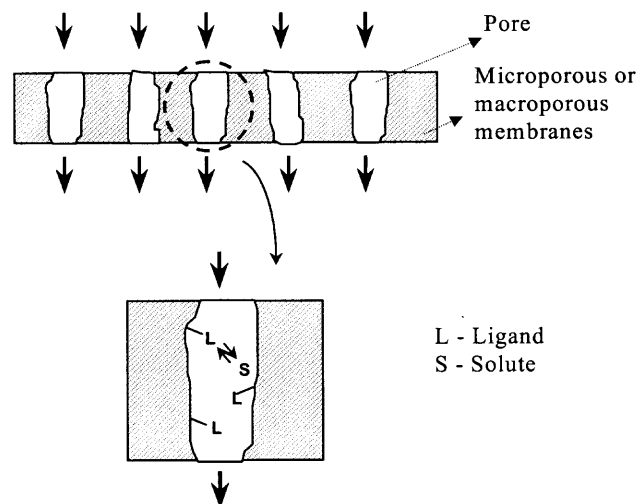
Figure 1.3 Schematic for membrane adsorption processes

One major problem facing this technique is the limited capacity of individual membranes along the liquid filtration path compared with that of chromatography beads as the specific surface area available for the ligands of these membranes is lower. Introducing a three dimensional ligand layer may overcome this problem to obtain similar capacity per unit volume to that of conventional adsorbents. However, these three dimensional ligand spheres compromise the superior mass transfer capability of membrane adsorption process.

Perfusion chromatography technology was introduced in 1989 (PerSeptive Biosystems Inc. 1996). It is a hybrid between conventional particulate resins and membrane adsorbents, as the new porous materials allow partial convective flow through the beads. But there are still interparticulate and intraparticulate voids remaining in a packed bed in this kind of chromatography. In addition, perfusion chromatography does not allow unclarified solution to be applied to the column as the particles and debris may lead to fouling of the beads.

Many of these aforementioned techniques require specially designed and costly adsorbents and unusual operational conditions in expanded/fluidized beds to accommodate the presence of an unclarified broth. More often than not, the specially designed bead may not have the required ligands for separating certain biomolecules in solutions. This is certainly true for membrane adsorption process as well. Further, perfusion chromatography technology can not be used for an unclaified broth or a homogenate yet.

Besides these aforementioned techniques with specialized adsorbents/membranes, aqueous two-phase system could be directly used for unclarified fermentation broths or homogenates. Particles and product biomolecules may be partitioned into opposite phases under appropriate conditions. After the phase disengagement, the product is enriched in an aqueous environment of much reduced particle concentration. This technique has the advantage of integrating clarification, concentration and partial purification, but phase separation can be slow because of high viscosity and small density differences and there is no separation of different molecules in the product phase (Subramanian 1998).

Microfiltration/Ultrafiltration-based cell-protein separation or lysate clarification is being increasingly employed in small as well as large-scale harvesting of protein (van Reis, Leonard, Hsu and Builder 1991) and other biomolecules. Further, a wide variety of adsorbent beads or chromatographic matrix particles are commercially available and routinely used for biomolecule fractionation and purification. An efficient integration of these functions in one device using commercially available and commonly utilized microfiltration/ultrafiltration membranes and adsorbent beads is highly desirable.

Employing this overall strategy, some work has been carried out. For example, adsorbent beads are added to a mixture consisting of the target biomolecule and impurities to allow adsorption of the target biomolecule onto the beads (Byers, Isacoff and Naples 1991); then the suspension is circulated through the lumen of hollow fiber membranes. This allows impurities to permeate through the membrane to the shell space. The product has to be recovered next from the adsorbent with another membrane filtration process. This technique still has to contend with the broth debris and the adsorbent particle interaction; further, running beads through the membrane fiber bore is

not a very desirable operational mode. Another example is the work by Davis (1990). An affinity bead-containing stream is circulated through one side of the membrane where the adsorbent has a dimension larger than that of the pores; feed containing different materials including the product is flowing in the second side of the membrane whereby certain biomolecules become bound to the adsorbent upon passing through the membrane to the first side and get separated. For this technique, a separate elution device or process is needed to remove the bound molecules from the beads.

Molinari et al. (1990) employed a hollow fiber membrane device with affinity beads or ion exchangers on the shell side. They circulated the feed through the fiber bore and operated the shell side in Starling flow (by having very low effective permeation rate) (Starling 1896). They continued this process for 5-7 hours; the permeate showed considerable activity of the target compound after one hour. Afterwards, the bioproduct was recovered by elution from the shell side beads. No chromatography was involved in this study. The beads packed on the shell side were used as adsorbent particles in an adsorbent bed. The long loading time resulted in breakthrough of the target protein through the adsorbent bed into the permeate (Figure 5 on page 576 shows breakthrough beyond 1 hour and continuing till 7 hours). As a result, ion exchange-based purification of the enzyme achieved via elution was limited. For example, they achieved only a 2.3–fold purification of carboxylesterase in the eluate compared with the feed solution.

1.3 New Technique in This Work

It is clear from the above that there is no study of a process for direct chromatographic purification of protein mixtures from a fermentation broth or a homogenate. An

investigation employing commercially available membrane ultrafiltration devices and chromatographic media was undertaken in this dissertation to separate binary protein mixtures from a clear feed solution or a cellular suspension.

The device consisted of ion exchange beads carefully packed on the shell side of a hollow fiber UF module. Loading of proteins on the stationary phase on the shell side was carried out for a short period (e.g., less than 30 minutes) from the UF permeate on the shell side produced from a tube-side feed containing protein mixtures in buffer or in a cellular suspension. The eluent was next introduced either from the shell-side inlet or tube-side inlet; the chromatographic fractions were collected from the shell-side outlet. The resolution of the proteins obtained for systems studied in one-run process from clean solutions containing several binary mixtures will be described in this dissertation. Continuous cyclic processes have also been developed by repeatedly loading, washing and eluting single protein and multiple protein mixtures without applying cleaning agents to the membrane cartridge at the beginning of each cycle except the first one. The extent of mixture separations and the yields in such processes were studied. A yeast-based cellular suspension containing a protein mixture was also applied to this device to recover and purify target proteins by the continuous cyclic process.

This cyclic process-based device integrates clarification, concentration and chromatographic purification of biomolecules and may be adopted for large-scale processing easily. It is suitable for both extracellular and intracellular products. The details of the process concept and device will be presented in the next chapter. The experimental details are provided in Chapter 3. The results for the performance of the integrated device are illustrated in Chapter 4.

A general mathematical model has been developed in Chapter 5 for the prediction of pressure, flow rate and solvent flux profiles in an ultrafiltration/microfiltration hollow-fiber membrane module whose shell side is filled with beads. The model was studied for a variety of operational modes in such modules, e.g., ultrafiltration/microfiltration, permeate flow control, Starling flow, elution and backflushing, etc. The model can predict the nature of the transmembrane pressure (TMP) profile and the solvent flux profile in situations that are quite different, namely, conventional ultrafiltration and Starling flow (Starling 1896). By using this model, preliminary descriptions for protein loading and elution behaviors in the bead-filled device have also been developed in Chapter 6.

CHAPTER 2

THE PROCESS CONCEPT AND THE DEVICE

2.1 The Process Concept and the Device

As stated in Chapter 1, microfiltration/ultrafiltration-based processes are currently used for cell-protein separation (extracellular products) or lysate clarification (intracellular products) in small- or large-scale harvesting of bioproducts. Many adsorbent beads or chromatographic matrix particles are commercially available and routinely used for biomolecule fractionation and purification. In this work, a new cyclic process concept has been developed by integrating the membrane filtration process and chromatographic purification process in a new apparatus assembled by combining a membrane module and chromatography beads.

A commercially available hollow fiber ultrafiltration cartridge is employed in this research (microfiltration cartridge can also be used). The hollow fiber cartridge (e.g., for ultrafiltration (UF)) may be chosen based on the molecular weight cut off (MWCO) or the pore size compared with the size of the targeted product(s) to be separated from the feed. Although the flux through the membrane is also an important consideration, the presence of shell-side beads tends to reduce the solvent flux significantly. The effective flux should be in the allowable/recommended range for the beads employed on the shell side for chromatographic applications. Appropriate adsorbent beads are carefully packed on the shell side of the hollow fiber cartridge (Figure 2.1a). Through the lumen of the fiber, the feed solution is allowed to flow for a defined period of time, say, 5 – 30 min. The feed solution may be a lysate for intracellular products or a fermentation broth for extracellular products. The feed solution pressure everywhere on the lumen side is greater

than that on the permeate (shell) side; permeate appearing through the membrane everywhere on the shell side flows out in the same direction as the feed solution and leaves the shell side via an outlet. No Starling flow (Starling 1896) is involved.

During this period of filtration-cum-loading in chromatography, bioproducts (e.g., DNAs, proteins) in the feed solution smaller than the membrane pores will go through the pores under appropriate transmembrane pressure (TMP) and then get partitioned onto the adsorbent under proper conditions (e.g. pH and ionic strength, etc.) (Figure 2.1a). The particles, cell debris, proteins, etc. which are larger than the pores are rejected by the membrane and are concentrated in the retentate stream. The conditions must be such that any bioproduct appearing on the shell side gets adsorbed on the shell side beads during this loading or feeding step. During the loading time, the bed was not allowed to be saturated. For those beads close to the fibers, there should be diffusion of proteins into the beads. For those beads relatively far away from the fibers, there may be surface adsorption of proteins on the beads. The permeate was monitored to assure that the protein products do not <u>breakthrough</u> into the permeate stream leaving the shell side. For columns in traditional ion exchange chromatography for protein purification, less than 30% of the beads' dynamic capacity is recommended (Sofer and Hagel 1997b) for loading purposes. Further the dynamic capacity is usually lower than that of the available resin capacity. These provide useful estimates for the loading time. In addition there is an additional length of column at the permeate outlet (Figures 2.1a, 2.1b and 2.1c) to provide a safety factor for preventing protein breakthrough.
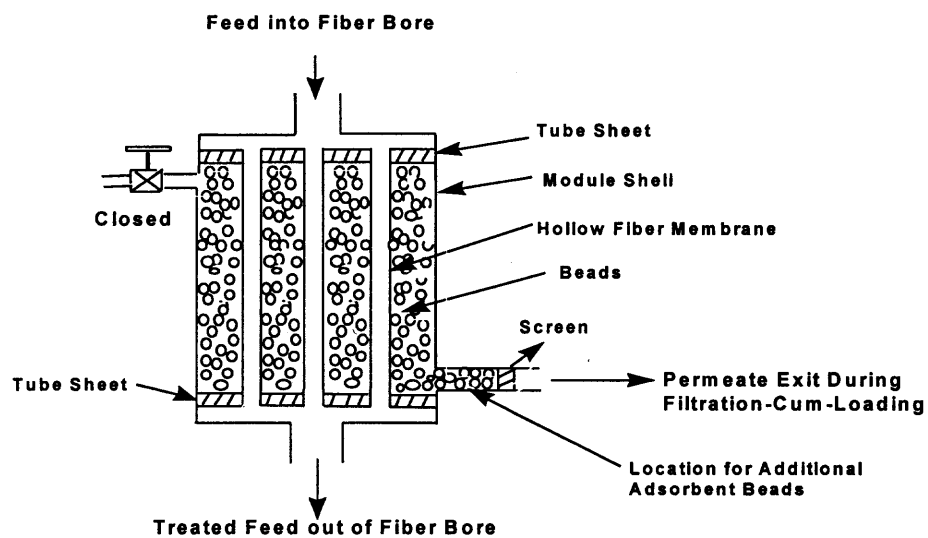
Figure 2.1a Configuration of the device containing membrane and adsorbent beads during filtration-cum-loading
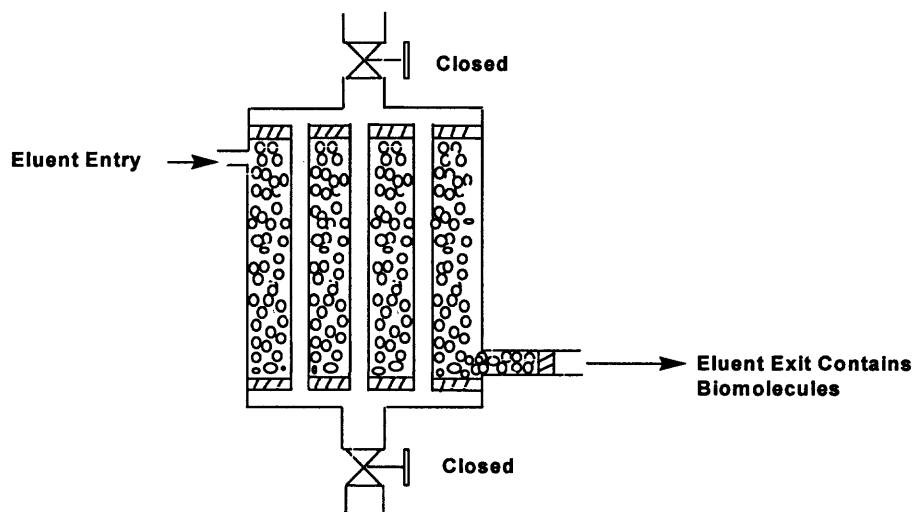
Figure 2.1b Configuration of the device containing membrane and adsorbent beads during chromatographic elution
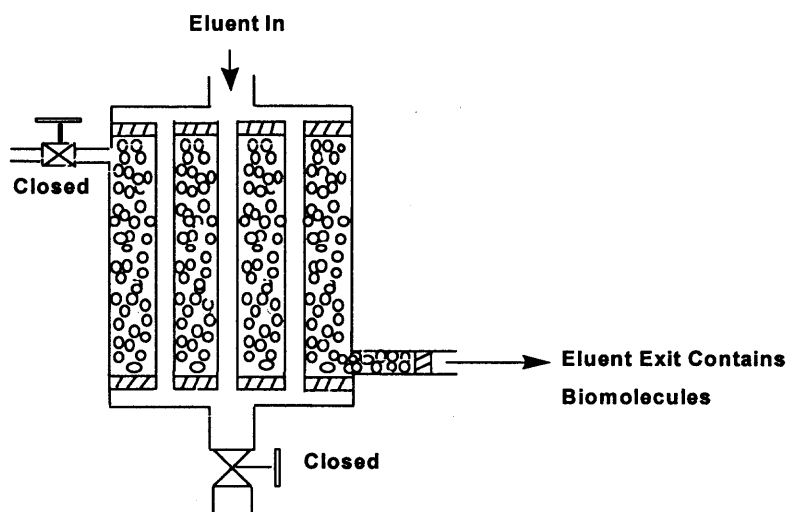
Figure 2.1c Alternative configuration of the device containing membrane and adsorbent beads during chromatographic elution

After the feed solution flow into the fiber lumen is stopped, the column can be washed by the starting buffer, and then elution of the bioproduct adsorbed on the shell-side beads is initiated by introducing the eluent. The eluent may be introduced on the shell side as shown in Figure 2.1b (which is called the shell-side elution) or through the fiber lumen inlet as shown in Figure 2.1c (which is called the tube-side elution). During this elution step, in the configuration of Figure 2.1b, both ends of the fiber lumen are kept closed; in the configuration of Figure 2.1c, the retentate end of the feed fiber lumen and the shell side inlet of Figure 2.1b are kept closed. The elution process is continued until the respective product peaks emerge from the permeate side outlet end. The duration of the elution step may vary widely and could run as long as 40 – 90 minutes or longer if it is not optimized.

After the elution is over, the bed could be regenerated using a specific regeneration buffer (e.g., NaCl solution in the starting buffer) followed by reequilibration with the starting buffer. Then the cyclic process of loading-elution-reequilibration or loading-elution-regeneration-reequilibration is initiated again.

The loading of the feed solution on the adsorbent beads in this process is quite different from that in an axial flow (conventional) chromatography column or radial chromatography column. In axial flow columns, loading takes place at the column top. Here loading occurs all along the length of the bed next to the fiber. Then it spreads out radially as well as axially further away from each fiber.

In addition to combining several downstream steps such as clarification, concentration and purification into one device, this cyclic filtration-adsorption-chromatography process may possess several unique characteristics, such as elimination of Starling flow, membrane fouling reduction, higher product recovery, modular unit facilitating scale-up, etc. These will be elaborated in the discussion section.

This process concept and device differ from those of Molinari et al. (1990) in a number of important aspects. First, the bed of resin beads packed on the shell side of the module was used as a chromatographic column for elution chromatography in this study. Thus the time used for loading was controlled and the permeate was monitored so that no breakthrough could take place. On the other hand, breakthrough during loading was routine in Molinari et al.'s work (1990). As a result, the extent of purification of carboxylesterase in their study was only 2.3 fold compared to that in the feed. In the present study, two separate peaks are obtained repeatedly in the eluent fractions as will be shown later in the results. Second, to ensure the above outcome, an additional amount of

resin beads has been packed at the permeate outlet port on the shell side. These resin particles used as an extended section of the chromatographic bed were kept in place by a 21 μm polyester mesh. This extended section, which can be made longer if necessary, serves several purposes. First, it catches protein molecules which may come out from the shell-side permeate exit due to the direct loading of proteins from the tube side to the shell side at the bottom of the module. Second, it helps in the separation of different species especially when the extended section is longer. Molinari et al. (1990) did not have any such section; their permeate ports on the shell side were packed with fiberglass. Third, the permeate flow rate was restricted in Molinari et al. (1990) to a low value (e.g. 0.67 ml/min) during the protein binding step by adopting Starling flow (Starling 1896). No Starling flow is involved in the present study and the system was operated with whatever permeate flow rate produced naturally in the system under the operating conditions. Fourth, the eluent in Molinari et al. (1990) was introduced through one of the ports in the shell space and taken out through the other port (Figure 2 and the write-up on page 577 in their paper, shell-side elution shown in Figure 2.1b in this Chapter). Study of eluent introduction through the tube-side inlet and its withdrawal through the shell-side outlet has been primarily conducted in this research. This has several important and possible beneficial features to be discussed later.

2.2 Other Engineering Applications with Similar Device Configurations

2.2.1 Hollow-Fiber Bioreactor (HFBR)

Hollow-fiber bioreactors (HFBRs) have been used extensively to immobilize mammalian cells on the shell side (the extracapillary space (ECS)) for the production of diagnostic

and therapeutic proteins. Substrate-containing solution flows through the tube side to supply nutrients and to remove metabolic wastes. There is no permeate flow at all. Fluid enters the ECS over an upstream portion of the reactor and then returns downstream to the fiber lumen creating a Starling flow as modeled by other authors (Heath, Belfort, Hammer, Mirer, and Pimbley 1990; Taylor, Piret, and Bowen 1994; Patkar, Koska, Taylor, Bowen and Piret 1995; Koska, Bowen and Piret 1997). HFBRs thus provide a low-shear environment for the immobilized cells and permit months of continuous production, for example, antibodies. High-molecular-weight products can be concentrated within the ECS in an ultrafiltration HFBR.

2.2.2 Hollow-Fiber Trickle Bed (HFTB)

Trickle beds are widely employed to carry out multiphase catalytic chemical reactions. Introducing hollow fibers to catalyst bed by packing the catalyst on the shell side and having the gas flow in the fiber bore and liquid flow in the shell-side bed independently, can reduce channeling, flooding and incomplete loading in a Hollow-Fiber Trickle-Bed Reactor (Yang and Cussler 1987).

2.2.3 Integrated Bioreactor-Separator

An integrated bioreactor-separator concept was introduced by Frank and Sirkar (1985). This integrated bioreactor-separator consists of a hollow fiber fermentor with yeast immobilized on wood chips on the shell side. The substrate is introduced on the shell side containing suspended wood chips and yeast. The lumen may be supplied with air or oxygen to improve the yeast cell growth and provide O_2 supplement as well as remove

CO_2 through the fiber exit. A solvent that may wet the membrane pores can also be supplied to the hollow fiber lumen to continuously remove the ethanol and CO_2 (due to the chemical potential gradient) as well as other inhibitory end products, e.g. acetic acid, lactic acid, etc. from the broth. Chopped microporous hollow-fiber-based cell immobilization technique was established by Shukla et al. (1989) thereafter to develop a high cell density on the shell side. This process was modeled by Frank (1986) and Kang et al. (1990).

2.2.4 Packed Bed Hollow-Fiber Reactor (PBHR)

The principle of the packed bed hollow fiber reactor (PBHR) and its use for aqueous-organic two-phase biocatalysis has been described by Vaidya et al. (1993); it is similar to that of the Integrated Bioreactor-Separator discussed above. The shell side of the hollow fiber membranes was packed with microporous particles bearing enzyme. A bicontinuous system was formed with reactants, supplied through the shell and the fiber lumen, forming an interface at pore mouth on the fibers, which allowed one of the reactants and/or the products preferentially to be dissolved in either organic phase or aqueous phase. The PBHR can reduce channeling, avoid emulsification which complicates downstream separation and offer a high area of interfacial contact between the two phases. Rosell et al. (1996) used a PBHR for esterification of dodecanol and decanoic acid in hexane. Lipase from *Candida rugosa*, immobilized on microporous polypropylene particles and packed in the shell side of the reactor, was used to catalyze the reaction. Substrate solution containing the reactants was recirculated through the packed bed at a certain flow rate. Appropriate saturated salt solution was pumped through the

microporous hollow fiber bores which can remove the water generated by the reaction in the organic phase under the proper water activity gradient. Thus water activity in the organic phase could be maintained at a certain level.

2.2.5 Hollow-Fiber Adsorber (HFA)

Pan and McMinis (1992) invented a hollow-fiber adsorber (HFA) which can be applied to adsorption processes. Minute adsorber particles were held in either the shell space or the fiber bore of microporous hollow-fiber membranes, with the gas stream flowing through the other side and maintaining good contact between the gas stream and the adsorbent. Separation occurs primarily by selective adsorption on the adsorbents and not by selective permeation through the fiber wall. The HFA offers the following advantages: low pressure drop; reduction of particle attrition; choice of fine particles which reduce the intraparticle mass-transfer resistance with large specific external areas; uniform contact of gas with adsorbents, reducing channeling and adsorbent dead-spacing problems; use of fast PSA cycles to enhance the process capacity (Feng, Pan, McMinis, Ivory and Ghosh 1998; Gilleskie, Parkar and Cussler 1995).

CHAPTER 3

EXPERIMENTAL MATERIALS AND
EXPERIMENTAL METHOD DEVELOPMENT

3.1 System Selection

3.1.1 Chromatography Beads

Ion exchange chromatography separates molecules based on differences in their accessible surface charges. It can be used for any charged molecule that is soluble in aqueous systems. Ion exchange-based elution chromatography is employed in this study to demonstrate the technique because it is widely used in the separation of proteins; the relatively mild binding and elution conditions allow high protein recovery with intact biological activity. Most protein separation schemes involve one or more ion exchange steps. It plays a critical role in the purification of many proteins, antibodies, nucleic acids, and to a lesser extent peptides.

Sepharose Fast Flow ion exchangers are a good choice for separation of crude mixtures early in the purification schemes and preferred for separation of larger biomolecules (Pharmacia Biotech Catalog 1996). DEAE Sepharose Fast Flow beads from Amersham Pharmacia Biotech (Piscataway, NJ) were chosen for this study. They are weak anion exchangers based on agarose beads having an optimized highly cross-linked bead structure with a particle size range of 45-165 µm; the mean particle size is 90 µm, which provides the media greatly improved physical and chemical stability compared to Sepharose CL-6B based ion exchangers. This stability allows the gel to be used at the higher flow rates that is required for many separations as well as meeting the throughput and CIP (cleaning-in-place) requirement of process scale chromatography. Table 3.1

provides details of DEAE Sepharose Fast Flow anion exchangers selected (Pharmacia

Biotech Catalog 1996). The functional groups of the beads are shown in Figure 3.1.

Table 3.1 Details of DEAE Sepharose Fast Flow anion exchangers (Pharmacia Biotech 1996)

Available capacity	100 mg/ml for α-Lactalbumin
Particle size range (μm)	45 - 165
Approximate mean particle size (μm)	90
Bead form	Spherical, diameter 45-165 μm in wet form
Bead structure	6% cross-linked agarose
pH stability (long term)	3 - 12
pH stability (short term)	1 - 14
Chemical stability	Stable in 1 M NaOH, 70% ethanol, etc.
Physical stability	Negligible volume variation due to changes in pH or ionic strength
Max. flow rate (cm/h)	750
Max. operating pressure (psi)	42
Autoclavable	With Cl⁻ as counter ions, at 121 °C, pH 7 for 30 min
Antimicrobial agent	20% ethanol

$$C_2H_5$$
$$/$$
$$Agarose - O - CH_2CH_2N^+\text{-}H$$
$$\backslash$$
$$C_2H_5$$
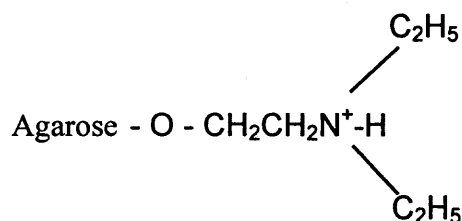
Figure 3.1 Functional group-oriented structure of DEAE (diethylaminoethyl-) Sepharose Fast Flow media

3.1.2 Membrane Module

Hollow fiber membrane cartridge used in this study was UFP-100-E-4A (A/G Technology Corporation, Needham, MA). It is an ultrafiltration membrane cartridge having a nominal membrane area 0.042 m^2; the membrane has a molecular weight cut off (MWCO) of 100,000. Table 3.2 provides details of UFP-100-E-4A cartridges (A/G Technology Corporation 1997a) used in this research.

Table 3.2 Details of the hollow fiber cartridge UFP-100-E-4A

	Length cm	O.D. cm	I.D. cm	Fiber No.	Fibers Material	Length cm	O.D. mm	I.D. mm	Pure water permeation parameter m/Pa.s
Module 1	36.20	1.90	1.524	50	Poly-sulfone	25.4	1.6	1.0	6.086×10^{-10}
Module 2	36.20	1.90	1.524	50	Poly-sulfone	25.4	1.6	1.0	1.439×10^{-9}

The fiber lumen diameter of 1.0 mm is suited for application to feeds with moderate suspended solid content and moderate viscosity. E. coli, mammalian cells, yeast cells and blood products can be treated in this cartridge. Figure 3.2 shows the cartridge configuration. Two permeate ports are on the same side. If the cartridge is installed in the system provided by the company (e.g., Quixstand^{TM} Benchtop system), standard standoffs and O-rings are available for the connections. The cartridge is autoclavable.

Two identical modules have been used in the study. Pure water permeation parameters for both modules were determined as shown in the last column of Table 3.2. The permeation fluxes are quite different with a significantly higher flux for module 2 although the modules are apparently similar. Module 1 was used for all the experiments

with protein mixtures in clean feeds. Module 2 was used for experiments with a simulated yeast-based broth.
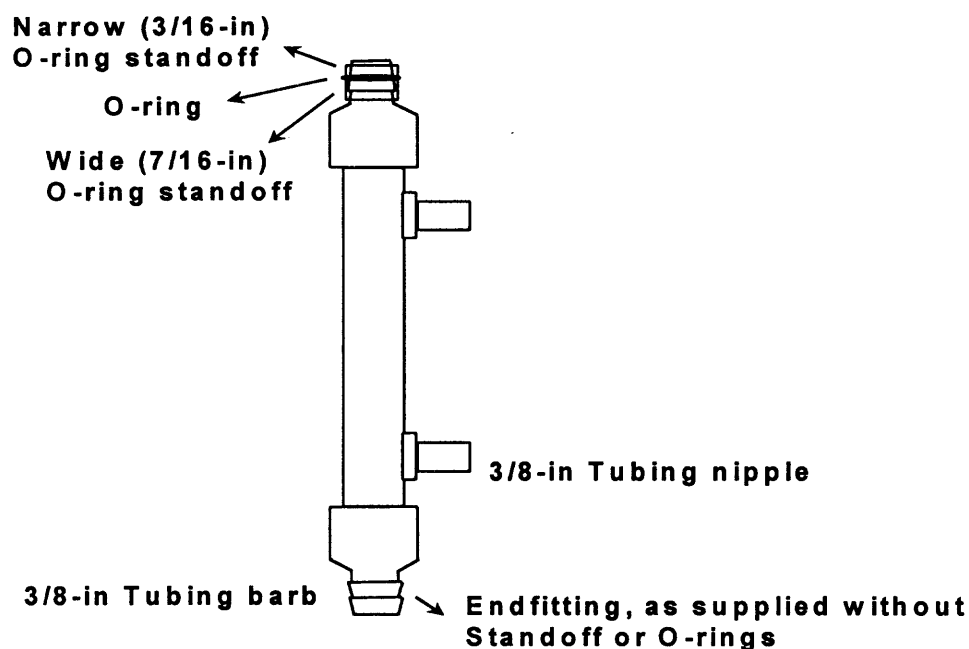
Figure 3.2 Configuration of the hollow fiber cartridge UFP-100-E-4A

3.1.3 Model Proteins

Hemoglobin (Hb, MW 64677 (Dickerson and Geis 1969), Lot 16H9315), bovine serum albumin (BSA, MW 66430 (Hirayama, Akashi, Furuya and Fukuhara 1990), Lot 99F00191), myoglobin (Mb, MW 17566 (Darbre, Romero-Herrera and Lehmann 1975), Lot 96H7035), β-lactoglobulin (β-LG, MW 35500 (Townend, Weinberger and Timasheff 1960), Lot 100H8185) and α-lactalbumin (α-LA, MW 14175 (Vanaman, Brew and Hill 1970), Lot 76H7130 and Lot 98H7003) were chosen as model proteins and purchased from Sigma (St. Louis, MO). These proteins were selected due to their differences in pI values. The pI values for Hb, BSA, Mb, β-LG and α-LA are respectively 6.8 (Lehninger

1975), 4.7 (Longsworth and Jacobsen 1949), 7.3 (Radola 1973), 5.3 (Kaplan and Foster 1971) and 4.2-4.5 (Kronman and Andreotti 1964).

3.1.4 Other Materials and Instruments

All other chemicals and materials were obtained commercially and were of the highest available quality. Tris-HCl (20 mM) at pH 8.5 was used as the starting buffer unless otherwise specified. All protein solutions were prepared using the starting buffer. Elution buffers were prepared by adding different amounts of NaCl to the starting buffer.

For the simulated broth, the yeast strain (NRRLY-12636), *Saccharomyces cerevisiae*, was purchased from the United States Department of Agriculture (Peoria, IL). For YM medium broth, yeast extract, malt extract, peptone and glucose were obtained from Sigma (St. Louis, MO). A G24 Environmental Incubator Shaker (New Brunswick Scientific Co., Inc., Edison, NJ) was used for the yeast cell culture and batch protein adsorption experiments.

A model U-2000 (Hitachi, Danbury, CT) UV-vis spectrophotometer was used to measure the protein concentration and the optical density of yeast suspension. Quartz cuvets (S-10C) (Sigma, St. Louis, MO) having a 10 mm path length were used in the spectrophotometer. The pumps used in filtration, washing, elution, regeneration and cleaning were Masterflex Model 7518-60 and Model 7518-10 (Cole Parmer, Chicago, IL). An IEC Clinical Centrifuge (International Equipment Co., Needham HTS, MA) was used to centrifuge all the samples wherever needed.

3.2 Experimental Methods

3.2.1 Pretreatment of the New Cartridges

Ultrafiltration (UF) membrane cartridges purchased from the company were supplied pretreated with a glycerol solution within the pore structure to prevent drying of the membrane. This solution must be thoroughly rinsed from the cartridge prior to use (A/G Technology Corporation 1997b). To enhance glycerol removal and maximize initial water flux, the cartridge was soaked in a 50:50 by volume mixture of ethanol : water overnight to replace the air in the module. Then the module was rinsed with clean water according to New Cartridge Rinsing Procedure recommended by the company to remove the alcohol.

New Cartridge Rinsing Procedure:

(1) Rinse with clean warm (up to 50°C) water for 90 minutes, adjust the permeate flow rate to around 20 ml/min and retentate flow rate to about 2 ml/min.

(2) Discharge both retentate and permeate to drain.

3.2.2 Cleaning of the Cartridges

Cleaning was performed at 5 psi tube-side outlet pressure and temperature of 40 - 50°C. Soaking the membrane overnight improves the effectiveness of the cleaning cycle. For protein products either in clean feed or in whole broth, 0.5 M NaOH is recommended as the cleaning agent. The procedure recommended is as follows:

(1) Flush with clean water, buffer or saline solution at 40 - 50°C.

(2) Circulate 0.5 M NaOH at 50°C for 30-60 min.

(3) Flush with clean water.

Up to 0.5 M NaOH circulated for 30-60 minutes or up to 70% ethanol in water could be used for sanitization of the cartridges.

3.2.3 Storage of the Cartridges

UF cartridge must be stored wet. For short-term storage up to 2 weeks, only water wetting is used after proper cleaning. For long term storage up to 1 month, 0.1 M NaOH or 30% ethanol in water are used. For storage longer than 1 month, the membrane should be periodically checked to be certain that it remains wetted.

3.2.4 Preparation, Regeneration and Cleaning of the Chromatographic Resin

DEAE Sepharose Fast Flow ion exchange media were supplied preswollen in 20% ethanol prior to use. The ethanol solution was decanted. The beads were washed and equilibrated with the starting buffer.

Regeneration was normally performed by washing the column with a high ionic strength buffer followed by re-equilibrating in starting buffer. A solution of 1.0 - 2.0 M NaCl was used in all experiments for regeneration. The UV absorbance was monitored to determine if bound substances have been completely washed out.

For cleaning-in-place (CIP) to remove ionically bound proteins, precipitated proteins, hydrophobically bound proteins and lipoproteins, and strongly hydrophobically bound proteins, lipoproteins and lipids respectively, 2.0 M NaCl, 1.0 M NaOH and 70% ethanol can be used. A solution containing 0.5-1.0 M NaOH is good for sanitization. The same solution was used in all the experiments for cleaning of the beads whenever needed in this study. After the CIP, the beads were equilibrated with the starting buffer before use.

3.2.5 Packing the Shell Side of the UF Cartridge

Packing beads on the shell side was the first critical step in this experimental research. Unlike the bead packing technique in traditional chromatography, no standard procedures can be followed and no standard devices can be adopted. Column packing technique for DEAE Sepharose Fast Flow beads suggested by the company is shown in Figure 3.3 (Amersham Pharmacia Biotech: Instruction for Fast Flow Media).

The packing method developed in this study is shown in Figure 3.4. The ethanol solution from the bottle containing the beads was decanted. The beads were washed and equilibrated with the starting buffer. The membrane cartridge was cleaned and soaked in the starting buffer before packing. The dilute bead suspension was pumped from the shell-side inlet while the shell-side outlet was blocked by a 21 μm polyester mesh (Spectrum, Houston, TX) to hold the beads and let the buffer pass through. This packing was continued until the shell side was full of beads. The beads were equilibrated with the starting buffer. The tube-side openings were kept closed during this operation. The device is shown in Figure 2.1a. This resulted in 20 ml and 20.5 ml DEAE Sepharose Fast Flow anion exchange beads packed in module 1 and module 2 respectively. The experimental setup for all filtration-cum-loading as well as elution steps is shown in Figure 3.5.
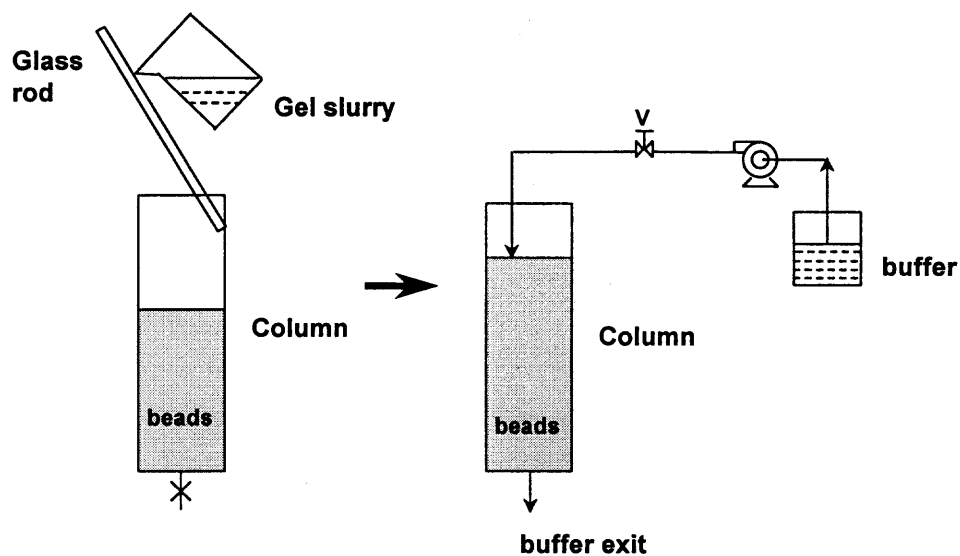
Figure 3.3 Schematic for column packing suggested by Amersham Pharmacia Biotech
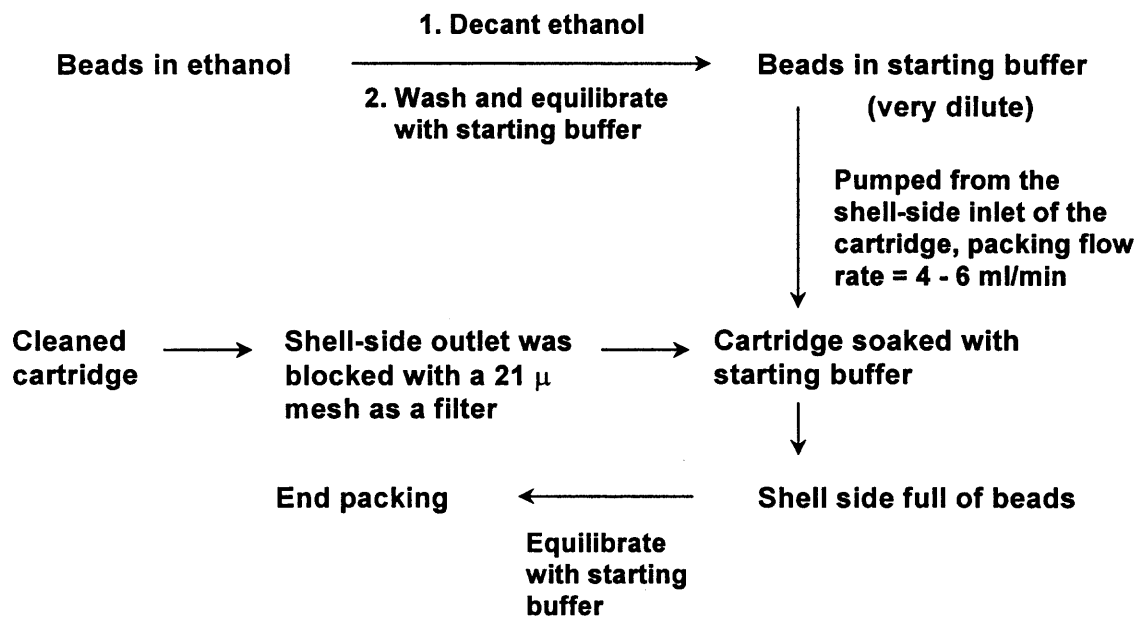
Figure 3.4 Method used for packing the beads on shell side of the HF cartridge

V: Valve
PG: Pressure Gauge
TWV: Three Way Valve
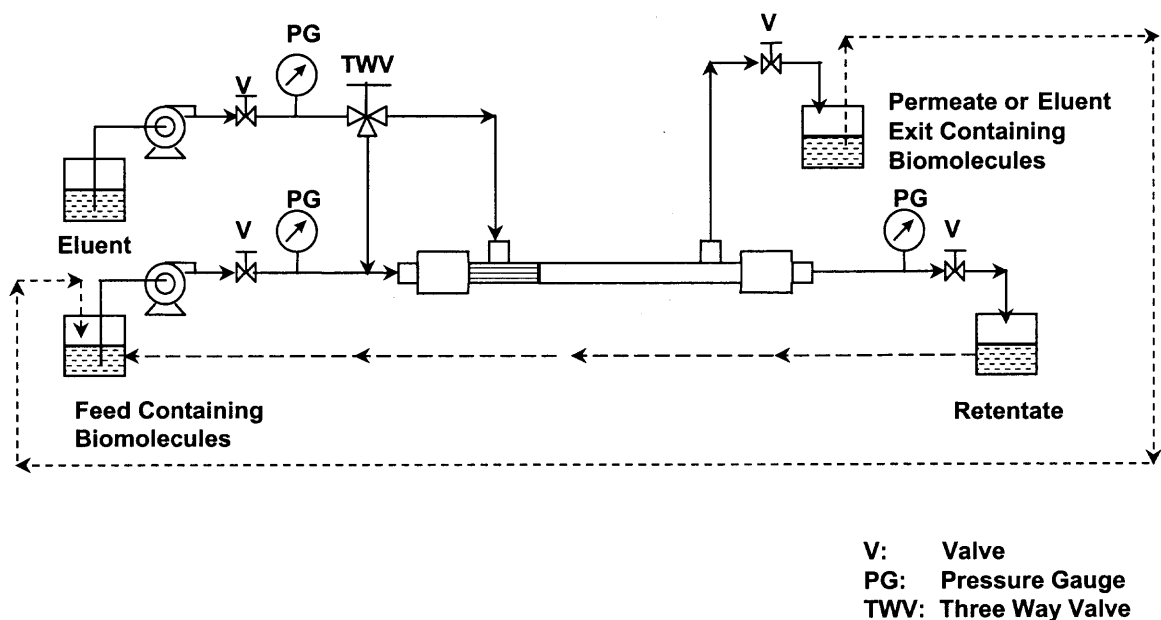
Figure 3.5 Schematic of the apparatus for hollow-fiber membrane-based filtration-loading-chromatography process

To check if the packed resin bed was functioning as a chromatographic column, 1.0 ml binary protein mixture (e.g., Mb and β-LG; BSA and Hb) was loaded onto the bed from the shell-side inlet in initial experiments. The elution was then conducted with a stepwise change of NaCl concentration in the starting buffer from shell-side inlet (shell-side elution). Fractions were collected and assayed for the protein concentrations.

3.2.6 Development of the Cleaning Protocol for the Integrated Device

Cleaning protocols need to be developed for the integrated device by combining the protocols for membrane and chromatography beads. Conditions selected must be effective for both parts without any harm to the membrane and the chromatography beads.

3.2.6.1 Use of NaOH: Alkalis are effective cleaning agents for many biological/organic foulants. They work by mechanisms including neutralization of acidic materials (e.g. fatty acids and humic acids), saponification (hydrolysis) of fat and oil, and dispersion/emulsification of colloidal material. Caustic soda (NaOH) is the simplest alkaline cleaner. It is a very effective saponification agent, and it is one of the most alkaline of different alkali cleaners due to its complete dissociation into Na^+ and OH^- (Zeman and Zydney 1996a).

The membrane in the UF hollow fiber membrane cartridge (A/G Technology) is made of polysulfone having a MWCO of 100,000. In their operating guide (A/G Technology Corporation 1997b), the manufacturer recommends customers use 0.5 M NaOH at 40-50°C to clean the membranes in the processes of cell culture, fermentation broth, enzymes, juice clarification and protein products, etc. The shear rate is 4000-8000 sec^{-1} with about 5 psi transmembrane pressure. Also, 0.5 M NaOH can be used for sanitization of the cartridge. A concentration of 0.1 M is recommended for use for storage (up to 1 month) of the UF cartridges.

Coincidentally, sodium hydroxide is widely accepted for cleaning, sanitizing and storing chromatography media and systems because of its efficacy, low cost and ease of detection, removal and disposal. NaOH has been shown to be effective in removing proteins and nucleic acid from chromatography media. It can saponify fats and dissolve precipitated proteins. It also has the ability to inactivate several viruses, bacteria, yeasts and molds (Amersham Pharmacia Biotech 1998).

For the DEAE Sepharose Fast Flow beads bought from Pharmacia Biotech, a high ionic strength buffer (e.g. starting buffer containing 1.0 - 2.0 M NaCl) is used as the

regeneration solution. But some denatured proteins or lipids may not be eluted in the regeneration procedure. NaOH can be used to remove precipitated proteins, hydrophobically bound proteins and lipoproteins (Amersham Pharmacia Biotech: Instructions for Fast Flow Media).

3.2.6.2 Developing a Protocol for Cleaning of the Integrated Device: Membrane cleaning is an essential component of nearly all membrane processes. All membranes will foul during operation, causing the membrane performance (flux and/or selectivity) to decline with time even if other operating conditions and fluid properties remain constant (Zeman and Zydney 1996b).

Traditionally, the indicator for most of the membrane cleaning process is the recovery of the permeate flux, say, the pure water flux after the cleaning will go up to 90-100% of the original level (Sirkar and Prasad 1986). But sometimes the flux is not very sensitive to gel layer formation or membrane fouling, especially when very dilute feeds with smaller molecule products are treated (e.g. in some ultrafiltration application), unless the process runs a reasonably long time. This is also valid for the case (no matter what feeds have been treated) when the membrane is not completely cleaned but the permeate flux seemed to have been recovered on the basis of the clean water flux.

For the integrated membrane-based chromatography device of this study, the situation is more complicated. The flux is generally lower compared to that from the membrane itself under the similar conditions. This makes the traditional indicator for membrane cleaning even more insensitive. Moreover, it was found that after performing the cleaning protocol shown in Figure 3.6, water fluxes went back to the original level;

but for some of the batches, there was still some absorbance reading at 280 nm by spectrophotometer for the fractions taken from the blank elution with 1.0 M NaCl after cleaning.

Soak the column with 0.5 M NaOH overnight

↓

Flush with DI water at 45-50 ºC

↓

Clean the cartridge with 0.5 M NaOH at 45-50ºC

↓

Rinse with DI water at 45 - 50ºC

↓

Equilibrate the column with starting buffer

↓

Reuse or Store the cartridge at 4ºC
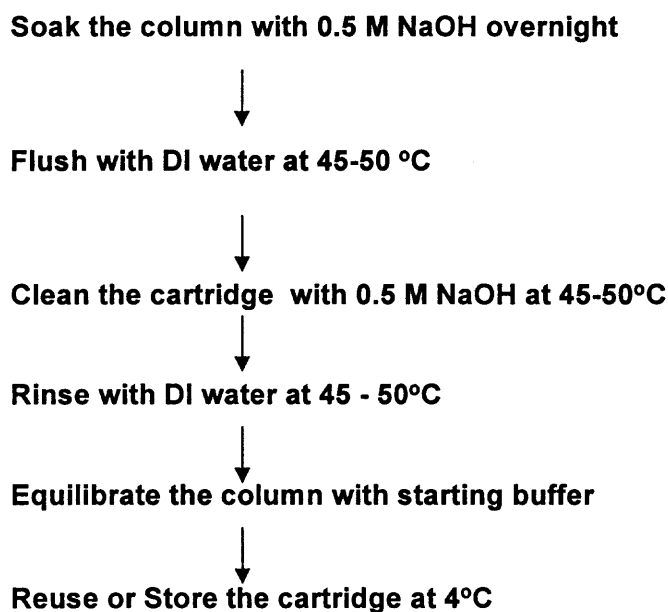
Figure 3.6 Initial cleaning method based on membrane and beads cleaning protocols

One difference in the protocols between traditional membrane cleaning methods and the integrated device cleaning method is that we could not use very high permeate flux. This high flux wash in the membrane cleaning cycle can flush a lot of fouling residuals (produced by the cleaning agent in chemical cleaning method) out of the membrane. Further, the influence of the chromatographic beads packed on the shell side needs to be considered as well. In this study, DEAE-Sepharose Fast Flow beads were used. This kind of beads can adsorb molecules with negative charges. The polysulfone

membrane has a pI value of 3.6 (Zeman and Zydney 1996, Bellara, Cui and Pepper 1997); it adsorbs positively charged molecules in the NaOH cleaning process, e.g., water rinse step if there are still some impurities left in the column. In this case, no matter what is left after the treatment with NaOH, both charged molecules are to be adsorbed in the cartridge and the high permeate flux could not be used to flush the dissolved and decomposed molecules out.

One solution proposed here is to "regenerate" the device with 1.0 - 2.0 M NaCl after the NaOH treatment in the cleaning cycle - blank elution. The improved cleaning protocol is shown in Figure 3.7. In this way, both charged, dissolved and decomposed molecules can be made to flow out of the cartridge. In order to ensure the full cleaning of the device, NaOH can be used to treat the membrane again after "regeneration" (or blank elution) until no absorbance at 280 nm (or say, no "ghost" peak) is detected during the next blank elution step. Reasonably low absorbance could also be the criterion for the cleaning based on the time and solution consumptions.

Soak the column with 0.5 M NaOH overnight

↓

Flush with DI water at 45-50 °C

↓

**Clean the cartridge with 0.5 M NaOH and
0.5 M NaCl at 45-50°C**

↓

Rinse with DI water at 45 - 50°C

NO

↓

**Blank elution of the bed with 1.0 M NaCl
in starting buffer until no absorbance
at 280nm**

↓

ABS @ 280 nm at
beginning=0 or low

YES

↓

Equilibrate the column with starting buffer

↓

Reuse or Store the cartridge at 4°C
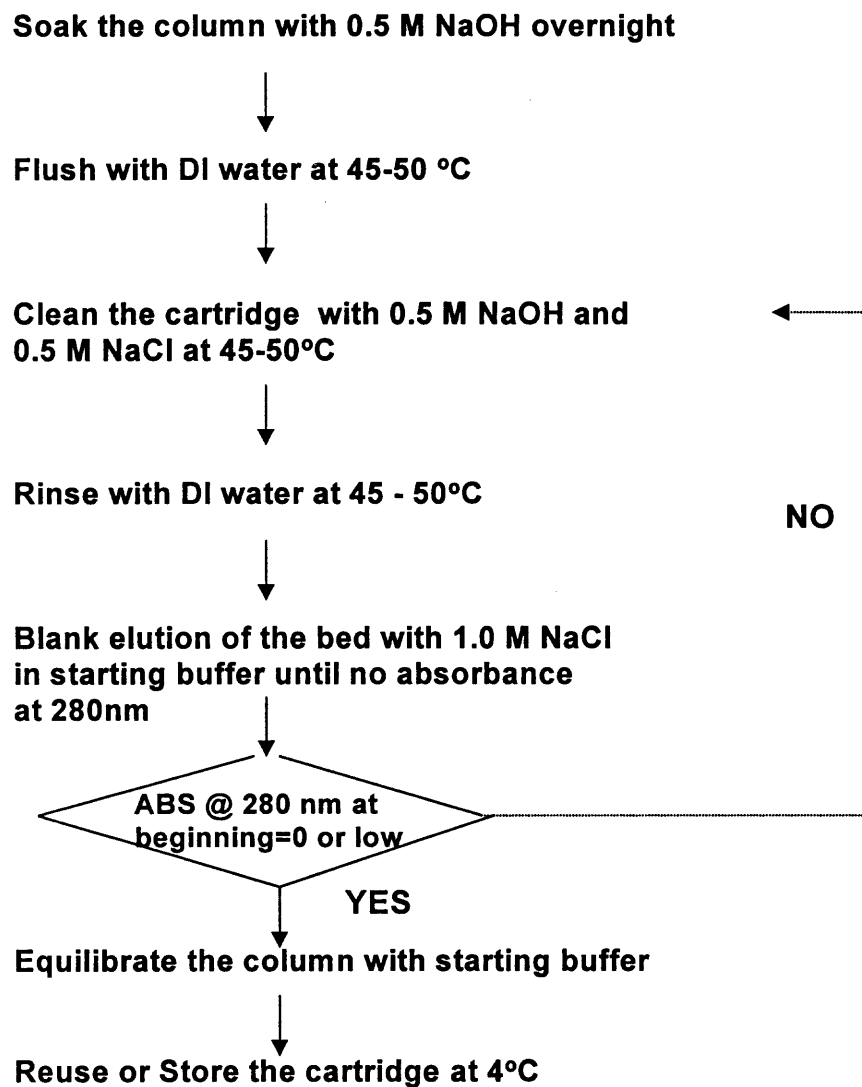
Figure 3.7 Cleaning protocol developed for the integrated device

3.2.7 Experimental Methods

3.2.7.1 One Cycle Experiment: For one-cycle-based filtration-cum-loading-cum-chromatography experiments of interest, 100 - 400 ml solution of either one protein or a protein mixture was directly loaded from the tube-side inlet; the permeate and the retentate could be recycled if necessary (Figure 3.5). The tube-side pressure was higher than that of the shell side to maintain a certain transmembrane pressure. Elution was carried out as shown in Figure 3.5 either from the shell side (corresponding to Figure 2.1b) or from the tube side (corresponding to Figure 2.1c) with NaCl in the starting buffer, using either isocratic or stepwise fashion. Fractions were collected and assayed for the protein concentrations. The whole cartridge was cleaned according to the cleaning protocol shown in Figure 3.7.

3.2.7.2 Cyclic Process: For cyclic processes where many cycles were run continuously without the NaOH-based module cleaning, there were three types of experiments. First, a cyclic process was carried out using a clean feed (i.e., without cells) containing myoglobin in module 1. 250 ml (0.027-0.029 mg/ml) of myoglobin solution was directly loaded from the tube-side inlet for 12 min at a flow rate of about 200 ml/min under an average transmembrane pressure* of 2.4 psi; the retentate was recycled (Figure 3.5). Tube-side elution was carried out with 0.5 M NaCl in 20 mM Tris-HCl (pH 8.5) at a flow rate of 2.2-2.5 ml/min. Fractions were collected every 2.5 minutes and assayed for the protein concentration. Displacement of the eluent was conducted after elution with

---

* Average transmembrane pressure in this dissertation = sum of TMP @ the beginning of the module length and TMP @ the end of the module length divided by 2.

starting buffer to take eluent out of the bed by using tube-side elution operation mode for 4-5 bed volumes followed by using shell-side elution operation mode for the same volume of buffer. A new cycle was then carried out after the displacement of the eluent with the starting buffer. In this manner as many cycles as necessary were conducted. After the experiment was over, the whole cartridge was cleaned by using the cleaning protocol shown in Figure 3.7.

In the second type of cyclic process, a binary protein mixture was employed. 150 ml (0.029-0.034 mg/ml) of a protein mixture solution was directly loaded from the tube-side inlet of module 1 for 10 min at a flow rate of about 200 ml/min under an average transmembrane pressure of 3.1 psi; the retentate was recycled (Figure 3.5). Tube-side elution was carried out with 0.05 M NaCl in 20 mM Tris-HCl (pH 8.5) for 55 minutes followed by 1.0 M NaCl for 45 minutes at a flow rate of 2.3-2.6 ml/min. After fractions were collected every 2.5 minutes and assayed for the protein concentrations, the device was treated following the same protocols mentioned earlier for a multi-cycle process for a single protein and it was continued for many cycles. After the experiment, the whole cartridge was cleaned by the same cleaning protocol previously mentioned (Figure 3.7).

In the third type of cyclic process, a yeast suspension was employed to simulate a fermentation broth. One loopful of cells was transferred from agar slope into 50-60 ml YM medium broth, which was prepared by dissolving 3 g yeast extract, 3 g malt extract, 5 g peptone and 10 g glucose in 1L water, autoclaving glucose solution and other ingredients in solution separately, and then mixing them before use. Cells were cultured for 20–24 hours until the optical density at 540 nm was in the range of 2.080-2.495. Cells were washed 3 times with water by centrifuging at 3000g for 3 minutes each time before

being diluted to 200 ml in the starting buffer. Then 0.038–0.043 mg/ml Mb and 0.037-0.042 mg/ml α-LA were added to the yeast suspension. For this suspension, the optical density reading at 540 nm was in the range from 1.264 to 1.400, corresponding to a cell concentration about 0.5 g/L (Kang 1989).

The above yeast–based synthetic broth was directly loaded from the tube-side inlet of module 2 for 12 min at a flow rate of about 200 ml/min under an average transmembrane pressure of 3.0 psi as the retentate was recycled. Tube-side elution was carried out with 0.05 M NaCl in 20 mM Tris-HCl (pH 8.5) for 45 minutes followed by 0.5 M NaCl for 55 minutes with an average flow rate of 2.5 ml/min. Fractions were collected every 2.5 minutes and assayed for the protein concentrations. The bed could be then regenerated by using 1.0 M NaCl in starting buffer for 4-5 bed volumes in tube-side elution operation mode if necessary. Displacement of the eluent was conducted after elution or regeneration with the starting buffer to remove the remaining cells and eluent out of the system by shell-side back flushing for 4-5 bed volumes (through the tube-side outlet), tube-side flushing for 2-4 bed volumes (shell-side and tube-side outlets open), followed by tube-side elution operation mode flushing for 4-5 bed volumes. A new cycle of operation was then carried out after reequilibration with the starting buffer. When the cyclic process was over after multiple cycles, the cartridge was cleaned and stored following the protocol shown in Figure 3.7.

3.2.7.3 One Cycle-Based Experiments with the Additional Extended Section on the Permeate Outlet: As stated in Chapter 2, to ensure the separation effect in the shell-side bed, an additional amount of resin beads was packed at the permeate outlet port on the

shell side. These resin particles used as an extended section (ES) of the bed were kept in place by the 21μ polyester mesh. There was a fixed ES on the permeate outlet on the module; for some of the experiments, an additional ES bed was packed over the fixed ES for module 1. The dimensions of the ES beds are shown in Table 3.3.

Table 3.3 Dimensions of the extended sections on the permeate outlets

	I.D. of the ES cm	Length of the ES cm	Percentage of beads in the ES[*]
Fixed ES for both modules	0.7	1.7	3.27
Additional ES for module 1	0.85	2.3	6.12
Fixed ES + Additional ES for module 1			9.20

[*]Based on total volume of beads packed on the shell-side bed and the ES bed.

The experimental method is similar to that in section 3.2.7.1, namely, "One cycle experiment" for a clean feed solution.

3.2.8 Measurement of Protein Concentrations

The concentrations of Hb, Mb, BSA, β-LG and α-LA were determined by measuring the absorbance at 430 nm (or 410 nm) and 280 nm. Standard calibration curves for various proteins are provided in Equations 3.1-3.7.

(1) Hemoglobin:

@ 280 nm: $Concentration(\mu g / ml) = 382.7 \times absorbance - 0.162$ (3.1)

Linear range: 0 – 200 μg/ml.

@ 430 nm: $Concentration(\mu g / ml) = 231.5 \times absorbance - 0.164$ $\qquad$ (3.2)

Linear range: $0 - 100$ µg/ml.

(2) Myoglobin:

@ 280 nm: $Concentration(\mu g / ml) = 620.0 \times absorbance - 0.176$ $\qquad$ (3.3)

Linear range: $0 - 1000$ µg/ml.

@ 410 nm: $Concentration(\mu g / ml) = 135.3 \times absorbance + 0.155$ $\qquad$ (3.4)

Linear range: $0 - 220$ µg/ml.

(3) BSA @ 280 nm: $Concentration(\mu g / ml) = 1253.0 \times absorbance - 3.396$ $\qquad$ (3.5)

Linear range: $0 - 600$ µg/ml.

(4) β-LG @ 280 nm: $Concentration(\mu g / ml) = 1222.0 \times absorbance - 3.25$ $\qquad$ (3.6)

Linear range: $0 - 1000$ µg/ml.

(5) α-LA @ 280 nm: $Concentration(\mu g / ml) = 514.8 \times absorbance - 0.556$ $\qquad$ (3.7)

Linear range: $0 - 550$ µg/ml.

In a binary protein mixture, concentrations of Hb and Mb were directly measured at 430 nm and 410 nm using their standard curves. The concentrations of BSA, β-LG and α-LA in a binary protein mixture were obtained using the method of Sokol, Hána and Albrecht (1961) by subtracting the corresponding 280 nm absorbances of Hb and Mb (calculated with their standard curves at 280 nm from their concentrations obtained at 430 nm and 410 nm) from the absorbance of the mixture (e.g., a mixture of Hb and BSA and a mixture of Mb and α-LA) at 280 nm. Sample calculations are illustrated in Figure 3.8.

This method is based on the assumption that the absorption coefficient of each protein in the mixture does not change, which is very close to reality especially when the protein concentration is low. For proteins in the study in a cellular suspension, the absorbances of protein fractions were measured at 280 nm.

Experimentally determine ABS at 280 nm and 410 nm	1. Absorbance of a binary mixture of Mb and α-LA @ 280 nm = A_{280T} 2. Absorbance of a binary mixture of Mb and α-LA @ 410 nm = A_{410T} =A_{410Mb} (α-LA has no absorbance @ 410 nm)

Four steps used for calculations to get protein concentrations	1. Concentration of Mb = 135.3 × A_{410Mb} +0.155 = C_{Mb} (eq 3.4) 2. The corresponding Mb absorbance @ 280nm A_{280Mb} =(C_{Mb}+0.176)/ 620.0 (eq 3.3) 3. Absorbance of α-LA @ 280 nm A_{280LA} = A_{280T} - A_{280Mb} 4. Concentration of α-LA = 514.8 × A_{280LA} -0.556 = C_{LA} (eq 3.7)

Figure 3.8 Schematic of the calculation method for determining protein concentrations in a binary mixture of Mb and α-LA

3.2.9 Adsorption Equilibrium

Equilibrium adsorption is a classical technique for characterizing the interactions involved in adsorption. The equilibrium adsorption studies were carried out in a manner similar to the procedure described by Chase (1984), Boyer (1991) and Noriega et al. (1997) but modified to correspond to the present situation. Known volumes of the adsorbent were prepared by allowing a suspension of the adsorbent to settle in a graduated cylinder for 48 hours. The operating systems were prepared by adjusting the buffer volume to that of the settled adsorbent to obtain a 75:25 (v/v) suspension.

Adsorption equilibrium studies were carried out in the G24 Environmental Incubator Shaker (New Brunswick Scientific Co., Inc, Edison, NJ) at room temperature. 1.0 – 2.0 ml of a 75:25 (v/v) suspension was added to flasks containing various amounts of protein of interest with or without certain concentrations of NaCl in 20 mM Tris-HCl buffer, pH 8.5, in a final volume of 50 ml. The flasks were shaken at 200 rpm in the Shaker. Samples (2.5 ml) were removed and centrifuged (4000-5000g, 1-1.5 min) and the supernatants were assayed for protein concentrations at 280 nm. Each adsorption experiment was carried out until no appreciable change was observed.

CHAPTER 4

RESULTS AND DISCUSSIONS

Experimental results will be presented and discussed in this Chapter. First, conditions for eluting a single protein using the shell-side packed bed of this system (Figure 3.5) will be addressed for the basis of separation for binary protein mixtures. Then the results of experiments for the separation of binary protein mixtures on the shell-side bed will be discussed. These results could be used as tests for the performance of the shell-side packed bed as a chromatographic column. Next, the results of tube-side filtration-based experiments using clean feed solutions will be presented in two categories: shell-side elution (according to Figure 2.1b) and tube-side elution (according to Figure 2.1c). These experiments will be illustrated using a binary protein mixture in a clean solution for one cycle of loading-and-elution. In the type of experiments that follows, a similar experiment will be carried out continuously for many cycles using a clean feed solution for a single protein and then for a protein mixture. Then, in the next series of experiments, a yeast-based simulated fermentation broth is employed, a synthetic protein mixture is added to this broth, the solution is filtered and the proteins are separated by elution chromatography. This cyclic process is carried out repeatedly using the simulated feed broth to explore the behavior of the integrated device and process. The effects of the extended section on the permeate port of the shell side will be discussed thereafter. The results of the adsorption isotherms from batch experiments will be presented at the end of this Chapter.

4.1 Preliminary Investigation of the Experimental Methods

Several proteins were used as model proteins for this study. Initial experiments were carried out using a single protein in a clean feed solution in order to find out the buffer conditions for the elution of these proteins. Shell-side inlet loading was employed in most of the initial experiments unless otherwise mentioned. Binary mixtures of model proteins were utilized thereafter to check if the shell-side bed was performing as a chromatographic column. Beads were positively charged, and the model proteins were negatively charged at the buffer pH of 8.0 or 8.5 in all experiments presented in this Chapter.

4.1.1 Myoglobin

The first experiment was carried out by loading about 0.45 ml of a 1.0 mg/ml myoglobin (Mb) sample on the shell-side bed from the shell-side inlet. Elution was performed by pumping 0.025 M NaCl in the starting buffer (pH 8.0) at a flow rate of 1.60 ml/min. Fractions were taken every 3 min for the assay of Mb concentrations. Figure 4.1 shows the result. Over 90 % of the Mb was recovered[*].

The second experiment was performed in a similar manner. About 0.80 ml of a 1.0 mg/ml Mb sample was loaded on the shell-side bed from the shell-side inlet. Elution was performed by a stepwise change of NaCl in the starting buffer (pH 8.0) at a flow rate of 1.61 ml/min: (1) 0.05 M NaCl for 60 minutes, (2) 0.1 M NaCl for 30 minutes and (3) 0.5 M NaCl for 40 minutes. Fractions were taken every 3 min for the assay of Mb concentrations. Figure 4.2 shows the elution profile. About 93.0 % of the Mb was eluted

---

[*] Recovered protein % was calculated by the sum of protein amount in each fraction (concentration × volume in each fraction) divided by the total amount of protein loaded.

out during first 60 minutes elution, 3.0 % of Mb was eluted out in the 2nd step elution and

2.0 % was recovered in the last elution step. The total protein recovered in the three steps

was about 99.0 % of the protein in the feed.

From these two experiments, it became clear that an ionic strength of 0.025 or

0.05 M NaCl in the starting buffer is strong enough for the elution of Mb out of the shell-

side bed in this device.
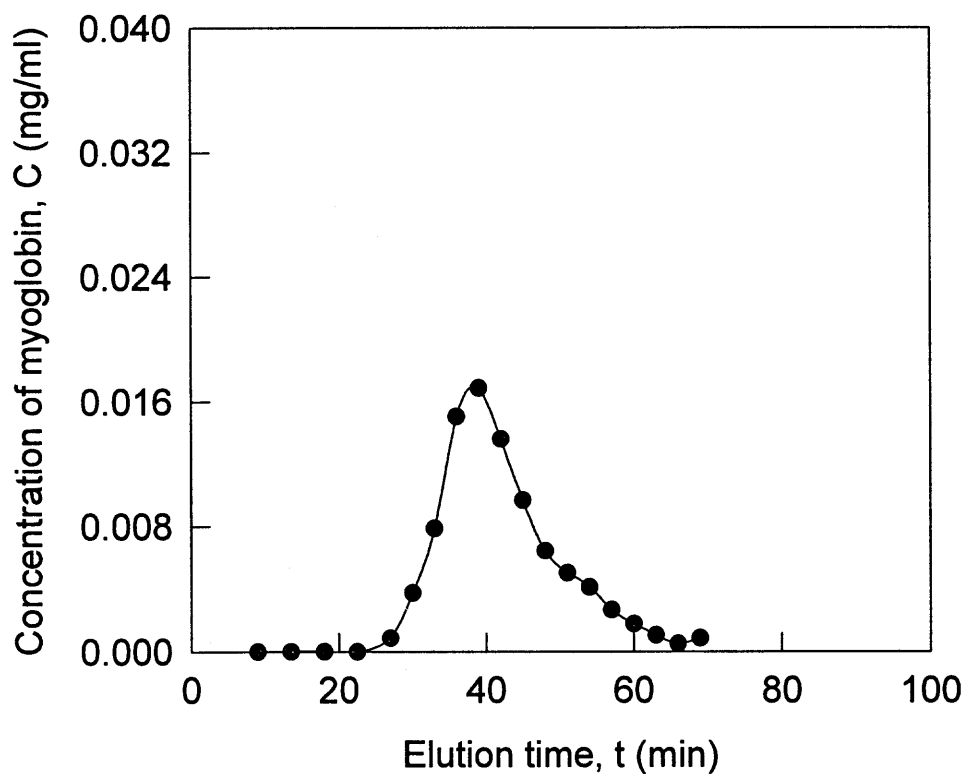
Figure 4.1 Shell-side elution for Mb with 0.025 M NaCl in the starting buffer (pH 8.0)
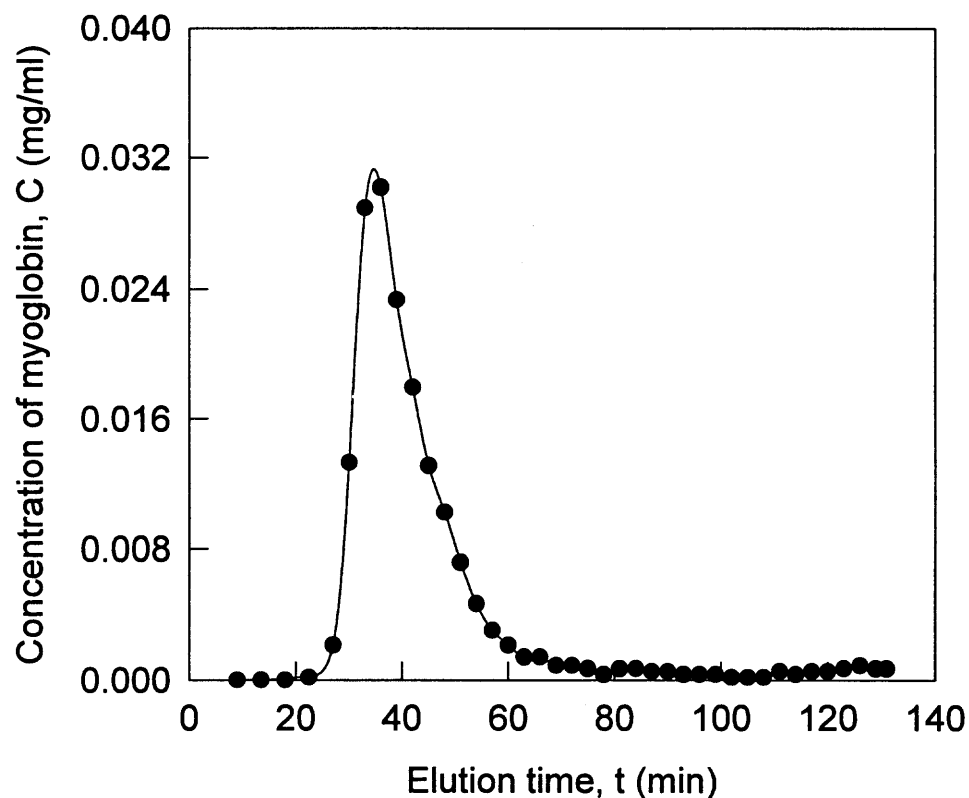
Figure 4.2 Shell-side elution for Mb with a 3 stepwise changes of NaCl concentration in the starting buffer (pH 8.0)

4.1.2 β-Lactoglobulin

About 0.20 ml of a 2.40 mg/ml β-lactoglobulin (β-LG) solution was loaded on the shell-side bed from the shell-side inlet. Elution was performed by a stepwise change of NaCl in the starting buffer (pH 8.0) at a flow rate of 1.74 ml/min: (1) 0.05 M NaCl for 54 minutes; (2) 0.5 M NaCl for 50 minutes. Fractions were taken every 4.5 min for the assay of β-LG concentrations. Figure 4.3 shows the protein concentration profile. It can be seen that 0.05 M NaCl is not effective for elution of β-LG.
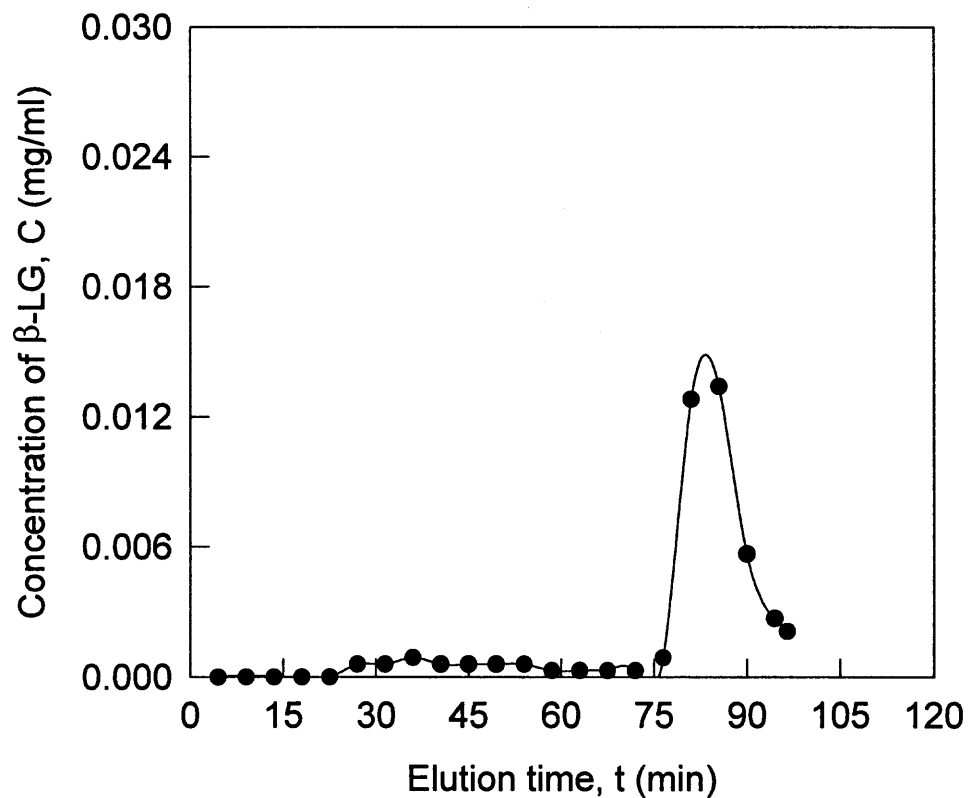
Figure 4.3 Shell-side elution for β-LG with a stepwise change of NaCl concentration in the starting buffer (pH 8.0)

The second experiment was carried out by loading about 0.20 ml of a 2.40 mg/ml

β-LG solution on the shell-side bed from the shell-side inlet. Elution was performed by a

stepwise change of NaCl in the starting buffer (pH 8.0) at a flow rate of 1.78 ml/min: (1)

0.1 M NaCl for 60 minutes; (2) 0.5 M NaCl for the next 48 minutes. Fractions were taken

every 4.5 min for the assay of β-LG concentrations. Figure 4.4 illustrates the protein

concentration profile during elution; the profile indicates that 0.1 M NaCl can only elute

part of the β-LG out of the bed.
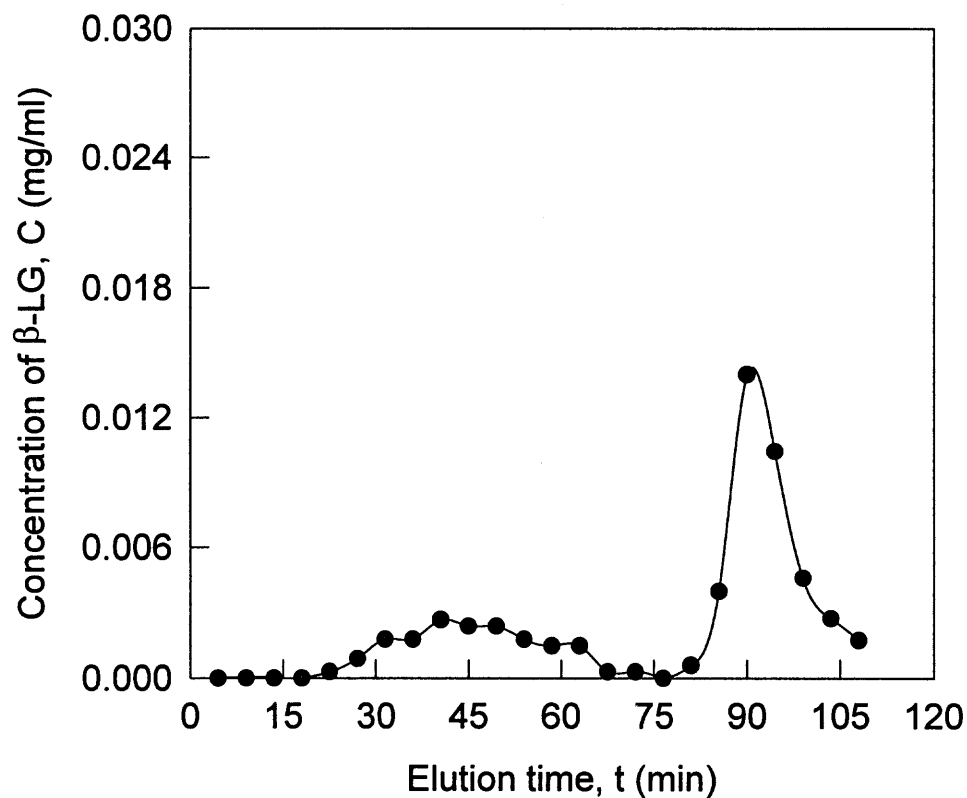
Figure 4.4 Shell-side elution for β-LG with a stepwise change of NaCl concentration in the starting buffer (pH 8.0)

A similar experiment was carried out at pH 8.5 by loading about 0.50 ml of a 1.2 mg/ml β-LG sample on the shell-side bed from the shell-side inlet. Elution was performed by a stepwise change of NaCl in the starting buffer (pH 8.5) at a flow rate of 1.89 ml/min: (1) 0.05 M NaCl for 60 minutes; (2) 0.5 M NaCl for the next 44 minutes. Fractions were taken every 3.0 min for the assay of β-LG concentrations. Figure 4.5 shows the protein concentration profile during elution. It can be seen that 0.5 M NaCl can elute β-LG out of the bed at pH 8.5.
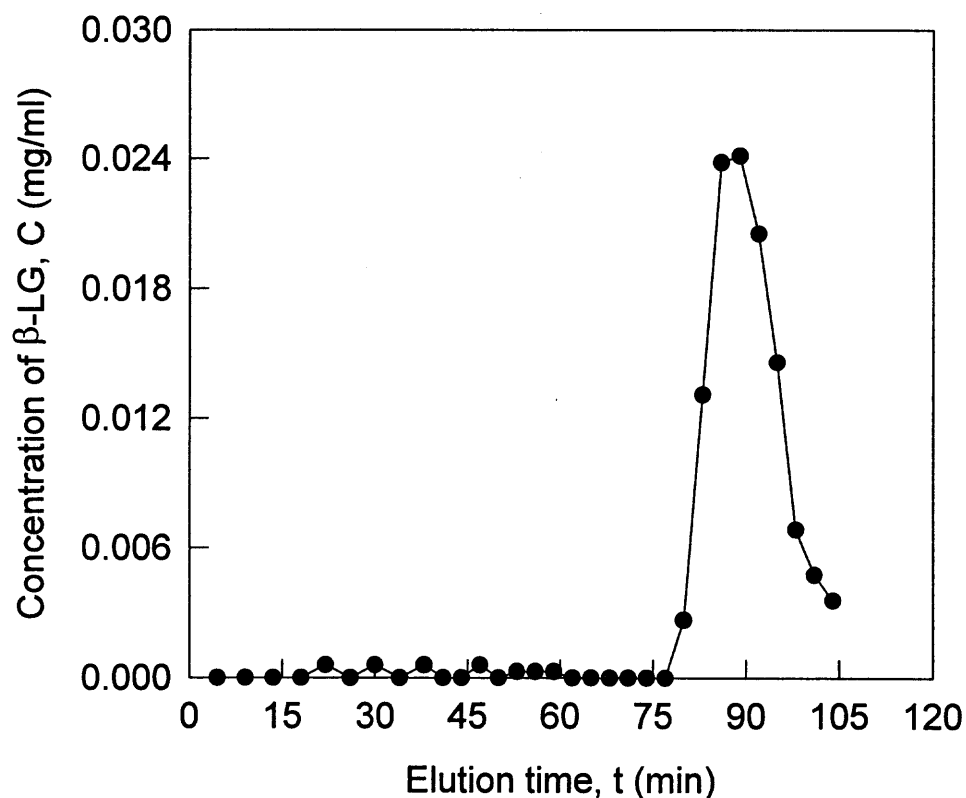
Figure 4.5 Shell-side elution for β-LG with a stepwise change of NaCl concentration in the starting buffer (pH 8.5)

Tube-side loading of β-LG onto the shell-side bed was carried by pumping 300 ml of a 44.3 µg/ml β-LG solution in the starting buffer (pH 8.0) through the hollow fiber lumen at an average TMP about 2.5 psi. Since the molecular weight of β-LG is smaller than the molecular weight cut off (MWCO) of the membrane, β-LG can partially pass through the pores of the membrane under the TMP and get adsorbed onto the beads at pH 8.0. Shell-side elution was implemented using 0.5 M NaCl in the starting buffer at a flow rate of 2.1 ml/min. Figure 4.6 illustrates the eluted concentration profile. About 90 % of the loaded protein were recovered.
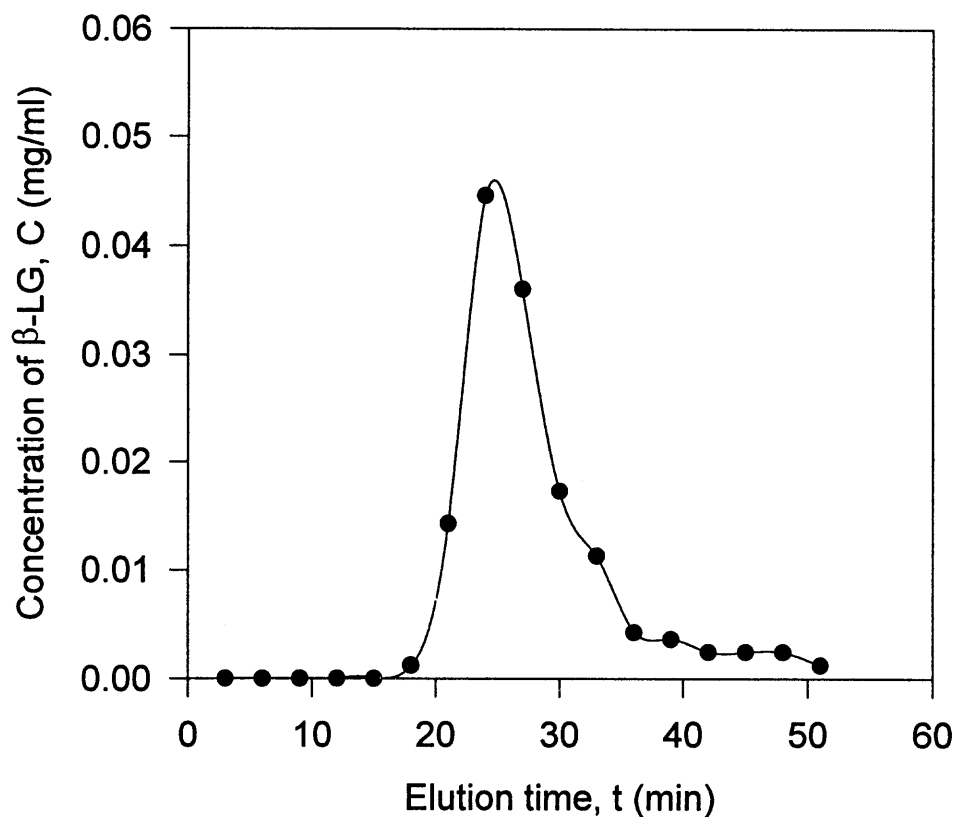
Figure 4.6 Shell-side elution for tube-side β-LG loading using 0.5 M NaCl in the starting buffer (pH 8.0)

4.1.3 BSA

About 0.60 ml of a 1.60 mg/ml BSA sample was loaded on the shell-side bed from the shell-side inlet. Elution was performed by a stepwise change of NaCl in the starting buffer (pH 8.0) at a flow rate of 1.82 ml/min: (1) 0.05 M NaCl for 51 minutes; (2) 0.1 M NaCl for 27 minutes; (3) 0.2 M NaCl for 50 minutes. Fractions were taken every 3 min to measure the protein concentrations. Figure 4.7 shows the protein concentration profile

during elution. It can be seen that 0.05 M and 0.1 M NaCl can not fully elute BSA from the beads.
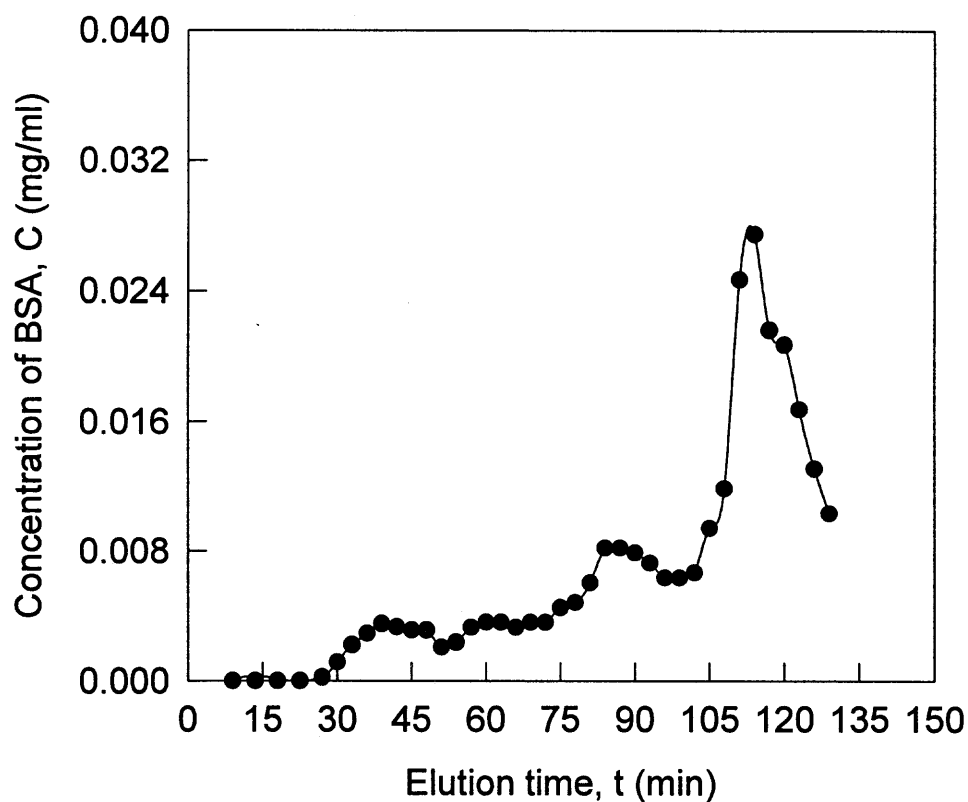
Figure 4.7 Shell-side elution for BSA with a stepwise change of NaCl concentration in the starting buffer (pH 8.0)

4.1.4 α-Lactalbumin

Tube-side loading of α-LA onto the shell-side bed was carried out by pumping 200 ml of a 47.9 μg/ml α-LA solution in the starting buffer (pH 8.5) through the fiber bore under an average TMP of 3.1 psi at a flow rate of 200 ml/min. Only the retentate was recycled. The molecular weight of α-LA is smaller than the MWCO of the membrane: it can pass through the membrane pores under a certain TMP. Tube-side elution was adopted in a

stepwise fashion: (1) 0.05 M NaCl in starting buffer for 45 minutes; (2) 0.5 M NaCl in starting buffer for 50 minutes at a flow rate of 2.54 ml/min. Figure 4.8 shows the concentration profile during elution. About 94 % of the loaded protein was recovered. Figure 4.8 also illustrates that 0.05 M NaCl could not elute α-LA properly from the beads. Only about 2.5 % of the protein was eluted in the first elution step.
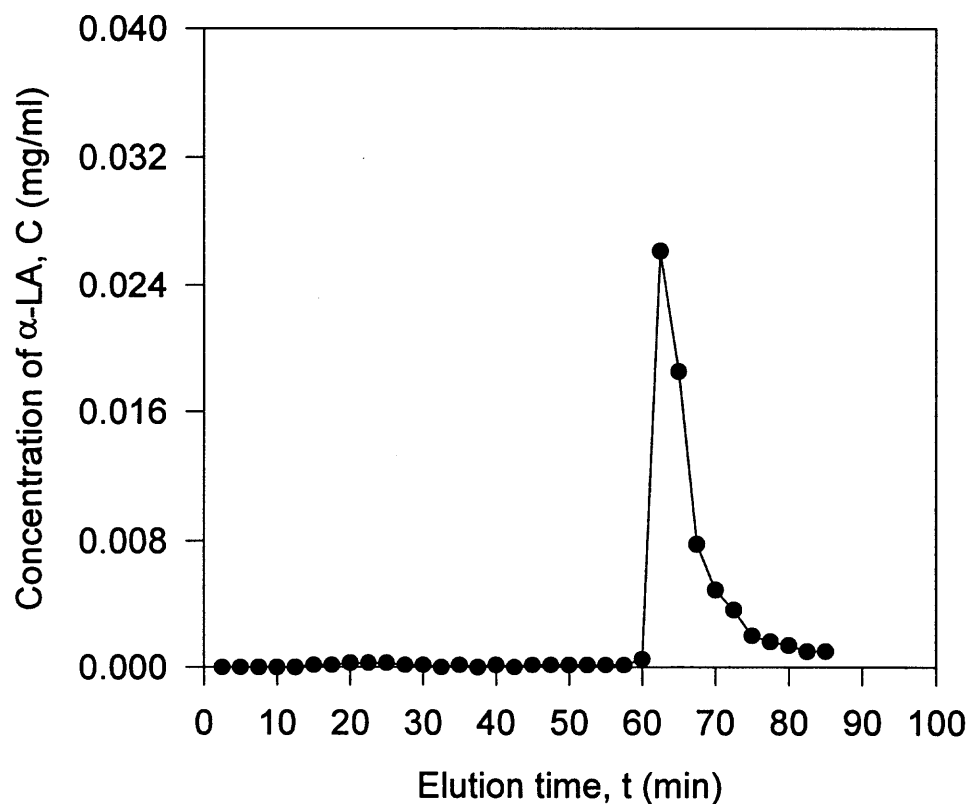
Figure 4.8 Tube-side elution using a stepwise change of NaCl concentration in the starting buffer (pH 8.5) for tube-side loading of α-LA

4.1.5 Separation of Binary Protein Mixtures Using Shell-Side Loading

The binary protein mixture of Mb and β-LG is one pair of model proteins studied. A sample consisting of 1.0 ml of a mixture of Mb (0.7 mg/ml) and β-LG (0.7 mg/ml) was loaded directly onto the shell-side bed. Based on the results from sections 4.1.1 and 4.1.2, a stepwise change in elution buffer was carried out with 0.05 M NaCl in 20 mM Tris-HCl (pH 8.0) for the first 60 minutes, and with 0.5 M NaCl for the following 40 minutes. The eluent flow rate was 1.65 ml/min. Figure 4.9 shows the chromatogram of the eluted proteins. The first peak is of Mb due to the weak interaction between the beads and Mb. The second peak is of β-LG; the interaction between the beads and this protein was stronger. The good separation achieved indicated that the packed beads in the shell side were working well as an anion exchanger; further, the packed bed column with the fibers was an effective axial flow chromatographic column. The peak shape for β-LG is quite similar to that obtained by Luo and Hsu (1997) in packed bed chromatography with DEAE-Sepharose beads in a bed which was 1.5 cm in diameter and 22.0 cm in length. The elution of β-LG could have been initiated earlier by an earlier introduction of 0.5 M NaCl.

BSA and hemoglobin (Hb) are another chosen pair of proteins for a binary mixture. The first experiment employed 0.2 M NaCl in the starting buffer (pH 8.0) to elute 1.0 ml sample of 0.75 mg/ml Hb and 0.63 mg/ml BSA loaded from the shell-side inlet. Fractions were taken every 1.5 minutes. The movement of Hb band could be observed during the elution for Hb and BSA as the housing shell of the cartridge is semi-transparent. Figure 4.10 shows the poor separation illustrating that isocratic elution using 0.2 M NaCl at pH 8.0 is not efficient for the separation of these two proteins.
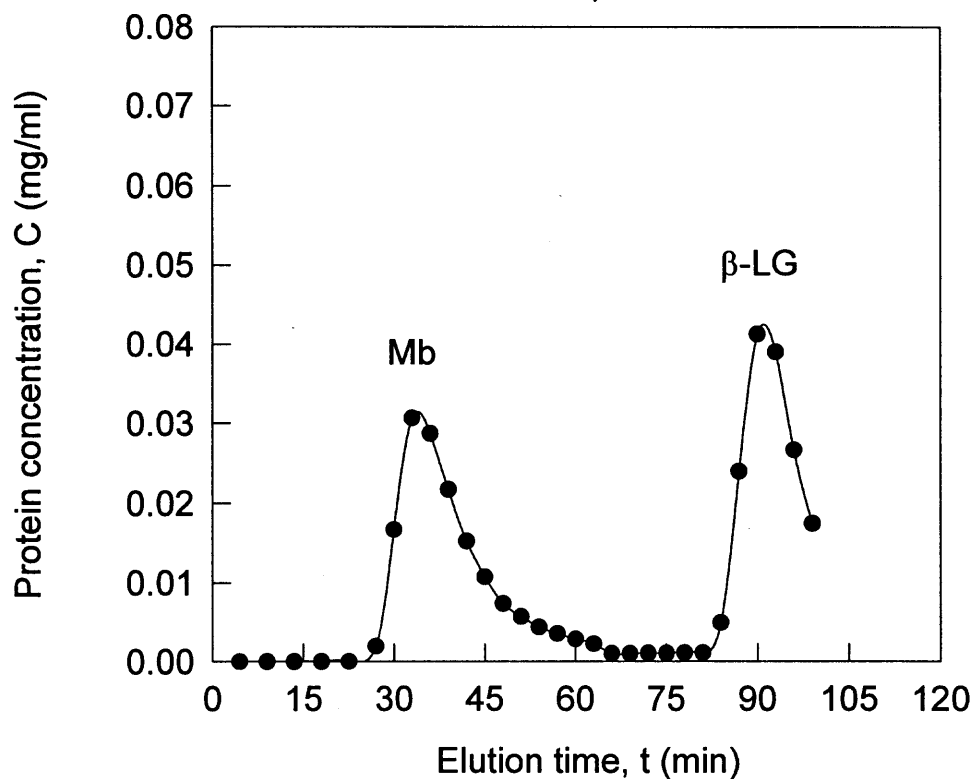
Figure 4.9 Separation of Mb and β-LG for shell-side loading using shell-side elution with a stepwise change of NaCl concentration (pH 8.0)

Improved separation of Hb and BSA was achieved by shell-side elution using a stepwise change of NaCl concentration in the starting buffer for the shell-side loading of the protein sample mixture. A sample consisting of an 1.0 ml mixture of about 0.6 mg/ml Hb and 0.65 mg/ml BSA was loaded directly on the shell-side bed from shell-side inlet. Elution was performed by using 0.05 M NaCl in the starting buffer (pH 8.0) for 50 minutes followed by 0.2 M NaCl in the starting buffer (pH 8.0). Fractions were taken every 1.5 minutes. Figure 4.11 illustrates the protein concentration profile during the

stepwise change elution. A higher resolution was achieved compared with that of Figure
4.10.
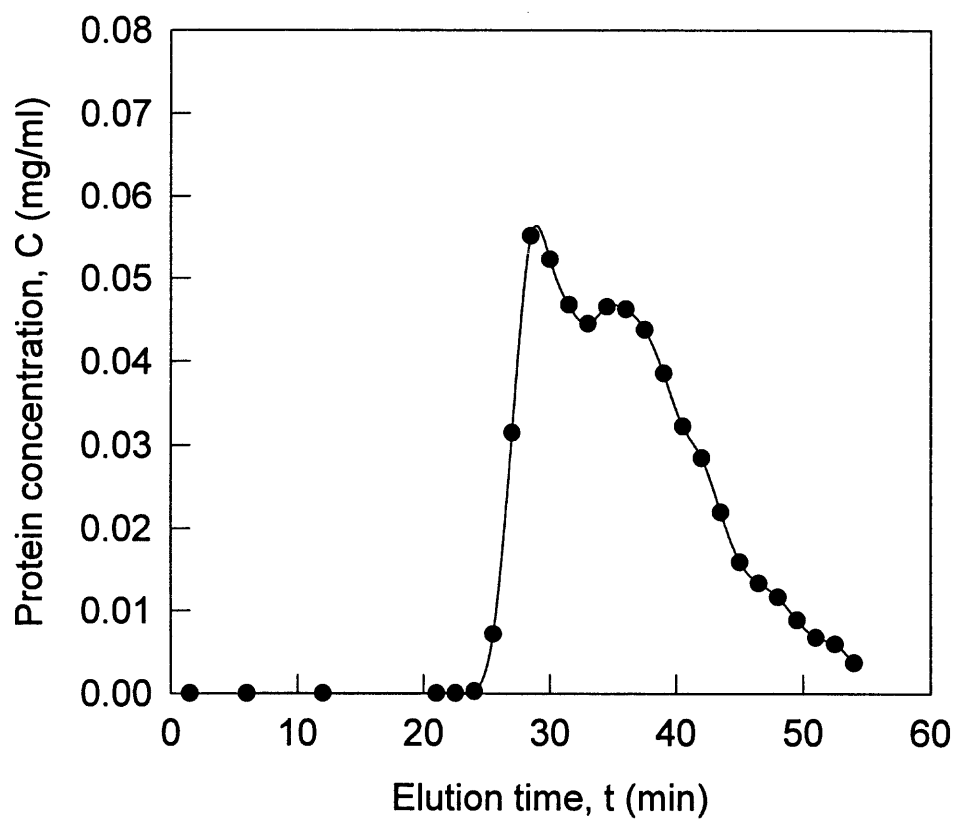
Figure 4.10 Poor separation of Hb and BSA for shell-side loading with a shell-side elution using 0.2 M NaCl (pH 8.0)
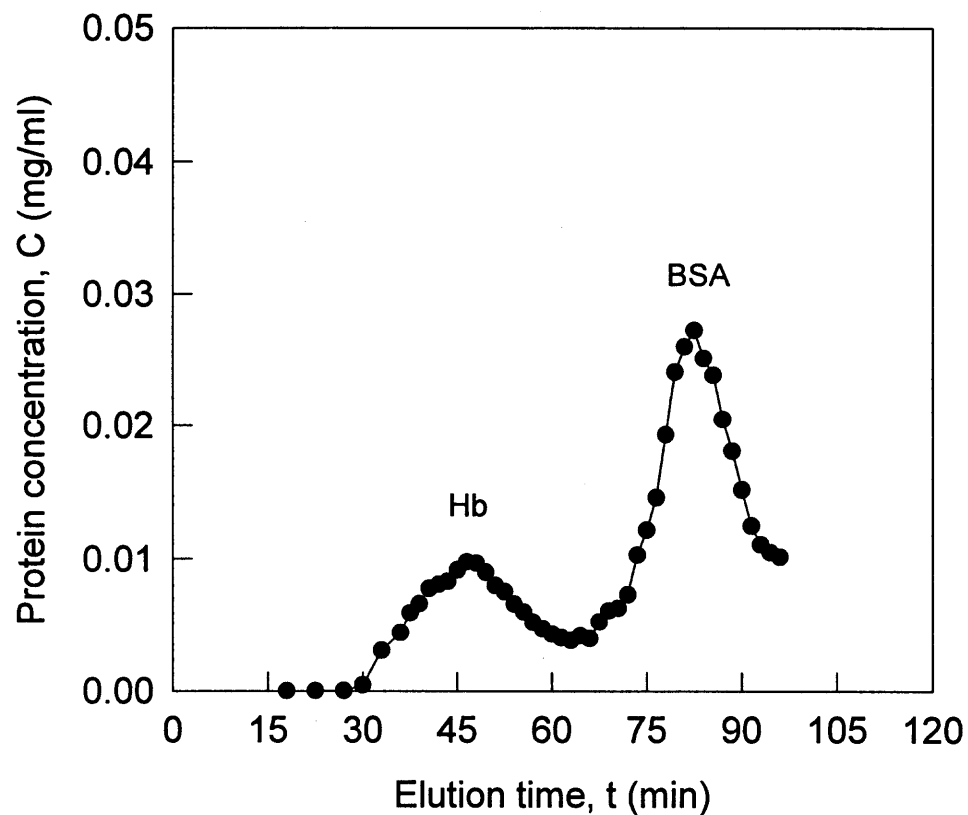
Figure 4.11 Improved Separation of Hb and BSA for shell-side loading with a shell-side stepwise elution (pH 8.0)

In this Section 4.1, experimental results have been presented for the preliminary investigation of the experimental conditions using the integrated device including mainly shell-side loading and shell-side elution of the protein samples as well as a small part of results for tube-side loading of the feed and tube-side elution. Further explorations of this technique using the integrated device will be discussed in the following sections.

4.2 One Cycle-Based Process of Filtration-cum-Loading-cum-Chromatography

One cycle-based process of tube-side filtration-cum-loading-cum-chromatography experiments was conducted using clean feed solutions of a binary protein mixture. The first experimental result presented in this section is the separation of Hb and BSA. An aqueous solution of 0.030 mg/ml Hb and 0.033 mg/ml BSA in the starting buffer (pH 8.0) was pumped through the hollow fiber bores. Full recycle was performed to return both permeate and retentate to the reservoir (Figure 3.5); the process was stopped before detecting any of the poorly adsorbed protein (Hb) on the permeate side. Filtration-cum-loading was run in this fashion for 12 minutes at a permeate flow rate of 9.1 ml/min - 13.6 ml/min (Figure 2.1a). Since the molecular weights of Hb and BSA are smaller than the MWCO of the membrane, both Hb and BSA can partially pass through the pores of the membrane under the transmembrane pressure. The red color of Hb could be seen during this loading operation from the outside of the cartridge which showed that Hb passed through the pores. A 3-stepwise change elution method based on the previous results was carried out next from the shell side (corresponding to Figure 2.1b): first (1) with 0.05 M NaCl in 20 mM Tris-HCl (pH 8.0, 42 min), then (2) with 0.1 M NaCl in 20 mM Tris-HCl (pH 8.0, 27 min), followed by (3) elution with 0.2 M NaCl in 20 mM Tris-HCl (pH 8.0, 60 min) at a flow rate of 1.845 ml/min. Figure 4.12 illustrates the separation achieved. Two separate peaks were obtained with a small amount of overlap in the middle. The peak widths are reasonable. There does not appear to be much band broadening.
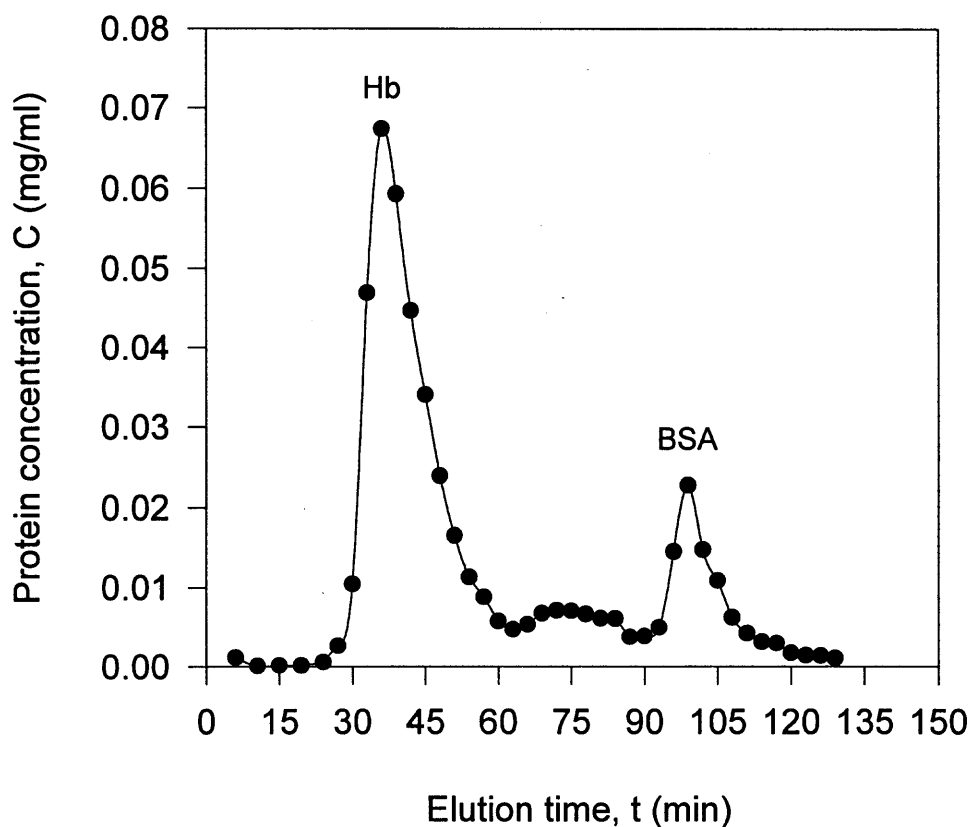
Figure 4.12 Separation of Hb and BSA for tube-side loading of feed by using a shell-side 3 stepwise change elution (pH 8.0).

Similar experiments were performed with a binary protein mixture of Mb and β-LG. Initial experiments showed that the starting buffer at pH 8.0 was not good for the loading of Mb on the beads. Mb "leaking" was detected in the permeate during very early stage of tube-side loading operation. Only part of Mb was loaded on the shell-side bed. In order to achieve a better adsorption of Mb onto the beads on the shell-side, a buffer pH of 8.5 was chosen for Mb-related experiments. Like most experiments discussed in Section 4.1, separation for a shell-side loading of a binary protein mixture of Mb and β-LG using shell-side elution was tried first. An 1.0 ml sample of 1.2 mg/ml Mb and 1.1 mg/ml β-LG

was loaded onto the shell-side bed from the shell-side inlet. The bed was washed with starting buffer (pH 8.5) for 30 minutes at a flow rate of 1.78 ml/min, neither Mb nor β-LG was washed out during this step, showing that both proteins were adsorbed well on the beads under the buffer pH at 8.5. Then 0.05 M NaCl in the starting buffer (pH 8.5) was used for the elution followed by 0.5 M NaCl in the starting buffer (pH 8.5) at a flow rate of 1.66 ml/min. Two separate peaks were obtained; the first one is of Mb and second one is of β-LG (Figure 4.13). Over 90 % of the proteins were recovered.
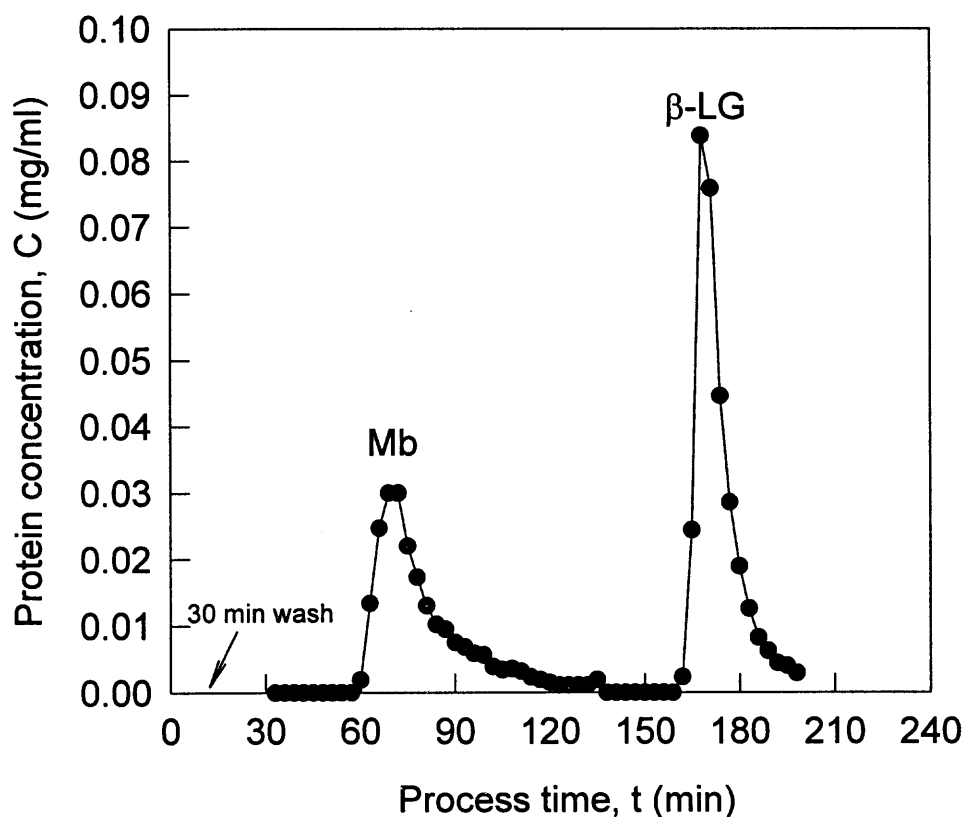
Figure 4.13. Separation of Mb and β-LG for shell-side loading with a shell-side elution (pH 8.5)

Based on this result, a series of experiments for separation of Mb and β-LG were conducted to study different operating modes and conditions for the integrated device. Four hundred ml of aqueous solution of around 0.030 - 0.032 mg/ml Mb and 0.029 – 0.037 mg/ml β-LG in the starting buffer was pumped through the fiber bores for 12 - 15 minutes. The average transmembrane pressure was around 2.7 psi at a permeate flow rate of 5 ml/min. In this case, both Mb and β-LG can pass through the membrane pores. A stepwise elution method was carried out first with 0.05 M NaCl in 20 mM Tris-HCl (pH 8.5) for about 90 minutes, followed by 0.5 M NaCl in 20 mM Tris-HCl (pH 8.5) for about 40 minutes at a flow rate of around 2.7 ml/min, either from the tube side or the shell side of the hollow fiber module. Figures 4.14 and 4.15 illustrate the results for tube-side elution and shell-side elution respectively. Two separate peaks were obtained in each of the two elution modes. For the elution mode from shell side, sharper peaks could be obtained, while for the elution from tube side, somewhat shorter retention times were observed. Yields of the separations shown in Figures 4.14 and 4.15 are summarized in Table 4.1.

Comparison of the eluted peaks indicated in Figures 4.14 and 4.15 show that the shell-side elution peaks have a sharper separation than those from tube-side elution. Possible explanations for this observation follows:

1. Tube-side elution is likely to desorb small amounts of proteins adsorbed on the membrane surface and pore surfaces. The introduction of these desorbed proteins on the shell side may broaden the peaks.

2. Tube-side elution introduces eluent into the bed along its whole length. The stationary phase near the column top is subjected to a certain volume of mobile phase flow. The

stationary phase further down the column is subjected to a larger volume of mobile

phase flow. The stationary phase near the bottom of the column is subjected to the

largest volume of mobile phase flow. Thus, in this configuration, there is a spectrum

of mobile phase volumes as well as a spectrum of stationary phase volumes for a

given partition coefficient of the sorbed species. As a result, the effective retention

time is probably reduced and the band somewhat broadened in the tube-side elution

vis-à-vis the shell-side elution.
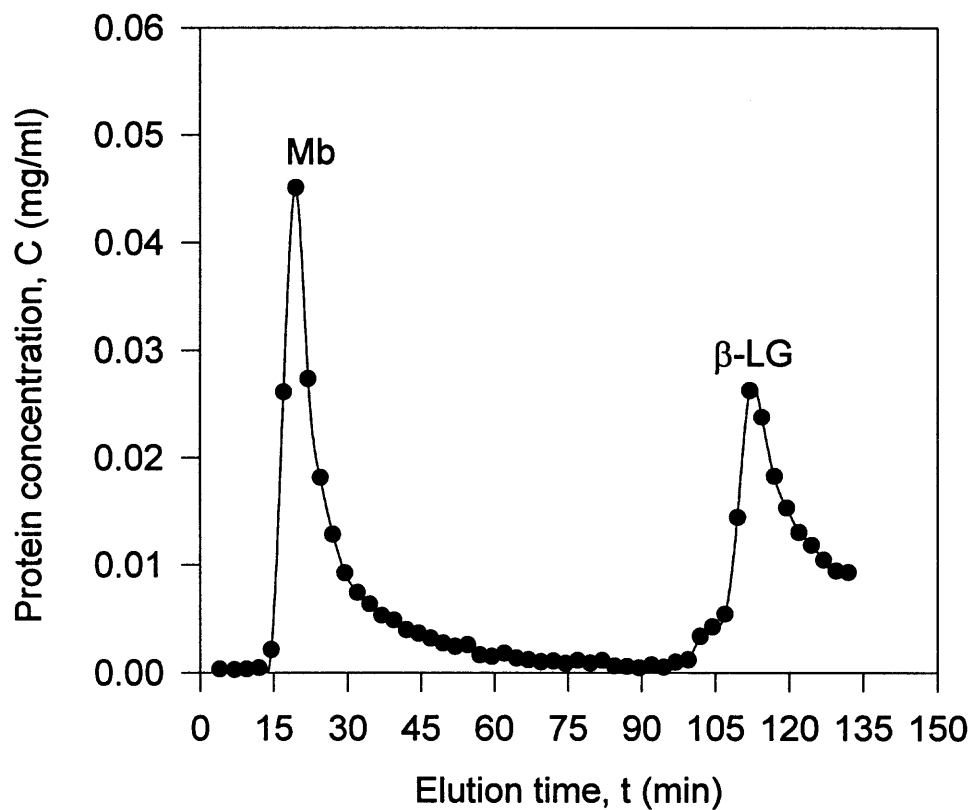
Figure 4.14 Separation of Mb and β-LG for tube-side loading by using tube-side elution (pH 8.5)
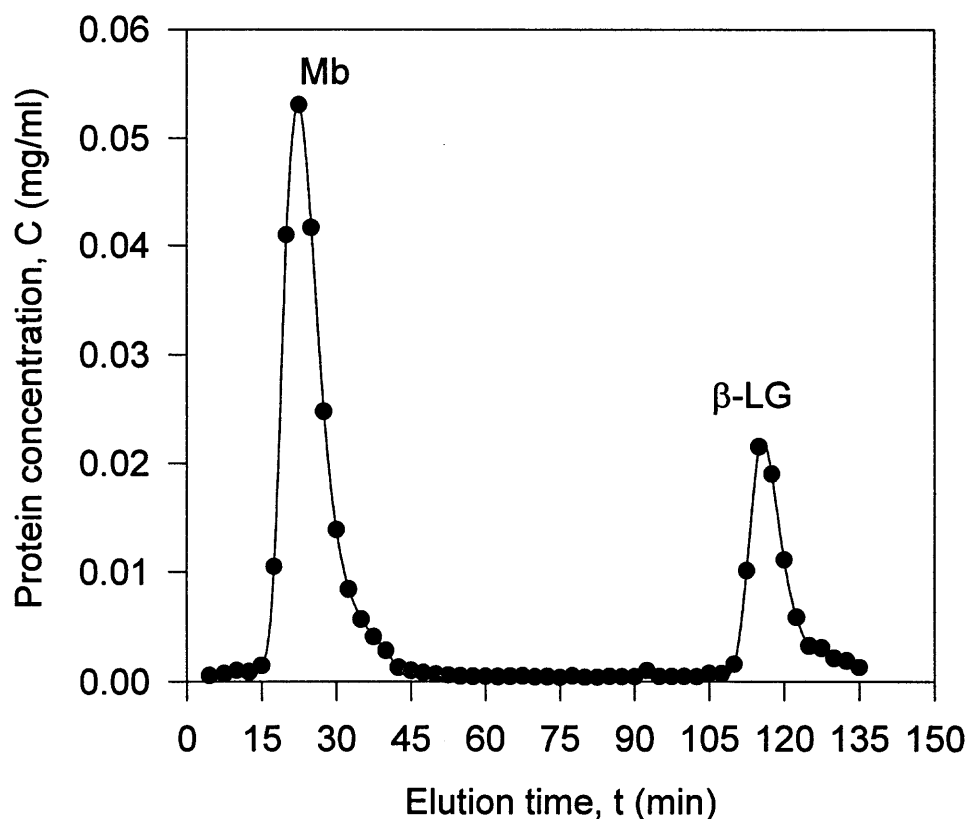
Figure 4.15 Separation of Mb and β-LG for tube-side loading by using shell-side elution (pH 8.5)

To optimize the elution conditions, 400 ml of an aqueous solution of around 0.031 mg/ml Mb and 0.032 mg/ml β-LG in the starting buffer was pumped through the fiber bores without retentate and permeate recycle for 11 minutes. The average transmembrane pressure was around 2.8 psi at a permeate flow rate of 5.6 ml/min. The stepwise elution method was modified to reduce the elution time, first with 0.05 M NaCl in 20mM Tris-HCl (pH 8.5) for 50 minutes instead of more than 90 minutes, then followed by 0.5 M NaCl in 20mM Tris-HCl (pH 8.5) for 38 minutes at a flow rate of around 2.85 ml/min,

which was carried out from the shell side of the hollow fiber module. Figures 4.16 shows

the result. Good separation was obtained with a much shorter elution time compared with

that of the experiment shown in Figure 4.15. Yet the bandwidth of each peak in Figure

4.16 is almost identical to that in Figure 4.15.
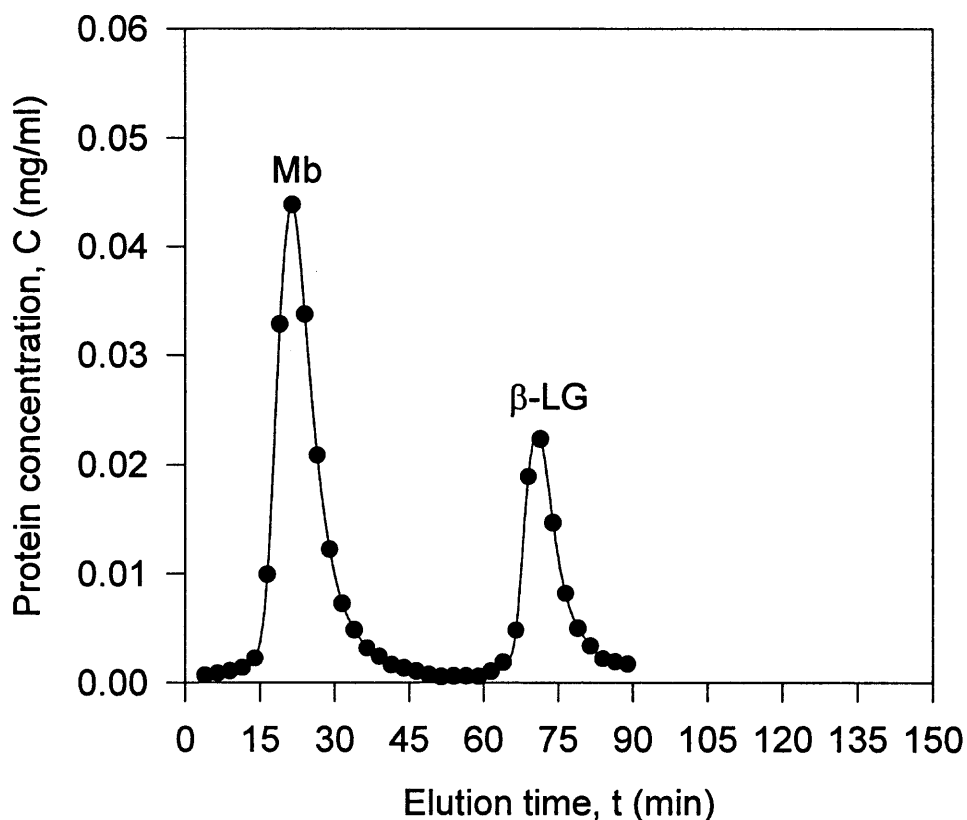
Figure 4.16 Separation of Mb and β-LG for tube-side loading by using shell-side elution for a reduced elution time (pH 8.5)

A similar reduction in elution time can also be achieved in tube-side elution

processes. Figure 4.17 illustrates the separation of Mb and β-LG from 400 ml of a

mixture of Mb (0.031 mg/ml) and β-LG (0.037 mg/ml) via tube-side elution. In this

experiment, 0.05 M NaCl was used in the standard eluent for 52 minutes, followed by 0.5 M NaCl for 40 minutes. Even though the elution took much less time here compared to that in Figure 4.14, the peaks and the peak shapes are almost identical in these figures. It also appears that one could cut down the time even further provided one accepts a somewhat higher impurity level of Mb in the β-LG fraction.
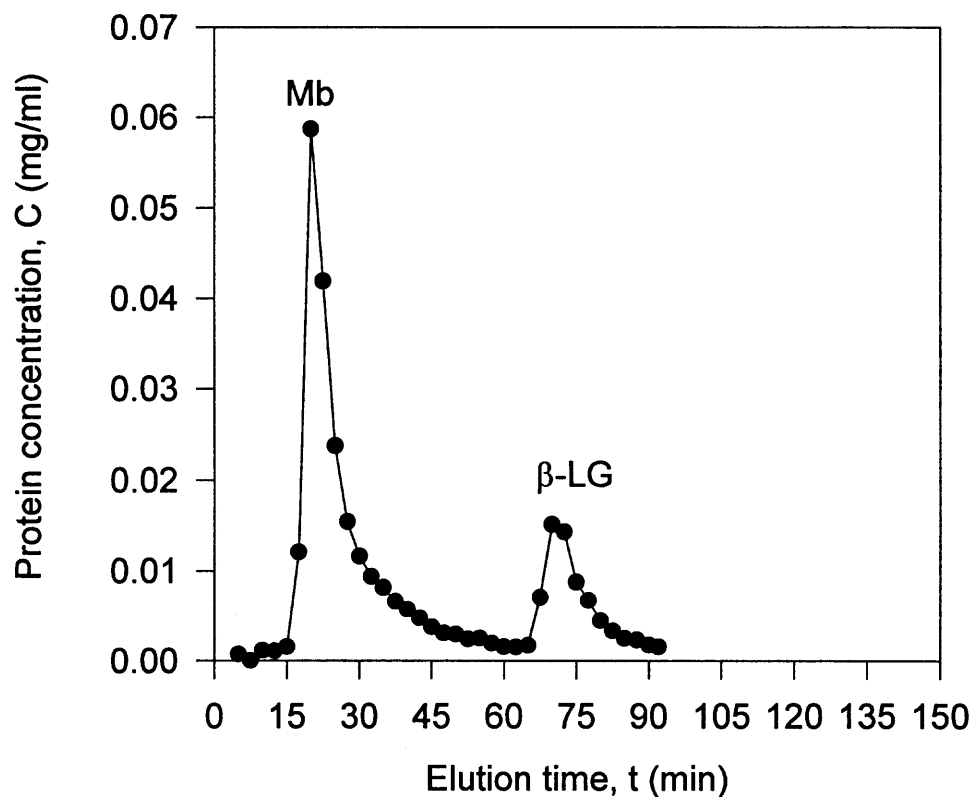
Figure 4.17 Separation of Mb and β-LG for tube-side loading by tube-side elution for a reduced elution time (pH 8.5)

Figures 4.14 to 4.17 illustrate results of chromatographic separations carried out from one-time loading of the shell-side beads from a tube-side filtration-based feed. How

would this device and process behave if such a process is carried out repeatedly? For practical application of this device, a repetitive process would be needed since as Table 1 shows the amount of protein recovered in the eluent fraction in one cycle in this case varies between 3-12 % of the amount present in the feed. While different devices, designs and operating conditions can increase this fractional recovery considerably (as shown later in the simulated yeast broth experiments), multiple cycles are needed in general.

Table 4.1 Yields from the filtration-loading-chromatography experiments for separation of Mb and β-LG

Elution Mode	Tube-side elution (shown in Figure 4.14)		Shell-side elution (shown in Figure 4.15)		Tube-side elution (shown in Figure 4.17)		Shell-side elution (shown in Figure 4.16)	
Proteins	Mb	β-LG	Mb	β-LG	Mb	β-LG	Mb	β-LG
Yield based on protein removed from feed solution*	98.9%	95.5%	98.9%	92.3%	100.0%	98.6%	96.6%	96.0%
Yield based on total protein in feed**	11.0%	5.1%	11.7%	4.2%	10.9%	3.1%	10.9%	4.4%

*Dividing the total recovered protein amount from the elution fractions in one cycle by the amount of protein removed from the feed solution in one cycle.
**Dividing the total recovered protein amount from the elution fractions in one cycle by the total amount of protein present in the feed solution.

4.3 Cyclic Processes

4.3.1 A Cyclic Process for a Solution Containing a Single Protein

Figure 4.18 illustrates the peaks for Mb in a 10-cycle process. The feed in this case had only Mb at a concentration of 0.027 –0.029 mg/ml. Two hundred and fifty ml of the feed solution was pumped through the fiber lumen at a flow rate of about 200 ml/min under an

average TMP of about 2.4 psig for each cycle with retentate recycle. Tube-side elution was performed by using 0.5 M NaCl in the starting buffer (pH 8.5) at a flow rate of 2.2 – 2.5 ml/min. The peak shapes in different cycles are essentially identical in this 10-cycle process. Any reduction or increase in the peak height may be ascribed to fluctuations in the permeate flux level in that cycle as shown in the Figure. The multi-step process carried out continuously in a cyclic fashion to load-elute-reequilibrate for a single protein in a feed demonstrates that a large volume of feed can be handled successfully over a period of time.
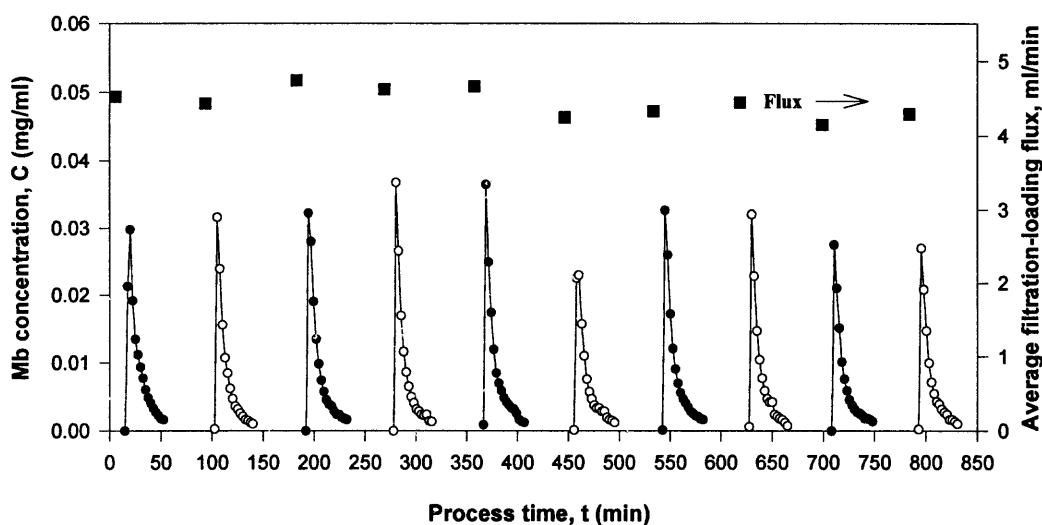
Figure 4.18 Cyclic process for recovery of a single protein Mb in a clean feed (pH 8.5)

4.3.2 A Cyclic Process for a Protein Mixture Present in a Clean Feed

In the set of experiments to be presented now, the feed was a mixture of Mb and α-LA. The feed had both Mb and α-LA at a concentration range of 0.028 –0.030 mg/ml. One hundred and fifty ml feed solution was pumped through the tube side at a flow rate of 200 – 250 ml/min under an average TMP of about 3.1 psig for each cycle with retentate

recycle. Tube-side stepwise elution was performed by first using 0.05 M NaCl in the starting buffer (pH 8.5) for 55 minutes, then changing to 1.0 M NaCl in the starting buffer (pH 8.5). Elution flow rate was in the range of 2.3 – 2.6 ml/min. As shown in Figure 4.19, the repeated process of loading-elution-reequilibration successfully yielded in each cycle a clean and identical separation of two peaks of Mb and α-LA (in each case the second peak). Any reduction or increase in the peak height or area in a given cycle can easily be correlated with a reduction or increase in the filtration flux in that cycle as shown in the Figure. Thus although the fractional recovery of proteins in the feed per cycle in this device is somewhat low, multiple and repetitive cycles are easily carried out. No deterioration in performance was observed as the number of cycles were increased (Figure 4.19 has 12 cycles).
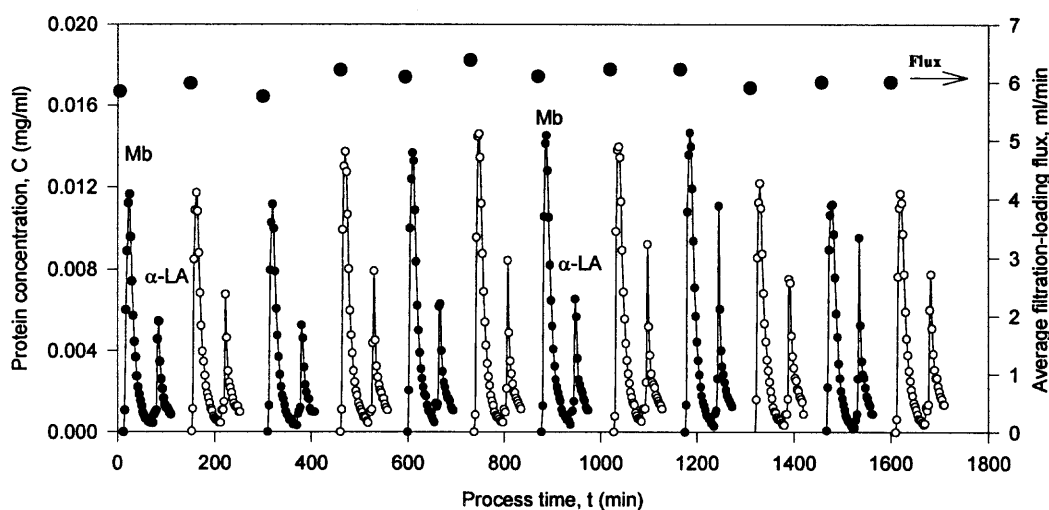
Figure 4.19 Cyclic separation process for mixtures of Mb and α–LA in a clean feed (pH 8.5)

4.3.3 A Cyclic Process for a Protein Mixture in a Simulated Yeast Broth

Every experiment described so far employed ultrafiltration of a clean solution of a single protein or a protein mixture from the tube side to load the proteins on the shell-side beads. The results described next in Figure 4.20 employed a mixture of Mb and α-LA in a yeast suspension simulating a fermentation broth. For this experiment module 2 was used. Figure 4.20 first shows the absorbance reading when the cellular suspension was passed; the small peaks are due to particular proteins present in the suspension. Then the system was regenerated using 1.0 M NaCl and reequilibrated with the starting buffer. Afterwards, a protein mixture in a clean solution without any cells was loaded. The elution of this tube-side loaded protein mixture of Mb and α-LA came out in two distinct peaks between 150-240 minutes (as shown on the right hand side of Figure 4.20). The bed was next regenerated and then the simulated yeast broth containing a mixture of Mb and α-LA (about 0.04 mg/ml respectively) was introduced from the tube side. The loading-elution-(regeneration)-reequilibration steps are as described in the Figure. This process was cyclically repeated six times. Any difference between the runs 1-3 and 4-6 are due to the additional step 7 (shown in the Figure 4.20) explored from runs 4-6. What is however clear is that the cyclic process studied before with clean solutions can be also implemented from a simulated broth system. The cyclic process output and the device behavior appear to be repeated. Recoveries of Mb and α-LA from the feed in each cycle were about 30% and 20% respectively.
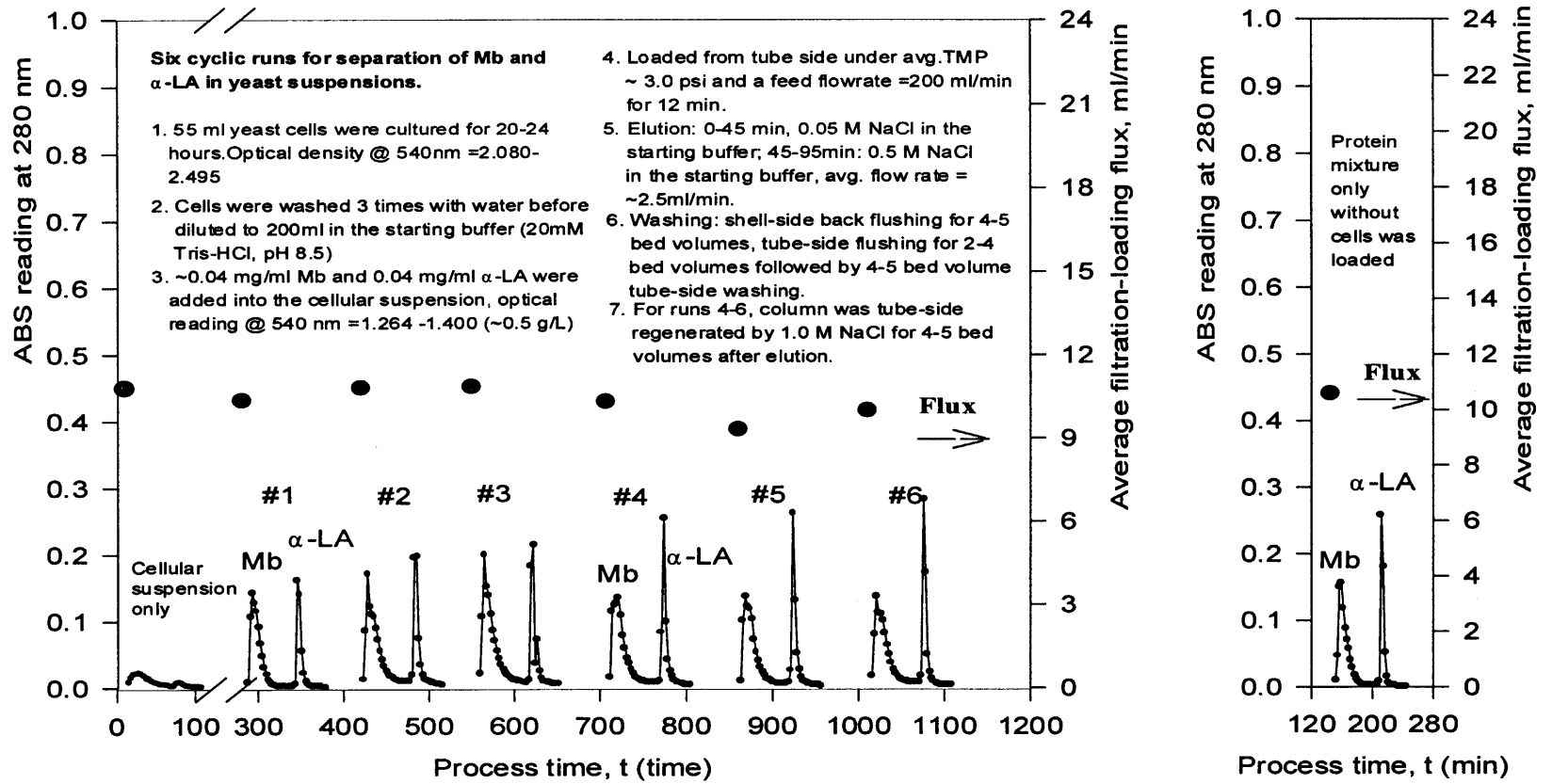
Figure 4.20 Cyclic process for separation Mb and α–LA in yeast suspensions using module 2 (pH 8.5)

The above results indicate that the integrated cyclic process can be implemented over many cycles for binary protein mixture separation via elution chromatography. Futher, the basic objective of this integrated process and single device, namely, chromatographic separation of a protein mixture from a cellular broth (among others) is achievable. There are a number of other aspects of this one device-based process which are worthy of further exploration. One of them concerns the rate of protein transmission through the membrane in the integrated device vis-à-vis the same membrane without any beads on the shell side. For example, the protein transmission rate (mg/min.m^2) of Mb obtained for membrane module 2 without shell-side beads at a feed concentration of about 0.030 mg/ml in a clean solution and a transmembrane pressure difference of 4 psi was found to be 2.14 mg/min.m^2 (see Table 4.2). For the same protein, the protein transmission rate is considerably higher using this integrated device (e.g. about 5.16 mg/min.m^2) under an average TMP of 3.0 psi. It must be due to a higher protein concentration difference across the membrane since the beads on the shell side act as a sink for the protein in the permeate.

Table 4.2 Comparison of protein (myoglobin) transmission in module 2 without beads and with beads* at a feed flow rate of 200 ml/min

	Feed conc. mg/ml	Average TMP psi	Loading time minutes	Permeate volume ml	Permeate conc. mg/ml	Permeate conc. / Feed conc.	Mass transfer rate mg/min.m^2
Without beads	0.03	4	2	150	0.0009-0.0015	0.03-0.05	2.14***
With beads	0.04	3	12	130	0.02**	0.5	5.16***

Table 4.2 Comparison of protein (myoglobin) transmission in module 2 without beads and with beads* at a feed flow rate of 200 ml/min (Continued)

*Experiment without beads was carried out by using a clean solution containing only myoglobin; the data for experiment with beads were from a cyclic process using a protein mixture in a yeast suspension.
**Dividing the total recovered protein amount from elution peak by permeate volume.
***Mass transfer rate = permeate concentration × permeate volume / (loading time × membrane area)

4.4 Effects of Higher Protein Concentration in Feed and the Extended Section

The concentration level of proteins used in each of the above experiments for tube-side loading (Figure 4.12 and Figures 4.14 - 4.20) varied between 0.027 mg/ml - 0.037 mg/ml. Can the particular device being studied be used to process feeds containing higher protein concentrations? Figure 4.21 illustrates the separation of Mb and α-LA present in the feed at concentration levels of 0.14 mg/ml and 0.137 mg/ml respectively. This is about 5 times larger than those in all of the earlier experiments employing 15 minutes tube-side loading. Tube-side stepwise elution method was used by pumping 0.05 M NaCl in the starting buffer (pH 8.5) for 45 minutes followed by 0.5 M NaCl in the starting buffer (pH 8.5) at a flow rate of 2.58 ml/min. The peak shapes and the peak separations in this one-cycle experiment are similar to those of Figure 4.19. A low level of α-LA was detected along with the Mb peak. This suggests that for higher feed concentration levels either the local bed volume is to be increased vis-à-vis the fiber membrane surface area or that an additional length of a column needs to be provided at the end of the permeate outlet beyond the current length.
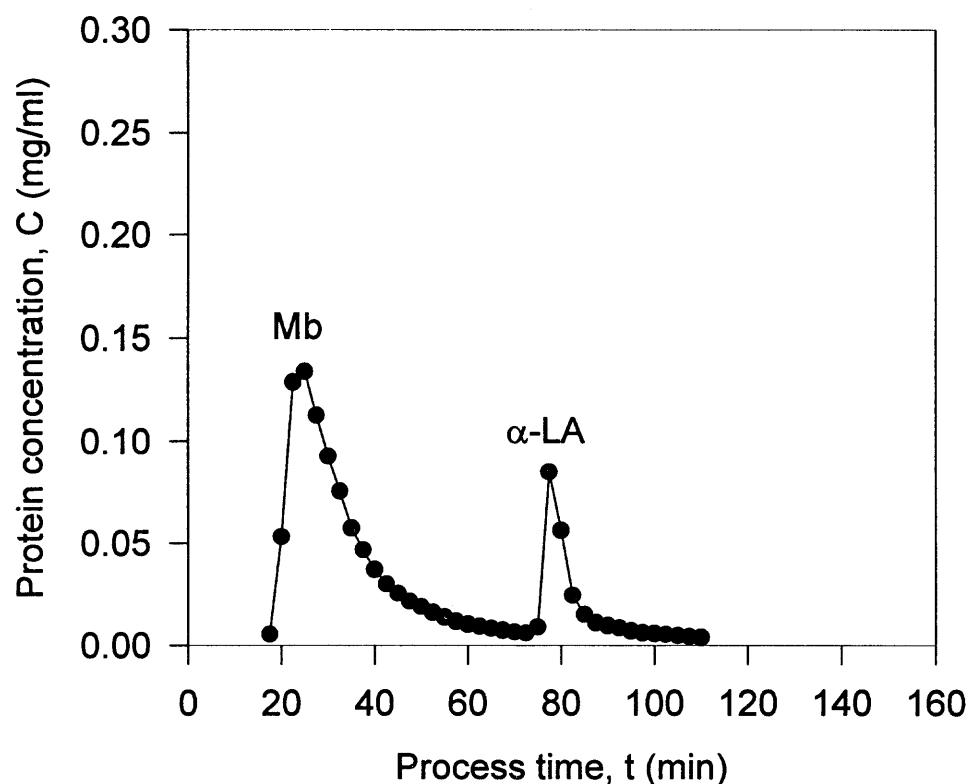
Figure 4.21 Separation of Mb and α-LA for higher protein concentrations (pH 8.5)

A similar experiment was performed by using module 1 with an additional extended section (Table 3.3). The total volume of the beads in both fixed and additional ES was about 9.2 % of the total volume of beads packed in module 1. Concentration levels similar to those in the above experiment were adopted by adding 0.150 mg/ml Mb and 0.156 mg/ml α-LA in 200 ml of feed. The loading time was 30 minutes instead of 15 minutes. The same elution method was used at a flow rate of 2.52 ml/min. Figure 4.22 provides the experimental result. Protein concentration profiles during elution show higher amounts of proteins recovered compared with those in Figure 4.21. Detailed comparisons of the two experiments are provided in Table 4.3.
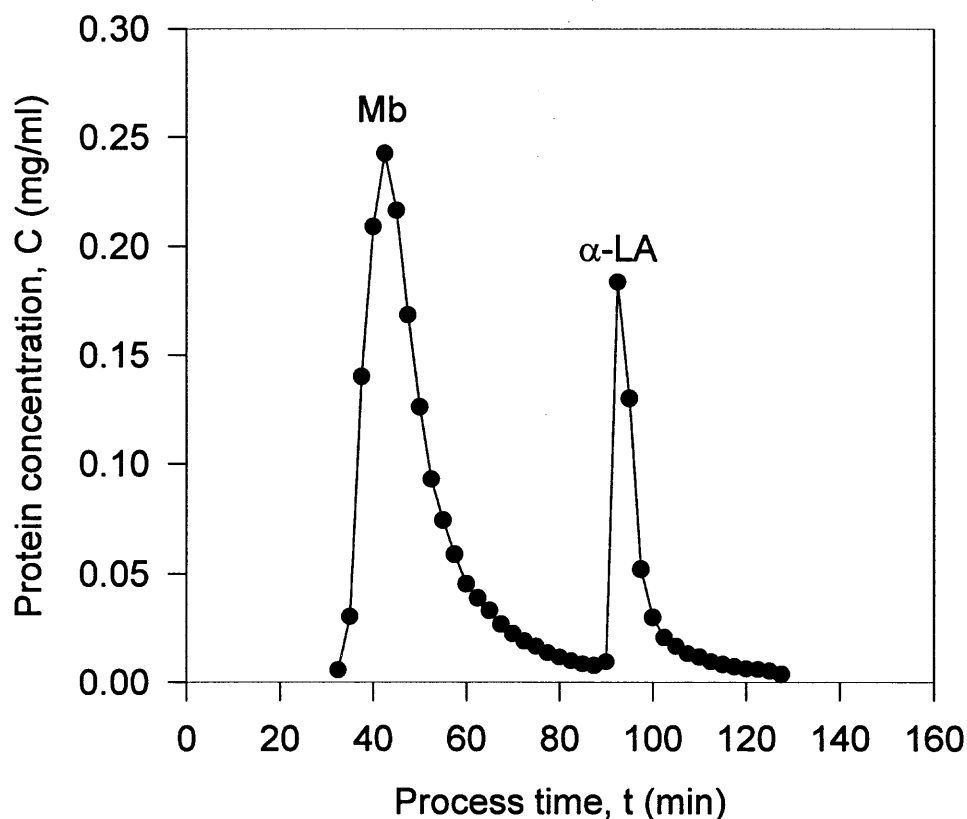
Figure 4.22 Separation of Mb and α-LA for tube-side loading of higher protein concentrations using the additional ES (Table 3.3) (pH 8.5)

From Table 4.3, it can be seen that although the additional ES lowered the TMP as well as the flux for similar experimental conditions, doubling the loading time did not increase the extent of protein "leaking" much (see "ABS @ 280 nm for the total permeate"). The averaged amount of recovered proteins in the permeate is similar for both cases but slightly higher for the case with the additional ES using longer loading time.

In order to further explore the function of the ES, additional sets of experiments were carried out with even higher protein concentrations in the feed. In this set of experiments, 200 ml of mixture of Mb (0.568 mg/ml) and α-LA (0.522 mg/ml) was loaded through tube-side filtration-loading. This is about 20 times larger than those in the earlier experiments employed in tube-side loading. The loading times for the two experiments were different: 15 minutes for the experiment without the additional ES and 30 minutes for the experiment with the additional ES. Similar stepwise elution method was adopted for both experiments by using 0.05 M NaCl in the starting buffer (pH 8.5) for 50 minutes followed by 0.5 M NaCl in the starting buffer (pH 8.5) for 50 minutes. Elution flow rate was 2.5 – 2.6 ml/min. Fractions were taken every 2.5 minutes and assayed for protein concentrations. Figure 4.23 shows the elution profiles for both cases. Detailed results are also provided in Table 4.3.

Similarly, it can be seen that the extent of protein leaking ("ABS @ 280 nm for the total permeate" (Table 4.3)) with the additional ES for 30 minutes loading is even lower than that without the additional ES for half of the loading time. Again, although the additional ES lowered the TMP as well as the flux for similar experimental conditions, the total recovered protein for the experiment with the additional ES is more than double that without the additional ES. The averaged amount of recovered protein in the permeate was also much higher for the experiment with the additional ES.
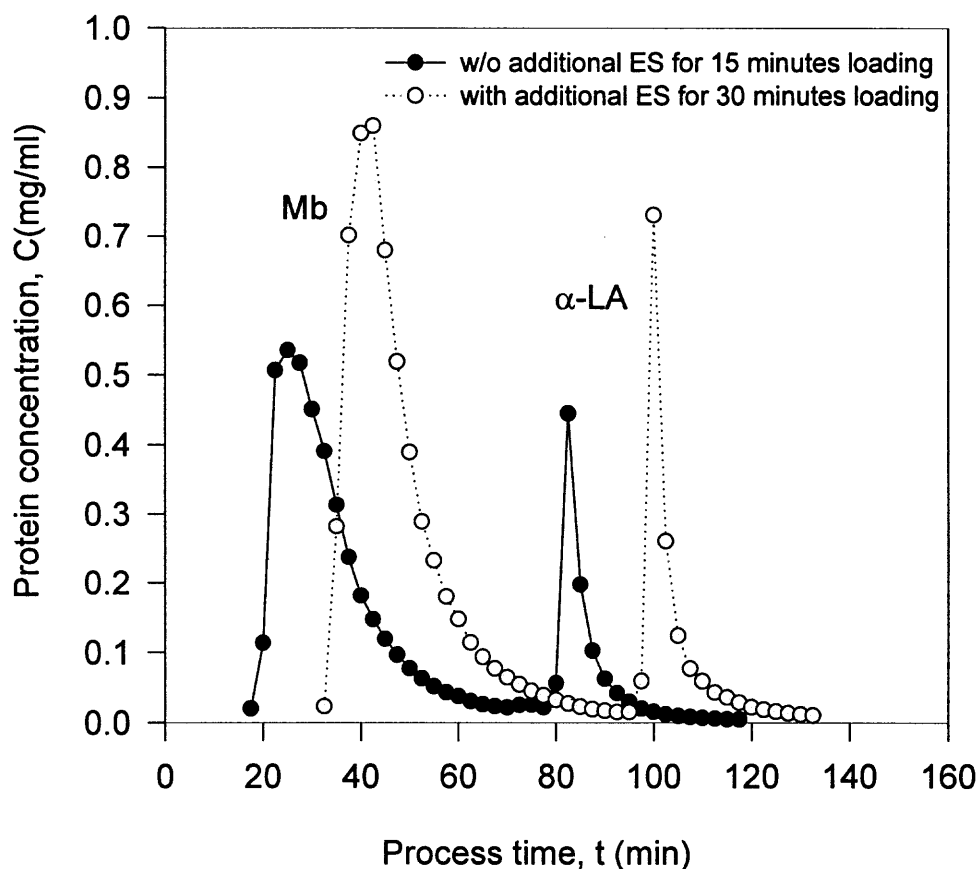
Figure 4.23 Effects of the additional ES (Table 3.3) at the permeate port on the separation for higher concentrations of Mb and α-LA (pH 8.5)

It is also useful to note here that the level of concentration of an individual protein eluted in a given fraction in all experiments is similar to its concentration level in the feed solution. That is expected in the elution chromatographic technique adopted here. Increasing the loading time may increase this concentration level to some extent in the present situation. If one were to adopt bed saturation as practiced in affinity adsorption processes, one can achieve a much higher concentration in the eluent at the cost of

substantial leakage through the permeate exit and a reduction in the resolution of the two proteins.

Table 4.3 Comparison of the effect of the ES in Figures 4.21-4.23

	Feed protein concentration 0.277 - 0.306 mg/ml		Feed protein concentration 1.04 -1.09 mg/ml	
	Figure 4.21 w/o additional ES	Figure 4.22 with additional ES	Solid line in Figure 23 w/o additional ES	Dotted line in Figure 23 with additional ES
Percentage of beads in the ES	3.27 %	9.20 %	3.27 %	9.20 %
Total feed concentration	0.277 mg/ml	0.306 mg/ml	1.09 mg/ml	1.04 mg/ml
Loading flow rate	200 ml/min	200 ml/min	200 ml/min	200 ml/min
Loading time	15 min	30 min	15 min	30 min
Average TMP @ loading	~3.1 psig	~2.8 psig	~3.1 psig	~2.8 psig
Average permeate flow rate	5.95 ml/min	4.92 ml/min	6.39 ml/min	5.08 ml/min
Total permeate volume	89.2 ml	147.5 ml	96 ml	152 ml
ABS @ 280 nm for the total permeate	0.002	0.003	0.0065	0.004
Total recovered protein for the run	7.55 mg	13.3 mg	30 mg	78 mg
Average amount of proteins in the permeate	0.085 mg/ml	0.090 mg/ml	0.31 mg/ml	0.51 mg/ml

4.5 Possible Advantages of this Integrated Process

There are many possible advantages of this integrated device and process. They are summarized as follows:

1. The process and the device proposed above clearly allows an integration of three major steps in bioseparations, namely, removal of insolubles, isolation and chromatographic purification in one device and in one cyclic process; further, the bioproduct may be extracellular or intracellular (after cell disruption).

2. There are major improvements in the process of microfiltration (MF) or ultrafiltration (UF) in such a configuration.

   a. Due to the presence of the beads on the shell side, the flow pressure drop in the permeate stream is increased significantly. As a result, it becomes easier to maintain a constant transmembrane pressure (TMP) along the module length. Maintenance of constant TMP is highly desirable (van Reis, Leonard, Hsu and Builder 1991). The possibility of reverse filtrate flow at the feed outlet region is easily eliminated.

   b. The loss of filtration flux that develops with time can be substantially reduced since the feeding step which involves the filtration of the cellular broth or the homogenate, lasts for a short time, e.g., 5 - 30 minutes. The advantages of operation in the initial period are obvious: the gel/fouling layer is not allowed to develop significantly on the membrane; the flux levels remain high. Further, elution from the shell-side inlet can even loosen and reduce the gel/fouling layer to some extent as it acts as a pseudo-backpulse. In the next cycle, the

unconsolidated deposit will be swept away to a great extent at the beginning of the cycle.

c. Introducing the eluent through the fiber bore will allow one to desorb any valuable product lost by adsorption on the fiber lumen membrane surface or pore surface. This will directly lead to an increased yield.

d. Although the flux is reduced a lot due to the beads packed on the shell side, the protein transmission rate is increased considerably.

3. Unless the permeate side pressure drops are excessive (which can develop under unusual conditions), most commercially available beads can be used in such a device/process. They need to withstand a small pressure drop (e.g., 2 - 8 psi) on the shell side which most beads are capable of. The vast majority of conventional hollow fiber membrane-based UF and MF devices could be utilized in this process. The fiber dimensions may vary from 100 μm ID to 2000 μm ID or higher. The adsorbent beads can have any functionality and structure and dimensions of 5 μm or upwards. Further, flat membrane-based devices may be easily adopted to this end.

4. Hollow fiber membrane modules can be cleaned-in-place (CIP) or sanitized by an appropriate sequence of cleaning solutions (van Reis, Leonard, Hsu and Builder 1991). The adsorbent particles may be subjected to a CIP procedure (Chang and Chase 1996). One has to ensure that the two procedures are reasonably compatible.

5. Membrane units employed for MF or UF are modular. Hence, the device for the proposed process containing adsorbents will also be modular. This will substantially reduce the problem of scale up; more than one packed hollow fiber module may be used in parallel operation to treat higher feed flow rates. Correspondingly, if steady

state feeding of the fermentation broth is desired, a number of units may be used in parallel so that at least one unit will always be in the filtration-cum-loading mode. This is illustrated in Figure 4.24 for several example cases.

Case 1: Loading time = Elution time = Re-equilibration time = One time unit

Operation time

Module 1

Module 2

Module 3

⌐__⌐ One time unit ········ Elution

▬▬ Loading ——— Re-equilibration

▬▬·····——— One cycle ▨▨▨ Idle time
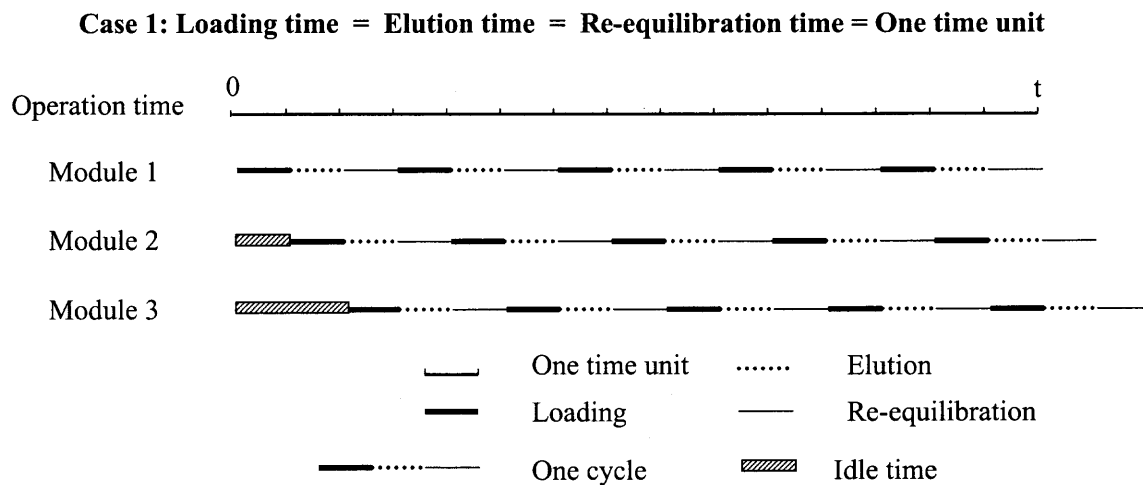
Figure 4.24a Schematic for continuous cyclic process using three integrated devices in parallel. Loading time = Elution time = Re-equilibration time = One time unit

Case 2: Loading time = 1/2 Elution time = Re-equilibration time = One time unit

Operation time

Module 1

Module 2

Module 3

Module 4

⌐__⌐ One time unit ·············· Elution

▬▬ Loading ——— Re-equilibration

▬▬············——— One cycle ▨▨▨ Idle time
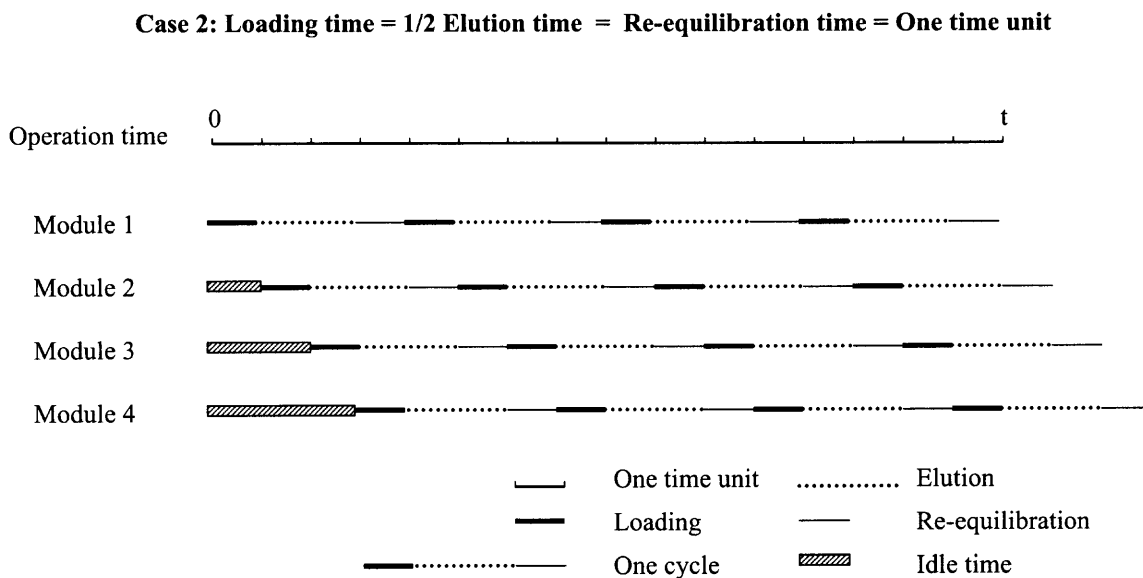
Figure 4.24b Schematic for continuous cyclic process using four integrated devices in parallel. Loading time = 1/2 Elution time = Re-equilibration time = One time unit

Case 3: Loading time = 1/3 Elution time = Re-equilibration time = One time unit
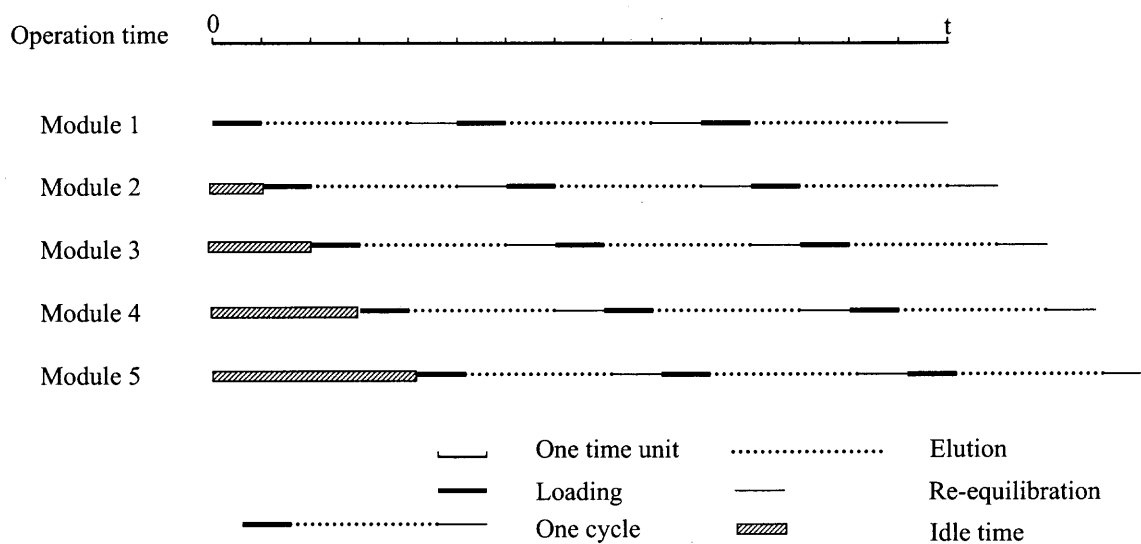
Figure 4.24c Schematic for continuous cyclic process using five integrated devices in parallel. Loading time = 1/3 Elution time = Re-equilibration time = One time unit

From Figure 4.24, it can seen that depending on the specific requirements for a process, i.e., different time needed for different stages of operation, a continuous cyclic process for several modules in parallel can be carried out. For example, Figure 4.24a describes a process having only three stages in each cycle, namely, loading, elution and re-equilibration in which loading time = elution time = re-equilibration time = one time unit. In this case, if one has three modules in parallel, there is always one module in the loading mode, one module in the elution mode and the third one in re-equilibration mode. In other words, all three operations (loading, elution and re-equilibration) are continuously running from module to module without interruption until some specific goals are achieved, e.g., the whole broth volume is treated. The process can be controlled by an automatic program designed for the system. Similarly for the case in Figure 4.24b, if loading time = $\frac{1}{2}$ elution time = re-equilibration time = one time unit, 4 modules can

be put in parallel to carry out a continuous process. There is always one module in four in the loading stage, two modules in elution stage and the fourth one in re-equilibration stage. For the case in Figure 4.24c, if loading time $= \dfrac{1}{3}$ elution time $=$ re-equilibration time $=$ one time unit, 5 modules can be put in parallel to carry out a continuous process. This figure illustrates that no matter what kind of specific requirements on operation time for different stages are needed for product purification, a continuous cyclic process can be easily designed; further the scale-up of the process is also relatively easy and convenient.

4.6. Adsorption Isotherm of the Model Proteins

Equilibrium adsorption experiments were carried out for proteins used most often in this dissertation: Mb, α-LA and β-LG. The experimental methods for equilibrium adsorption have been described in Chapter 3. It was found that adsorption of Mb on DEAE Sepharose Fast Flow beads could reach equilibrium within 15 minutes. Figure 4.25 shows typical experimental results for the isotherm relationship between concentrations in the liquid phase and the solid phase. Concentration in solid phase is calculated by eq 4.1:

$$q^* = \frac{(C_0 - C^*) \times liquid\ volume}{Bead\ volume \times (1-\varepsilon)} \qquad (4.1)$$

Where C_0 is the initial protein concentration of liquid phase, q^* and C^* are equilibrium concentrations for solid and liquid phases, respectively, and ε is the void fraction assumed for the bead bed settled in the graduated cylinder after 48 hours.
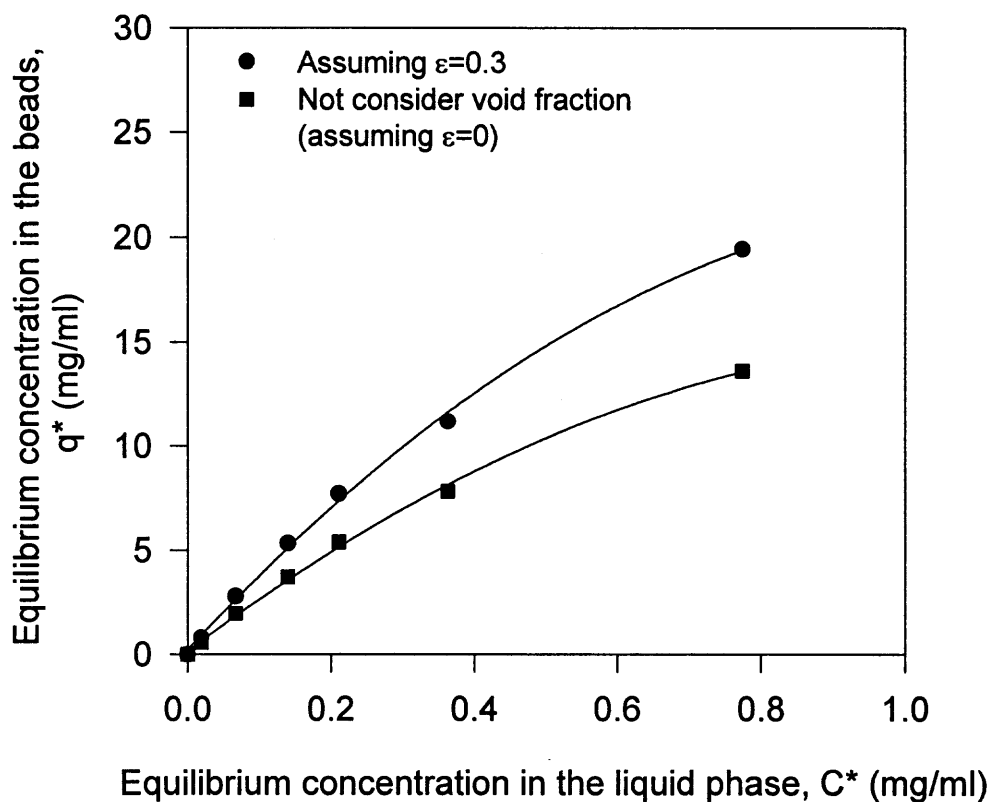
Figure 4.25 Adsorption isotherm for Mb on DEAE Sepharose Fast Flow beads (pH 8.5)

If one assumes that Langmuir isotherm is valid, then

$$q^* = \frac{q_m C^*}{K_d + C^*}$$
(4.2)

Where q_m is the maximum adsorption capacity and K_d is the dissociation constant. This equation can be written in the following double-reciprocal plot form (useful for the experimental data obtained with the protein(s) at low concentration(s) (Mao and Hearn 1996)):

$$\frac{1}{q^*} = \frac{K_d}{q_m}\frac{1}{C^*} + \frac{1}{q_m} \qquad (4.3)$$

Alternatively, a semireciprocal plot (provides more weight to the data obtained at higher adsorbate concentrations (Mao and Hearn 1996)) can be developed:

$$\frac{C^*}{q^*} = \frac{1}{q_m}C^* + \frac{K_d}{q_m} \qquad (4.4)$$

Additionally, the Scatchard plot (nonlinear Scatchard plots are indicative for adsorption away from Langmuir behavior (Mao and Hearn 1996)):

$$\frac{q^*}{C^*} = -\frac{1}{K_d}q^* + \frac{q_m}{K_d} \qquad (4.5)$$

When the protein concentration in the liquid is low, a linear relationship can be used.

$$q^* = \frac{q_m C^*}{K_d} = KC^* \qquad (4.6)$$

The analysis for isotherm of Mb adsorption on DEAE Sepharose Fast Flow beads using eqs 4.4 and 4.5 is shown in Figure 4.26. Double reciprocal plot is not shown in Figure 4.26 because it does not give the intercept value which provides the information on q_m. Results in Figure 4.26 show that the adsorption isotherm of Mb on the beads is quite close to the Langmuir adsorption type. The maximum adsorption capacity of Mb on DEAE Sepharose Fast Flow beads is 31.1 mg/ml according to Scatchard plot without considering the void fraction ε. If $\varepsilon = 0.3$ is considered, the maximum adsorption capacity of Mb on the beads is 44.46 mg/ml according to the Scatchard plot.
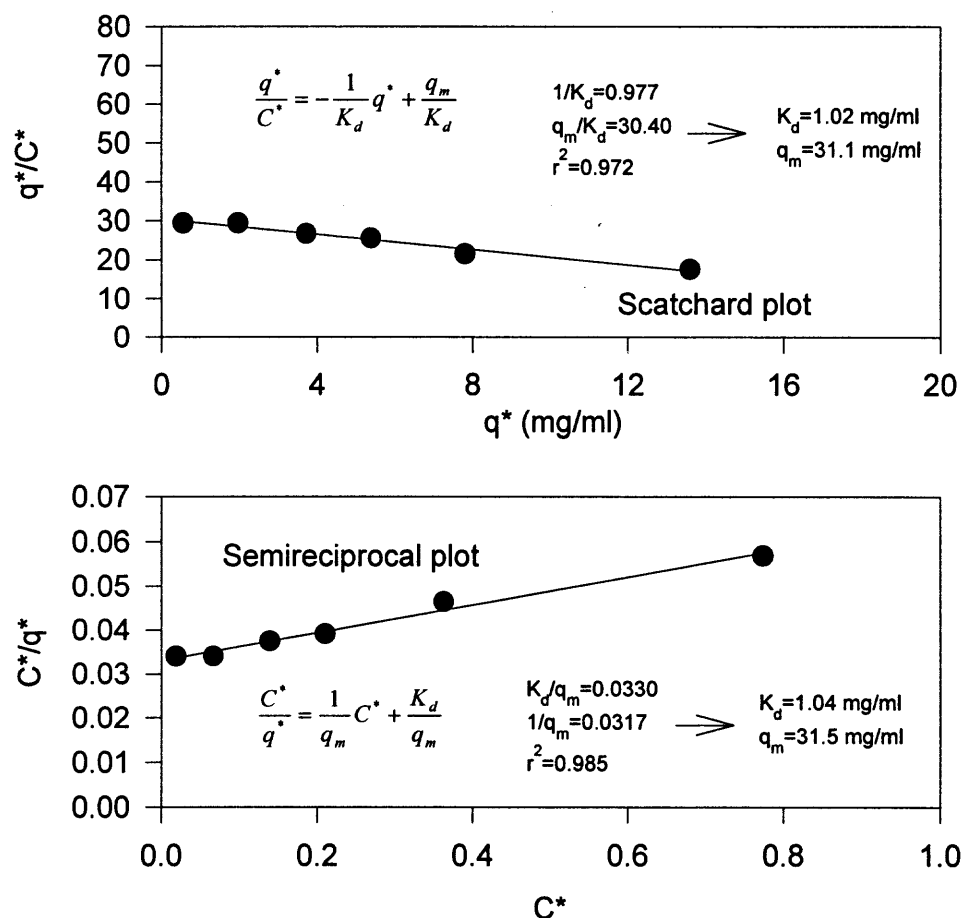
Figure 4.26 Scatchard plot and semireciprocal plot for the isotherm of Mb adsorption on DEAE Sepharose Fast Flow beads using the data in Figure 4.25 without considering ε

Results of the measurements of the adsorption isotherm of β-LG on DEAE Sepharose Fast Flow beads are shown in Figure 4.27. It took much longer time for the adsorption of β-LG on the beads to reach equilibrium. The experiment needed to be continued overnight. Results shown in Figure 4.27 are a typical set of data from 24 hours adsorption. Solid phase concentrations were calculated by eq 4.1. Figure 4.28 provides the regression results using eqs 4.3, 4.4 and 4.5 showing that the adsorption equilibrium

is essentially Langmuir type and the three methods yield very close values of q_m which

from the Scatchard plot yields q_m = 115 mg/ml. Similarly if the void fraction ε = 0.3 is

considered, the maximum adsorption capacity of β-LG adsorption on the beads is 164.2

mg/ml according to Scatchard plot.
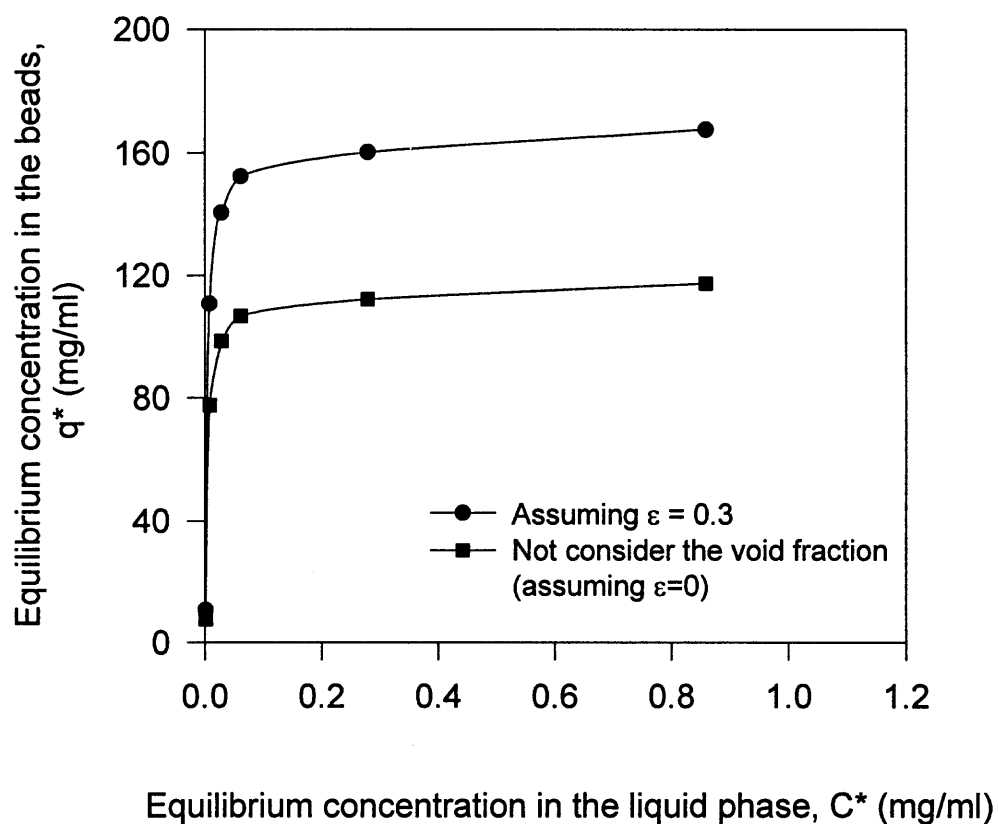
Figure 4.27 Adsorption isotherm of β-LG on DEAE Sepharose Fast Flow beads (pH 8.5)
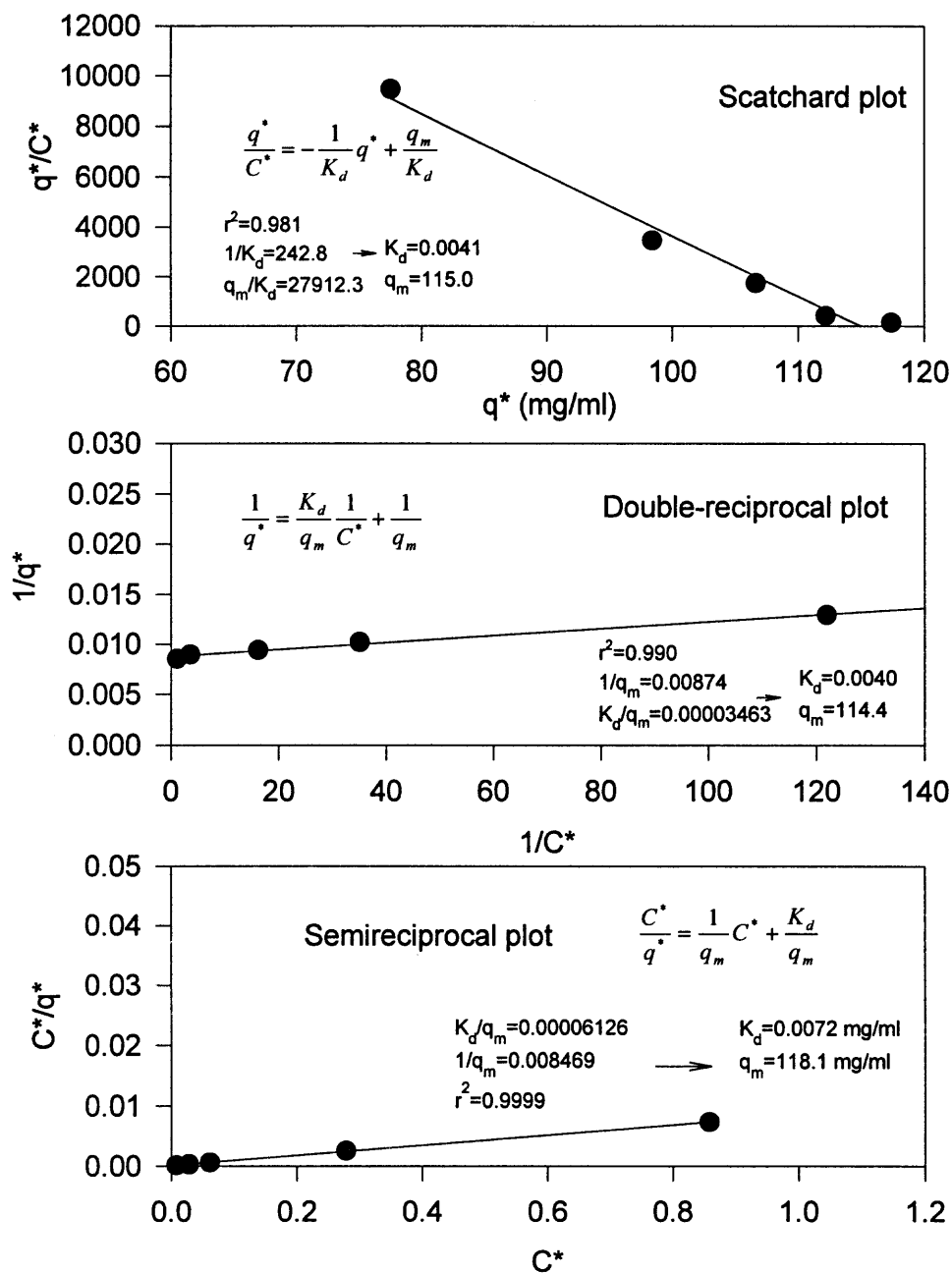
Figure 4.28 Analysis for the isotherm of β-LG adsorption on DEAE Sepharose Fast Flow beads using the data in Figure 4.27 without considering the void fraction ε

A similar approach was used for adsorption of α-LA on DEAE Sepharose Fast Flow beads. The adsorption isotherm is shown in Figure 4.29. It took less than one hour for the adsorption of α-LA on the beads to reach equilibrium. Solid phase concentrations were calculated by eq 4.1. Figure 4.30 provides the regression results using eqs 4.3, 4.4 and 4.5; the figures show that by the method of Scatchard plot the adsorption equilibrium deviates considerably from Langmuir type although the three methods give very close values of q_m (q_m = 76.6 mg/ml from the Scatchard plot). Similarly if ε = 0.3 is considered, the maximum adsorption capacity of α-LA adsorption on the beads is 109.4 mg/ml according to the Scatchard plot.

Freundlich isotherm (eq 4.7) was also employed to describe the adsorption of α-LA on the beads:

$$q^* = K \ C^{*\frac{1}{n}} \tag{4.7}$$

which can be written as

$$\ln q^* = \ln K + \frac{1}{n}\ln C^* \tag{4.8}$$

The result is shown in Figure 4.31 where Freundlich isotherm is used to describe α-LA adsorption on the beads. If the first two sets of data in the low concentration range are neglected, a linear relationship can be obtained for $\ln q^*$ with $\ln C^*$. The value of K = 79.0 for the case without considering the void fraction ε and K = 112.8 for the case assuming ε = 0.3. These values are quite close to q_m values from Langmuir type analysis. The available capacity of DEAE Sepharose Fast Flow beads for α-LA is 100 mg/ml which was determined under conditions using 50 mM Tris-HCl .at pH 8.3 (Amersham Pharmacia Biotech 1995) (void fraction of the bed is not indicated in the information).

Thus, the values of q_m for α-LA obtained in this study are close to that indicated by the

manufacturer of the beads.
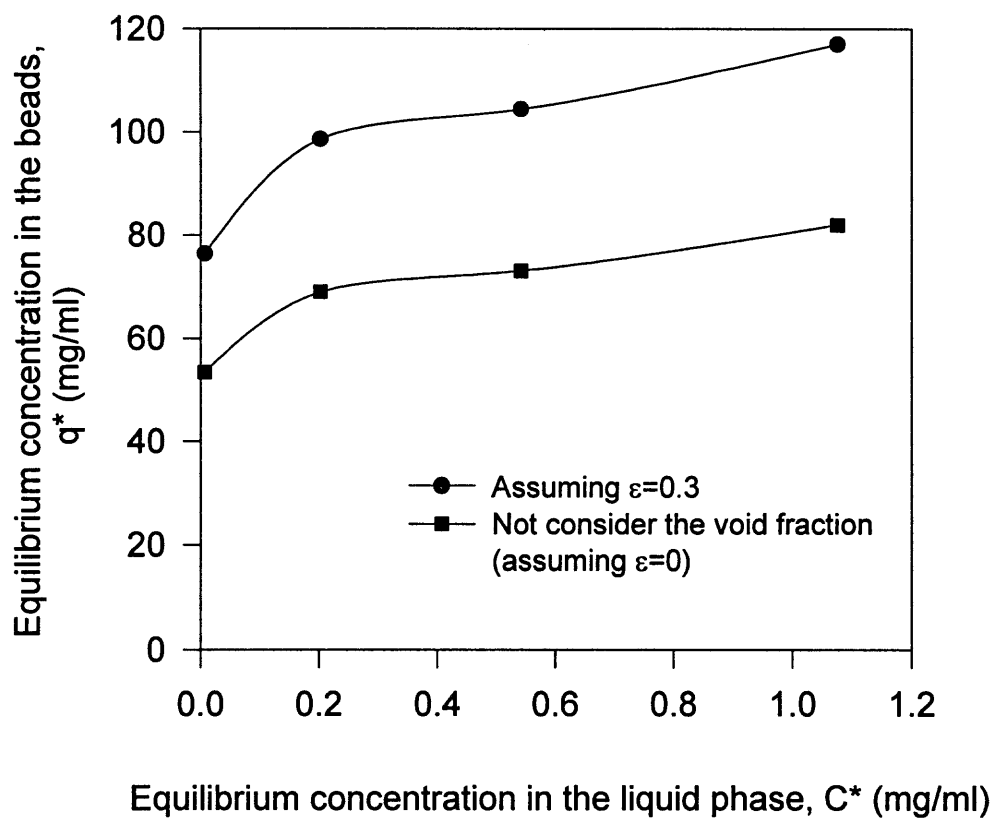
Figure 4.29 Adsorption isotherm of α-LA on DEAE Sepharose Fast Flow beads (pH 8.5)

Scatchard plot

$$\frac{q^*}{C^*} = -\frac{1}{K_d}q^* + \frac{q_m}{K_d}$$

r^2=0.815
$1/K_d$=284.23 → K_d=0.0035
q_m/K_d=21769.6 q_m=76.6

q* (mg/ml)

Double-reciprocal plot

$$\frac{1}{q^*} = \frac{K_d}{q_m}\frac{1}{C^*} + \frac{1}{q_m}$$

r^2=0.898
$1/q_m$=0.0134 → K_d=0.0028
K_d/q_m=0.0000375 q_m=74.6

1/C*

Semireciprocal plot $\dfrac{C^*}{q^*} = \dfrac{1}{q_m}C^* + \dfrac{K_d}{q_m}$

K_d/q_m=0.00037596 K_d=0.031 mg/ml
$1/q_m$=0.0121   → q_m=82.6 mg/ml
r^2=0.996

C*
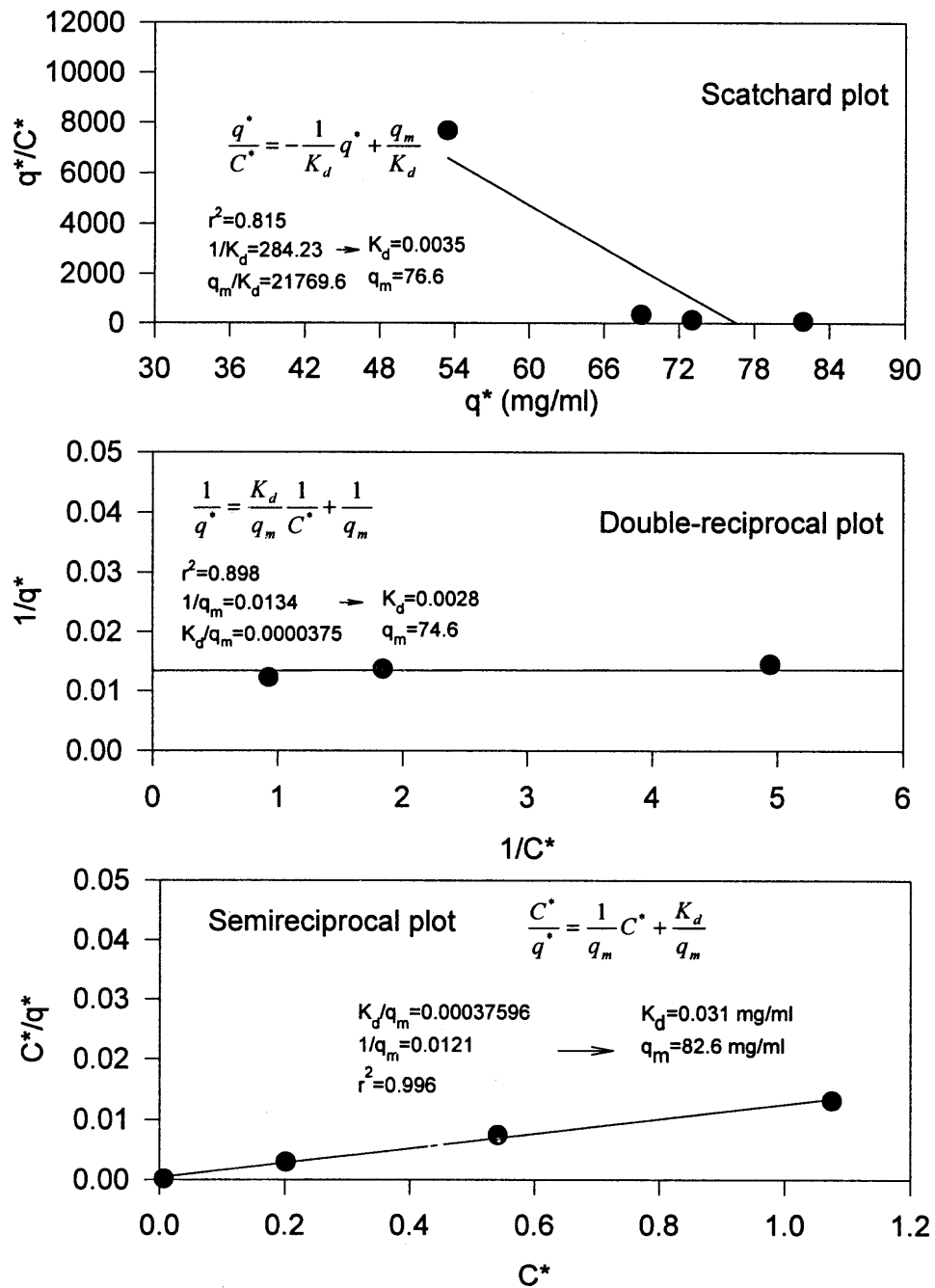
Figure 4.30 Analysis for the adsorption isotherm of α-LA on DEAE Sepharose Fast Flow beads using the data in Figure 4.29 without considering the void fraction ε
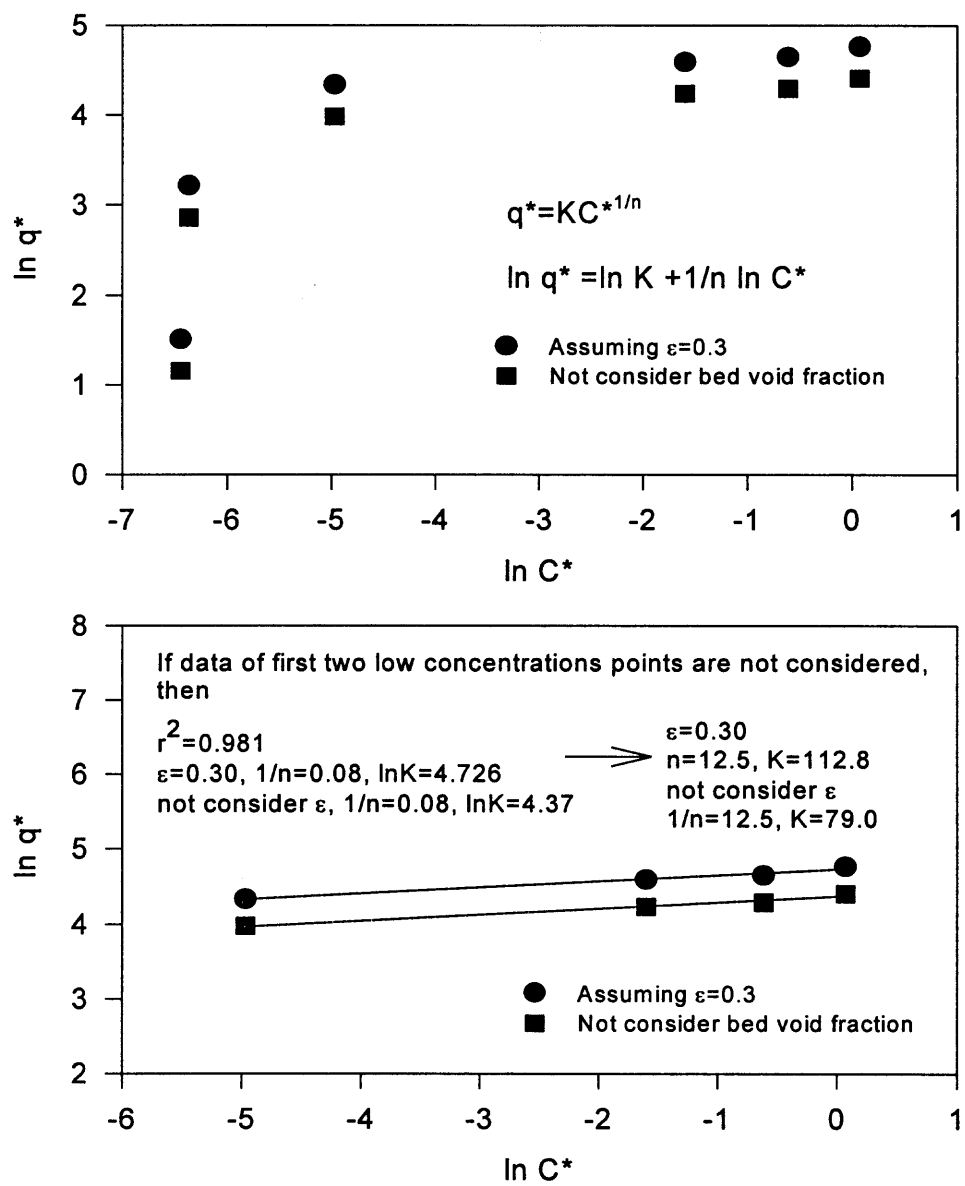
Figure 4.31 Freundlich isotherm relationship for α-LA adsorption on DEAE Sepharose Fast Flow beads (pH 8.5)

4.7. Concluding Remarks

This Chapter presented the experimental results of this research for different operations using the integrated device: these include one cycle operation with different combinations of loading and elution modes as well as cyclic operation of this process with clean feeds or with a yeast suspension using tube-side elution (Table 4.4). Several binary protein mixtures have been separated through these processes via this device. At this point, mathematical descriptions are needed to help us further understand and efficiently use this integrated process.

Table 4.4 Different combinations of the operating modes presented in this Chapter using the integrated device

	One cycle operation	Cyclic operation
Shell-side loading + Shell-side elution	X	
Shell-side loading + Tube-side elution		
Tube-side loading + Shell-side elution	X	
Tube-side loading + Tube-side elution	X	X

CHAPTER 5

PRESSURE AND FLUX PROFILES IN THE INTEGRATED DEVICE

5.1 Introduction

Hollow fiber membranes are extensively employed in a variety of bioseparation processes, e.g., ultrafiltration, microfiltration, reverse osmosis, etc. Adsorbents and chromatographic resin beads are also widely used in downstream processing. In this study, two hollow fiber ultrafiltration cartridges were packed on the shell side with chromatographic resin beads. Such devices and the corresponding separation methods integrate feed broth clarification by the microfiltration/ultrafiltration membrane with bioproduct purification by the shell-side resin beads either as an adsorbent or as a stationary phase in elution chromatography. The potential attractiveness of such integrated bioseparation devices needs to be evaluated and compared against traditional sequential processing. A first step in this direction involves the determination of pressure and flux profiles in the integrated devices.

In this study, the flow patterns in tube-side elution-based processes are such that any permeate, produced from the tube-side feed or eluent, flows out through the regular shell-side permeate outlet (Figure 2.1). There is no Starling flow. On the other hand, the flow pattern in Molinari et al. (1990) (Figure 5.1) is dominated by the highly restricted flow through the shell-side permeate outlet during the solute loading stage which causes a considerable amount of permeate to come back to the retentate stream; there is therefore Starling flow to some extent. The flow situation in Molinari et al. (1990) is also quite close to that in hollow-fiber bioreactors (HFBRs) in which mammalian cells are immobilized on the shell side (the extracapillary space (ECS)) and the substrate-

containing solution flows through the tube side. However, there is one difference, namely, there is no permeate flow at all in HFBRs and there is pure Starling flow as modeled by a number of investigators (Heath, Belfort, Hammer, Mirer, and Pimbley 1990; Taylor, Piret, and Bowen 1994; Patkar, Koska, Taylor, Bowen and Piret 1995; Koska, Bowen and Piret 1997).

Permeate

Closed port

Retentate

Crude protein mixture
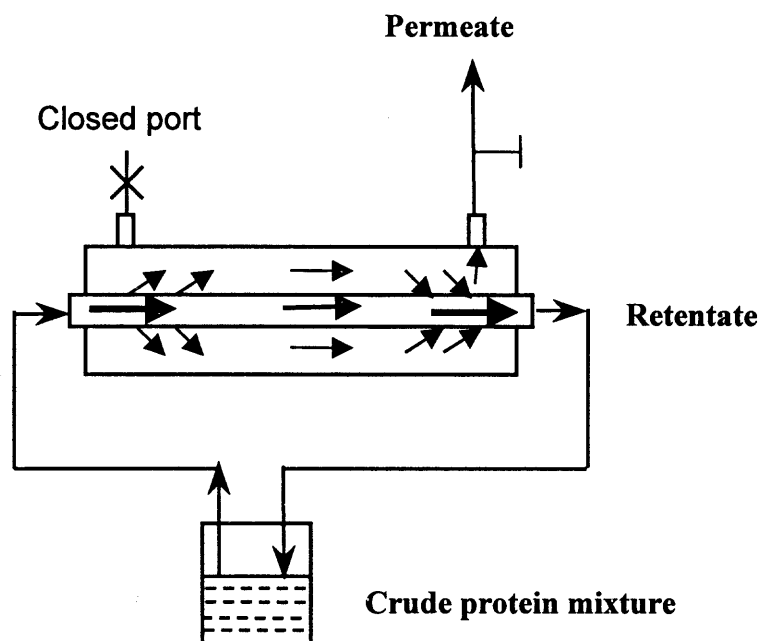
Figure 5.1 Configuration of the device containing membrane and adsorbent beads during filtration-cum-loading in Molinari et al. (1990)

There are other engineering applications where beads are located on the shell side of microporous hollow fiber module with the fluid phase introduced through the fiber bore. For example, Pan and McMinis (1992) described a hollow-fiber adsorber (HFA) that can be applied to adsorption processes. Minute adsorbent particles were held in either the shell space or the fiber bore of the microporous hollow-fiber membranes, with the gas stream flowing through the other side and maintaining good contact between the gas

stream and the adsorbent. Separation occurs primarily by selective adsorption on the adsorbents and not by selective permeation through the fiber wall. As mentioned in Chapter 2, the HFA offers many attractive advantages such as low pressure drop; reduction of particle attrition; choice of fine particles; uniform contact of gas with adsorbents; use of fast PSA cycles to enhance the process capacity (Feng, Pan, McMinis, Ivory and Ghosh 1998; Gilleskie, Parkar and Cussler 1995).

This Chapter is focused on developing pressure profiles and solvent flux profiles in bead-filled hollow fiber microfiltration/ultrafiltration devices for different operational modes. First, the operation modes for which the feed is flowing in the fiber bore and the permeate goes out from the shell-side outlet will be discussed. Since some other types of operations such as shell-side elution and backflushing were also performed in this research, the operation modes for introducing the eluent (shell-side elution) or buffer (for backflushing) from the shell-side inlet will be discussed at the end of this Chapter. Due to the presence of the ES packed at the permeate outlet port on the shell side (Figures 2.1), pressure profiles and solvent flux profiles will be developed and discussed for this configuration as well.

5.2 Feed Introduced from the Fiber Bore

5.2.1 Theory

An analysis of the integrated device will be provided to develop quantitative estimates of length-wise profiles of flow rates, fluxes and transmembrane pressures in the bead-filled hollow fiber modules; emphasis will be placed on how these are interrelated for different modes of operations of such devices. Only steady state operation is considered. The

configurations of the devices are shown in Figures 2.1 and 5.1. For the process of

filtration, the feed is assumed to be pure water so that the permeation velocity or volume

flux J_{vz} (m^3/m^2.s) through the membrane at any axial location z is given by

$$J_{vz} = A(P_F - P_P)_z \qquad (5.1)$$

Where A is the pure water membrane permeation parameter (m/Pa.s). The feed is flowing

in the tube side of the module; the local volumetric flow rate in tube side, Q_{Fz} (m^3/s), is

such that

$$\frac{d Q_{Fz}}{dz} = -N_0 (\pi d_i J_{vz}) \qquad (5.2)$$

where N_0 is the number of fibers inside the module and d_i is the I.D. of the fiber lumen.

The total mass balance for the flow distribution in the hollow fiber module at any

location z in the module is

$$Q_{F0} = Q_{Fz} + Q_{Pz} \qquad (5.3)$$

where Q_{Pz} is the local volumetric permeate flow rate in the shell side and Q_{F0} is the

volumetric feed flow rate at the tube-side inlet (z = 0). Integrating eq 5.2, the following

expression for Q_{Fz} is obtained:

$$Q_{Fz} = Q_{F0} - N_0 \pi d_i \int_0^z J_{vz} \, dz \qquad (5.4a)$$

Combine with eq 5.3

$$Q_{Pz} = N_0 \pi d_i \int_0^z J_{vz} \, dz \qquad (5.4b)$$

The pressure drop inside each fiber is described by the Hagen-Poiseuille flow law:

$$\frac{dP_F}{dz} = -\frac{128\mu_F Q_{si}}{\pi d_i^4} = -\frac{8\mu_F Q_{si}}{\pi r_i^4} \qquad (5.5)$$

where Q_{si} is the volumetric flow rate in a single fiber:

$$Q_{si} = \frac{Q_{Fz}}{N_0} = \frac{Q_{F0}}{N_0} - \pi \ d_i \int_0^z J_{vz} \ dz \qquad (5.6)$$

and $r_i = d_i/2$. Substitute eq 5.6 into eq 5.5

$$\frac{dP_F}{dz} = -\frac{128\mu_F}{\pi d_i^4} \times (\frac{Q_{F0}}{N_0} - \pi \ d_i \int_0^z J_{vz} \ dz) = -\frac{128\mu_F}{d_i^3} \times (\frac{Q_{F0}}{N_0\pi d_i} - \int_0^z J_{vz} \ dz) \qquad (5.7)$$

For pressure drop in the shell-side bed, Blake-Kozeny equation (Bird, Stewart and Lightfoot 1960) for a packed bed is used:

$$\frac{dP_P}{dz} = -\frac{150 \ (1-\varepsilon)^2}{d_p^2 \varepsilon^3} \ \mu_P \ u_P \qquad (5.8)$$

Here d_p is the particle diameter, ε is the void fraction of the shell-side bed, u_p is the superficial velocity which can be expressed by

$$u_P = \frac{Q_{Pz}}{S_s} = \frac{4N_0\pi d_i}{\pi(D_i^2 - N_0 d_o^2)} \int_0^z J_{vz} dz \qquad (5.9a)$$

Where S_s is the cross-sectional area of the shell side,

$$S_s = \frac{(\pi D_i^2 - N_0\pi d_o^2)}{4} \qquad (5.9b)$$

and D_i is the housing internal diameter, d_o is the O.D. of a single fiber. Substituting eq 5.9a into eq 5.8, the following equation is obtained:

$$\frac{dP_P}{dz} = -\frac{150 \ (1-\varepsilon)^2}{d_p^2 \varepsilon^3} \ \mu_P \ \frac{4N_0\pi d_i}{\pi(D_i^2 - N_0 d_o^2)} \int_0^z J_{vz} dz \qquad (5.10)$$

Rewrite eqs 5.7 and 5.10 appropriately and get the following three governing equations:

$$J_{vz} = A(P_F - P_P)_z \qquad (5.1)$$

$$\frac{dP_F}{dz} = -M \times (N - \int_0^z J_{vz} \ dz) \qquad (5.11)$$

$$\frac{dP_P}{dz} = -B \int_0^z J_{vz} dz \qquad (5.12)$$

where

$$M = \frac{128\mu_F}{d_i^3} \ , \ N = \frac{Q_{F0}}{N_0 \pi d_i} \quad (5.13); \quad B = \frac{150 \ (1-\varepsilon)^2}{d_p^2 \varepsilon^3} \ \mu_P \ \frac{N_0 \pi d_i}{\pi (D_i^2 - N_0 d_o^2)/4} \quad (5.14)$$

Here parameters A and B are assumed not to change along the module length. Therefore, by differentiating eq 5.1 and combining with eqs 5.11 and 5.12, one gets

$$\frac{dJ_{vz}}{dz} = A \times (\frac{dP_F}{dz} - \frac{dP_P}{dz})$$

$$= -AMN + AM \int_0^z J_{vz} dz + AB \int_0^z J_{vz} dz \qquad (5.15)$$

and by differentiating eq 5.15 again, a second-order differential equation is obtained as follows:

$$\frac{d^2 J_{vz}}{dz^2} = A \times (M+B)J_{vz} \qquad (5.16)$$

Let
$$\beta^2 = A(M+B) \qquad (5.17)$$

The solution of eq 5.16 is

$$J_{vz} = A_1 \cosh(\beta z) + A_2 \sinh(\beta z) \qquad (5.18a)$$

@ z=0,
$$J_{v0} = A_1 = A(P_{F0} - P_{P0}) \qquad (5.18b)$$

@ z=L,
$$J_{vL} = A_1 \cosh(\beta L) + A_2 \sinh(\beta L) = A(P_{FL} - P_{PL}) \qquad (5.18c)$$

Equation 5.18a provides the local permeation flux profile in the module during filtration operation. By substituting eq 5.18a into eq 5.11, and rearranging, one gets

$$\frac{dP_F}{dz} = -MN + \frac{M}{\beta}\{A_1 \sinh(\beta z) + A_2[\cosh(\beta z) - 1]\} \qquad (5.19)$$

Integrate from z = 0 to z

$$P_{Fz} = P_{F0} - M(N + \frac{A_2}{\beta})z + \frac{M}{\beta^2}\{A_1[\cosh(\beta z) - 1] + A_2 \sinh(\beta z)\} \tag{5.20a}$$

@ z=0, $P_{Fz} = P_{F0}$

$$\tag{5.20b}$$

@ z=L, $P_{FL} = P_{F0} - M(N + \frac{A_2}{\beta})L + \frac{M}{\beta^2}\{A_1[\cosh(\beta L) - 1] + A_2 \sinh(\beta L)\}$

Substitute eq 5.18a into eq 5.12, and rearrange; this leads to

$$\frac{dP_P}{dz} = -\frac{B}{\beta}\{A_1 \sinh(\beta z) + A_2[\cosh(\beta z) - 1]\} \tag{5.21}$$

Integrating from z to L yields

$$P_{Pz} = P_{PL} + \frac{B}{\beta^2}\{A_1[\cosh(\beta L) - \cosh(\beta z)] + A_2[\sinh(\beta L) - \sinh(\beta z)] - A_2\beta(L - z)\} \tag{5.22a}$$

@ z=0, $\qquad P_{P0} = P_{PL} + \frac{B}{\beta^2}\{A_1[\cosh(\beta L) - 1] + A_2 \sinh(\beta L) - A_2\beta L\}$

$$\tag{5.22b}$$

@ z=L, $\qquad P_{Pz} = P_{PL}$

Equations 5.20a and 5.22a are the solutions for pressure profiles in tube side and shell side respectively for known boundary conditions, namely, P_{F0}, P_{PL} and Q_{F0}.

Substituting eq 5.18a into eqs 4.4a and 4.4b, the flow rates in both sides can be obtained via the following expressions:

$$Q_{Fz} = Q_{F0} - \frac{N_0\pi d_i}{\beta}\{A_1 \sinh(\beta z) + A_2[\cosh(\beta z) - 1]\} \tag{5.23a}$$

$$Q_{Pz} = \frac{N_0\pi d_i}{\beta}\{A_1 \sinh(\beta z) + A_2[\cosh(\beta z) - 1]\} \tag{5.23b}$$

@ z= 0, $\qquad Q_{F0} = Q_{F0}, \qquad Q_{P0} = 0$

@ z= L, $\qquad Q_{FL} = Q_{F0} - \frac{N_0\pi d_i}{\beta}\{A_1 \sinh(\beta L) + A_2[\cosh(\beta L) - 1]\} \tag{5.24a}$

$$Q_{PL} = \frac{N_0 \pi d_i}{\beta} \{A_1 \sinh(\beta L) + A_2 [\cosh(\beta L) - 1]\} \tag{5.24b}$$

Equations 5.24a and 5.24b provide the flow rates at the end point of the tube side and the shell side of the module during filtration. Total permeate collected at the permeate port could be calculated by eq 5.24b. The average velocities at any location z in both sides could be obtained by dividing eqs 5.23a and 5.23b by the cross-sectional areas of tube side and shell side, respectively.

5.2.1.1 Constants A_1 and A_2: To use the model, constants A_1 and A_2 have to be determined first based on the specific experimental conditions. This will be considered under several categories.

Case 1: The permeate flows out through the bead-filled shell-side permeate outlet without any restriction – conventional filtration

For this case, the feed flow rate (Q_{F0}), the feed inlet pressure (P_{F0}) and the permeate exit pressure (P_{PL}) (which is the atmospheric pressure) are the known boundary conditions. Expressions for A_1 and A_2 which are given below can be obtained by solving the group of eqs 5.18b, 5.18c, 5.20b and 5.22b:

$$A_2 = -\frac{AMN}{\beta} \tag{5.25}$$

$$A_1 = \frac{A\{(P_{F0} - MNL - P_{PL}) - [\frac{ML}{\beta} + \frac{B}{\beta^2} \sinh(\beta L)]A_2\}}{\cosh(\beta L) - \frac{AM}{\beta^2}[\cosh(\beta L) - 1]} \tag{5.26}$$

Substituting eqs 5.25 and 5.26 into eqs 5.20a, 5.22a, 5.23a, 5.23b and 5.18a, the pressure, flow rate and flux profiles for a particular filtration-loading operation of a specific bead-filled hollow fiber membrane module can be obtained.

Case 2: Permeate flow control

In this case, the permeate exit pressure P_{PL} is unknown; however, the permeate flow rate Q_{PL} has a fixed value. Feed flow rate (Q_{F0}) and feed inlet pressure (P_{F0}) are the other known boundary conditions. Solving eqs 5.18b, 5.18c, 5.20b, 5.22b, and 5.24b, one gets A_1 and A_2:

$$A_1 = \frac{\dfrac{Q_{PL}\beta}{N_0 \pi d_i} - A_2[\cosh(\beta L) - 1]}{\sinh(\beta L)} \tag{5.27}$$

$$A_2 = -\frac{AMN}{\beta} \tag{5.25}$$

Rearranging eq 5.18b leads to

$$P_{P0} = P_{F0} - \frac{A_1}{A} \tag{5.28}$$

Integrate eq 5.21 from z = 0 to z,

$$P_{Pz} = P_{P0} - \frac{B}{\beta^2}\{A_1[\cosh(\beta z) - 1] + A_2 \sinh(\beta z) - A_2 \beta z\} \tag{5.29}$$

Substituting eqs 5.25 and 5.27 into eqs 5.20a, 5.29, 5.23a, 5.23b and 5.18a, the pressure, flow rate and flux profiles for a particular permeate flow control-based filtration-loading operation (fixed Q_{PL}) of a specific bead-filled hollow fiber membrane module will be obtained.

There are two special cases in this category: (i) Starling flow without permeate flow at all ($Q_{PL} = 0$) which is actually the case of HFBRs as stated in the Section 5.1 - the permeate side outlet is closed to achieve Starling flow only; and (ii) the tube-side elution situation ($Q_{PL} = Q_{F0}$) which was studied extensively in the experimental part of this dissertation. Expressions of A_1 for the two cases are, respectively,

$$Q_{PL}=0; \qquad A_1 = \frac{A_2[\cosh(\beta L)-1]}{\sinh(\beta L)} \qquad (5.30a)$$

$$Q_{PL}= Q_{F0}; \qquad A_1 = \frac{\dfrac{Q_{F0}\beta}{N_0\pi d_i} - A_2[\cosh(\beta L)-1]}{\sinh(\beta L)} \qquad (5.30b)$$

However, the boundary condition for tube-side elution is different; instead of a known tube-side feed pressure (P_{F0}), the permeate exit pressure (P_{PL}) which is atmospheric is used. Therefore the shell-side pressure profile and shell-side inlet pressure (P_{P0}) can be obtained by substituting eqs 5.25 and 5.30b into eq 5.22a and 5.22b. The corresponding P_{F0} can be calculated by eq 5.18b:

$$P_{F0} = P_{P0} + \frac{A_1}{A} \qquad (5.31)$$

The pressure profile in the fiber lumen is obtained by the substitution of eqs 5.25, 5.30b and 5.31 into eq 5.20a. Flux and flow rate distributions can be obtained by substituting eqs 5.25, 5.30b into eqs 5.18a, 5.23a and 5.23b.

It is clear from above that the permeate flow rate could be controlled at a particular point by varying appropriate parameters.

5.2.1.2 Applying the Model to a Module Having an Extended Section at the Permeate Outlet: In the study of this dissertation, a short extended section (ES) is

packed with resin particles at the permeate outlet port on the shell side (Figure 2.1 and Table 3.3). The particles are kept in place by a 21 μm polyester mesh. The solutions obtained above need to be modified to include the effects of the ES on the module operation.

In the case of the ES, if one neglects the outlet mesh resistance, P_{PL} (at z = L) can be related to the atmospheric pressure. Use Blake-Kozeny equation (Bird, Stewart and Lightfoot 1960) for P_E, the local pressure in the ES:

$$\frac{dP_E}{dz_E} = -\frac{150(1-\varepsilon)^2}{d_p^2 \varepsilon^3} \mu_P \, u_E \tag{5.32a}$$

where u_E is the superficial velocity in the ES bed (obtained by dividing the total permeate flow rate by the cross-sectional area in the ES). Equation 5.32a can be rewritten as follows:

$$\frac{dP_E}{dz_E} = -B^* \, u_E = -B^{**} Q_{PL} \tag{5.32b}$$

$$B^* = \frac{150(1-\varepsilon)^2}{d_p^2 \varepsilon^3} \mu_P \, , \qquad B^{**} = \frac{B^*}{S_E} \tag{5.32c}$$

where S_E is the cross-sectional area of the ES. Integrate eq 5.32b from 0 to z_E corresponding to P_{PL} and P_E:

$$P_E = P_{PL} - B^{**} z_E Q_{PL} \tag{5.33a}$$

This prescribes the pressure profile in the ES of the hollow fiber module. At $z_E = L_E$ (length of the ES), eq 5.33a leads to

$$P_{PL} - P_{atm} = B^{**} L_E Q_{PL} = B' Q_{PL} \tag{5.33b}$$

where $\qquad\qquad B' = B^{**} L_E \tag{5.34a}$

From eq 5.14, one obtains

$$B = \frac{150\ (1-\varepsilon)^2}{d_p^2 \varepsilon^3}\ \mu_p\ \frac{N_0 \pi d_i}{\pi(D_i^2 - N_0 d_o^2)/4} = \frac{150\ (1-\varepsilon)^2}{d_p^2 \varepsilon^3}\ \mu_p\ \frac{N_0 \pi d_i}{S_S}$$

Since the same beads are used in the shell-side bed and the ES bed, one can assume that all the characteristics of the shell-side bed and the extended bed are the same; therefore combining eqs 5.14, 5.32c and 5.34a, one gets

$$B = B^*\frac{N_0 \pi d_i}{S_S} = B^{**}N_0 \pi d_i \frac{S_E}{S_S} = \frac{B'}{L_E}\frac{S_E}{S_S}N_0 \pi d_i \qquad (5.34b)$$

Write eq 5.34b as follows

$$B' = \frac{\phi L_E}{N_0 \pi d_i}B \qquad (5.34c)$$

Here ϕ is the ratio of the cross-sectional areas of the shell-side bed over the ES bed. In one case studied in this dissertation, module 1 has an additional ES packed over the fixed ES (Table 3.3). B' for the two ES can be obtained from the sum of B's for the fixed ES (B'_1) and the additional ES (B'_2).

For the pressure and flux profiles of the filtration-loading operation in the module with the extended section, constants A_1 and A_2 should be obtained first. Here consider only case 1 in Section 5.2.1.1 where all of the permeate flows out through the bead-filled shell-side permeate outlet and none comes back to the reject solution leaving the fiber bore exit. Substitution of eq 5.24b into eq 5.33b leads to

$$
\begin{aligned}
P_{PL} &= P_{atm} + B'\frac{N_0 \pi d_i}{\beta}\{A_1 \sinh(\beta L) + A_2[\cosh(\beta L)-1]\}\\
&= P_{atm} + T\{A_1 \sinh(\beta L) + A_2[\cosh(\beta L)-1]\}
\end{aligned} \qquad (5.35)
$$

where
$$T = B'\frac{N_0 \pi d_i}{\beta} \qquad (5.36)$$

Substituting eq 5.35 into eq 5.26, expression for A_1 is obtained,

$$A_1 = \frac{A[(P_{F0} - MNL - P_{atm}) - \{\frac{ML}{\beta} + T[\cosh(\beta L) - 1] + \frac{B}{\beta^2}\sinh(\beta L)\}A_2]}{AT\sinh(\beta L) + \cosh(\beta L) - \frac{AM}{\beta^2}[\cosh(\beta L) - 1]} \qquad (5.37)$$

A_2 is not changed in this case (see eq 5.25).

Therefore one can substitute eqs 5.25 and 5.37 into eqs 5.20a, 5.22a, 5.23a, 5.23b and 5.18a to get the pressure, flow rate and flux profiles for both shell side and tube side of the module with an ES. Same boundary conditions are applied as for case 1 in Section 5.2.1.1. Eq 5.33a could be used to describe the pressure profile in the ES. Flow rate in the ES is the total permeate flow rate Q_{PL}. The superficial velocity u_E can be obtained by dividing Q_{PL} by the cross-sectional area S_E.

5.2.1.3 Estimation of the Parameters A and B: In order to use the equations describing the pressure and flux profiles, two important parameters are needed: A, the membrane permeation parameter and B, the composite parameter for the bed reflecting the size of beads, void fraction, fiber number and dimensions, module housing size, and the fluid. Since the beads packed on the shell side are on the side of membrane back support and contact the porous backing, resistance is added to the convection of the fluid through the porous backing of the membrane. Thus the permeation rate (via the observed parameter A) is expected to decrease to some extent from that corresponding to the case of fibers-only situation without beads. Even if the same beads were packed for the same type of modules, the packing effect may be different (as will be seen later).

To obtain the values of the parameters A and B, experiments need to be done at particular values of the tube-side inlet pressure (P_{F0}) and shell-side inlet pressure (P_{P0}). For this problem, the relevant set of equations is as follows:

$$J_{v0} = A_1 = A(P_{F0} - P_{P0})$$

(5.18b)

$$J_{vL} = A_1 \cosh(\beta L) + A_2 \sinh(\beta L) = A(P_{FL} - P_{PL})$$

(5.18c)

$$P_{FL} = P_{F0} - M(N + \frac{A_2}{\beta})L + \frac{M}{\beta^2}\{A_1[\cosh(\beta L) - 1] + A_2 \sinh(\beta L)\}$$

(5.20b)

$$P_{P0} = P_{PL} + \frac{B}{\beta^2}\{A_1[\cosh(\beta L) - 1] + A_2 \sinh(\beta L) - A_2\beta L\}$$

(5.22b)

$$Q_{PL} = \frac{N_0 \pi d_i}{\beta}\{A_1 \sinh(\beta L) + A_2[\cosh(\beta L) - 1]\}$$

(5.24b)

$$P_{PL} - P_{atm} = B'Q_{PL}$$

(5.33b)

The boundary conditions (which can be experimentally measured) are:

@ z=0, $P_{Fz} = P_{F0}$, $P_{Pz} = P_{P0}$, $Q_{Fz} = Q_{F0}$

@ z=L, $Q_{Pz} = Q_{PL}$

@ $z_E = L_E$, $P_E = P_{atm}$, $Q_{PLE} = Q_{PL}$.

The ES is considered here since a module having an ES was used to measure A and B. A similar method can be used to determine these two parameters for a module without an ES. Trial and error was used to get A and B. Starting from eq 5.12, one has

$$\int_0^z J_{vz}dz = -\frac{1}{B}\frac{dP_P}{dz}$$

(5.38)

Substituting eq 5.38 into eq 5.11 leads to

$$\frac{dP_F}{dz} = -M \times (N + \frac{1}{B}\frac{dP_P}{dz})$$

(5.39)

$$dP_F = - MNdz - \frac{M}{B} dP_P \tag{5.40}$$

Integrate equation 5.40: P_F varies from P_{F0} to P_{FL}, z varies from 0 to L and P_P varies from P_{P0} to P_{PL}. Rearrange and obtain:

$$B = \frac{P_{P0} - P_{PL}}{NL - \frac{P_{F0} - P_{FL}}{M}} \tag{5.41}$$

An algorithm for programming based on the above equation group is given in Figure 5.2. By following this procedure, a Qbasic program is written to get the values of parameters A and B based on the experimentally measured data. For those modules without an ES, $B' = 0$, $P_{PL} = P_{atm}$; then parameters A and B can be obtained following the same procedure in Figure 5.2.

5.2.2 Experimental Methods

The experimental setup is described in Figure 3.5. To determine parameters A and B for the empty/bead-filled module, starting buffer was pumped through the fiber lumen at a certain feed flow rate and tube-side feed pressure. The shell-side inlet pressure and the permeate flow rate were measured during the filtration. The permeate port on the shell side was open to the atmosphere. Other experiments were run in a similar manner.

```
              ┌──────────────────┐
        ┌────►│  Input: guess A  │
        │     └──────────────────┘
        │              │
        │              ▼
        │     ┌──────────────────────────────┐
        │     │ A₁=A (P_F0-P_P0), eq 5.18b    │
        │     └──────────────────────────────┘
        │              │
        │              ▼
        │     ┌──────────────────┐
        │  ┌─►│  Input: guess B  │
        │  │  └──────────────────┘
        │  │           │
        │  │           ▼
        │  │  ┌──────────────────────────────────────┐
        │  │  │ Calculate β (eq 5.17), B' (eq 5.34c), A₂│
        │  │  │ (eq 5.25), P_PL (eq 5.33b) and P_FL    │
        │  │  │ (eq 5.20b)                             │
        │  │  └──────────────────────────────────────┘
        │  │           │
        │  │           ▼
        │  │  ┌──────────────────┐
        │  │  │ Calculate B using│
        │  │  │ equation 5.41    │
        │  │  └──────────────────┘
        │  │           │
        │  │           ▼
        │  │    No  ◄─────◇ B=input B? ◇
        │  └───────────         │ Yes
        │                       ▼
        │              ┌──────────────────┐
        │              │ Calculate Q_PL   │
        │              │ using equation   │
        │              │ 5.24b            │
        │              └──────────────────┘
        │                       │
        │   No                  ▼
        └──────◄──── ◇ Q_PL=experimental Q_PL? ◇
                               │ Yes
                               ▼
              ┌──────────────┐     ┌──────┐
              │ Output A and B│──►  │ End  │
              └──────────────┘     └──────┘
```
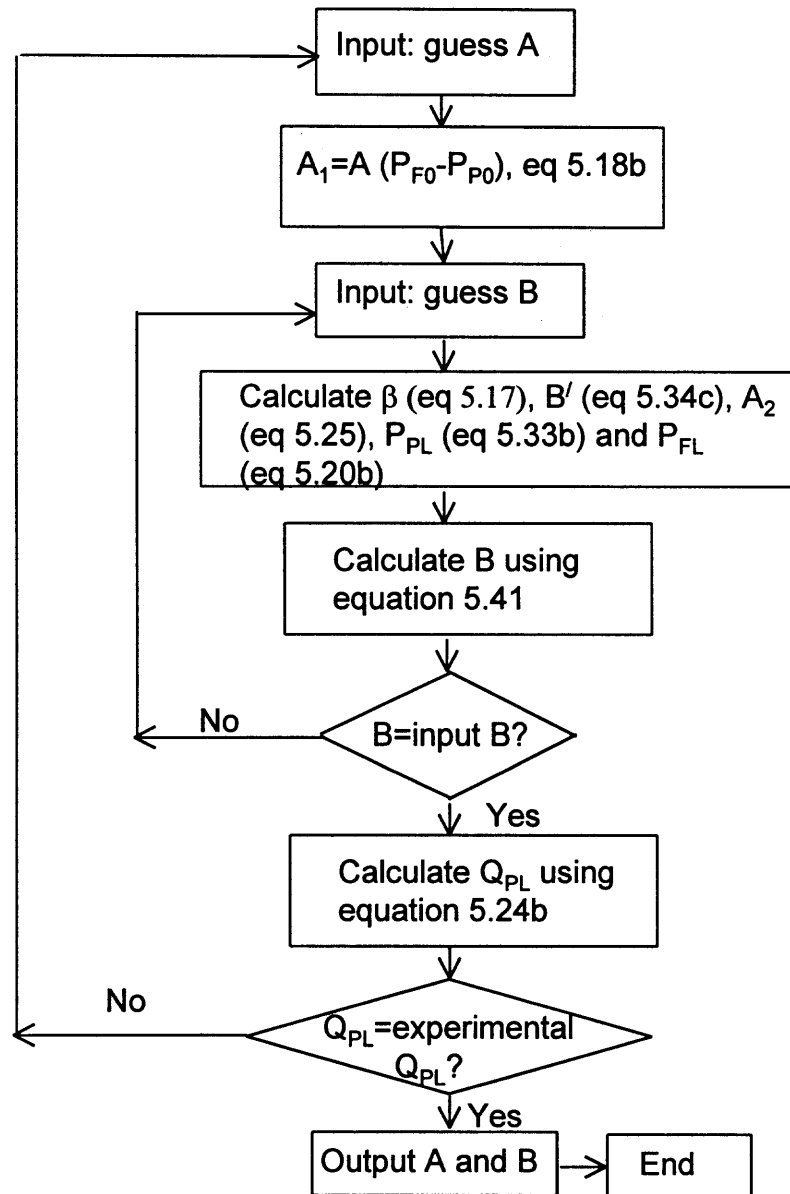
Figure 5.2 Program algorithm for determination of the parameters A and B

5.2.3 Results and Discussions

5.2.3.1 Parameters A and B for the Device: It was found experimentally that the

observed permeation rate parameter A was increased gradually with an increase of TMP

at the same feed flow rate Q_{F0}. A possible reason is that the increased TMP and the

increased flux pushes the beads further away from the porous support side of the

membrane which actually decreases the extra resistance encountered by the solvent flow due to the beads. For this calculation, the value of A was assumed to be constant along the module length. Values of the lumped parameter B were however, reasonably constant as a function of TMP for both modules which shows that the shell-side beds of both modules were essentially unaffected by the range of fluxes studied. Changes of A and B values with an increase in TMP are shown in Figure 5.3 for both modules 1 and 2 for an ES of ID 0.70 cm and length 1.7 cm at room temperature. Table 5.1 provides the averaged values for A and B for the TMP range of 2.0 - 4.0 psig which was used for loading in most of the experiments performed for this dissertation.

Table 5.1 Averaged A and B values and related information for modules 1 and 2 packed with DEAE Sepharose Fast Flow Beads

	A, m/Pa.s	B, Pa.s/m³	$\dfrac{A_{without\ beads}}{A_{with\ beads}}$	Void Fraction, ε
Module 1	1.857×10^{-10}	4.724×10^{11}	3.27	0.325
Module 2	3.225×10^{-10}	3.003×10^{11}	4.77	0.362

The length-averaged value of the permeation rate parameter A was reduced by about 3.27 and 4.77 times for modules 1 and 2 respectively compared to those without beads packed on the shell side (Table 3.2); this is to be expected. However, experiments using proteins in feed solution interestingly indicate that the protein transmission rate was increased due to the presence of the beads packed on the shell side (Table 4.2). Values of B are different for the two modules as well. Void fractions for the shell-side beds can be estimated from the B values by eq 5.14 to be 0.325 for module 1 and 0.362 for module 2.
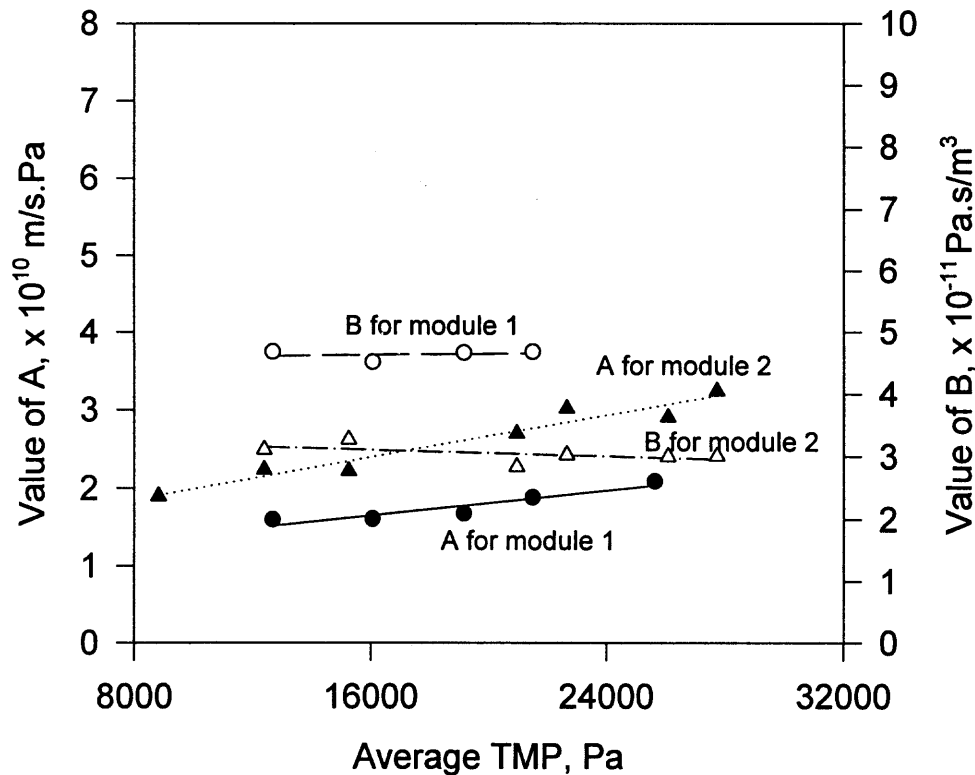
Figure 5.3 The effect of TMP on the parameters A and B. Average TMP = {(P_{F0} + P_{FL}) - (P_{P0} + P_{PL})}/2

The equation uses: Average TMP = $\{(P_{F0} + P_{FL}) - (P_{P0} + P_{PL})\}/2$

5.2.3.2 Simulations for Case 1- Conventional Filtration without any Restriction in the Permeate Outlet: In the experiments carried out, due to the pumping limitations, only 200-300 ml/min feed flow rate (Q_{F0}) was adopted; typically a feed inlet pressure of 7 psig was used. Figure 5.4 illustrates the simulation results for module 1 with the fixed ES (Table 3.3) using the above conditions. Values of A and B in Table 5.1 for module 1 were utilized. The solvent flux profile changes with the TMP profile. As the TMP increases, the solvent flux increases. Similarly, Figure 5.5 shows such a result using values of A and B in Table 5.1 for module 2. Flux for module 2 is higher than that of module 1 as module

2 has a higher A value, however, higher flux will cause higher shell-side pressure drop. From these two cases, it can be seen that due to the low feed flow rate used, tube-side pressure is essentially unchanged along the module length. Figure 5.6 shows a similar simulation result for module 1 with both fixed ES and the additional ES (Table 3.3). Comparing the results in Figures 5.4 and 5.6, lower flux and more uniform TMP are obtained for that with two ESs. The simulation results for the above three cases are quite close to the experimental data shown in Table 5.2.

Table 5.2 Comparison of the experimental data and the simulation results

	Q_{PL}, ml/min		P_{PO}, psig		P_{FL}, psig	
	Experi-mental	Calculated	Experi-mental	Calculated	Experi-mental	Calculated
Module 1 with fixed ES	6.39	6.57	5.95	6.00	6.9	6.87
Module 1 with 2 ESs	5.08	5.34	6.00	6.18	6.9	6.87
Module 2 with fixed ES	10 - 10.85	10.75	6.15	6.12	6.9	6.87

The experimental data shown in Table 5.2 are from the experiments for higher protein concentrations (20 times, see Figure 4.23 and Table 4.3) and for the yeast suspensions which are detailed in Chapter 4.
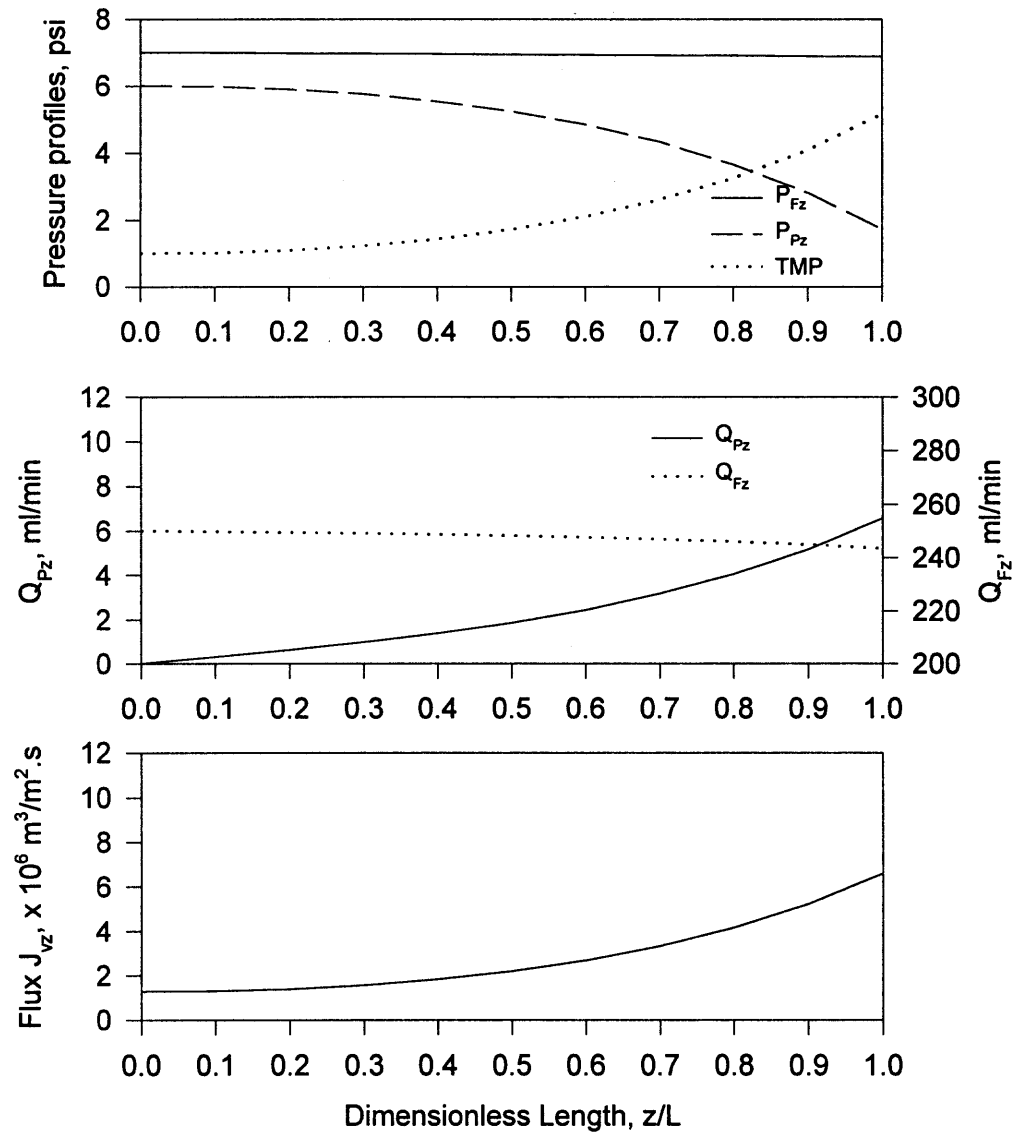
Figure 5.4 Simulation of the profiles for pressure, flow rate and flux. $A = 1.857 \times 10^{-10}$ m/Pa.s, $B = 4.724 \times 10^{11}$ Pa.s/m^3. Feed flow rate $Q_{F0} = 250$ ml/min. Feed inlet pressure $P_{F0} = 7.0$ psig. Module 1 (Table 3.2) with the fixed ES (Table 3.3).
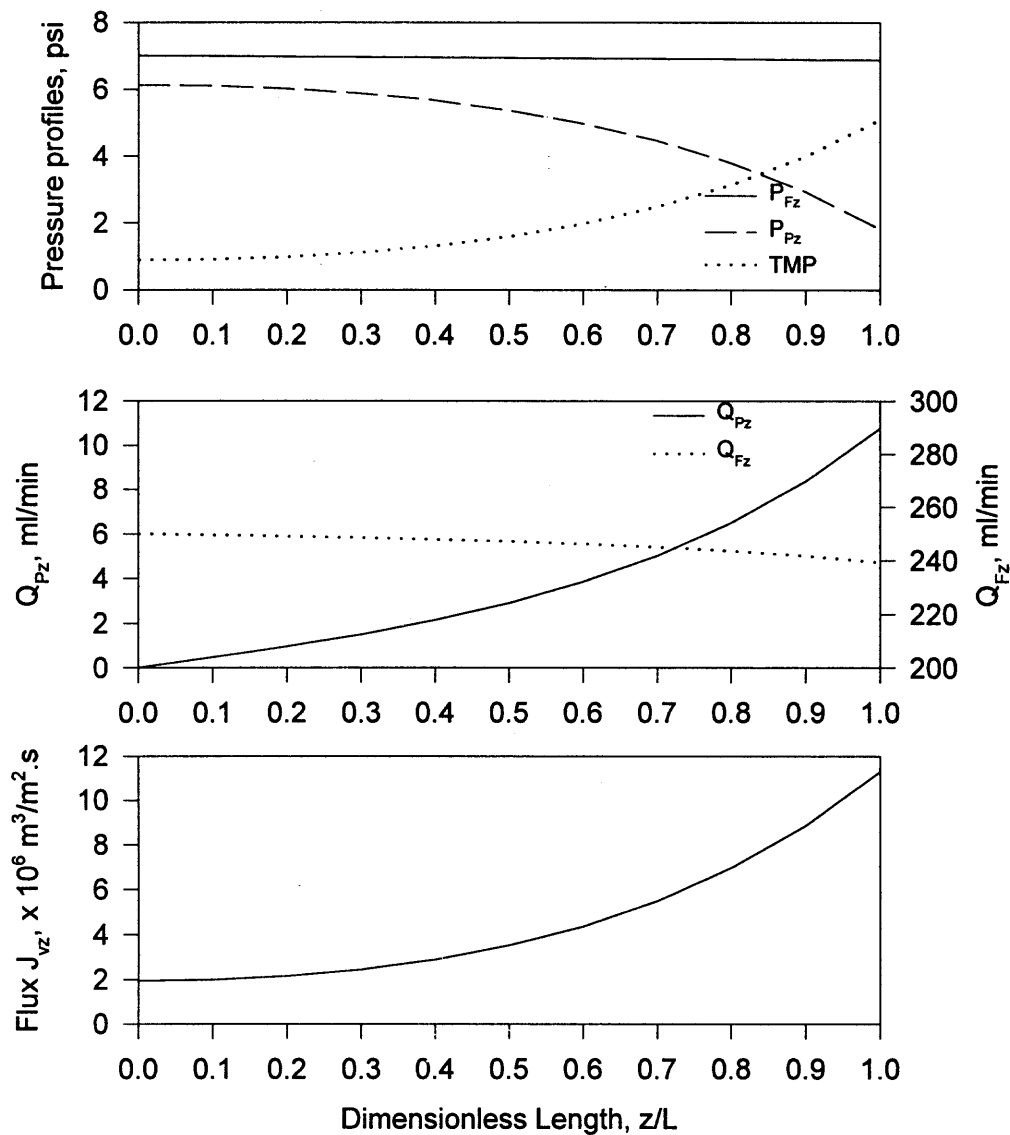
Figure 5.5 Simulation of the profiles for pressure, flow rate and flux. A = 3.225 × 10⁻¹⁰ m/Pa.s, B = 3.003 × 10¹¹ Pa.s/m³. Feed flow rate Q_{F0} = 250 ml/min. Feed inlet pressure P_{F0} = 7.0 psig. Module 2 (Table 3.2) with the fixed ES (Table 3.3).
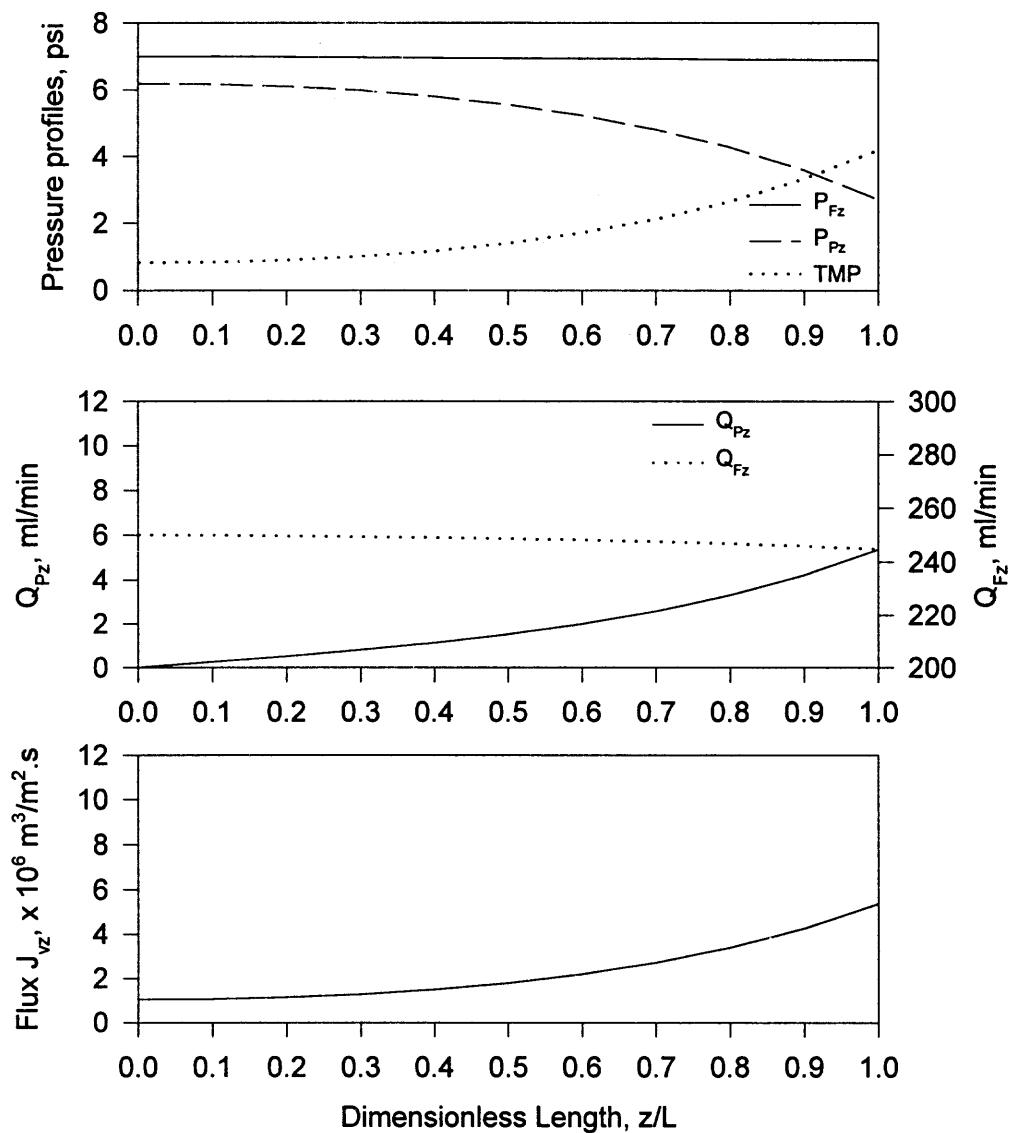
Figure 5.6 Simulation of the profiles for pressure, flow rate and flux. A = 1.857 × 10⁻¹⁰ m/Pa.s, B = 4.724 × 10¹¹ Pa.s/m³. Feed flow rate Q_{F0} = 250 ml/min. Feed inlet pressure P_{F0} = 7.0 psig. Module 1 (Table 3.2) with the fixed ES and the additional ES (Table 3.3).

In order to describe the uniformity of the transmembrane pressure profile, here a new parameter – uniformity factor α, is defined by eq 5.42.

$$\alpha = \frac{|TMP_0 - TMP_L|}{MAX(TMP_0, TMP_L)} \qquad \text{when } TMP > 0 \qquad (5.42)$$

The range of this parameter is 0-1: the lower the α, the more uniform the transmembrane pressure profile. The values of the uniformity factor α for the simulation results in Figures 5.4, 5.5 and 5.6 are 0.8062, 0.8270 and 0.8039 respectively, which show very low uniformity of TMP profiles. The major reason for this is that the low feed flow rates were adopted in these studies. If much higher feed flow rates, e.g., 5000 ml/min, are used, the situation will be quite different. Figures 5.7 and 5.8 show such results for module 1 with and without the fixed ES using 5000 ml/min feed flow rate at a feed inlet pressure 7 psig. Comparing the two results in Figures 5.7 and 5.8, the transmembrane pressure profile is less uniform along the module length but the flux is increased without an ES. The values of α for the two cases are 0.4886 and 0.5864 respectively. This shows agreement with the results in Figure 5.4 and 5.6: the longer the ES, the more uniform the TMP and the lower the permeate flow rate. Further, by the comparison of the results in Figures 5.4 and 5.7, it can be seen that increasing feed flow rate from 250 ml/min to 5000 ml/min does increase the TMP uniformity considerably based on a change of α from 0.8062 to 0.4886. The influence of the feed flow rate on TMP uniformity will be discussed in detail later in this Section.
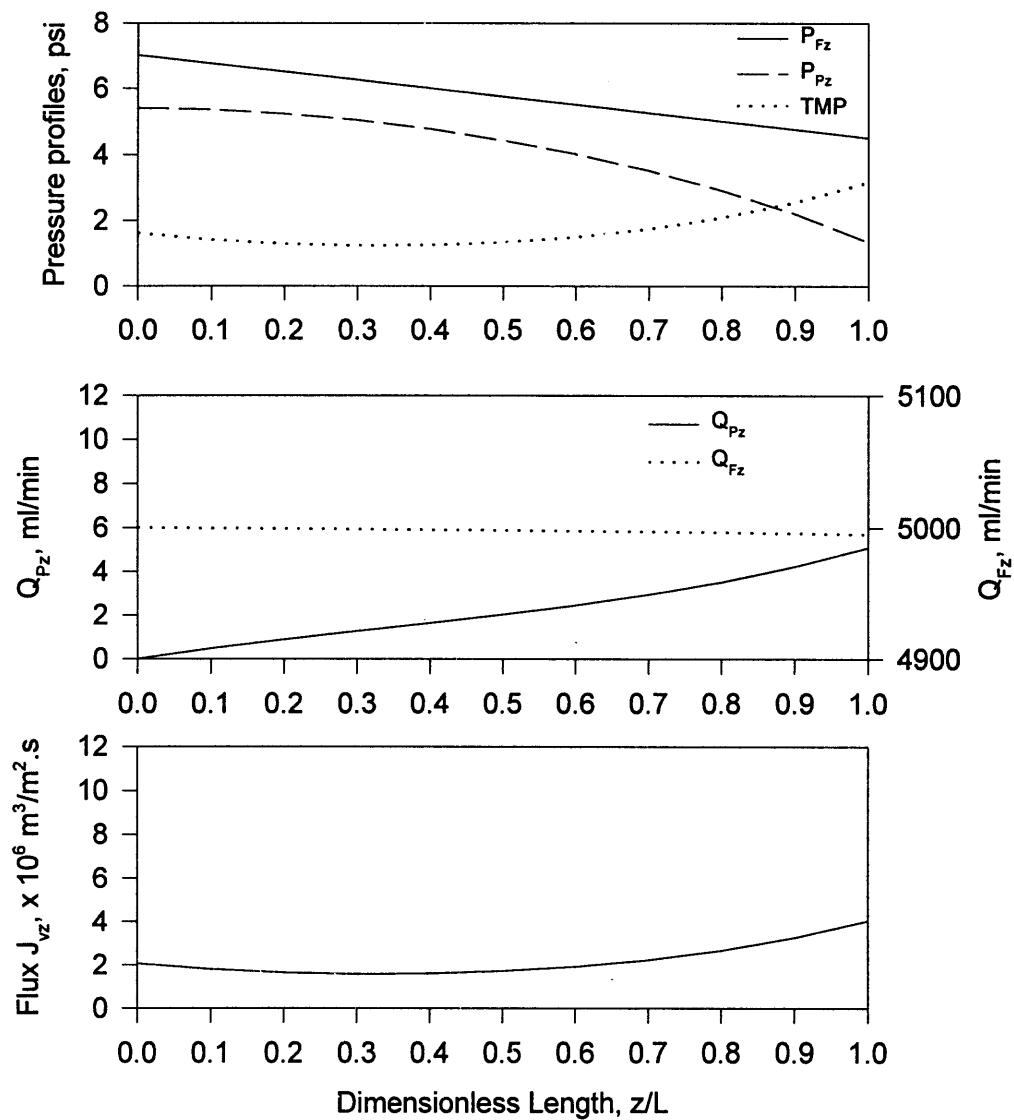
Figure 5.7 Simulation of the profiles for pressure, flow rate and flux. A = 1.857 × 10⁻¹⁰ m/Pa.s, B = 4.724 × 10¹¹ Pa.s/m³. Feed flow rate Q_{F0} = 5000 ml/min. Feed inlet pressure P_{F0} = 7.0 psig. Module 1 (Table 3.2) with the fixed ES (Table 3.3).
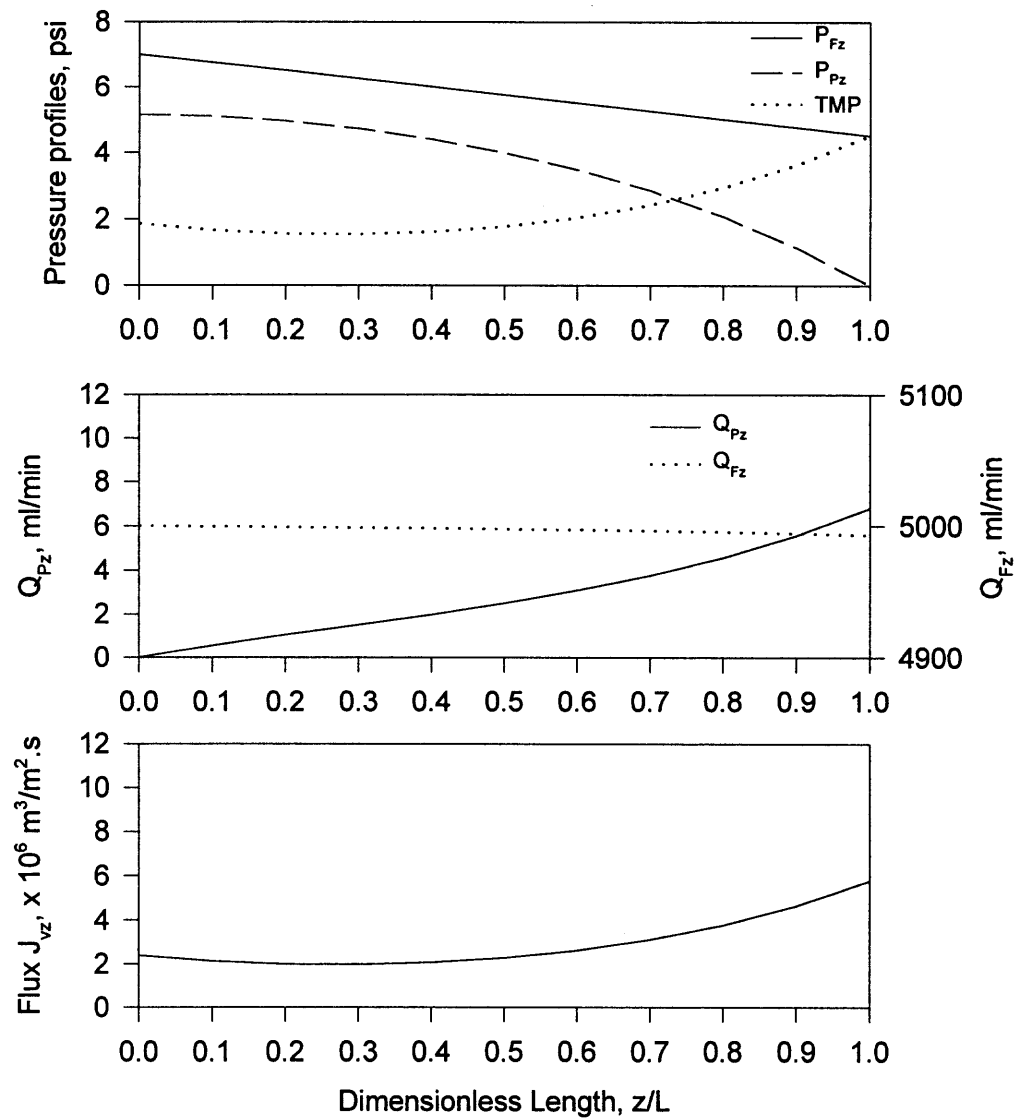
Figure 5.8 Simulation of the profiles for pressure, flow rate and flux. A = 1.857 × 10⁻¹⁰ m/Pa.s, B = 4.724 × 10¹¹ Pa.s/m³. Feed flow rate Q_{F0} = 5000 ml/min. Feed inlet pressure P_{F0} = 7.0 psig. Module 1 (Table 3.2) without the fixed ES (Table 3.3).

Similar systematic simulations were carried out using different values of various parameters influencing α. Figure 5.9 illustrates the effects of a change in A on the permeate flow rate and the uniformity factor α when B value is 4.724×10^{11} Pa.s/m^3 for a feed flow rate of 5000 ml/min at a feed inlet pressure of 7 psig. It was found that, as the permeation rate parameter A is increased, the solvent flux is increased, the TMP and TMP uniformity are decreased. This conclusion is consistent with that shown in Figures 5.4 and 5.5 but with different B values. The ES on the permeate port increases the TMP uniformity but decreases the flux. Note that the values of the parameter A for UF membranes are usually in the range of 10^{-11}-10^{-9} m/Pa.s (Ho and Sirkar 1992).
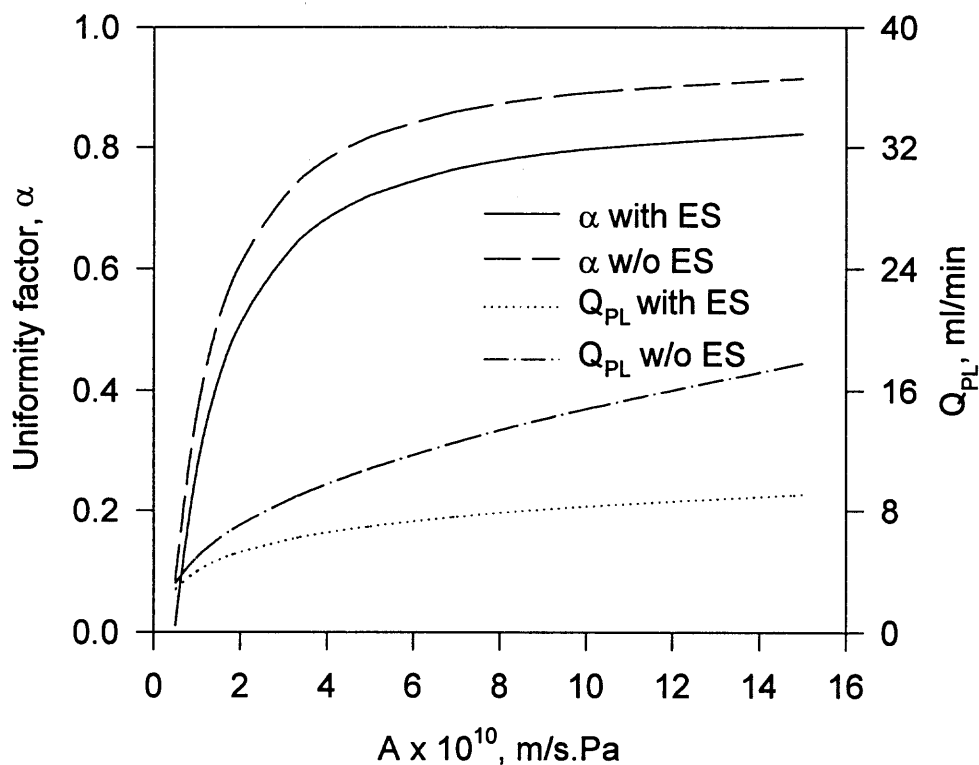
Figure 5.9 Effect of A value on the uniformity factor α and the permeate flow rate. B = 4.724 × 10^{11} Pa.s/m^3. Feed flow rate Q_{F0} = 5000 ml/min. Feed inlet pressure P_{F0} = 7.0 psig. Module 1 (Table 3.2) with and without the fixed ES (Table 3.3).

Figure 5.10 shows the effects of a change in B on the uniformity factor α and the permeate flow rate when A value is 1.857 × 10^{-10} m/Pa.s using the same conditions as above. Increasing B will decrease the TMP and the flux. However, it is very interesting to see that there is a minimum in α with an increase of B in the lower range of Bs. This implies that at a certain low value of B (say, B$^{\#}$), one can achieve the highest level of uniformity in the TMP profile. The TMP nonuniformity increases on both sides of B$^{\#}$. The α value for B close to 0 corresponds to the situation for the hollow fiber membrane module without any beads packed on the shell side. One can conclude that filling beads

on the shell side with B less than $B^{\#}$ or larger than $B^{\#}$ in a certain range can get more uniform TMP profile with a different flux value. The effect of ES is also shown in Figure 5.10. The presence of an ES can shift the curve of α as a function of B to a higher value of $B^{\#}$ even though the starting α value remains the same corresponding to B being 0 i.e. no beads packed on the shell side. At a certain value of B, say B^c, same TMP uniformity can be obtained for both with and without an ES but with a lower permeate flow rate for the situation with an ES. The presence of an ES increases the TMP uniformity factor α with B before B^c and then decreases the TMP uniformity factor α after B^c.

It can be expected that increasing the feed flow rate Q_{F0} will shift $B^{\#}$ to a higher value and change the curve shape to some extent. Figure 5.11 provides such a result using the conditions as in Figure 5.10 but for a higher feed flow rate Q_{F0} of 7000 ml/min. In this case, α for B = 0 is higher than that in the Figure 5.10, demonstrating that increasing the feed flow rate actually decreases the TMP uniformity for the ordinary ultra/microfiltration operations and this is more prominent especially when the feed flow rate is higher. It can be seen that the effect of ES is considerable, it not only shifts the α profile to the right side but also lowers α significantly leading to a more uniform TMP profile at higher B values. The B values for the shell-side bed can be calculated by eq 5.14 if the particle diameter and void fraction ε of the bed are known. Table 5.3 provides some values of the ECS hydraulic conductivities (m^2) for the porous medium in HFBRs and their corresponding B values for module 1. These are typical values when the cultures are approaching the end.
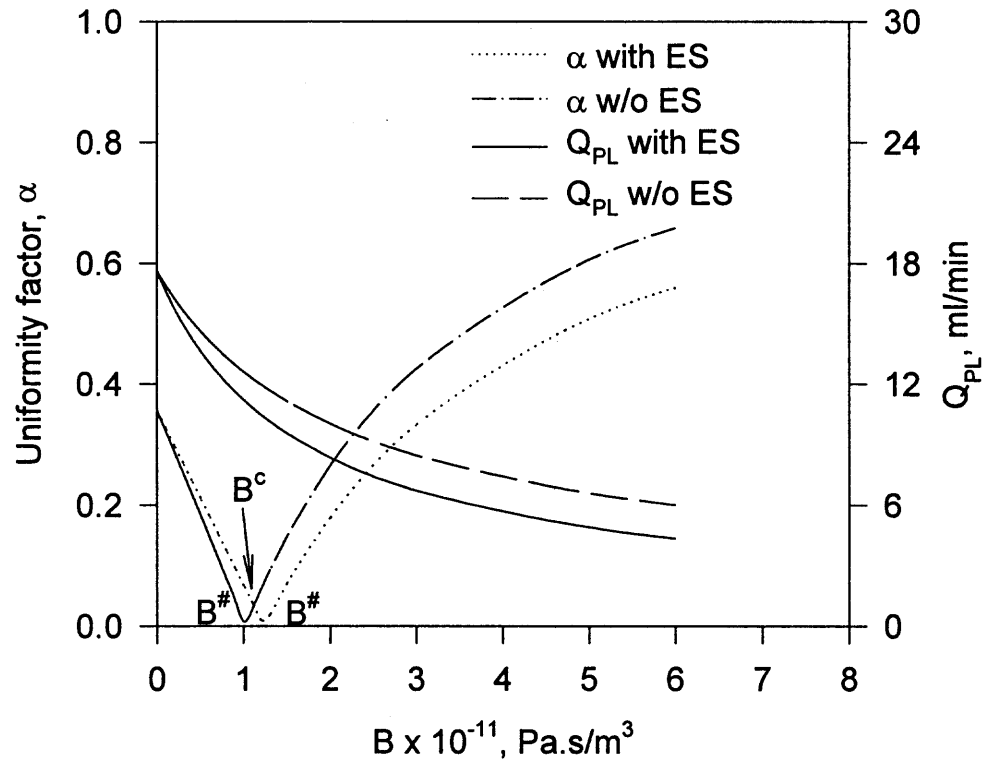
Figure 5.10 Effect of B value on the uniformity factor α and the permeate flow rate. A = 1.857 × 10^{-10} m/Pa.s. Feed flow rate Q_{F0} = 5000 ml/min. Feed inlet pressure P_{F0} = 7.0 psig. Module 1 (Table 3.2) with and without the fixed ES (Table 3.3).
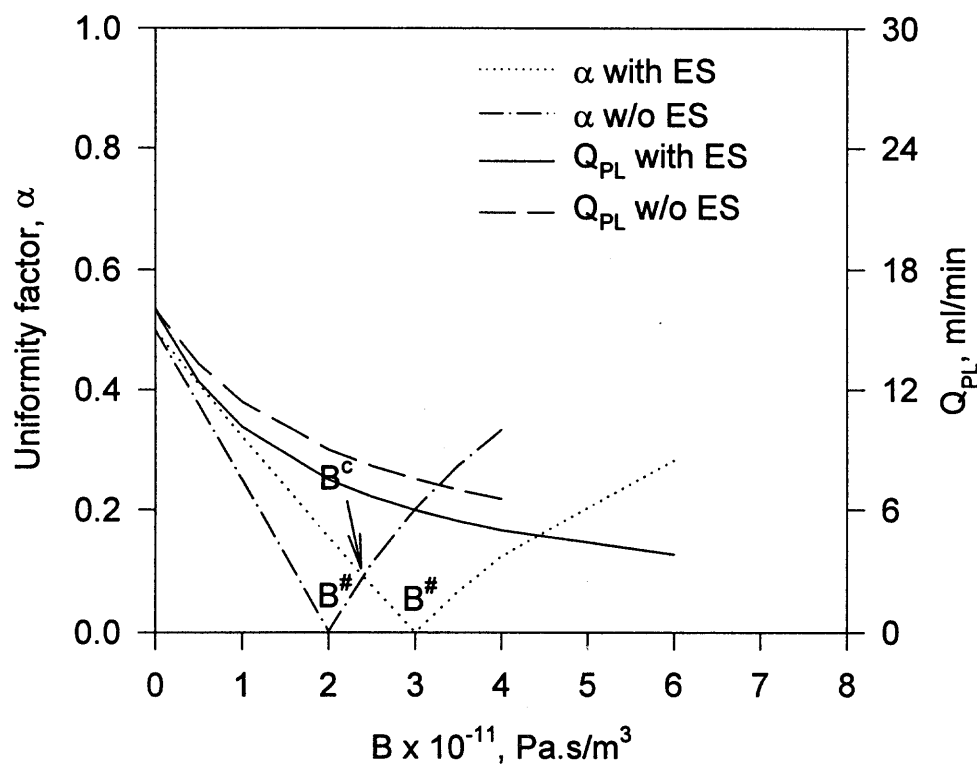
Figure 5.11 Effect of B value on the uniformity factor α and the permeate flow rate. A = 1.857×10^{-10} m/Pa.s. Feed flow rate Q_{F0} = 7000 ml/min. Feed inlet pressure P_{F0} = 7.0 psig. Module 1 (Table 3.2) with and without the fixed ES (Table 3.3).

Table 5.3 Representative B values from literature for cells and tissues in ECS of HFBRs

Porous media in ECS	Hydraulic conductivity (m^2)	Source	Corresponding B (Pa.s/m^3) values for module 1
Red blood cells	7×10^{-15}~3×10^{-18}	Zydney, Saltzman and Colton 1986	1.08×10^{15}~2.52×10^{18}
Rat tissue	6.4×10^{-18}~31×10^{-18}	Swabb, Wei and Gullion 1974	1.18×10^{18}~2.44×10^{17}
Tissue	1×10^{-18}	Apelblat, Katzir-Katchalsky and Silberberg 1974	7.5528×10^{18}

Figure 5.12 shows the influence of the feed flow rate Q_{F0} on α and the permeate flow rate Q_{PL} using A = 1.857 × 10^{-10} m/Pa.s, B = 4.724 × 10^{11} Pa.s/m^3 and a feed inlet pressure of 7 psig. One can see that Q_{PL} decreases monotonically with an increase of Q_{F0}. Similarly, there is another minima type of behavior of α with an increase of Q_{F0}. This means that at a certain Q_{F0} ($Q_{F0}^{\#}$), one can achieve the highest level of uniformity in the TMP profile. The TMP uniformity increases with Q_{F0} increase before $Q_{F0}^{\#}$, then decreases after $Q_{F0}^{\#}$. Therefore choosing Q_{F0} in a certain range can get a more uniform TMP profile. For example, as mentioned before, the TMP uniformity increases a lot (α change from 0.8062 to 0.4886) due to the increase in feed flow rate from 250 ml/min to 5000 ml /min (compare the results in Figures 5.4 and 5.7). This is a case where Q_{F0} is less than $Q_{F0}^{\#}$. The effect of an ES is also shown in Figure 5.12. The presence of an ES can shift the curve as well but when Q_{F0} is low, the values of α in the two cases remain close. Similarly, the same level of uniformity of TMP can be obtained with and without an ES at a certain value of Q_{F0}, say Q_{F0}^{c}, but with a lower permeate flow rate for the situation with an ES. Unlike the ES effect on α as a function of B value, ES increases the TMP uniformity before Q_{F0}^{c} and then decreases the TMP uniformity after Q_{F0}^{c}.
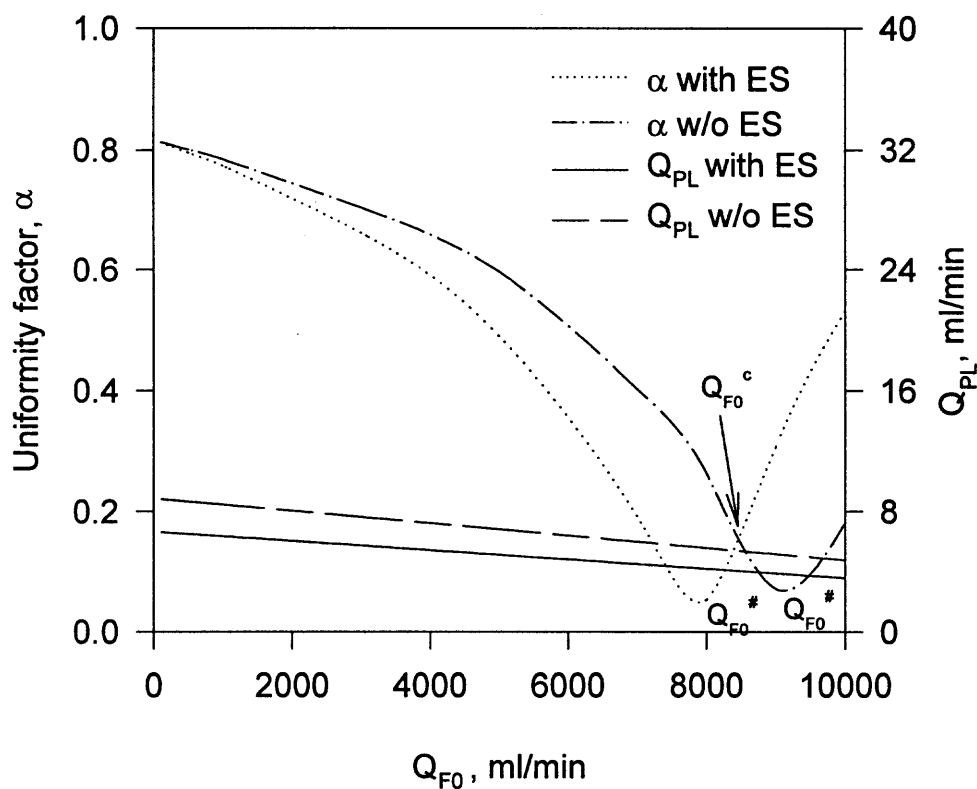
Figure 5.12 Effect of feed flow rate Q_{F0} on the uniformity factor α and the permeate flow rate. $A = 1.857 \times 10^{-10}$ m/Pa.s. $B = 4.724 \times 10^{11}$ Pa.s/m^3. Feed inlet pressure $P_{F0} = 7.0$ psig. Module 1 (Table 3.2) with and without the fixed ES (Table 3.3).

5.2.3.3 Simulation for Case 2 - Permeate Flow Control: No ES exists in the module in this case since other applications did not utilize or need this extended section. However it is not difficult to include ES in the simulation. Figure 5.13 provides the simulation results for the case of a restricted permeate flow rate. The conditions are similar to those shown in Figure 5.8, namely, 5000 ml/min feed flow rate at a feed inlet pressure 7 psig. Permeate flow rate was restricted to 4 ml/min in this case. The TMP profile is more uniform with the uniformity factor α being 0.3641 compared with that of 0.5864 in

Figure 5.8 without the restriction of the permeate flow due to the lowered flux, which reduces the pressure drop in the shell side bed. Figure 5.14 shows similar results but for an even more restricted permeate flow rate of Q_{PL} = 1 ml/min. There is Starling flow to some extent near the end of the module: the permeate comes back to the tube side. This case is similar to that in the study by Molinari, et al. (1990). Figure 5.15 provides the results of Starling flow only for similar operating conditions except there is no permeate flow at all. The flow situation in the case corresponds to that in hollow-fiber perfusion bioreactors (HFBRs). TMP profile is symmetrical along the module length; so is the flux profile. Typical B values are provided in Table 5.3 for porous media on the shell side in HFBRs. From these simulations, it can be concluded that using this model one can control the permeate flow rate such that Starling flow is actually prevented.

Considering the tube-side elution situation used in this work, Figure 5.16 shows the simulation results for an elution flow rate of 2.5 ml/min. The ES is supposed to be present here. The calculated tube-side inlet pressure is 2.63 psi which is quite close to the experimental values of 2.7 psi. Figure 5.16 also illustrates the pressure, flux and flow rate profiles in the module. Flow rate profiles in both sides are symmetrical to each other.
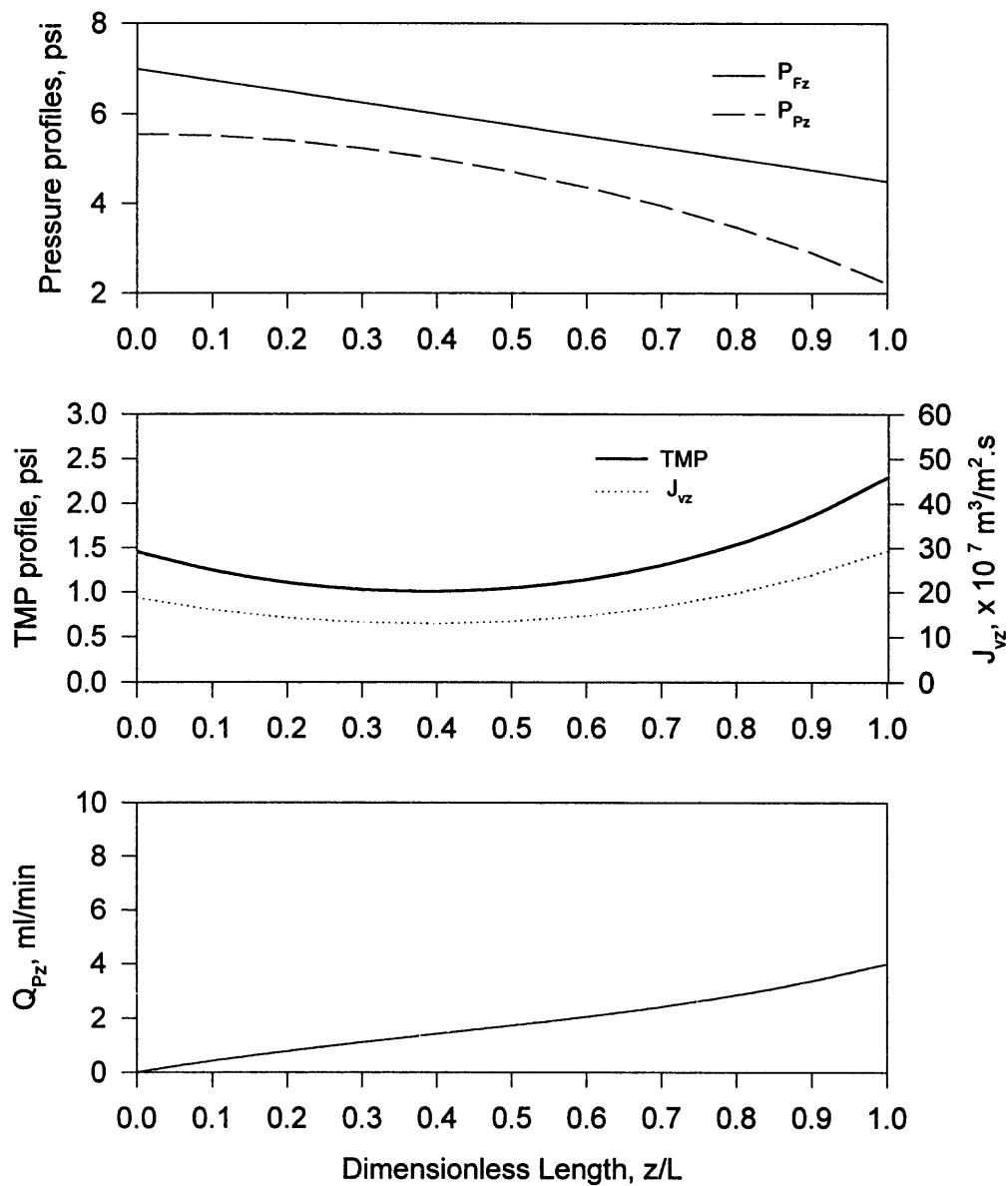
Figure 5.13 Simulation of the profiles for pressure, flow rate and flux for a fixed permeate flow rate Q_{PL}= 4 ml/min. A = 1.857 × 10^{-10} m/Pa.s, B = 4.724 × 10^{11} Pa.s/m^3. Feed flow rate Q_{F0} = 5000 ml/min. Feed inlet pressure P_{F0} = 7.0 psig. Module 1 (Table 3.2) without the fixed ES (Table 3.3).
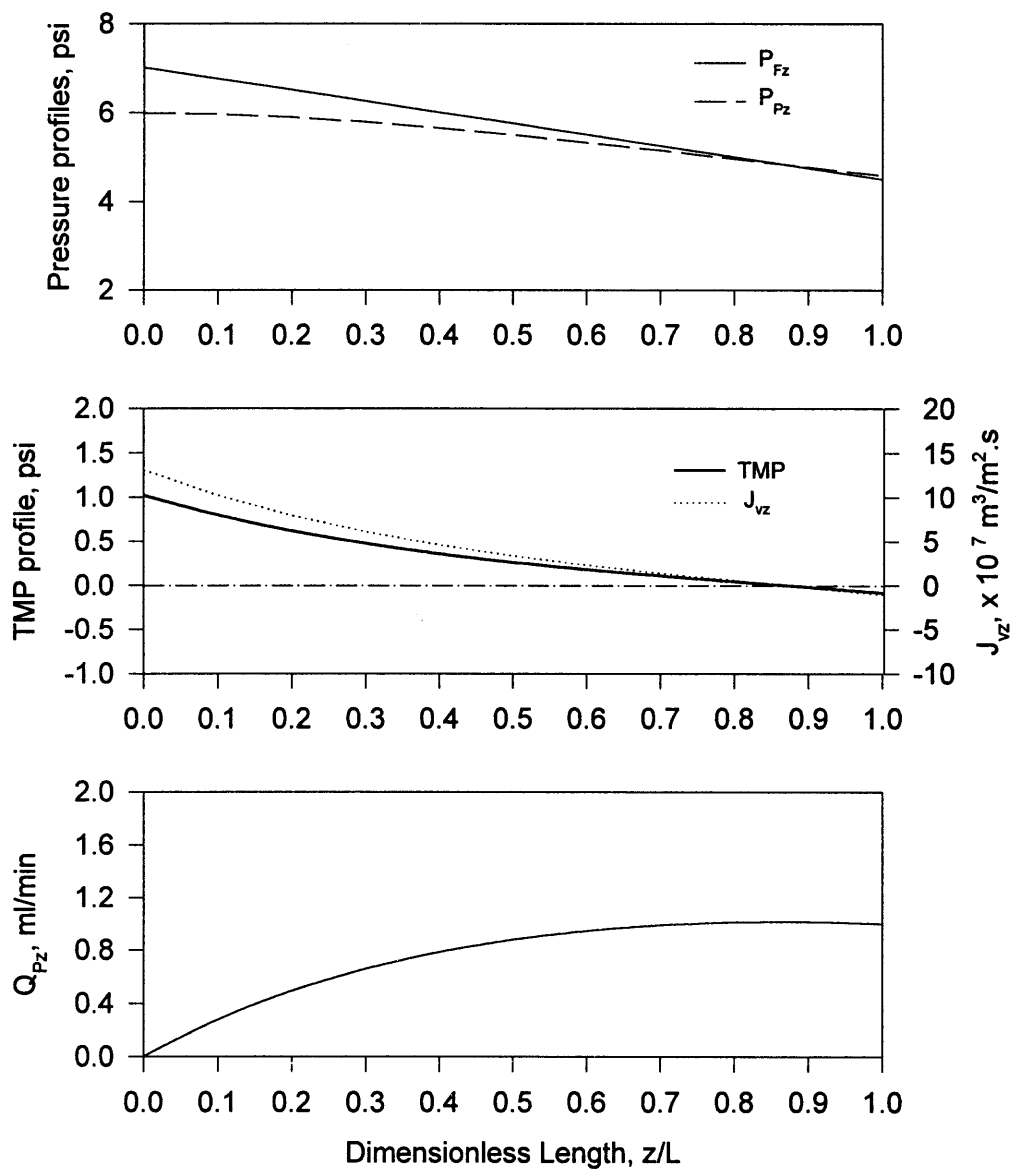
Figure 5.14 Simulation of the profiles for pressure, flow rate and flux for some extent of Starling flow (Q_{PL} = 1 ml/min). A = 1.857 × 10^{-10} m/Pa.s, B = 4.724 × 10^{11} Pa.s/m^3. Feed flow rate Q_{F0} = 5000 ml/min. Feed inlet pressure P_{F0} = 7.0 psig. Module 1 (Table 3.2) without the fixed ES (Table 3.3).
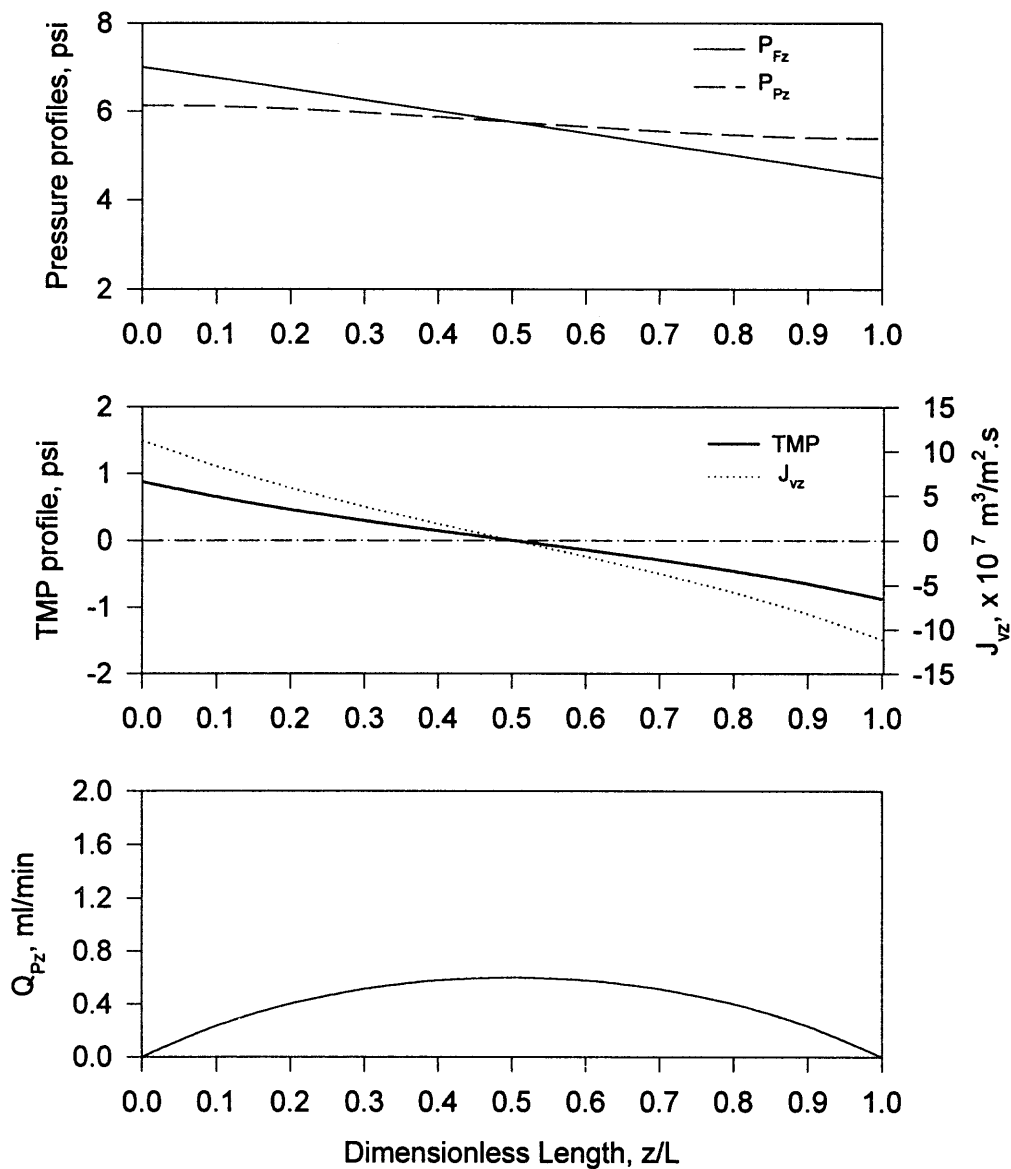
Figure 5.15 Simulation of the profiles for pressure, flow rate and flux with no permeate flow rate (Starling flow). $Q_{PL} = 0$. $A = 1.857 \times 10^{-10}$ m/Pa.s, $B = 4.724 \times 10^{11}$ Pa.s/m^3. Feed flow rate $Q_{F0} = 5000$ ml/min. Feed inlet pressure $P_{F0} = 7.0$ psig. Module 1 (Table 3.2) without the fixed ES (Table 3.3).
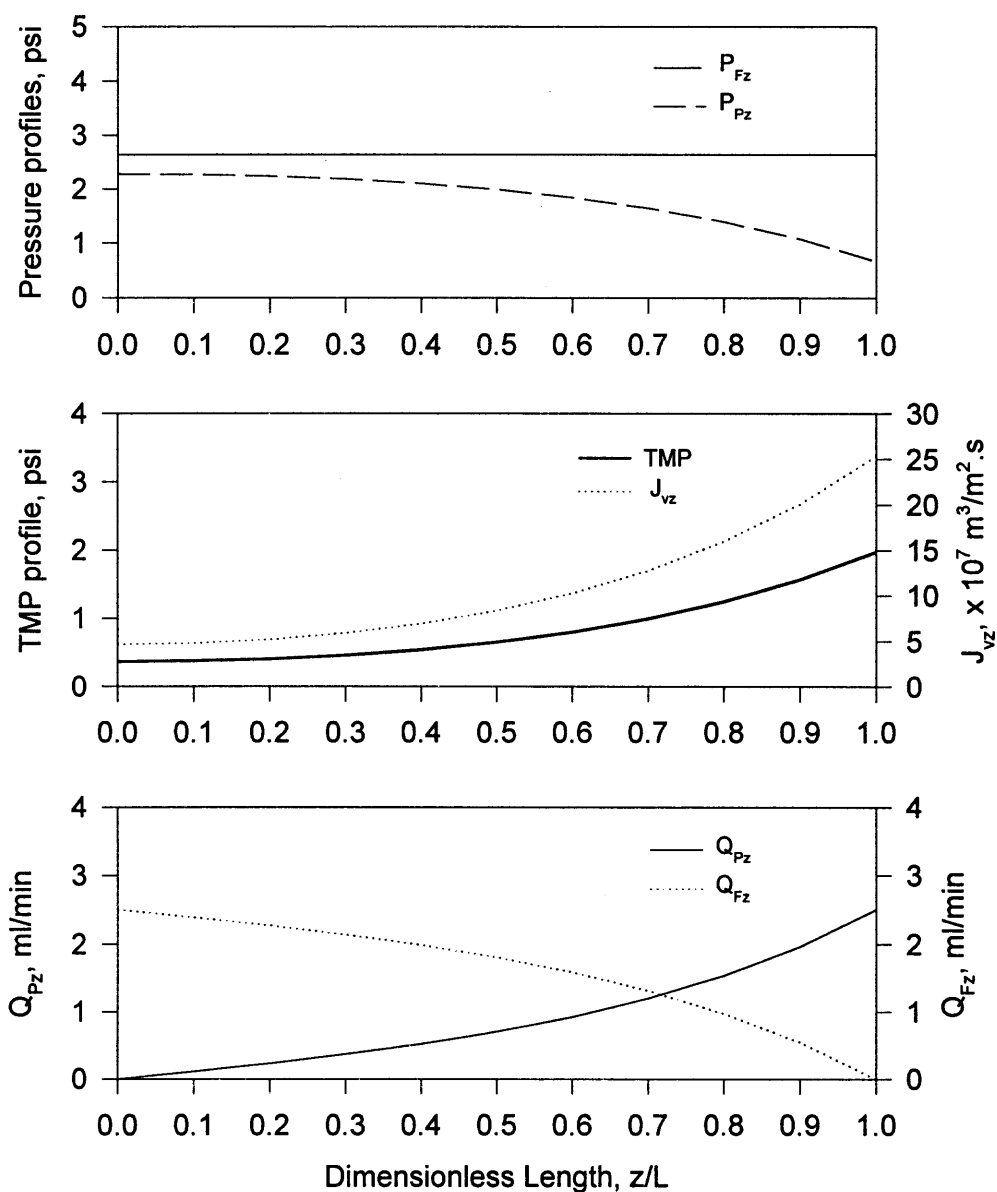
Figure 5.16 Simulation of the profiles for pressure, flow rate and flux in tube-side elution. A = 1.857 × 10⁻¹⁰ m/Pa.s, B = 4.724 × 10¹¹ Pa.s/m³. Elution flow rate Q_{F0} = 2.5 ml/min. Module 1 (Table 3.2) with the fixed ES (Table 3.3).

5.3 Feed Introduced from the Shell-Side Inlet

Besides the descriptions of different operational modes using the integrated device for which the feed is introduced from the tube-side inlet, there are some other situations such as shell-side elution and backflushing (Figure 5.17). Some other researchers also use shell-side inlet of a hollow fiber module as the feed port and tube-side outlet as the permeate exit. Therefore it is necessary to develop a similar model describing this kind of operational situations.
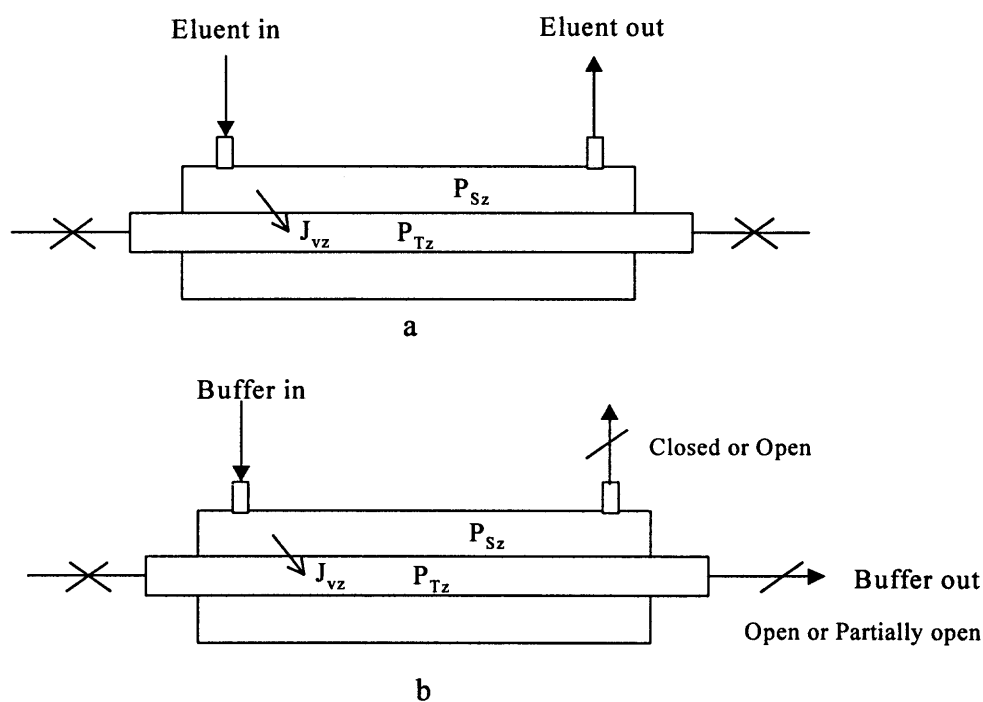
Figure 5.17 Schematic for the operation of shell-side elution (a) and backflushing (b)

5.3.1 Theory

An analysis similar to that in Section 5.2.1 will be provided briefly in this Section. First a general solution will be developed for the description of using shell-side inlet as the feed port and tube-side outlet as the permeate exit. Then two special operations will be

considered: (i) shell-side elution and (ii) backflushing. Quantitative estimates of lengthwise profiles of flow rates, fluxes and transmembrane pressures will be developed. Same set of symbols will be used to describe the behaviors at different positions in a hollow fiber module except using subscript T for the tube side and subscript S for the shell side (Figure 5.17). Correspondingly, the permeation velocity or volume flux J_{vz} (Figure 5.17) through the membrane at any axial location z is given by

$$J_{vz} = A(P_S - P_T)_z \qquad (5.43)$$

The local volumetric flow rate in the tube side Q_{Tz} (m^3/s) is described by

$$\frac{dQ_{Tz}}{dz} = N_0(\pi d_o J_{vz}) \qquad (5.44)$$

The total mass balance for the flow distribution in the hollow fiber module at any location z in the module is

$$Q_{S0} = Q_{Tz} + Q_{Sz} \qquad (5.45)$$

Q_{S0} is the volumetric feed (or eluent and buffer) flow rate at the shell-side inlet (z = 0). Integrating eq 5.44, an expression for Q_{Tz} is obtained:

$$Q_{Tz} = N_0 \pi d_o \int_0^z J_{vz} \, dz \qquad (5.46a)$$

Combine with eq 5.45

$$Q_{Sz} = Q_{S0} - N_0 \pi d_o \int_0^z J_{vz} \, dz \qquad (5.46b)$$

The pressure drop inside each fiber is described by the Hagen-Poiseuille flow law:

$$\frac{dP_T}{dz} = - \frac{128 \mu_F Q_{si}}{\pi d_i^4} = - \frac{8 \mu_F Q_{si}}{\pi r_i^4} \qquad (5.47)$$

where μ_F is the viscosity of the feed (or eluent, buffer), and Q_{si} is the volumetric flow rate in a single fiber, which can be expressed by

$$Q_{si} = \frac{Q_{Tz}}{N_0} = \pi \ d_i \int_0^c J_{vz} \ dz \tag{5.48}$$

Substitute eq 5.48 into eq 5.47

$$\frac{dP_T}{dz} = - \frac{128\mu_F}{\pi d_i^4} \times (\pi \ d_o \int_0^c J_{vz} \ dz) = -\frac{128\mu_F d_o}{d_i^4} \times \int_0^c J_{vz} \ dz \tag{5.49}$$

For pressure drop in the shell-side bed, Blake-Kozeny equation (Bird, Stewart and Lightfoot 1960) for a packed bed is used:

$$\frac{dP_S}{dz} = - \frac{150(1-\varepsilon)^2}{d_p^2 \varepsilon^3} \mu_F u_P = -\frac{150(1-\varepsilon)^2}{d_p^2 \varepsilon^3} \mu_F \frac{Q_{S0} - N_0 \pi d_o \int_0^c J_{vz} dz}{S_s} \tag{5.50}$$

Rewrite eqs 5.49 and 5.50 appropriately and get the following three governing equations:

$$J_{vz} = A(P_S - P_T)_z \tag{5.43}$$

$$\frac{dP_T}{dz} = - E \int_0^c J_{vz} \ dz \tag{5.51}$$

$$\frac{dP_S}{dz} = -V + W \int_0^c J_{vz} dz \tag{5.52}$$

where

$$E = \frac{128\mu_F d_o}{d_i^4} \tag{5.53}$$

$$V = \frac{150(1-\varepsilon)^2}{d_p^2 \varepsilon^3} \mu_F \frac{Q_{S0}}{S_s}, \qquad W = \frac{150(1-\varepsilon)^2}{d_p^2 \varepsilon^3} \mu_F \frac{50\pi d_o}{S_s} \tag{5.54}$$

Here parameters A and B are assumed not to change along the module length. Therefore, by differentiating eq 5.43 and combining with eqs 5.51 and 5.52, one obtains

$$\frac{dJ_{vz}}{dz} = A \times \left(\frac{dP_S}{dz} - \frac{dP_T}{dz}\right)$$

$$= -AV + AW \int_0^z J_{vz}dz + AE \int_0^z J_{vz}dz \qquad (5.55)$$

and by differentiating eq 5.55 again, a second-order differential equation is obtained as follows:

$$\frac{d^2 J_{vz}}{dz^2} = A \times (E + W)J_{vz} \qquad (5.56)$$

Let $\qquad\qquad \beta^2 = A(E + W) \qquad\qquad\qquad\qquad (5.57)$

The solution of eq 5.56 has the same form as that of eq 5.18a but with different expressions of A_1 and A_2.

$$J_{vz} = A_1 \cosh(\beta z) + A_2 \sinh(\beta z) \qquad (5.58a)$$

@ z=0, $\qquad\qquad J_{v0} = A_1 = A(P_{S0} - P_{T0}) \qquad (5.58b)$

@ z=L, $\qquad J_{vL} = A_1 \cosh(\beta L) + A_2 \sinh(\beta L) = A(P_{SL} - P_{TL}) \qquad (5.58c)$

Equation 5.58a provides the local permeation flux profile in the module during shell-side elution or backflushing. Substituting eq 5.58a into eq 5.51, and rearranging, one gets

$$\frac{dP_T}{dz} = -\frac{E}{\beta}\{A_1 \sinh(\beta z) + A_2[\cosh(\beta z) - 1]\} \qquad (5.59)$$

Integrate from z = 0 to z

$$P_{Tz} = P_{T0} - \frac{E}{\beta^2}\{A_1[\cosh(\beta z) - 1] + A_2[\sinh(\beta z) - \beta z]\} \qquad (5.60a)$$

@ z=0, $P_{Tz}=P_{T0}$

$\qquad\qquad\qquad\qquad\qquad\qquad\qquad\qquad\qquad\qquad\qquad\qquad (5.60b)$

@ z=L, $P_{TL} = P_{T0} - \frac{E}{\beta^2}\{A_1[\cosh(\beta L) - 1] + A_2[\sinh(\beta L) - \beta L]\}$

Substitute eq 5.58a into eq 5.52, and rearrange:

$$\frac{dP_S}{dz} = -V + \frac{W}{\beta}\{A_1 \sinh(\beta z) + A_2[\cosh(\beta z) - 1]\} \tag{5.61}$$

Integrating from z to L leads to

$$P_{Sz} = P_{SL} + V(L-z) - \frac{W}{\beta^2}\{A_1[\cosh(\beta L) - \cosh(\beta z)] + A_2[\sinh(\beta L) - \sinh(\beta z)] - A_2\beta(L-z)\} \tag{5.62a}$$

@ z=0, $\qquad P_{S0} = P_{SL} + VL - \frac{W}{\beta^2}\{A_1[\cosh(\beta L) - 1] + A_2 \sinh(\beta L) - A_2\beta L\}$ $\qquad$ (5.62b)

@ z=L, $\qquad P_{Sz} = P_{SL}$

Equations 5.60a and 5.62a are the solutions for pressure profiles in tube side and shell side respectively for known boundary conditions, namely, Q_{S0}, P_{S0} and P_{TL} (related to atmospheric pressure). P_{T0} in eq 5.60a can be obtained from P_{S0} in eq 58b.

Substituting eq 5.58a into eqs 5.46a and 5.46b, the flow rates in both sides can be obtained via the following expressions:

$$Q_{Tz} = \frac{N_0 \pi d_o}{\beta}\{A_1 \sinh(\beta z) + A_2[\cosh(\beta z) - 1]\} \tag{5.63a}$$

$$Q_{Sz} = Q_{S0} - \frac{N_0 \pi d_o}{\beta}\{A_1 \sinh(\beta z) + A_2[\cosh(\beta z) - 1]\} \tag{5.63b}$$

@ z= 0, $\qquad Q_{T0} = 0, \qquad Q_{S0} = Q_{T0}$

@ z= L, $\qquad Q_{TL} = \frac{N_0 \pi d_i}{\beta}\{A_1 \sinh(\beta L) + A_2[\cosh(\beta L) - 1]\} \tag{5.64a}$

$$Q_{SL} = Q_{S0} - \frac{N_0 \pi d_i}{\beta}\{A_1 \sinh(\beta L) + A_2[\cosh(\beta L) - 1]\} \tag{5.64b}$$

Equations 5.64a and 5.64b provide the flow rates at the end point of the tube side and the shell side of the module. The average velocities at any location z in both sides could be

obtained by dividing eqs 5.63a and 5.63b by the cross-sectional areas of tube side and shell side, respectively.

5.3.2 Constants A_1 and A_2

Constants A_1 and A_2 have to be determined first based on the specific experimental conditions. This will be discussed under the following two categories.

Case 1: Shell-side elution ($Q_{S0} = Q_{SL}$)

For this case, the eluent flow rate from the shell-side inlet (Q_{S0}), the eluent exit flow rate (Q_{SL}) and the shell-side exit pressure at $z = L$ (P_{SL}) (which is related to the atmospheric pressure) are the known boundary conditions. Expressions for A_1 and A_2 which are given below can be obtained by solving the group of eqs 5.58b, 5.58c, 5.60b, 5.62b and 5.64b:

$$A_2 = -\frac{AV}{\beta} \tag{5.65}$$

$$A_1 = -\frac{A_2[\cosh(\beta L) - 1]}{\sinh(\beta L)} \tag{5.66}$$

Because of the presence of the ES, the relationship in eq 5.33b can be used to relate P_{SL} to the atmospheric pressure

$$P_{SL} - P_{atm} = B'Q_{SL} \tag{5.67}$$

Substituting eqs 5.65, 5.66 and 5.67 into eqs 5.62a and 5.62b, the pressure profile in the shell side of the module and P_{S0} can be obtained. Substituting P_{S0} into eq 5.58b, P_{T0} has the following expression:

$$P_{T0} = P_{S0} - \frac{A_1}{A} \tag{5.68}$$

Substituting eqs 5.65, 5.66 and 5.68 into eq 5.60a, pressure profile in the tube side of the module can be obtained. Profiles of flow rates can be developed by substitution of eqs 5.65 and 5.66 into eqs 5.63a and 5.63b. Velocity profiles can be obtained by dividing the flow rates by the cross-sectional areas of shell side and tube side, respectively.

Case 2: Backflushing

Two kinds of problems will be discussed. (i) Only part of the feed goes out from the tube-side outlet; the rest goes out from the shell-side exit. (ii) All the feed goes out from the tube-side exit ($Q_{TL}=Q_{S0}$).

For the first kind of problem, the related group of equations is eqs 5.58b, 5.58c, 5.60b, 5.62b, 5.64a and 5.67 by considering the ES. Known conditions are P_{SL} (which is related to the atmospheric pressure), Q_{S0} and $Q_{TL}=1/n\ Q_{S0}$ and $n>1$. Six unknowns, namely, Q_{SL}, P_{S0}, P_{T0}, P_{TL}, A_1, A_2 can be obtained by solving the above group of equations. Expressions of A_1 and A_2 (same as that for shell-side elution) are following:

$$A_2 = -\frac{AV}{\beta} \tag{5.65}$$

$$A_1 = \frac{Q_{TL}\dfrac{\beta}{N_0\pi d_0} - A_2[\cosh(\beta L)-1]}{\sinh(\beta L)} \tag{5.69}$$

Procedures similar to those used for solving the shell-side elution problem can be followed to get the profiles of flow rates, pressures and flux.

For the second kind of problem, same group of equations is related by considering the ES and the boundary conditions are P_{TL} (which is the atmospheric pressure), Q_{S0} and with $n = 1$ instead of $n > 1$ for $Q_{TL}=1/n\ Q_{S0}$. In this case, the expression for A_1 becomes

$$A_1 = \frac{Q_{S0} \dfrac{\beta}{N_0 \pi d_0} - A_2[\cosh(\beta L) - 1]}{\sinh(\beta L)} \qquad (5.70)$$

and that for A_2 remains unchanged. The problem can be solved following the same procedure. Therefore problem (ii) is just a special case for problem (i). In fact, shell-side elution is also a special case for problem (i) with $Q_{TL} = 0$ (n= ∞ for $Q_{TL}=1/n\ Q_{S0}$). If there is no ES at the shell-side outlet, just set $B'=0$ by using above solutions.

5.3.3 Results and Discussions

5.3.3.1 Simulation Results for Shell-Side Elution: For the shell-side elution configuration used in this dissertation, Figure 5.18 shows the simulation results for an elution flow rate of 2.5 ml/min for module 1 having a fixed ES. Here A = 1.857×10^{-10} m/Pa.s and B = 4.724×10^{11} Pa.s/m^3 are used. The calculated shell-side inlet pressure is 3.27 psi which is close to the experimental values of 3.5-3.6 psi. Figure 5.18 also illustrates the pressure, flux and flow rate profiles in the module. Both TMP and flux profiles are symmetrical along the module length; there is Starling flow in this case. From the flow rate profiles, one can directly observe the change of eluent flow rate along the module length; some of the eluent goes into the tube side from the upper part of the module and comes back to the shell side at the bottom of the module.
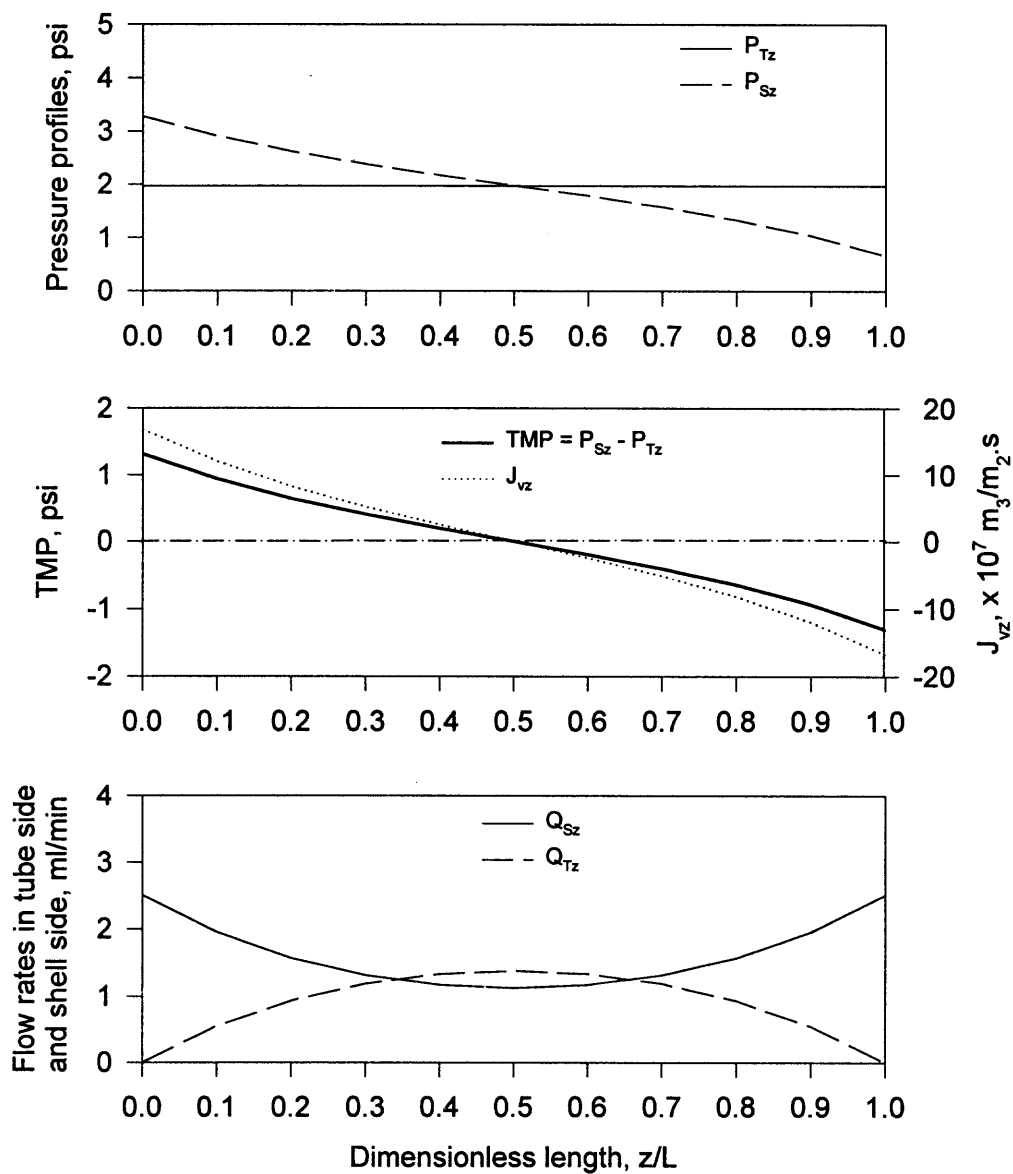
Figure 5.18 Simulation of the profiles for pressure, flow rate and flux in shell-side elution. A = 1.857 × 10⁻¹⁰ m/Pa.s, B = 4.724 × 10¹¹ Pa.s/m³. Elution flow rate Q_{S0} = 2.5 ml/min. Module 1 (Table 3.2) with the fixed ES (Table 3.3).

5.3.3.2 Simulation Results for Backflushing: For backflushing used to clean the module, the configuration where the tube-side outlet is open and the shell-side outlet is closed will be simulated. Figure 5.19 provides the results for a backflushing flow rate of 5 ml/min. The buffer entered from the shell-side inlet and goes out from the tube-side outlet. The flow rates in the shell side and the tube side are symmetrical to each other.

Results of simulations for the other situation discussed before, namely, the situation where flow rate control is used to keep the tube-side outlet flow rate at a fixed value ($Q_{TL} = 1/n \ Q_{S0}$, n>1 and n $\neq \infty$), are provided in Figure 5.20 using the same conditions as above but with $Q_{TL} = 4.0$ ml/min (n=5/4). Both TMP and flux become negative at the bottom of the module (Starling flow). Flow rate profiles in both sides are symmetrical to each other.
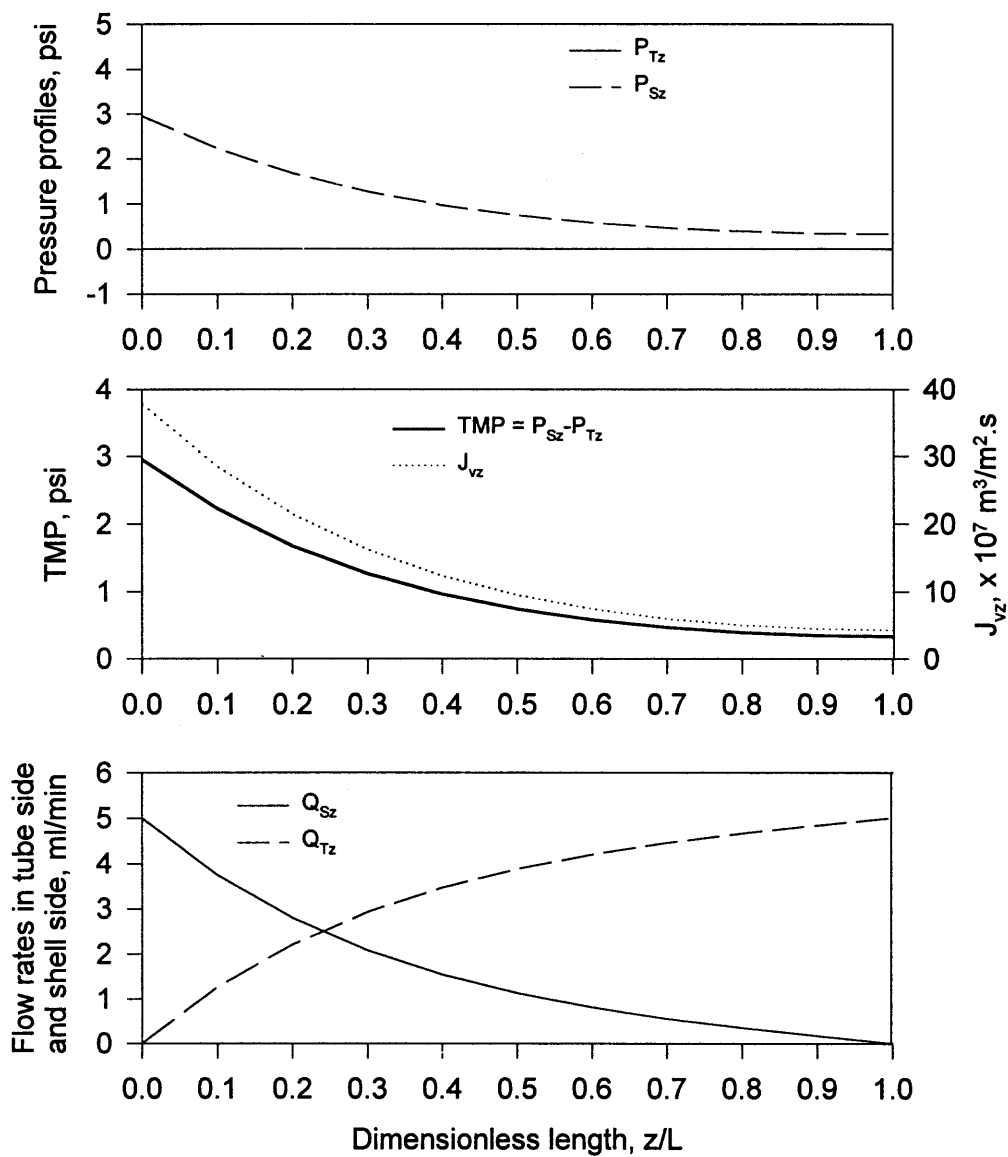
...

Figure 5.19 Simulation of the profiles for pressure, flow rate and flux in backflushing with tube-side outlet open and shell-side outlet closed. A = 1.857 × 10⁻¹⁰ m/Pa.s, B = 4.724 × 10¹¹ Pa.s/m³. Backflushing flow rate Q$_{S0}$ = 5.0 ml/min. Module 1 (Table 3.2) with the fixed ES (Table 3.3).

Figure 5.19 Simulation of the profiles for pressure, flow rate and flux in backflushing with tube-side outlet open and shell-side outlet closed. A = 1.857×10^{-10} m/Pa.s, B = 4.724×10^{11} Pa.s/m³. Backflushing flow rate Q_{S0} = 5.0 ml/min. Module 1 (Table 3.2) with the fixed ES (Table 3.3).
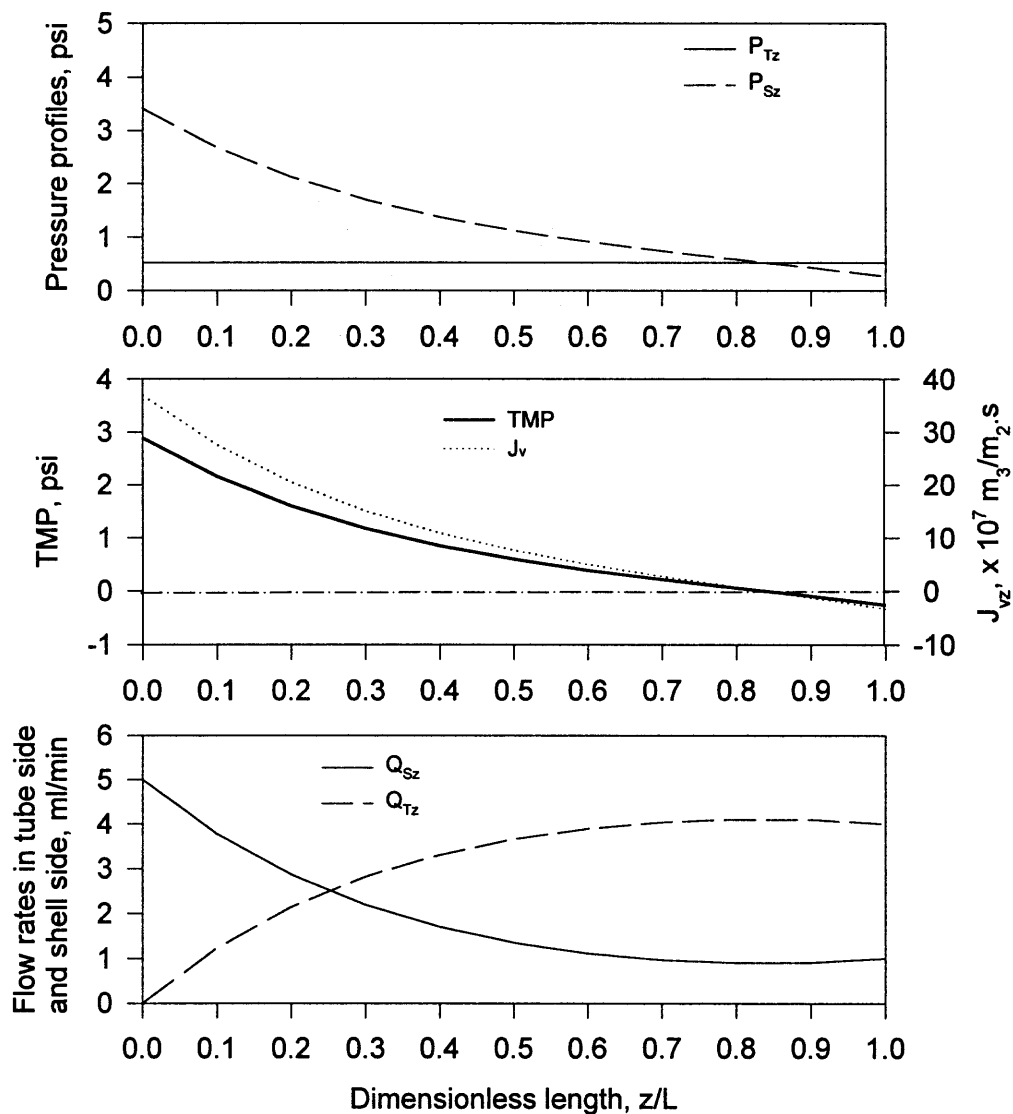
Figure 5.20 Simulation of the profiles for pressure, flow rate and flux in backflushing for fixed $Q_{TL} = 4.0$ ml/min by using $Q_{S0} = 5.0$ ml/min, $A = 1.857 \times 10^{-10}$ m/Pa.s, $B = 4.724 \times 10^{11}$ Pa.s/m^3. Module 1 (Table 3.2) with the fixed ES (Table 3.3).

5.4. Concluding Remarks

The model discussed in this Chapter can be applied to different operating modes of a bead-filled UF/MF hollow fiber membrane module. Pressure and flux profiles for different operating modes are predicted by the model for appropriate boundary conditions. Parameters A and B which are specific for a particular membrane module can be easily determined by the method proposed here. A parametric study of the uniformity of TMP shows that this model can provide a good tool for process design directed to achieving improved operation for diverse applications. Other operational modes such as backflushing and shell-side elution can also be described following a similar procedure. For all problems discussed in this Chapter, one can observe that as long as one knows the appropriate boundary conditions, the unknowns can be obtained by solving the related group of equations. The model discussed in this Chapter can be used as the basis for developing a more complicated model to describe the chromatographic behaviors for the integrated device. Those applications employing similar device configurations may also employ the model developed here to predict the pressure and flux profiles to facilitate the design of the process and the operating conditions.

CHAPTER 6

PRELIMINARY MODELING STUDY FOR THE DESCRIPTION OF LOADING AND ELUTION BEHAVIORS IN THE INTEGRATED DEVICE

6.1 Preliminary Remarks

In the development of a chromatographic system for bioseparation, it is important to design an efficient system having minimum capital and operating cost and maximum throughput. To better understand, optimize and scale up the process, the process should be accurately modeled (Subramanian 1998b). The production rate of conventional UF or MF membrane module is generally likely to be different from that of a chromatographic column. It is desirable to have each part of the device - membranes and the packed bed operated close to their designed capacities. This may require a somewhat special design of the hollow fiber modules, perhaps with fewer fibers in a given shell volume. Therefore it is important to develop a mathematical model for the cyclic filtration-loading-elution based chromatographic purification of a binary protein mixture in the bead-filled hollow fiber membrane device. One would like to know from the solution of the governing equations what should be the duration of the feeding step for a given feed flow rate and feed concentration without having much protein breakthrough at the permeate exit. One would also like to know during the elution step the retention time and the band height and width of each product peak, in fact, the complete peak profile. To achieve this objective, here a clean cell-free feed is assumed. Further, an ultrafiltration membrane is used. The main part of this Chapter will develop a mathematical model for the description of concentration profiles in both liquid and solid phases on the shell-side bed as well as the breakthrough curve at the permeate exit in the loading step and present the simulation

results. The preliminary description for the elution behaviors by a modified model will be provided briefly at the end of this Chapter.

6.2 Assumptions Used in the Model

In the development of the model proposed here, two basic assumptions are made:

1) Steady state ultrafiltration behavior with a bead-filled shell side is employed to model the time-dependent protein breakthrough behavior on the shell side during the loading step;

2) The "free-surface model" of Happel (1959) is employed so that one can model the whole device of N_0 fibers as a collection of individual fibers each having associated with it a given shell-side volume with no interaction between the corresponding volumes of the adjacent fibers (Gill 1973; Karoor 1993) (Figure 6.1).

Additional assumptions are:

3) Extent of concentration polarization is limited for the dilute feed solutions and permeable proteins;

4) No axial (z-direction) dispersion on the tube-side;

5) Liquid in plug flow on the shell side;

6) Constant rejection $R_i{}^/$ of an individual protein species i along the fiber length;

7) The behavior for each species may be modeled independently.

8) Local equilibrium exists between C_{ip} and C_{is} where C_{ip} is the mobile phase protein concentration and C_{is} is the lumped protein concentration on the stationary phase.

9) Constant feed concentration, no retentate recycle.

10) The osmotic pressures on both sides of the membrane will be neglected since the protein concentration in the feed is low. Solutions from Chapter 5 for the profiles of the axial velocities and pressures on both the feed side and the permeate side will be utilized.

11) Extended section at the permeate exit will not be considered in this Chapter.
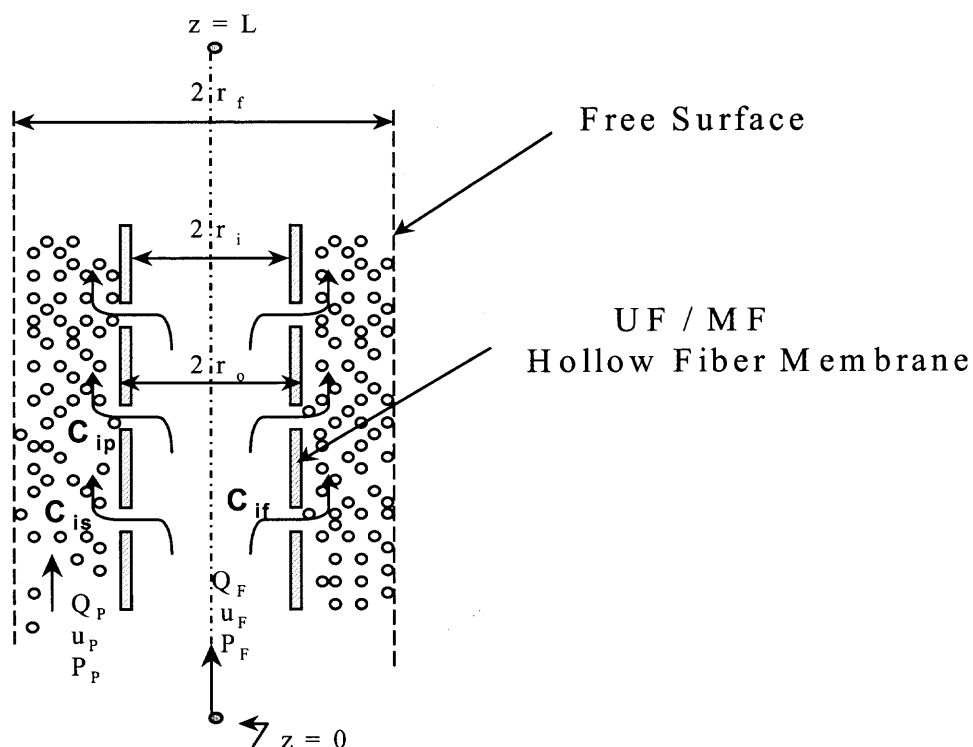
Figure 6.1 Schematic of the unit cell around any hollow fiber surrounded by a "free surface" in the cell model

6.3 Equivalent Radius of Free Surface

To determine the equivalent radius of free surface, it is considered that the relative volume of adsorbents surrounding a single fiber is the same as the relative volume of the total adsorbents surrounding all hollow fibers in the module (Happel 1959). Therefore, one has

$$\frac{(\pi R_i^2 - N_0 \pi r_o^2)L}{N_0 \pi r_o^2 L} = \frac{\pi (r_f^2 - r_o^2)L}{\pi r_o^2 L} \tag{6.1}$$

Where r_f is the free surface radius. Then

$$r_f = \frac{R_i}{\sqrt{N_0}} \tag{6.2}$$

6.4 Mass Balance of Species i in the Feed on the Tube Side

First, $R_i^/$, the solute rejection, is defined as

$$R_i^/ = 1 - \frac{C_{ipz}}{C_{ifz}} \tag{6.3}$$

where C_{ipz} and C_{ifz} are the local concentrations of species i in the permeate and the feed on the opposite sides of the fiber wall. In fact, $R_i^/$ is a function of feed and permeate concentrations, TMP and the membrane characteristics, e.g. permeation parameter, A, etc. In the present work, $R_i^/$ is assumed to be a constant when feed concentration C_{if0} and TMP are fixed. Then

$$\frac{d(Q_{Fz} C_{ifz})}{dz} = -\pi d_i J_{vz} C_{ifz} (1 - R_i^/) N_0 = -\pi d_i N_0 J_{i,z} \tag{6.4}$$

where

$$J_{i,z} = J_{vz} C_{ifz} (1 - R_i^/) \tag{6.5}$$

is the local species flux. One also has

$$\frac{d(Q_{Fz} C_{ifz})}{dz} = Q_{Fz} \frac{dC_{ifz}}{dz} + C_{ifz} \frac{dQ_{Fz}}{dz} = -\pi d_i J_{vz} C_{ifz} (1 - R_i^/) N_0 \tag{6.6}$$

From eq 5.4a, $\quad Q_{Fz} = Q_{F0} - N_0 \pi d_i \int_0^z J_{vz}\, dz$

one can get:

$$\frac{dQ_{Fz}}{dz} = -\pi \, d_i \, J_{vz} \, N_0 \tag{6.7}$$

Substitute eq 6.7 into the right-hand side of eq 6.6, and rearrange; one gets

$$Q_{Fz} \frac{dC_{ifz}}{dz} + C_{ifz} \frac{dQ_{Fz}}{dz} = C_{ifz} \, (1 - R_i') \frac{dQ_{Fz}}{dz} \tag{6.8}$$

Then

$$Q_{Fz} \frac{dC_{ifz}}{dz} = -R_i' \frac{dQ_{Fz}}{dz} C_{ifz} \tag{6.9}$$

Rearranging eq 6.9, one obtains:

$$\frac{dC_{ifz}}{C_{ifz}} = -R_i' \frac{dQ_{Fz}}{Q_{Fz}} \tag{6.10}$$

Integrate C_{ifz} from C_{if0} to C_{ifz} and Q_{Fz} from Q_{F0} to Q_{Fz}, the following expression can be obtained

$$\ln \frac{C_{ifz}}{C_{if0}} = -R_i' \ln \frac{Q_{Fz}}{Q_{F0}} \tag{6.11}$$

Rearrange eq 6.11, one gets eq 6.12.

$$C_{ifz} = C_{if0} (\frac{Q_{F0}}{Q_{Fz}})^{R_i'} \qquad (0 \le R_i' \le 1) \tag{6.12}$$

where Q_{Fz} can be calculated by eq 5.23a. Q_{F0} and C_{if0} are known boundary conditions. When $R_i' = 1$, nothing can pass through the membrane pores, total amount of species i will not change along the membrane length and it gets concentrated.

$$C_{ifz} \, Q_{Fz} = C_{if0} Q_{F0} \tag{6.13}$$

When $R_i' = 0$, the membrane has no rejection for the solute, therefore feed side concentration is not going to change, therefore one has:

$$C_{ifz} = C_{if0} \tag{6.14}$$

6.5 Mass Balance of Species i in the Permeate on the Shell Side

Unlike the situation in traditional chromatography column, the process studied in the integrated device is different. First, the velocity along the module length is not constant due to the presence of a permeation-based flux. Secondly, in the shell-side bed, there are biomolecules coming from upstream of the chromatographic column as well as biomolecules coming from the tube side of the cartridge (Figure 6.2).

Shell-Side Bed

$u_{ip|z}$

From the tube side

Dispersion

r_o

r_f

$z=0$

z

Δz

$z=L$

Solid phase $1-\varepsilon$ Liquid phase ε

$r = 0$
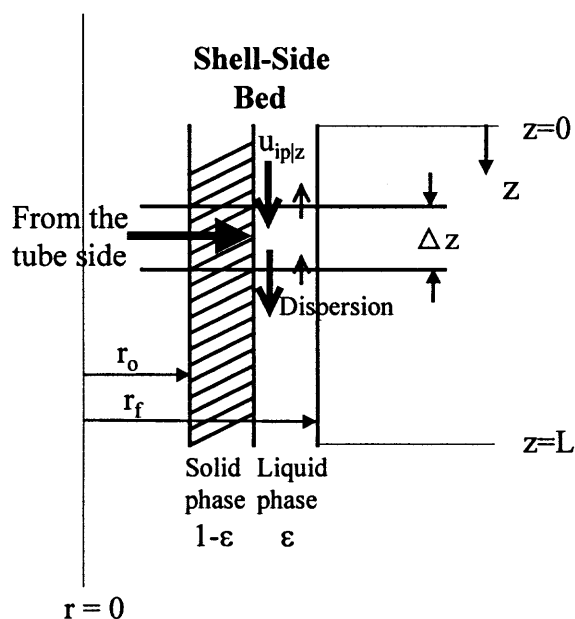
Figure 6.2 Schematic of the species flow pattern in the shell-side bed of the integrated device by using free surface model

To develop the governing equation for mass balance in the shell-side bed, the column is modeled as an one-dimensional system with the void fraction being constant throughout the bed. Here an elemental length of Δz is analyzed (Figure 6.2). Besides the axial convection and dispersion terms, there is an extra source coming from the tube side with the permeate flux (Eq 6.5). Therefore the mass balance in the Δz section is following:

$$[\varepsilon S_F u_{ip} C_{ip}\big|_{z,t} - \varepsilon S_F D_{ieff} \frac{\partial C_{iP}}{\partial z}\big|_{z,t}] - [\varepsilon S_F u_{ip} C_{ip}\big|_{z+\Delta z,t} - \varepsilon S_F D_{ieff} \frac{\partial C_{iP}}{\partial z}\big|_{z+\Delta z,t}]$$

$$+ 2\pi r_i J_{vz} \Delta z C_{ifz} (1 - R_i')\big|_{z,t} = S_F \Delta z [\varepsilon \frac{\partial C_{ip}}{\partial t} + (1 - \varepsilon) \frac{\partial C_{is}}{\partial t}] \tag{6.15}$$

where D_{ieff} is the effective axial dispersion coefficient of species i. S_F is the cross-sectional area outside a hollow fiber in one unit cell by applying the "free surface model", and

$$S_F = (r_f^2 - r_o^2)\pi \tag{6.16}$$

Dividing eq 6.15 by $\varepsilon S_F \Delta z$,

$$\frac{\partial C_{ip}}{\partial t} + \frac{(1 - \varepsilon)}{\varepsilon} \frac{\partial C_{is}}{\partial t} = \frac{u_{ip} C_{ip}\big|_{z,t} - u_{ip} C_{ip}\big|_{z+\Delta z,t}}{\Delta z} - \frac{D_{ieff} \frac{\partial C_{iP}}{\partial z}\big|_{z,t} - D_{ieff} \frac{\partial C_{iP}}{\partial z}\big|_{z+\Delta z,t}}{\Delta z}$$

$$+ \frac{2\pi r_i J_{vz} C_{ifz} (1 - R_i')\big|_{z,t}}{\varepsilon S_F} \tag{6.17}$$

Here u_{ip} is the interstitial velocity in the shell-side bed. Superficial velocity u_p is

$$u_p = u_{ip}\varepsilon \tag{6.18}$$

Substitute eqs 6.16 and 6.18 into eq 6.17, and get the following governing equation:

$$\frac{\partial C_{ip}}{\partial t} + \frac{(1 - \varepsilon)}{\varepsilon} \frac{\partial C_{is}}{\partial t} + \frac{\partial (u_p C_{ip})}{\varepsilon \partial z} = \frac{\partial}{\partial z}(D_{ieff} \frac{\partial C_{ip}}{\partial z}) + \frac{2\pi r_i J_{vz} C_{ifz} (1 - R_i')}{\varepsilon (r_f^2 - r_o^2)\pi} \tag{6.19a}$$

By substitution of eq 6.2 into eq 6.19a, eq 6.19a can be written as

$$\frac{\partial C_{ip}}{\partial t} + \frac{(1 - \varepsilon)}{\varepsilon} \frac{\partial C_{is}}{\partial t} + \frac{\partial (u_p C_{ip})}{\varepsilon \partial z} = \frac{\partial}{\partial z}(D_{ieff} \frac{\partial C_{ip}}{\partial z}) + \frac{2\pi r_i N_0 J_{vz} C_{ifz} (1 - R_i')}{\varepsilon (\pi R_i^2 - N_0 \pi r_o^2)} \tag{6.19b}$$

The basic difference between equation 6.19 and the conventional chromatographic/packed bed models lies in the extra source term on the right hand side and a z-dependent axial superficial velocity u_p through the bed (shell side). From eq 5.9a, one gets:

$$\frac{du_p}{dz} = \frac{2\pi r_i N_0 J_{vz}}{(R_i^2 - N_0 r_o^2)\pi}$$

(6.20)

Substituting eq 6.20 into eq 6.19b and rearranging leads to

$$\frac{\partial C_{ip}}{\partial t} + \frac{(1-\varepsilon)}{\varepsilon}\frac{\partial C_{is}}{\partial t} + \frac{u_p}{\varepsilon}\frac{\partial C_{ip}}{\partial z} = \frac{\partial}{\partial z}(D_{ieff}\frac{\partial C_{ip}}{\partial z}) + \frac{2 r_i J_{vz} N_0}{(R_i^2 - N_0 r_o^2)}\frac{[C_{ifz}(1-R_i')-C_{ip}]}{\varepsilon}$$

(6.21)

6.6 Estimation of the Parameters

Due to the porous backing of the membrane, the "dispersion model" (Levenspiel 1972) for determining ε and the axial dispersion coefficient D_{ieff} in the traditional column could not be used here. However, the bed void fraction ε can be estimated by Kozeny-Blake equation (Bird, Stewart and Lightfoot 1960) for a packed bed from the B values determined from experimental data. Results are provided in Table 5.1. For the estimation of D_{ieff}, Yamamoto (1983a and 1983b) found that D_{ieff}/u_i is constant regardless of flow rate and the type of gel particles and solutes, and is a unique function of the particle size of gel. Here u_i is the interstitial velocity in the packed bed. So D_{ieff}/u_i would remain constant despite any change in ionic strength. Luo and Hsu (1997) obtained the D_{ieff} for DEAE Sepharose CL-6B ion exchanger to be 0.235 cm^2/min (3.917 $\times$ 10^{-7} m^2/s). The experimental conditions in Luo and Hsu are shown in Table 6.1. The value of D_{ieff}/u_i is 7.83 $\times$ 10^{-4}m for the beads used in their study. The resin bead employed in this study is DEAE Sepharose Fast Flow media which has the same size distribution as that of DEAE Sepharose CL-6B ion exchanger. Therefore it can be assumed that the ratio of D_{ieff}/u_{ip} in this study is equal to that of Luo and Hsu (1997), i.e., 7.83 $\times$ 10^{-4} m (Table 6.1); therefore the following equation can be adopted:

$$D_{ieff}(m^2/s) = 7.83 \times 10^{-4}(m) \times u_{ip}(m/s)$$ (6.22)

Other empirical correlations for dispersion coefficient are given by Chung and Wen (1968), Gunn (1987), Hejimánek and Schneider (1993) and Koch and Brady (1985).

Table 6.1 Experimental conditions in Luo and Hsu (1997)

Void fraction ε	Column I.D., cm	Cross-sectional area, cm^2	Flow rate, ml/min	Interstitial velocity, u_i, m/s	D_{ieff}/u_i, m
0.28	1.5	1.77	1.5	5.0×10^{-4}	7.83×10^{-4}

For the adsorption process, the solvent is not adsorbed. Therefore the mass balance of the mobile phase is not considered here. The adsorption kinetics are assumed to be very fast and can be represented by an equilibrium isotherm. This is close to the real situations for Mb and α-LA. It takes less than 15 min and one hour for the adsorption of Mb and α- LA to achieve equilibrium. Further linear isotherm is assumed because the protein concentration in the liquid phase of the shell-side bed is low. According to eq 4.6 in Chapter 4, $q^* = \dfrac{q_m C^*}{K_d} = KC^*$, and K for Mb ($K_{Mb}$, assuming void fraction ε=0.3) by Scatchard plot (Figure 4.26) is:

$$K_{Mb} = \frac{q_m}{K_d} = \frac{30.40}{(1-\varepsilon)} = \frac{30.40}{1-0.3} = 43.43$$ (6.23)

K for α-LA (K_{LA}, assuming void fraction ε=0.3) by Scatchard plot (Figure 4.30) is:

$$K_{Mb} = \frac{q_m}{K_d} = \frac{21769.6}{(1-\varepsilon)} = \frac{21769.6}{1-0.3} = 31099$$ (6.24)

The solute rejection, $R_i^{/}$, assumed to be constant along the length although TMP may not be constant. Estimation of $R_i^{/}$s from the experimental data is made in the

following way. Use the method in Table 4.2 to get the ratio of (permeate concentration)/(feed concentration) first, then use eq 6.3 to obtain an estimate of R_i'. C_{if0} is used instead of C_{ifz} since the module length (0.254 m) is not long. Results are shown in Table 6.2. Average values are taken for the cyclic processes.

Table 6.2 Estimated R_i' from the experimental data

Module 1					
For Figure 4.19		For Figure 4.21		For Figure 4.23, solid line	
Mb					
C_{ip}/C_{if0}	R_i'	C_{ip}/C_{if0}	R_i'	C_{ip}/C_{if0}	R_i'
0.35	0.65	0.44	0.56	0.44	0.56
α-LA					
0.12	0.88	0.11	0.89	0.14	0.86

Module 2 from data in Figure 4.20			
Mb		**α-LA**	
C_{ip}/C_{if0}	R_i'	C_{ip}/C_{if0}	R_i'
0.56	0.44	0.37	0.63

The results in the above table are estimated from the experiments with the fixed ES (Table 3.3); the ES has the function of capturing biomolecules exiting from the permeate outlet. So it is expected that the actual value of R_i' is somewhat higher than those in Table 6.2. This will be adjusted in the simulations.

6.7 Boundary Conditions and Initial Conditions

The boundary conditions for equations 6.12 and 6.21 are as follows:

$$@ \ z = 0: \qquad P_{Fz}=P_{F0}, \quad Q_{Fz}=Q_{F0}, \quad C_{ifz}=C_{if0}, \qquad (6.25)$$

For the shell-side bed, Danckwerts boundary conditions (Danckwerts 1953) are employed by assuming that the mass transport outside the column is caused by convection only. Therefore,

@ z = 0: $\qquad (u_{iP} C_{iP})\big|_{z=0^-} - (u_{iP} C_{iP})\big|_{z=0^+} + D_{ieff} \dfrac{\partial C_{ip}}{\partial z}\bigg|_{z=0^+} = 0$ (6.26a)

However the shell-side bed is unlike the traditional chromatographic column, there is no flow in z-direction at z = 0, which is $u_{iP}\big|_{z=0} = 0$; therefore, eq 6.26a becomes

$$D_{ieff} \frac{\partial C_{ip}}{\partial z}\bigg|_{z=0} = 0 \Rightarrow \frac{\partial C_{ip}}{\partial z}\bigg|_{z=0} = 0$$ (6.26b)

At the permeate exit, the concentration in the liquid phase will not change after the solvent leaves the shell-side outlet, thus one can write:

@ z = L: $\qquad \dfrac{\partial C_{ip}}{\partial z}\bigg|_{z=L} = 0$ (6.27a)

Since the ES is not considered here, thus one has

@ z = L: $\qquad P_{PL} = P_{atm}$ (6.27b)

The initial conditions for loading are

@ t = 0 $\qquad C_{iP_z} = 0, \quad 0 \le z \le L$ (6.28a)

$$C_{isz} = 0, \quad 0 \le z \le L$$ (6.28b)

6.8 Solution Procedure

There are a variety of methods such as finite difference, orthogonal collocation and method of lines available for the numerical solution of PDEs in time and spatial dimensions. The technique of method of lines is adopted here. In this method, only the

spatial gradients are discretized by finite difference equations thus reducing the system of PDEs to a coupled system of ODEs in the time domain (Brian, Zwiebel and Artigue 1987)

Following Brian et al. (1987), the effective chromatographic column length on the shell-side bed in the axial direction has been discretized into NB points as shown in Figure 6.3. Equation 6.21 can be transformed to NB ordinary differential equations in the time domain by the following procedure.

0 1 2 m-1 m m+1   NB-1 NB NB+1

z=0   Δz   z=L
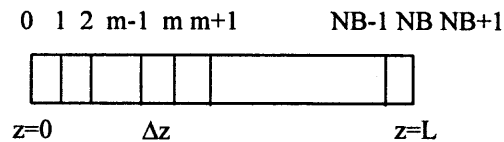
Figure 6.3 Axial grid for finite difference approximation of the spatial derivatives.

First, D_{ieff} is assumed to be a constant throughout the column corresponding to the average velocity in the shell-side bed. With the previous assumption of linear isotherm between the liquid phase and the solid phase, Eq 6.21 can be written as:

$$\frac{\partial C_{ip}}{\partial t} + \frac{(1-\varepsilon)}{\varepsilon} K \frac{\partial C_{ip}}{\partial t} + \frac{u_p}{\varepsilon} \frac{\partial C_{ip}}{\partial z} = D_{ieff} \frac{\partial^2 C_{ip}}{\partial z^2} + \frac{2 r_i J_{vz} N_0}{(R_i^2 - N_0 r_o^2)} \frac{[C_{ifz}(1 - R_i')-C_{ip}]}{\varepsilon} \qquad (6.29a)$$

Thus

$$(1 + \frac{1-\varepsilon}{\varepsilon} K) \frac{\partial C_{ip}}{\partial t} + \frac{u_p}{\varepsilon} \frac{\partial C_{ip}}{\partial z} = D_{ieff} \frac{\partial^2 C_{ip}}{\partial z^2} + \frac{2 r_i J_{vz} N_0}{(R_i^2 - N_0 r_o^2)} \frac{[C_{ifz}(1 - R_i')-C_{ip}]}{\varepsilon} \qquad (6.29b)$$

Let
$$S = (1 + \frac{1-\varepsilon}{\varepsilon} K) \qquad (6.30a)$$

$$F_1(z) = \frac{u_p}{\varepsilon} = \frac{Q_{Pz}}{\varepsilon S_s} \qquad (6.30b)$$

$$F_2(z,C_{ip}) = \frac{2\,r_i\,J_{vz}\,N_0}{(R_i^2 - N_0\,r_o^2)}\frac{[C_{ifz}(1-R_i')-C_{ip}]}{\varepsilon} \tag{6.30c}$$

Q_{Pz}, J_{vz} and C_{ifz} can be calculated by eqs 5.23b, 5.18a and 6.12, respectively. Therefore eq. 6.29b can be written as

$$\frac{\partial C_{ip}}{\partial t} = \frac{D_{ieff}}{S}\frac{\partial^2 C_{ip}}{\partial z^2} - \frac{F_1(z)}{S}\frac{\partial C_{ip}}{\partial z} + \frac{F_2(z,C_{ip})}{S} \tag{6.31}$$

Now the finite difference formulas for the liquid phase on the shell-side bed are as follows:

For m = 0, five point forward differences lead to

$$\frac{\partial C_{ip}}{\partial z}\bigg|_{m=0} = \frac{-25C_{ip}\big|_{m=0}+48C_{ip}\big|_{m=1}-36C_{ip}\big|_{m=2}+16C_{ip}\big|_{m=3}-3C_{ip}\big|_{m=4}}{12\Delta z} \tag{6.32}$$

For m = 1 through NB, three point central differences are used for the second order term and upwind differences are used for the convective term; therefore

$$\frac{\partial C_{ip}}{\partial z}\bigg|_m = \frac{C_{ip}\big|_m - C_{ip}\big|_{m-1}}{\Delta z} \tag{6.33}$$

and

$$\frac{\partial^2 C_{ip}}{\partial z^2}\bigg|_m = \frac{C_{ip}\big|_{m+1} - 2C_{ip}\big|_m + C_{ip}\big|_{m-1}}{\Delta z^2} \tag{6.34}$$

From the finite difference formulas shown above, eq 6.31 can be rewritten at each axial location m, $1 \le m \le NB$, as follows

$$\frac{dC_{ip}}{dt}\bigg|_m = \frac{D_{ieff}}{S}\frac{C_{ip}\big|_{m+1} - 2C_{ip}\big|_m + C_{ip}\big|_{m-1}}{\Delta z^2} - \frac{F_1(z)}{S}\frac{C_{ip}\big|_m - C_{ip}\big|_{m-1}}{\Delta z} + \frac{F_2(z,C_{ip}\big|_m)}{S} \tag{6.35}$$

For m = 1, the partial differential equation in finite difference form becomes

$$\frac{dC_{ip}}{dt}\bigg|_{m=1} = \frac{D_{ieff}}{S}\frac{C_{ip}\big|_{m=2}-2C_{ip}\big|_{m=1}+C_{ip}\big|_{m=0}}{\Delta z^2} - \frac{F_1(z=\Delta z)}{S}\frac{C_{ip}\big|_{m=1}-C_{ip}\big|_{m=0}}{\Delta z}$$
$$+\frac{F_2(z=\Delta z, C_{ip}\big|_{m=1})}{S}$$

(6.36)

where $C_{ip}\big|_{m=0}$ is determined from the boundary condition at $z = 0$. Combine eq 6.26b and

eq 6.32,

$$\frac{\partial C_{ip}}{\partial z}\bigg|_{m=0} = \frac{-25C_{ip}\big|_{m=0}+48C_{ip}\big|_{m=1}-36C_{ip}\big|_{m=2}+16C_{ip}\big|_{m=3}-3C_{ip}\big|_{m=4}}{12\Delta z} = 0$$

(6.37)

one gets

$$C_{ip}\big|_{m=0} = \frac{48C_{ip}\big|_{m=1}-36C_{ip}\big|_{m=2}+16C_{ip}\big|_{m=3}-3C_{ip}\big|_{m=4}}{25}$$

(6.38)

For m = NB, the exit boundary condition $\dfrac{\partial C_{ip}}{\partial z}\bigg|_L = 0$ (eq 6.27a) is applied. The finite

difference approximation of this boundary condition leads to the following unstable

condition, if central difference formula is used

$$C_{ip}\big|_{m=NB-1} = C_{ip}\big|_{m=NB+1}$$

(6.39)

However, the protein concentration in the liquid phase does not change after point NB,

therefore it is assumed that

$$C_{ip}\big|_{m=NB+1} = C_{ip}\big|_{m=NB}$$

(6.40)

The partial differential equation at point NB is represented by:

$$\frac{dC_{ip}}{dt}\bigg|_m = \frac{D_{ieff}}{S}\frac{C_{ip}\big|_{m=NB-1}-C_{ip}\big|_{m=NB}}{\Delta z^2} - \frac{F_1(z=L)}{S}\frac{C_{ip}\big|_{m=NB}-C_{ip}\big|_{m=NB-1}}{\Delta z}$$
$$+\frac{F_2(z=L, C_{ip}\big|_{m=NB})}{S}$$

(6.41)

The equations to be solved are summarized in Table 6.3.

Table 6.3 Summary of ODEs for liquid phase on the shell-side bed

1. Equation for m = 1

$$\frac{dC_{ip}}{dt}\bigg|_{m=1} = \frac{D_{ieff}}{S} \frac{C_{ip}\big|_{m=2} - 2C_{ip}\big|_{m=1} + C_{ip}\big|_{m=0}}{\Delta z^2} - \frac{F_1(z = \Delta z)}{S} \frac{C_{ip}\big|_{m=1} - C_{ip}\big|_{m=0}}{\Delta z}$$
$$+ \frac{F_2(z = \Delta z, C_{ip}\big|_{m=1})}{S}$$

(6.36)

where, $C_{ip}\big|_{m=0} = \dfrac{48C_{ip}\big|_{m=1} - 36C_{ip}\big|_{m=2} + 16C_{ip}\big|_{m=3} - 3C_{ip}\big|_{m=4}}{25}$

(6.38)

2. Equation for 1 < m < NB

$$\frac{dC_{ip}}{dt}\bigg|_{m} = \frac{D_{ieff}}{S} \frac{C_{ip}\big|_{m+1} - 2C_{ip}\big|_{m} + C_{ip}\big|_{m-1}}{\Delta z^2} - \frac{F_1(z)}{S} \frac{C_{ip}\big|_{m} - C_{ip}\big|_{m-1}}{\Delta z} + \frac{F_2(z, C_{ip}\big|_{m})}{S}$$

(6.35)

3. Equation for m = NB

$$\frac{dC_{ip}}{dt}\bigg|_{m} = \frac{D_{ieff}}{S} \frac{C_{ip}\big|_{m=NB-1} - C_{ip}\big|_{m=NB}}{\Delta z^2} - \frac{F_1(z = L)}{S} \frac{C_{ip}\big|_{m=NB} - C_{ip}\big|_{m=NB-1}}{\Delta z}$$
$$+ \frac{F_2(z = L, C_{ip}\big|_{m=NB})}{S}$$

(6.41)

The resulting ordinary differential equations in time domain for the shell-side bed have been solved using IMSL subroutine, IVPRK; the program was run in the mainframe computer, VAX/VMS environment. The computer code was written in Fortran 77. The liquid phase protein concentration in each differential section was obtained from the solution of the ODEs mentioned above. The adsorbed amount of protein in each section was then calculated using the equilibrium constant and the solid phase volume of the differential section.

6.9 Results and Discussions

6.9.1 Effects of Axial Dispersion

As shown in eq 6.22, the axial dispersion coefficient changes with the change of velocity. In the ordinary differential equations developed above, it is assumed that D_{ieff} is a constant. Figure 6.4 shows the effects of different D_{ieff} on the breakthrough curve of Mb. The parameters used in the simulation are shown in Table 6.4. The module dimensions are provided in Table 3.2. No ES is considered here.
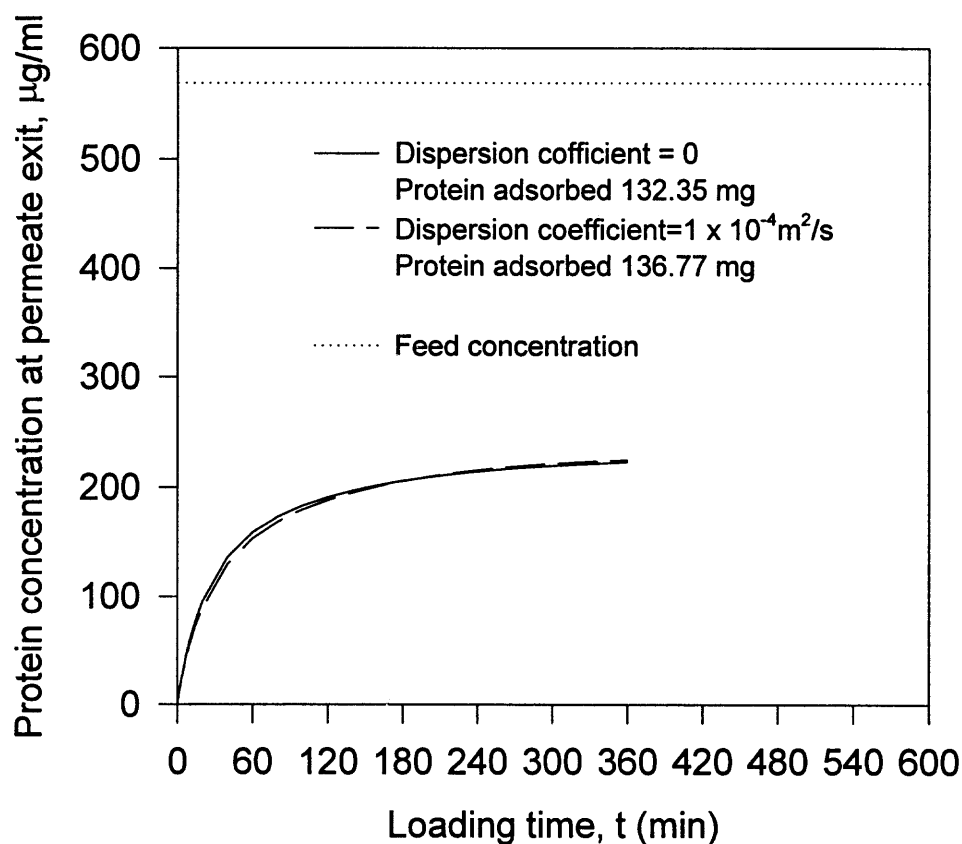
Figure 6.4 Effect of D_{ieff} on the simulation result for the breakthrough curve of Mb

Table 6.4 Parameters utilized in the simulation of Figure 6.4

Feed flow rate Q_{F0}, ml/min	200
Feed Inlet pressure P_{F0}, psi	7.0
Linear equilibrium coefficient, K_{Mb}	43.43
Feed inlet concentration C_{if0}, mg/ml	0.568
Rejection factor $R_i^{/}$	0.6
Void fraction ε	0.325
A, m/Pa.s	1.857×10^{-10}
B, Pa.s/m^3	4.724×10^{11}
Permeate exit pressure	Atmospheric pressure
Loading time, min	360
Axial dispersion coefficient, D_{ieff}, m^2/s	0 and 1×10^{-4}

In Figure 6.4, the solid line shows the breakthrough curve for the ideal case which has no axial dispersion. The dashed line provides the breakthrough curve for the situation which has considerable axial dispersion ($D_{ieff} = 1 \times 10^{-4}$ m^2/s). It is seen that the effect of axial dispersion is not very important for the breakthrough behavior. The total adsorbed amounts of the protein are quite similar for both cases for six hours' loading. It is obvious that the ES will reduce the breakthrough to some extent. Figure 6.5 shows the concentration profiles in both tube and shell sides under the same conditions as those in Table 6.4 except that the loading time is 15 minutes. There is little difference between the two cases having no axial dispersion and having considerable axial dispersion. Therefore the assumption for the constant D_{ieff} is reasonable for the prediction of loading and breakthrough behaviors. In the following simulations, D_{ieff} for average mobile phase velocity in the shell-side bed will be adopted by calculation from eq 6.22.
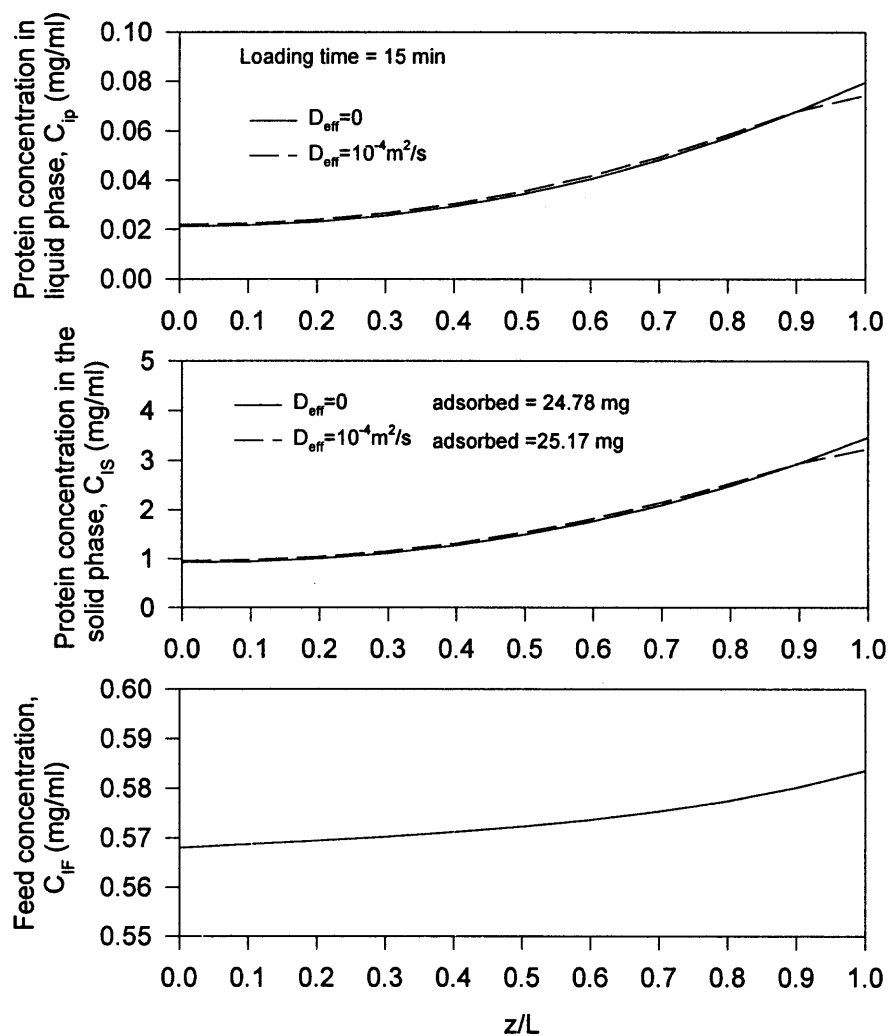
Figure 6.5 Effect of the axial dispersion on the simulation for concentration profiles in both tube and shell sides

6.9.2 Comparison of the Simulation and the Experimental Results

Simulations for loading behaviors using feed concentration of 0.568 mg/ml for Mb are

shown in Figure 6.6. All the parameters in Table 6.4 were used except $R_i^{\prime}$, loading time

and D_{ieff}. The conditions selected were those in the experiment of higher feed protein

concentrations with only a fixed ES using module 1 (Figure 4.23, solid line and Table

4.3). Loading time was 15 minutes in the experiment. R_i' was assumed to be 0.625. D_{ieff} was calculated by eq 6.22 by using the average superficial velocity u_p (which is

$$\frac{5.95 \text{ ml/min}}{2S_s} \approx \frac{3 \text{ ml/min}}{0.8188 \text{ cm}^2} = 6.107 \times 10^{-4} \text{ m/s (Table 4.3) for module 1 (Table 3.2)}$$

used in this dissertation) in the loading operation and $\varepsilon = 0.325$ (Table 5.1):

$$D_{ieff} = 7.83 \times 10^{-4} \times \frac{6.107 \times 10^{-4}}{0.325} = 1.50 \times 10^{-5} (m^2 / s)$$

In the simulation, a constant feed concentration was used as the boundary condition (eq. 6.25). From Figure 6.6, it can be seen that the tube-side concentration is increased along the module length due to a partial rejection of the protein by the membrane and its profile does not change with an increase in loading time. In the experiment actually conducted, the retentate was recycled. In addition, no ES was considered in the simulation. Therefore the adsorbed amount of protein should be less than the experimentally recovered amount of protein if it is assumed that all of the protein can be recovered by elution. The total adsorbed amount of Mb is 23.25 mg from the simulation which is somewhat less than the experimental value, which was 24.1 mg. At the permeate exit, Mb concentrations from simulation are 7.3 - 74.6 µg/ml corresponding to the loading time of 1 – 15 minutes. The optical absorbance reading at 280 nm was 0.002 (Table 4.3) for the total permeate of 89.3 ml. If it is assumed that all of the "leaking" protein was Mb, this absorbance reading is equivalent to 1.064 µg/ml by using eq 3.3 which is equivalent to the total amount of Mb in the permeate being 95 µg. At this point, one can conclude that adding the ES at the permeate exit can reduce the breakthrough and increase the yield. The corresponding pressure, flux and flow rate profiles are shown in Figure 6.7. It is seen that with the increase of TMP along the

module length, the flux increases and the concentrations on the shell-side bed increase. It can be expected that a uniform TMP profile will produce a more uniform loading concentration profile on the shell-side bed.
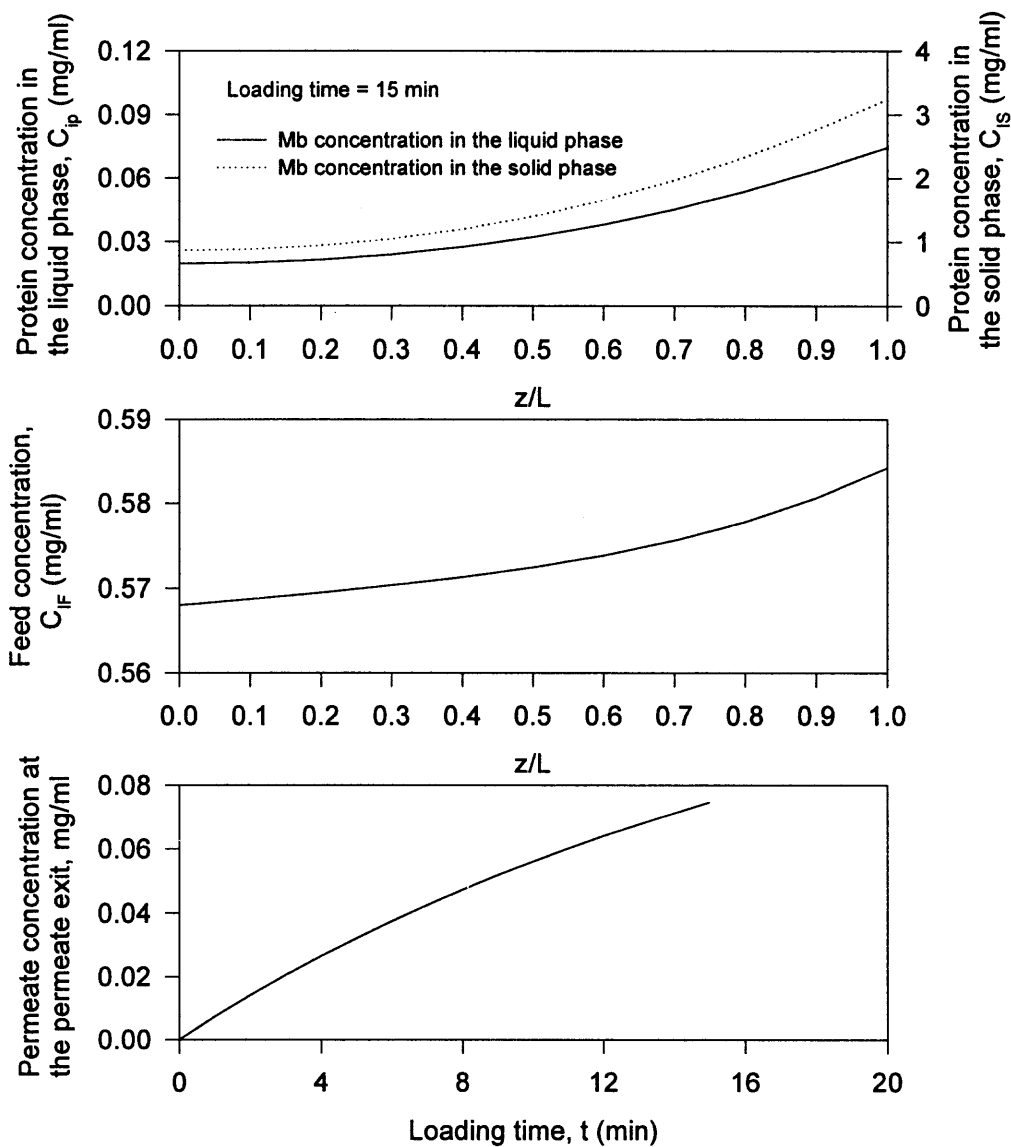
Figure 6.6 Simulation results for a feed concentration of 0.568 mg/ml for Mb on concentration profiles and breakthrough curve
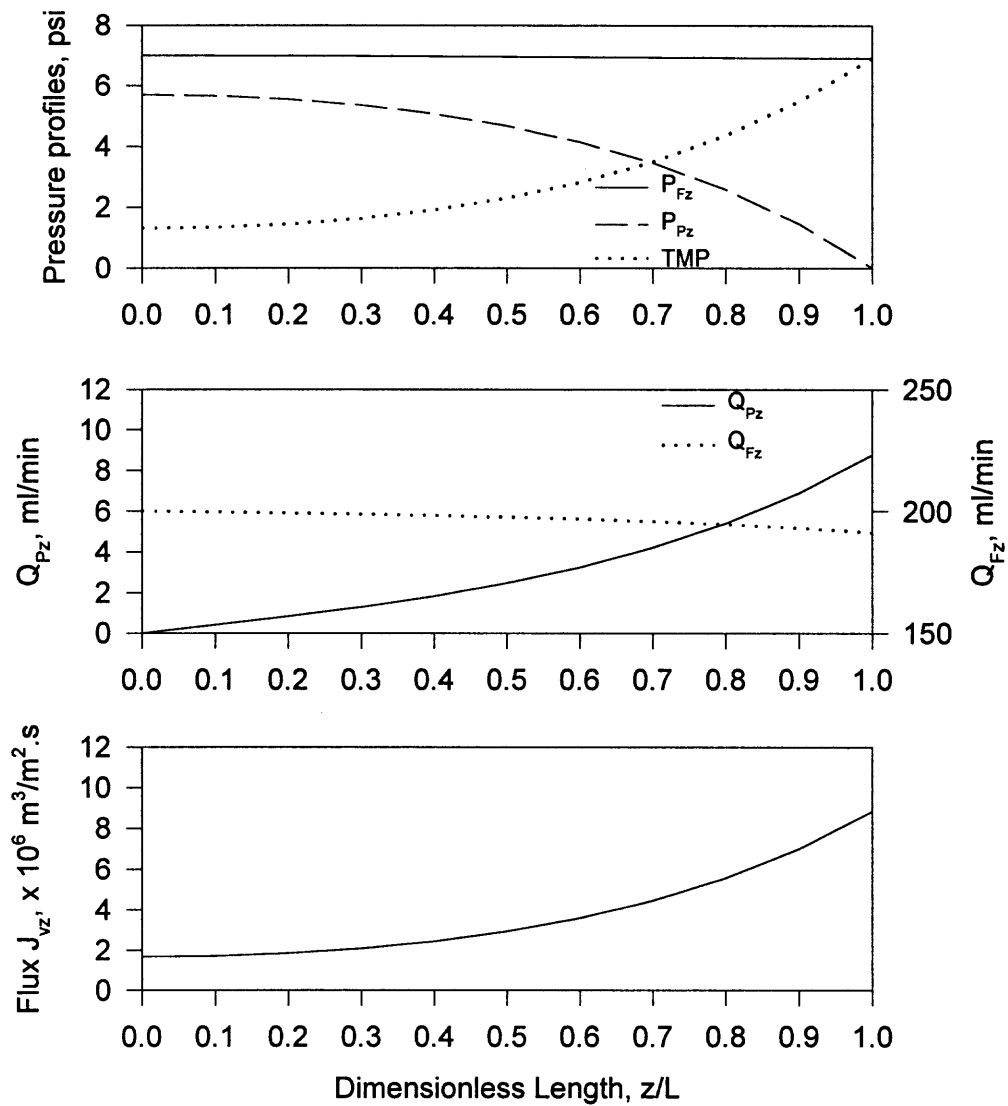
Figure 6.7 Simulation of the profiles for pressure, flow rate and flux. $A = 1.857 \times 10^{-10}$ m/Pa.s, $B = 4.724 \times 10^{11}$ Pa.s/m^3. Feed flow rate $Q_{F0} = 200$ ml/min. Feed inlet pressure $P_{F0} = 7.0$ psig. Module 1 (Table 3.2) without ES.

Similarly, adsorption of α-LA was also simulated as shown in Figure 6.8. Here the following values were adopted: $R_i^{/}$ =0.92; K_{LA}=31099; feed concentration C_{if0} = 522 μg/ml. Other parameters utilized here were same as those for Mb simulation in Figure 6.6. Tube-side concentration increases along the module length and does not change with the loading time. Concentration profiles for both liquid and solid phases on the shell-side bed change with a change of the TMP and flux. The total amount of adsorbed protein from simulation is 5.78 mg; the recovered amount from the experiment was 5.8 mg. The concentration in the liquid phase is quite low due to the high value of K_{LA} = 31099. So are the concentrations at the permeate exit. Much more amount of protein is adsorbed on the beads due to the higher value of K_{LA}. Breakthrough concentrations were also reduced considerably and it can be assumed that there was no "leaks" at the permeate exit.
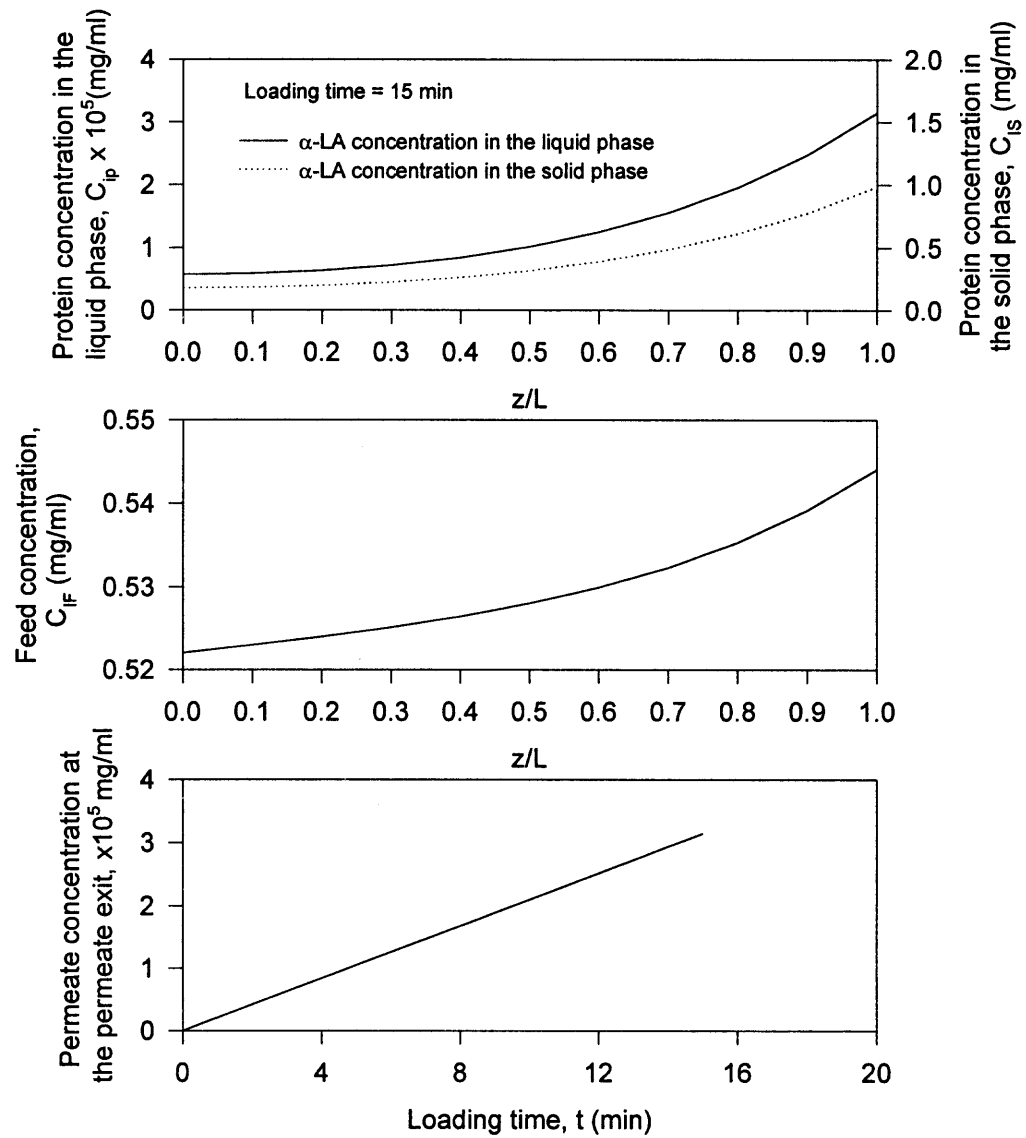
Figure 6.8 Simulation results for a feed concentration of 0.522 mg/ml for α-LA on concentration profiles and breakthrough curve

Similar simulations have been done for lower feed concentrations. Profiles are not shown here but the results are provided in Table 6.5. The same set of R_i's used in the above simulations are adopted for module 1. Total adsorbed amounts of proteins from the simulation are more than the experimentally recovered amounts of proteins when feed concentrations are in the range of 30 μg/ml. A possible reason is that the driving force in mass transfer increases when the feed concentration increases, the beads on the shell side can quickly adsorb the protein molecules passing through the membrane pores within the capacity of the beads and leave a very low liquid phase concentration for either low or high feed concentration. The lower is the feed concentration, the lower is the mass transfer driving force. Therefore the value of R_i' may vary.

Appropriate R_i's are assumed for the simulation for module 2. Results are also provided in Table 6.5. Module 2 has a higher pure water permeation rate (Table 3.2 and Table 5.1). This may cause lower R_i's compared to those of module 1.

Table 6.5 Comparison of the experimental data and the simulation results

		Mb, mg		α-LA, mg	
		Simulation	Recovered	Simulation	Recovered
Module 1 $R_{Mb}' = 0.625$ $R_{LA}' = 0.92$	Experiment from Figure 4.21 $C_{if0} \approx 140$ μg/ml	5.73	6.00	1.52	1.56
	Experiment from Figure 4.19 $C_{if0} \approx 30$ μg/ml	0.75	Avg. 0.72	0.27	Avg. 0.19
Module 2 $R_{Mb}' = 0.5$ $R_{LA}' = 0.75$	Experiment from Figure 4.20 $C_{if0} \approx 40$ μg/ml	2.68	Avg. 2.60	1.85	Avg. 1.70

6.9.3 Effect of the Water Permeation Parameter A

Figure 6.9 shows the effects of the parameter A on the total amount of protein adsorbed

and the breakthrough curve. Parameters utilized in the simulation are the same as those in

Table 6.4 except A was varied.
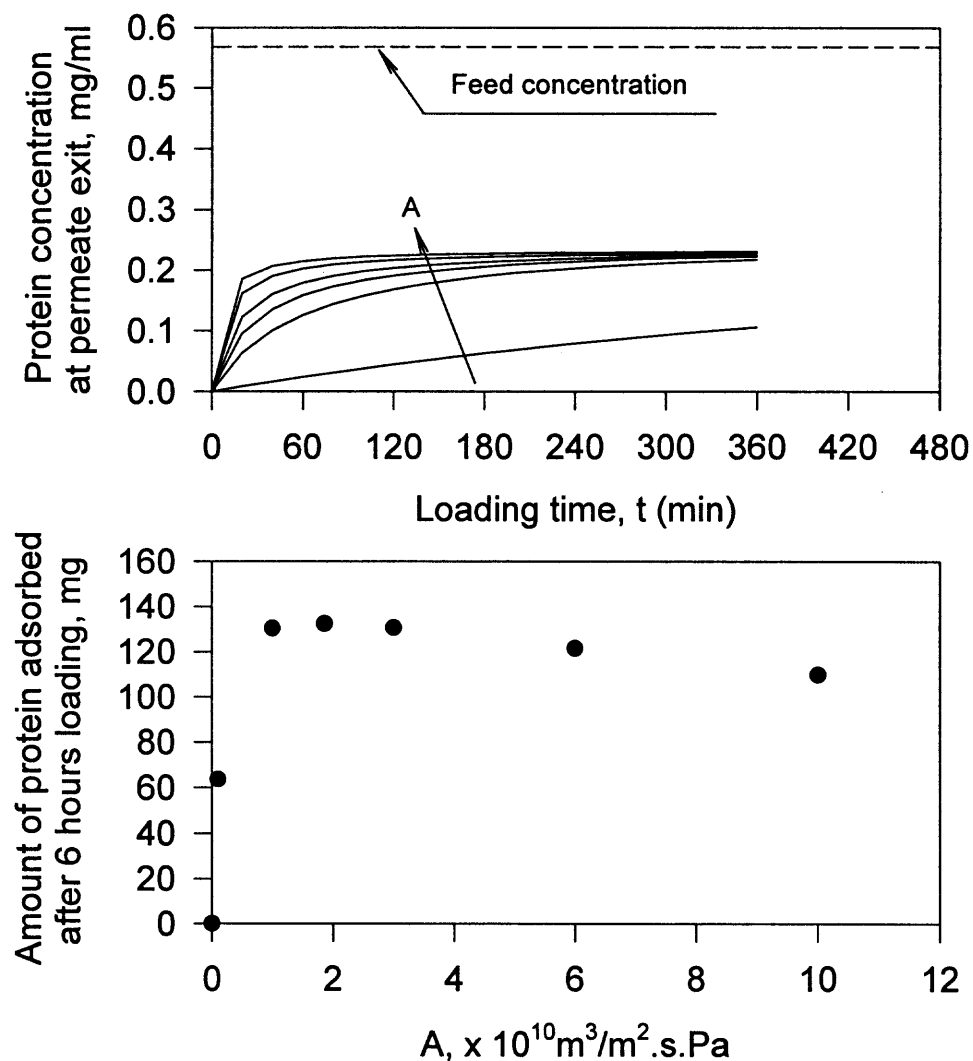
Figure 6.9 Effect of parameter A on the breakthrough curve and adsorbed amount of protein. $D_{ieff} = 0$ m^2/s. $R_i^/ = 0.6$

From Figure 6.9, it is seen that the higher the value of A, the earlier the breakthrough since more protein molecules pass through the membrane pores with the higher solvent flux. However, the total adsorbed amount of protein first increases with the increase of A and then decreases slowly after a certain value of A. Higher permeation rate brings in higher solvent flux as well as solute flux which leads to more adsorbed biomolecules on the beads. But, an even the higher solvent flux increases the pressure drop on the shell-side bed which reduces the TMP, correspondingly, the solvent flux and solute flux will decrease which can reduce the amount of protein adsorbed on the beads.

6.9.4 Effect of the Feed Flow Rate

The effect of the feed flow rate was also studied. Comparison is provided in Figure 6.10. For a feed flow rate of 2000 ml/min, more uniform tube-side concentration profile can be obtained compared to that of 200 ml/min feed flow rate although the amount of adsorbed protein decreases about 7% due to higher pressure drop in the tube side which lowers the TMP. Concentrations at the permeate exit are reduced due to the same reason. Lower TMP decreases the solvent and solute fluxes. However, a higher feed flow rate can offer higher wall shear rate on the membrane surfaces which can reduce gel layer formation and improve the flux. Also an increased feed flow rate in a certain range can increase the uniformity of the TMP profile (Figure 5.12). Therefore one can improve the feed flow rate within the biomolecule's shear tolerance as long as the pressure drop in the tube side is not excessive.
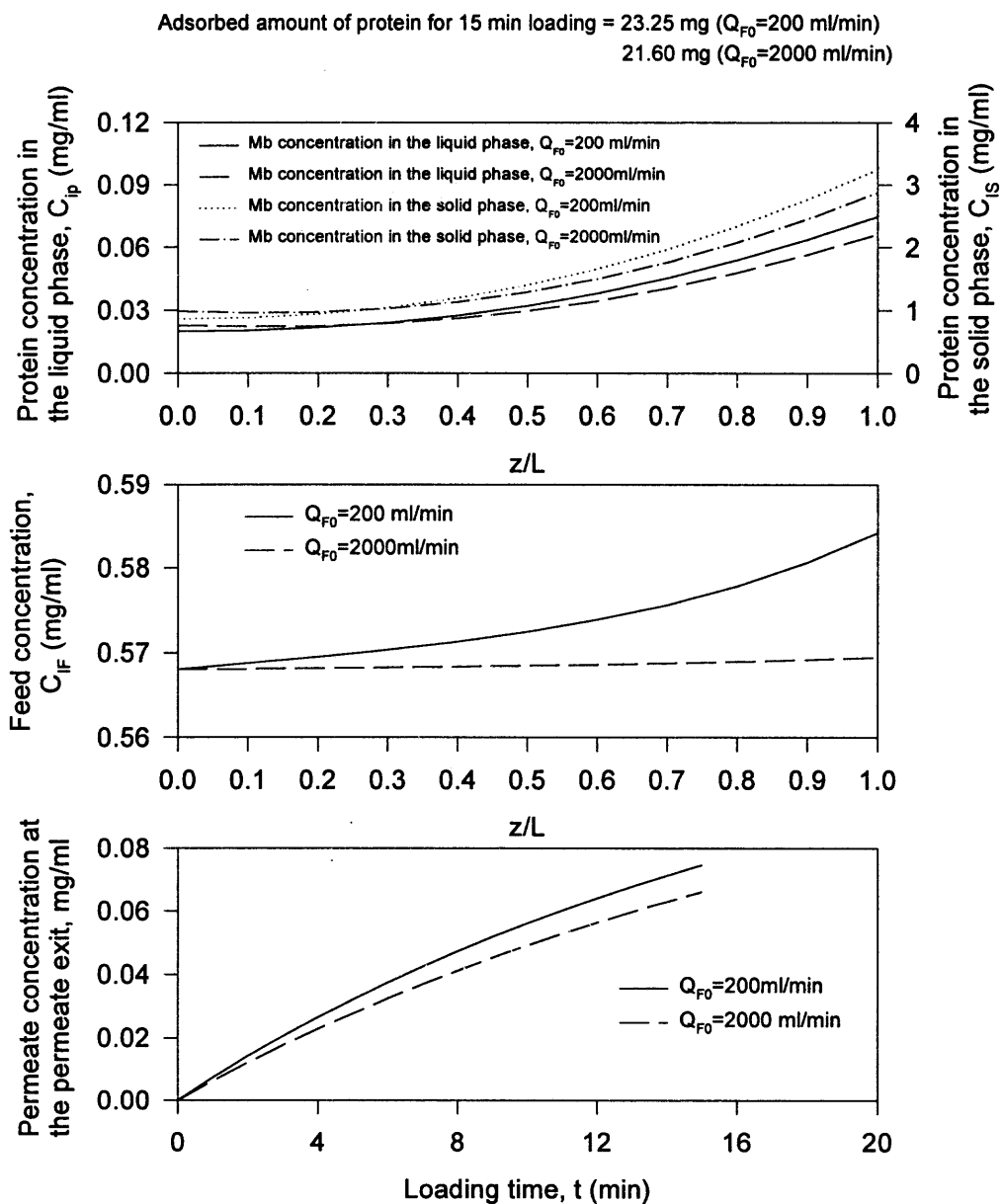
Figure 6.10 Effect of feed flow rate on the breakthrough curve and concentration profiles

6.10 Preliminary Study of the Tube-Side Elution

The physical situation in the tube-side elution is similar to that in the loading operation except no biomolecules are introduced from the tube side to the shell-side bed. Therefore eq 6.15 becomes

$$[\varepsilon S_F u_{ip} C_{ip}\big|_{z,t} - \varepsilon S_F D_{ieff} \frac{\partial C_{iP}}{\partial z}\big|_{z,t}] - [\varepsilon S_F u_{ip} C_{ip}\big|_{z+\Delta z,t} - \varepsilon S_F D_{ieff} \frac{\partial C_{iP}}{\partial z}\big|_{z+\Delta z,t}] = S_F \Delta z[\varepsilon \frac{\partial C_{ip}}{\partial t} + (1-\varepsilon)\frac{\partial C_{is}}{\partial t}]$$

(6.42)

Divide by $\varepsilon S_F \Delta z$, combine with eq 6.18 and rearrange; one gets

$$\frac{\partial C_{ip}}{\partial t} + \frac{(1-\varepsilon)}{\varepsilon}\frac{\partial C_{is}}{\partial t} + \frac{\partial(u_P C_{ip})}{\varepsilon \partial z} = \frac{\partial}{\partial z}(D_{ieff}\frac{\partial C_{ip}}{\partial z})$$

(6.43)

This is the equation for the traditional chromatographic/packed bed. However, there is one difference – unlike regular columns, u_p varies here along the length. It is assumed here that the equilibrium is instantly established when the eluent is introduced from the tube side to the shell-side bed. For the stepwise elution utilized for the separation of the binary mixture in this dissertation, it is also assumed that the lower NaCl concentration (e.g. 0.05 M NaCl) in the starting buffer can not elute the difficult-to-elute protein from the beads (e.g. α-LA, β-LG and BSA). The same procedure can be used to solve eq 6.43 except for a different initial condition for C_{ip}. The concentration profiles on the shell-side bed at the end of the loading step obtained from the previous program can be used as the initial condition in each Δz section for the elution simulation. A Fortran 77 program was written by modifying the previous program for the loading step calculation.

Results for the separation of the binary mixture of Mb and α-LA using stepwise change elution method (0.05 M NaCl to 0.5 M NaCl) are provided in Figure 6.11. The

experimental data of 2.5 min fraction concentrations from the experiment (see Figure 4.23) are also shown in the Figure. Initial condition was from the previous loading simulation for Mb and α-LA (see Figures 6.6 and 6.8). Parameters utilized here were those used in Table 6.4 except D_{ieff}, P_{F0}, Q_{F0}, C_{if0}, K and elution time. Here an elution flow rate of 2.5 ml/min was used and there was no protein present in the eluent. P_{F0} is not a boundary condition for the simulation (see Chapter 5, tube-side elution part in Section 5.2.1). D_{ieff} was calculated by eq 6.22 by using the average superficial velocity u_p (which

is $\dfrac{2.5 \text{ ml/min}}{2 \times S_s} = \dfrac{1.25 \text{ ml/min}}{0.8188 \text{ cm}^2} \approx 2.544 \times 10^{-4}$ m/s) in the elution and ε = 0.325 (Table 5.1).

$$D_{ieff} = 7.83 \times 10^{-4} \times \frac{2.544 \times 10^{-4}}{0.325} \approx 6.13 \times 10^{-7} (m^2/s)$$

Both equilibrium constants K_{Mb} and K_{LA} were assumed to be 0.1 based on over 90% recovery of proteins from the beads by using 0.05 M and 0.5 M NaCl in the starting buffer as the eluent to elute these two components from the shell-side bed. Fifty minutes were used as the elution times for the two proteins.

For a coarse estimation of the retention time for a given protein, three factors need to be considered. First, a small length of tubing was connected to each of the feed inlet and the permeate exit ports. The inside volume of the tubing was about 7.0 ml for the one connected to the permeate exit and was about 10.9 ml for the one connected to the feed inlet. The times needed to replace the fluid in the feed inlet and the permeate port tubing

are about $\dfrac{10.0 \text{ ml}}{2.5 \text{ ml/min}} = 4.0$ minutes and $\dfrac{7.0 \text{ ml}}{2.5 \text{ ml/min}} \approx 2.8$ minutes respectively for an elution flow rate of 2.5 ml/min. Secondly, the time needed to replace tube-side fluid can

be estimated by dividing the tube-side volume (can be calculated by module dimension from Table 3.2) by the average flow rate in the tube-side which is about $\dfrac{9.9 \text{ ml}}{2.5 \text{ ml/min/2}} \approx 7.9$ minutes. Third, the theory developed here does not take into account the time needed to replace the fluid in the shell-side bed and the ES bed. A rough estimation for the <u>average</u> time needed to replace the fluid in the shell-side bed and the ES bed is made as follows:

$$\frac{(\text{Total bead volume in the shell} - \text{side bed and the fixed ES bed}) \times \varepsilon}{\text{Average volumetric flow rate in the shell-side bed}} =$$

$$\frac{(20 + 0.65) \text{ ml} \times 0.3248}{2.5 \text{ ml/min/2}} \approx 5.3 \text{ min} \tag{6.44}$$

For Mb elution performed in the experiment shown in Figure 6.11, the fluid in the feed inlet tubing and the tube side was replaced before the elution was initiated. Therefore the total estimated retention time needed in addition for Mb is 8.1 minutes. The corresponding additional total retention time estimated for α-LA is 20.0 min. If these retention times are added to the calculated values and plotted in Figure 6.11, the predicted retention times appear to be quite close to the experimental retention times. The difference between the estimated and experimental retention time for α-LA may be caused by the presence of the lower ionic strength eluent in the bed before the higher ionic strength eluent was introduced.

It is seen from Figure 6.11 that both liquid and solid phase concentrations are quite low for the two proteins. However, the elution profiles from the simulations deviate somewhat from the experimental data shown in the Figure 6.11. The possible reasons are: (1) the desorption by the eluent did not reach equilibrium instantly; there were some

resistances such as film mass transfer, pore diffusion and adsorption kinetics presented in the process which were not considered in the simulation; (2) the concentration of the eluent did not instantly reach its original concentration in the entire shell-side bed; therefore concentration gradient was present in the column: this also makes the assumption for instant equilibrium not valid; (3) assumption for value of $K = 0.1$ is not accurate; (4) the protein adsorbed on the ES bed was not considered. One can conclude that the mass balance of eluent in the column should be considered for a more accurate description in the future study. The adsorption equilibrium at different NaCl concentrations in the starting buffer should also be obtained experimentally for the proper simulation of the elution behaviors. However, it is seen in Figure 6.11 that the model can predict the sharp front and tailing to some extent in the elution. The peak shape of α-LA from the simulation is quite similar to that from the experiment.
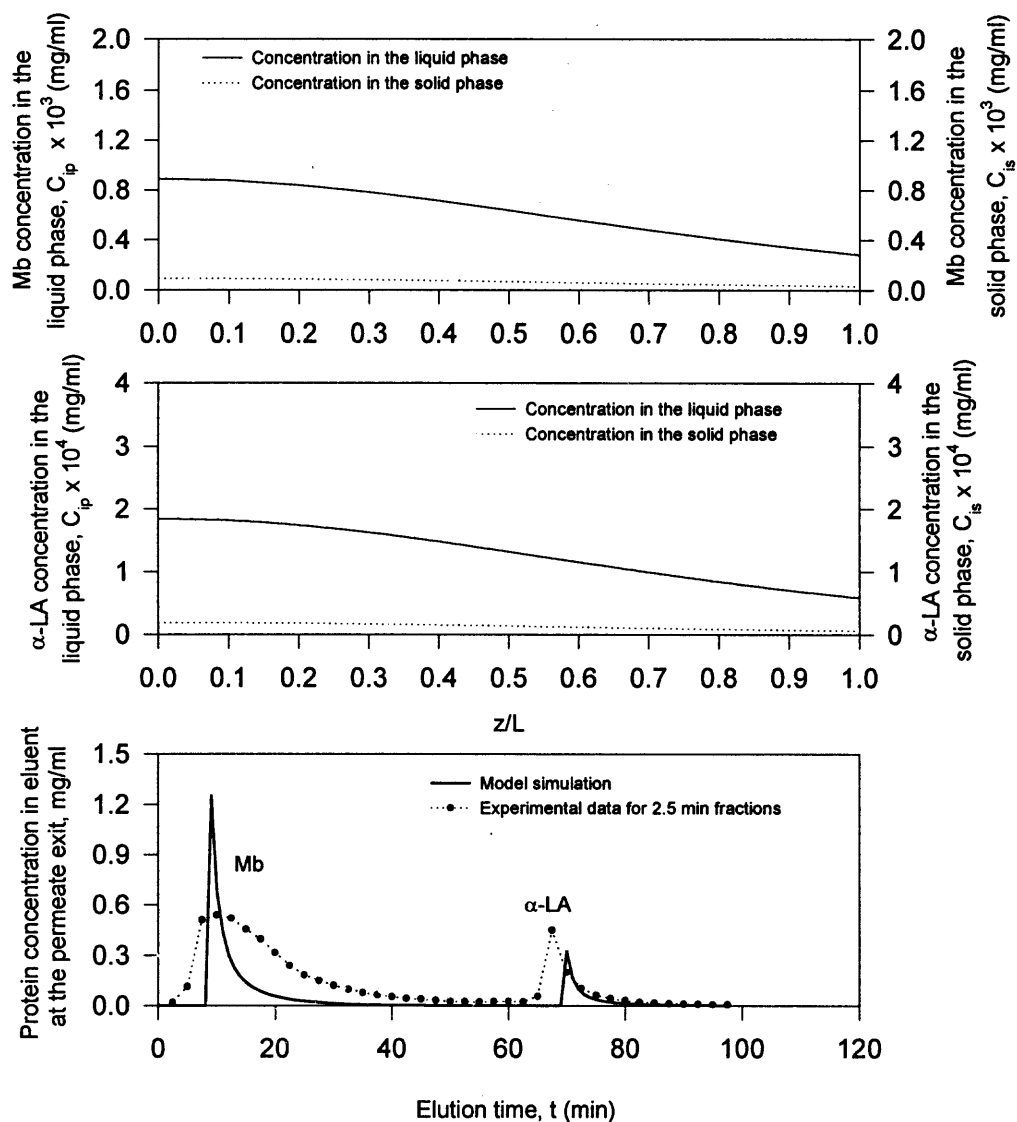
Figure 6.11 Simulation for concentration profiles on the shell-side bed and elution profiles for Mb and α-LA in tube-side elution and comparison with the experimental data (Figure 4.23)

6.11 Concluding Remarks

In this Chapter, a preliminary study has been carried out to develop a mathematical model for the prediction of the chromatographic behavior of the integrated device. Numerical solutions have been obtained for several typical cases by solving the governing equations using the Method of Lines. The model can reasonably describe the concentration profiles and breakthrough behavior in the loading step. From the simulation study, one can conclude that (1) the axial dispersion is not important for the loading behavior in the integrated device; (2) the higher is the feed concentration, the higher is the mass transfer driving force, the lower is the solute rejection by the membrane, the more protein is loaded by the shell-side bed; (3) effect of the permeation parameter of the membrane on loading is complex: the higher is the A, the quicker is the breakthrough; the amount of protein adsorbed changes with an increase of A, first it increases and then it slowly decreases; (4) a higher feed flow rate benefits filtration-loading but should be controlled within the shear tolerance for either biomolecule or cells in the feed. Further study needs to be done to improve the model utility by considering the effect of various factors such as resistances present in the process of chromatography (adsorption), mass balance for the eluent as well as the effect of the extended section packed on the permeate exit.

CHAPTER 7

CONCLUDING REMARKS AND RECOMMENDATIONS

Hollow fiber ultrafiltration cartridges have been successfully packed on the shell side with DEAE Sepharose Fast Flow anion exchange beads for the separation of mixtures of biomolecules via an integrated filtration-cum-loading-cum-chromatography process. Several binary mixtures of proteins were separated using either shell-side elution or tube-side elution via this device. Continuous cyclic processes were also studied by repeatedly loading, washing and eluting single protein and binary protein mixtures in either a clean feed or a yeast suspension without applying cleaning agents to the membrane cartridge at the beginning of each cycle except the first one. Good separations and stable yields were obtained. Since proteins are routinely separated from cellular broths or homogenates by microfiltration or ultrafiltration, these results suggest the following: 1) it is possible to separate mixtures of proteins effectively and efficiently by a cyclic process in one device using an integrated filtration-cum-loading-cum-chromatography process in a bead-filled membrane system from a fermentation broth or a lysate; 2) one may be able to scale up the process by putting a few large modules in parallel; 3) hollow fiber membrane-based modules appear to be quite suitable for such processes. Using the same concept, other simple geometrical configurations of devices could be designed easily and used for biomolecule separation.

A general mathematical model for the prediction of pressure, flow rate and flux profiles in a bead-filled UF/MF hollow-fiber membrane system has been developed. The model was studied for a variety of operational modes in such modules, e.g., conventional UF/MF, permeate flow control, Starling flow, elution, and backflushing, etc. The model

predicts successfully the nature of the transmembrane pressure profile and the solvent flux profile in situations that are quite different, namely, conventional ultrafiltration and Starling flow. By using this model, preliminary mathematical descriptions for protein loading and elution behaviors in the bead-filled device have also been developed.

However, the results in this dissertation were obtained only from ultrafiltration modules packed with DEAE Sepharose Fast Flow ion exchanger. An investigation using a microfiltration module is necessary since microfiltration is widely used for the application of fermentation broth clarification and concentration. Controlling the flux in any MF module packed with beads within the allowed range for chromatographic resin on the shell-side bed will be a critical subject for the future study. Further, other chromatographic resins can be employed in the integrated device such as perfusion chromatography beads which may decrease the shell-side pressure drop and lead to a more uniform TMP for the same conditions used in this dissertation. Perfusion beads also allow a higher flow rate than the ordinary beads which may be compatible with the solvent flux from a MF module. Hydrophobic chromatography beads can also be adopted since many real feed solutions such as the fermentation broth, have significant conductivities. Higher ionic strength is generally used as loading condition in the hydrophobic chromatography. Therefore the step of dilution can be eliminated before loading the feed onto the bed.

More work needs to be done for a more accurate mathematical description of the chromatographic behaviors in the integrated device. Mass transfer resistances such as film mass transfer, pore diffusion and adsorption kinetics should be considered in the modeling to improve the utility of the model. For the elution, mass balance of the eluent

needs to be considered and the relationship between the ionic strength and the

equilibrium constant needs to be obtained experimentally in the future study.

REFERENCES

A/G Technology Corporation. 1997a. *Selection Guide and Price List, United States and Canada.* pp. 6-12.

—. 1997b. *Operating Guide.*

Amersham Pharmacia Biotech.: Instructions for Fast Flow Media.

Amersham Pharmacia Biotech. 1995. Ion Exchange Chromatography: Principles and Methods. pp. 48.

Amersham Pharmacia Biotech. 1998. " Use of Sodium Hydroxide for Cleaning and Sanitizing Chromatography Media and Systems." *Science tools*® - *Results, Reports and Refinements for Life Science Researchers.* 3(1): 32.

Amersham Pharmacia Biotech. 1999a. *Expanded Bed Adsorption – Principles and Methods.* pp. 52.

—. 1997b. *Expanded Bed Adsorption – Principles and Methods.* pp. 9.

Apelblat, A., A. Katzir-Katchalsky, and A. Silberberg. 1974. "A Mathematical Analysis of Capillary-Tissue Fluid Exchange." *Biotechnology.* 11: 1-49.

Bellara, S. R., Z. Cui, and D. S. Pepper. 1997. "Fractionation of BSA and Lysozyme Using Gas-Sparged Ultrafiltration in Hollow Fiber Membrane Modules." *Biotechnol. Prog.* 13: 869-872.

Belter, P. A., E. L. Cussler, and W. Hu. 1988. *Bioseparations: Downstream Processing for Biotechnology.* John Wiley & Sons, Inc.

Bird, R. B., W. E. Stewart, and E. N. Lightfoot. 1960. *Transport Phenomena.* John Wiley & Sons. pp. 199.

Boyer, P. M. 1991. "Engineering Analysis of Protein Adsorption by Dye-Ligand Adsorbents." Doctoral Dissertation: Chapter 3. Lehigh University, Bethelham, PA.

Brian III, R. W., I. Zwiebel, and R. S. Artigue. 1987. "Numerical Simulation of Fixed-Bed Adsorption Dynamics by the Method of Lines." *AIChE Symp. Ser.,* 259: 80.

Byers, M. J., E. G. Isacoff, and J. O. Naples. Dec. 10, 1991. "Separation or Purification of Biomaterials with Particulate Polymeric Adsorbents." Canadian Patent 1,292,952.

Chang, Y. K., and H. A. Chase. 1996. "Ion Exchange Purification of G6PDH from Unclarified Yeast Cell Homogenates Using Expanded Bed Adsorption." *Biotechnol. Bioeng.* 49: 204 - 216.

Chase, H. A. 1984. "Prediction of the Performance of Preparative Affinity Chromatography." *Journal of Chromatography.* 297: 179-202.

Chung, S. F., and C. Y. Wen. 1968. "Longitudinal Dispersion of Liquid Flowing Through Fixed and Fluidized Beds." *AIChE J.* 14: 857.

Danckwerts, P. V. 1953. "Continuous Flow System: Distribution of Residence Times." *Chem. Eng. Sci.* 2(1): 1-18.

Darbre, P. D., A. E. Romero-Herrera, and H. Lehmann. 1975. "Comparison of the Myoglobin of the Zebra (*Equus Burchelli*) with that of the Horse (*Equus caballus*)." *Biochimica et Biophysi2ca Acta.* 393: 201 - 204.

Davis, J. C. 1990. "Process for Selective Dialysis Using Polymeric Affinity Adsorbents and Size Selective Membranes." US Patent 4,963,264.

Dickerson, R. E., and I. Geis. 1969. *The Structure and Action of Proteins.* Harper and Row Publisher, New York. pp. 52.

Diehl, P. 1998. "Expended-Bed Adsorption for BioManufacturing." *Genetic Eng. News.* Oct. 1: 1.

Feng, X., C. Y. Pan, C. W. McMinis, J. Ivory, and D. Ghosh. 1998. "Hollow-Fiber-Based Adsorbers for Gas Separation by Pressure-Swing Adsorption." *AIChE J.* 44(7): 1555-1562.

Finette, G. M. S., B.Baharin, Q. M. Mao, and M. T. W. Hearn. 1998. "Optimization Consideration for Purification of α_1-Antitrypsin Using Silica-Based Ion-Exchange Adsorbents in Packed and Expanded Beds." *Biotechnol. Prog..* 14: 286-293.

Frank, G. T. 1987. "Membrane Solvent Extraction with Hydrophobic Microporous Hollow Fibers and Extractive Bioreactor Development for Fuel Ethanol Production." Doctoral Dissertation. Department of Chemistry and Chemical Engineering, Stevens Institute of Technology, Hoboken, NJ.

Frank, G. T., and K. K. Sirkar. 1985. "Alcohol Production by Yeast Fermentation and Membrane Extraction." *Biotechnol. & Bioeng. Symp. Ser.* 15, 621-631.

Gill, W. N., and B. Bansal. 1973. "Hollow Fiber Reverse Osmosis Systems Analysis and Design." *AIChE J.* 19(4), 823-831.

Gilleskie, G. L., J. L. Parkar, and E. L. Cussler. 1995. "Gas Separations in Hollow-Fiber Adsorbers." *AIChE J.* 41(6): 1413-1425.

Gunn, D. J. 1987. "Axial and Radial Dispersion in Fixed Beds." *Chem. Eng. Sci.* 42: 363.

Happel, J. 1959. "Viscous Flow Relative to Arrays of Cylinders," *AIChE J.* 5(2), 174-177.

Harrison, R.G. (ed.). 1994. *Protein Purification Process Engineering*. Preface. Marcel Dekker, New York.

Heath, C. A., G. Belfort, G., B. E. Hammer, S. D. Mirer, and J. M. Pimbley. 1990. "Magnetic Resonance Imaging and Modelling of Flow in Hollow-Fiber Bioreactors." *AIChE J.* 36(4): 547 –558.

Hejtmánek, V., and P. Schneider. 1993. "Axial Dispersion under Liquid-Chromatography Conditions." 48: 1163-1168.

Hirayama, K., S. Akashi, M. Furuya, and K. Fukuhara. 1990. "Rapid Confirmation and Revision of the Primary Structure of Bovine Serum Albumin by Esims and Frit-Fab LC/MS." *Biochemical and Biophysical Research Communications.* 173: 639 – 646.

Ho, W. S. W., K.K. Sirkar. 1992. *Membrane Handbook.* Chapman & Hall, New York. Chapter 28.

Johansson, H. J., C., Jagerstern, and J. Shiloach. 1996. "Large Scale Recovery and Purification of Periplasmic Recombinant Protein from *E.coli* Using Expended Bed Adsorption Chromatography followed by New Ion Exchange Media." *J. Biotechnol.* 48: 9-14.

Kang, W. 1989. "Hollow Fiber Membrane – Based Extractive Bioreactors and a Whole Cell Immobilization Technique." Doctoral Dissertation: pp. 20. Stevens Institute of Technology. Hoboken, NJ.

Kang, W., R. Shukla, and K. K. Sirkar. 1990. "Ethanol Production in a Microporous Hollow-Fiber-Based Extractive Fermentor with Immobilized Yeast." *Biotechnol. Bioeng.* 36: 826 – 833.

Kaplan, L. J., and J. F. Foster. 1971. "Isoelectric Focusing Behavior of Bovine Plasma Albumin, Mercaptalbumin, and β-Lactoglobulin A and B." *Biochemistry.* 10: 630 – 636.

Karoor, S., and K.K. Sirkar. 1993. "Gas Absorption Studies in Microporous Hollow Fiber Membrane Modules." *I&EC Res.* 32(4), 674-684.

Koch, D. L., and J. F. Brady. 1985. "Dispersion in Fixed Beds." *J. Fluid Mech.* 154: 399.

Koska, J., B. D. Bowen, and J. M. Piret. 1997. "Protein Transport in Packed-Bed Ultrafiltration Hollow-Fiber Bioreactors." *Chemical Engineering Science.* 52(14): 2251 – 2263.

Kronman, M. J., and R. E. Andreotti. 1964. "Inter- and Intramolecular Interactions of α-Lactalbumin. I. The Apparent Heterogeneity at Acid pH." *Biochemistry.* 3(8): 1145-1151.

Lehninger, A. L.1975. *Biochemistry.* 2nd Ed. Worth Publisher, New York. pp. 162.

Levenspiel, O. 1972. Chemical Reaction Engineering. 2nd Ed. John Wiley & Sons. pp. 72.

Longsworth, L. G., and C. F. Jacobsen. 1949. "An Electrophoretic Study of the Binding of Salt Ion by β-Lactoglobulin and Bovine Serum Albumin." *J. Phys. Colloid Chem.* 53: 126 - 135.

Luo, R. G., and J. T. Hsu. 1997. "Rate Parameter and Gradient Correlations for Gradient Elution Chromatography." *AIChE J.* 43: 464-474.

Mao, Q. M., and M.T.W. Hearn. 1996. "Optimization of Affinity and Ion-Exchange Chromatographic Processes for the Purification of Proteins." *Biotechnol. Bioeng.* 52: 204.

McCormick, D. K. 1993. "Expanded Bed Adsorption – The First New Unit Process Operation in Decades." *Bio/Technology.* 11: 295-303.

Molinari, R., J. L. Torres, A. S. Michaels, P. K. Kilpatrick, and R.G. Carbonell. 1990. "Simultaneous Ultrafiltration and Affinity Sorptive Separation of Proteins in a Hollow Fiber Membrane Module." *Biotechnol. Bioeng.* 36: 572 – 580.

Nigam, S. C., A. Sakoda, and H. Y. Wang. 1988. "Bioproduct Recovery from Unclarified Broth and Homogenates Using Immobilized Adsorbent." *Biotechnol. Prog.* 4(3): 166 – 172.

Noriega, J. A., A. Tejeda, I. Magana, J. Ortega, and R. Guzman. 1997. "Modeling Column Regeneration Effects on Dye-Ligand Affinity Chromatography." *Biotechnol. Prog.* 13: 296-300.

Pan, C. Y., and C. W. McMinis. 1992. "Hollow Fiber Bundle Element." US Patent: 5,139,668.

Patkar, A.Y., J. Koska, D. G. Taylor, B. D. Bowen, and J. M. Piret. 1995. "Protein Transport in Ultrafiltration Hollow-Fiber Bioreactors." *AIChE J.* 41(2): 415-425.

PerSeptive Biosystems, Inc. 1996. *The Busy Researcher's Guide to Biomolecule Chromatography.*

Pharmacia Biotech. 1996. *BioDirectory.* pp. 363-364.

Radola, B. J. 1973. "Isoelectric Focusing in Layers of Granulated Gels: I. Thin-Layer Isoelectric Focusing of Proteins." *Biochimica et Biophysica Acta.* 295: 412 – 428.

Sirkar, K. K., and R. Prasad, 1996. "Protein Ultrafiltration - Some Neglected Considerations." from W. C. McGregor (Ed.), *Membrane Separations in Biotechnology.* Marcel Dekker, New York.

Sokol, F., L. Hána and P. Albrecht. 1961. "Fluorescent Antibody Method: Quantitative Determination of 1-Dimethylaminonaphthalene-5-Sulphonic Acid and Protein in Labelled γ-Globulin." *Folia Microbiologica.* 6: 145 – 150.

Rosell, C. M., A. M. Vaidya, and P. J. Halling. 1996. "Continuous In Situ Water Activity Control for Organic Phase Biocatalysis in a Packed Bed Hollow Fiber Reactor." *Biotechnol. & Bioeng.* 49: 284-289.

Shiloach, J., and J. B. Kaufman. 1999. "The Combined Use of Expended-Bed Adsorption and Gradient Elution for Capture and Partial Purification of Mutant Diphtheria Toxin (CRM 9) from *Corynebacterium diphtheriae.*" *Separation Science and Technology.* 34(1): 29-40.

Shukla R., W. Kang, and K. K. Sirkar. 1989. "Novel Hollow Fiber Immobilization Techniques for Whole Cells and Advanced Bioreactors." *Appl. Biochem. Biotechnol.* 20: 571.

Sofer, G., and L. Hagel. 1997a. *Handbook of Process Chromatography: A Guide to Optimization, Scale-up and Validation.* Chapter 10. Academic Press, New York.

—. 1997b. *Handbook of Process Chromatography: A Guide to Optimization, Scale-up and Validation.* Chapter 5. Academic Press, New York.

Starling, E. H. 1896. "On the Adsorption of Fluid from the Connective Tissue Space." J. Physiol. 19: 312-326.

Subramanian, G. 1998a. *Bioseparation and Bioprocessing - A Handbook. Volume II: Processing, Quality and Characterization, Economics, safety and Hygiene.* Wiley-VCH, Weinheim. pp. 19.

—. 1998b. *Bioseparation and Bioprocessing - A Handbook. Volume II: Processing, Quality and Characterization, Economics, safety and Hygiene.* Wiley-VCH, Weinheim. pp. 329.

Swabb, E., J. Wei, and P. M. Gullion. 1974. "Diffusion and Convection in Normal Neoplastic Tissues." *Cancer Res.* 34: 2814-2822.

Taylor, D. G., J. M. Piret, and B. D. Bowen. 1994. "Protein Polarization in Isotropic Membrane Hollow-Fiber Bioreactors." *AIChE J.* 40(2): 321 – 333.

Thömmes, J., M. Halfar, S. Lenz, and M-R. Kula. 1995. "Purification of Monoclonal Antibodies from Whole Hybridoma Fermentation Broth by Fluidized Bed Adsorption." *Biotechnol. Bioeng.* 45: 205 - 211.

Thömmes, J. 1999. "Investigation on Protein Adsorption to Agarose-Dextran Composite Media." *Biotechnol. Bioeng.* 62(3): 358.

Thömmes, J., and M-R. Kula.1995. "Membrane Chromatography – An Integrative Concept in the Downstream Processing of Proteins." *Biotechnol. Prog.* 11: 357.

Townend, R., L. Weinberger, and S. N. Timasheff. 1960. "Molecular Interactions in β-lactoglobulin Close to its Isoelectric Point." *J. Amer. Chem. Soc.* 82: 3157 – 3161.

Vaidya, A. M., P. J. Halling, and G. Bell. 1993. "Novel Reactor For Aqueous-Organic Two-Phase Biocatalysis: A Packed Bed Hollow Fiber Membrane Bioreactor." *Biotechnology Techniques.* 7(7): 441-446.

van Reis, R., L. C. Leonard, C. C. Hsu, and S. E. Builder. 1991. "Industrial Scale Harvest of Proteins from Mammalian Cell Culture by Tangential Flow Filtration." *Biotechnol. Bioeng.* 38: 413 - 422.

Vanaman, T. C., K. Brew, and R. L. Hill. 1970. "The Disulfide Bonds of Bovine α-Lactalbumin." *The Journal of Biological Chemistry.* 245 (17): 4583-4590.

Yamamoto, S., K. Nakanishi, R. Matsuno and T. Kamikubo. 1983a. "Ion Exchange Chromatography of Protein - Prediction of Elution Curves and Operating Conditions. I. Theoretical Considerations." *Biotechnol. Bioeng.* 25: 1465-1483.

Yamamoto, S., K. Nakanishi, R. Matsuno and T. Kamikubo. 1983b. "Ion Exchange Chromatography of Protein - Prediction of Elution Curves and Operating Conditions. I. Experimental Verification." *Biotechnol. Bioeng.* 25: 1373-1391.

Yang, M.-C., and E. L. Cussler. 1987. "A Hollow-Fiber Trickle-Bed Reactor." *AIChE J.* 33(10): 1754 – 1756.

Zeman, L. J., and A. L. Zydney. 1996a. *Microfiltration and Ultrafiltration.* Chapter 10, Marcel Dekker, New York.

—. 1996b. *Microfiltration and Ultrafiltration.* Chapter 9, Marcel Dekker, Inc, New York.

Zeng, X., E. Ruckenstein. 1999. "Membrane Chromatography: Preparation and Applications to Protein Separations." *Biotechnol. Prog..* 15(6): 1003 –1019.

Zydney, A. L., W.M. Saltzman, and C. K. Colton. 1986. "Hydraulic Resistance of Red Cell Beds in an Unstirred Filtration Cell." *Chem. Eng. Sci.* 44: 147-159.